Title	Studies on Quinoidal Non-alternant Hydrocarbons: Effect of the Molecular Symmetry of Quinoidal Structure on the Delocalization of π-Electrons and Open-shell Character
Author(s)	掘井, 康稀
Citation	大阪大学, 2022, 博士論文
Version Type	VoR
URL	https://doi.org/10.18910/88015
rights	
Note	

Doctoral Dissertation

Studies on Quinoidal Non-alternant Hydrocarbons:

Effect of the Molecular Symmetry of

Quinoidal Structure on the Delocalization of

π-Electrons and Open-shell Character

Koki Horii

January 2022

Department of Applied Chemistry

Graduate School of Engineering

Osaka University

Preface and Acknowledgements

The study of this doctoral dissertation was carried out under the guidance of Prof. Dr. Makoto Yasuda at the Department of Applied Chemistry, Graduated School of Engineering, Osaka University from April 2016 to March 2022. The thesis describes the study of π-extended bicyclic non-alternant hydrocarbons and the effect of the molecular symmetry of quinoidal strtucture on the (anti)aromaticity and open-shell characters.

First and foremost, I would like to express my deepest appreciation to Prof. Dr. Makoto Yasuda for his precise guidance, heart-warming encouragements and helpful suggestions throughout this work. His keen insights and enthusiasm for chemistry have broadened my horizons and provided me with many valuable experiences.

I would also like to thank Professors Dr. Yutaka Ie and Dr. Shinobu Itoh for their helpful advice and kind assistance.

I really wish to make a grateful acknowledgement to Associate Prof. Dr. Yoshihiro Nishimoto for his great assistance, helpful suggestion and stimulating discussion. His multifaceted point of view was very essential and helped me to improve my research.

I gratefully express acknowledgement to Assistant Prof. Dr. Akihito Konishi for his energetic and precise guidance in many situations, including the basics of research and daily discussions. He taught me the depth and interest of chemistry, and they were very valuable experiences for me.

I would sincerely like to thank Associate Prof. Dr. Shuntaro Tsubaki for his grateful support and heartwarming kindness.

I am deeply thankful to Ms. Yoshimi Shinomiya and Ms. Tomoko Shimizu for giving me their grateful support and heartwarming kindness.

I would like to thank Pofessors Dr. Masayoshi Nakano, Dr. Ken-ichi Nakayama, Dr. Takeshi Kawase and Dr. Takeaki Iwamoto, and Associate Professors Dr. Ryohei Kishi, Dr. Mitsuharu Suzuki, Dr. Daisuke Shiomi and Dr. Shintaro Ishida for their helpful suggestion and stimulating discussion in our cooperative researches.

I wish to acknowledge to all the members of Yasuda group for their hearty encouragement and constant support. I gratefully wish to thank Ms. Yui Okada, Ms. Haruna Iwasa, and Mr. Michiyoshi Hirose for their active working, untiring efforts and helpful assistance.

I would also like to thank Associate Professor Dr. Taro Uematsu and Assistant Professor Dr. Takuya Kodama for their sharp comments about my experiments and kind encouragement.

I would like to express my heartfelt thanks to Mr. Hiroshi Moriguchi, Dr. Nobuko Kanehisa, Dr. Kyoko Inoue, Dr. Hiroaki Tanaka Mr. Kunihiko Kamon and Mr. Hiromi Ohi with analytic assistance at the analytical instrumentation facility.

I wish to thank Japan society for the promotion of science (JSPS) for the financial support.

Finally, I would like to express my gratitude to my parents, Takahiro Horii and Maki Horii, and my groundmother, Taeko Ikoma for their understanding to my work, constant assistance and financial support. I also thank my sister, Miduki Horii for her encouragement.

<div align="right">

January, 2022

Koki Horii

</div>

Department of Applied Chemistry
Graduate School of Engineering
Osaka University
2-1 Yamadaoka, Suita, Osaka 565-0871, JAPAN

List of Publications

1) Open-shell and Antiaromatic Character Induced by the Highly Symmetric Geometry of the Planar Heptalene Structure: Synthesis and Characterization of a Non-alternant Isomer of Bisanthene
   Akihito Konishi, Koki Horii, Daisuke Shiomi, Kazunobu Sato, Takeji Takui, Makoto Yasuda
   J. Am. Chem. Soc. **2019**, *141*, 10165-10170.
   DOI: 10.1021/jacs.9b04080

2) Characterization of Benzo[*a*]naphtho[2,3-*f*]pentalene: Interrelation between Open-shell and Antiaromatic Characters Governed by Mode of the Quinoidal Subunit and Molecular Symmetry
   Akihito Konishi, Koki Horii, Haruna Iwasa, Yui Okada, Ryohei Kishi, Masayoshi Nakano, Makoto Yasuda
   Chem. Asian J. **2021**, *16*, 1553-1561.
   DOI: 10.1002/asia.202100398

3) Synthesis and Characterization of Dinaphtho[2,1-*a*:2,3-*f*]pentalene: A Stable Antiaromatic/Quinoidal Hydrocarbon Showing Appropriate Carrier Mobility in the Amorphous Layer
   Koki Horii, Akira Nogata, Yusuke Mizuno, Haruna Iwasa, Mitsuharu Suzuki, Ken-ici Nakayama, A. Konishi, M. Yasuda
   Chem. Lett. Accepted.
   DOI: 10.1246/cl.210809

4) Bis-periazulene as a Non-alternant isomer of Pyrene: Synthesis and Characterization of Triaryl Derivatives
   Koki Horii, Ryohei Kishi, Masayoshi Nakano, Daisuke Shiomi, Kazunobu Sato, Takeji Takui, Akihito Konishi,, Makoto Yasuda
   Submitted.

<Supplementary Publications>

1) Isolation and characterisation of a stable 2-azaphenalenyl azomethine ylide
   Koji Katayama, Akihito Konishi, Koki Horii, Makoto Yasuda, Chitoshi Kitamura, Jun-ichi Nishida, Takeshi Kawase
   Commun. Chem. **2019**, *2*, 136.
   DOI: 10.1038/s42004-019-0236-y

Contents

General Introduction

Understanding the structure–property relationship of π-conjugated molecules is essential in designing and controlling the electronic properties of these molecules. Consequently, the optoelectronic characteristics of π-conjugated systems, including photo-absorptions, emissions, redox behaviors, magnetisms, and carrier mobility, have received considerable attention for the potential applications of organic devices. Furthermore, various chemical functionalization toward π-conjugated systems has allowed chemists to address the precise control of the electronic properties.[1] As a result, many aromatic molecules consisting of benzene-like hexagons have been developed as fundamental units for functional organic materials.[2]

Unsaturated hydrocarbons composed of cyclic sp^2-carbon networks are the essential skeleton of π-conjugated molecules. Depending on the topology of the sp^2-carbon network, unsaturated hydrocarbons can be divided into two categories.[3] π-Conjugated carbocycles containing odd-membered rings are called as non-alternant hydrocarbons. When one alternately assigns stared (*) and non-stared marks (○) to the sp^2 carbon atoms of these hydrocarbons, the same marks are inevitably next to each other (Figure 1A). On the other hand, in alternant hydrocarbons such as benzene and naphthalene, the alternative assignment of the two marks to the sp^2 carbons is always realized (Figure 1B).
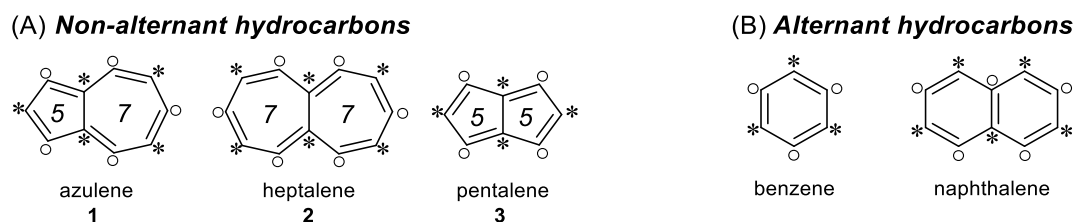

(A) *Non-alternant hydrocarbons*

azulene
1

heptalene
2

pentalene
3

(B) *Alternant hydrocarbons*

benzene

naphthalene

Figure 1. Examples of (A) non-alternant and (B) alternant hydrocarbons.

The intriguing sp^2-carbon network of non-alternant hydrocarbons has been a significant motivation for the research because of their optoelectronic properties, (anti)aromaticity, and magnetisms, which are never shared by alternant hydrocarbons. Over the passed 15 years, the chemistry of nonalternant hydrocarbons has experienced a remarkable renaissance thanks to advances in synthetic methodologies, computational techniques, and surface syntheses and observations. Ring-annulated nonalternant π-systems, in which some benzenoid rings are attached into the nonalternant frameworks, are the key players in their resurgence.[4] A fusion of benzenoid rings to the nonalternant π-systems (benzo-annulation) is the simplest way to construct the π-extended nonalternant hydrocarbons. The ring annulation impacts the electronic structures of nonalternant subunits, which modulates the highest occupied molecular orbital (HOMO)–the lowest unoccupied molecular orbital (LUMO) gap and creates perturbations in their inherent (anti)aromatic nature. For example, non-alternant hydrocarbons in which the naphthalene ring in benzo[*a*]pyrene is replaced by one and more azulene ring(s) have provided profound insights into the relationship between molecular structure
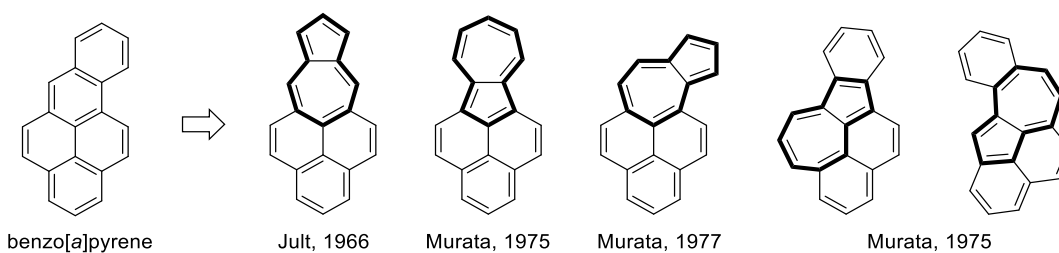
and the main π-conjugated system (Figure 2).[5]

benzo[*a*]pyrene   Jult, 1966   Murata, 1975   Murata, 1977   Murata, 1975

Figure 2. Non-alternant isomers of benzo[*a*]pyrene. Bold lines represent the embedded azulene skeleton.

On the other hand, benzo-annulations of a non-alternant hydrocarbon provide another aspect of incorporating quinoid structures into the non-alternant system. There are three types of quinoidal structures, *o*-, *p*-, and *m*-quinoidal scaffold (Figure 3). Although they have open-shell characters in their ground states, the most significant difference among them is the spin multiplicity in the ground state. The ground states of *o*- and *p*-quinoid are singlet because of the contribution of closed-shell Kekulé canonical structures. In contrast, *m*-quinoid is a non-Kekulé diradical. Due to the degenerate singly occupied molecular orbitals (SOMOs) with a non-disjoint feature, *m*-quinoid has a triplet ground state. The embedment of quinoidal scaffold significantly impacts the electronic properties of π-extended non-alternant hydrocarbons.
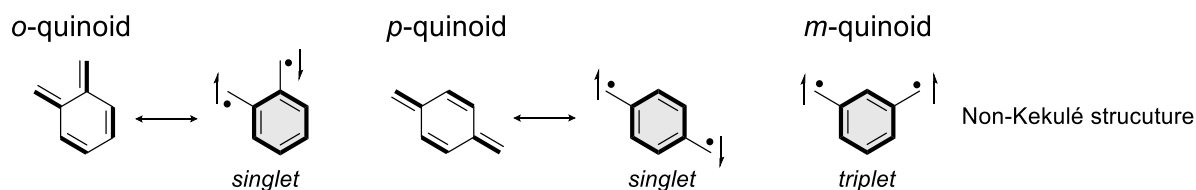

o-quinoid   *p*-quinoid   *m*-quinoid

singlet   singlet   triplet   Non-Kekulé strucuture

Figure 3. Quinoidal structures.

Recent studies on the π-extended indacenes (indenofluorenes) are landmark examples of how the embedded quinoidal structures can affect the electronic properties of the indacene core. The reported ground states vary from closed-shell to open-shell singlet/triplet states depending on the ring-fusion patterns (Figure 4).[6] The small HOMO–LUMO gaps, ambipolar redox properties and near-infrared absorptions of these π-extended non-alternant systems demonstrate the possibility of their application as functional organic materials.

In this thesis, the author focused on bicyclic non-alternant hydrocarbons, azulene **1**, heptalene **2**, and pentalene **3**, which are the most fundamental scaffolds in a series of non-alternant hydrocarbons.

Azulene **1** is an aromatic 10π-electron system consisting of a fused pentagon-heptagon network. While naphthalene, a structural isomer of azulene, is a colorless (λ_{max} = 312 nm) and nonpolar compound, azulene exhibits a blue color (λ_{max} = 585 nm) with an abnormal anti-Kasha's emission and a significant dipole moment (1.08 D). The charge-separated canonical structures of azulene, which are described as the superposition of an aromatic cyclopentadienide and tropylium ions, nicely explain the dipole moment (Figure 5A).
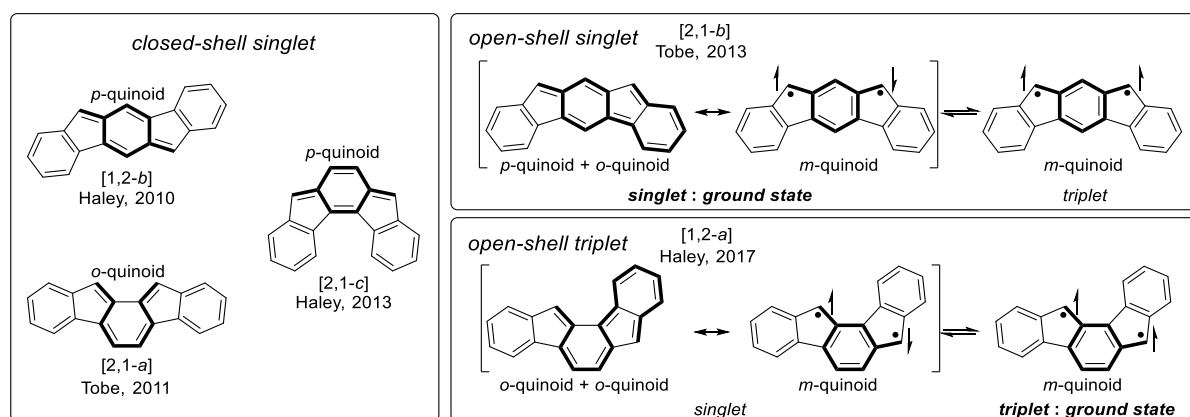
Figure 4. π-Extended indacenes (indenofluorenes) with their ground state electronic configurations.

Its HOMO is mainly distributed on the pentagon, but the LUMO exists on the heptagon (Figure 5B). This unsymmetric distribution of the coefficients of the frontier orbitals leads to a decrease in the mutual electron repulsions in the first excited state, giving a lower transition energy than that anticipated from the HOMO–LUMO gap. These peculiar properties of azulene have driven many chemists to the development of azulene-based materials as multi-stage and stable redox systems[7], near-infrared absorbers[8], and electronic devices[9] (Figure 5C).
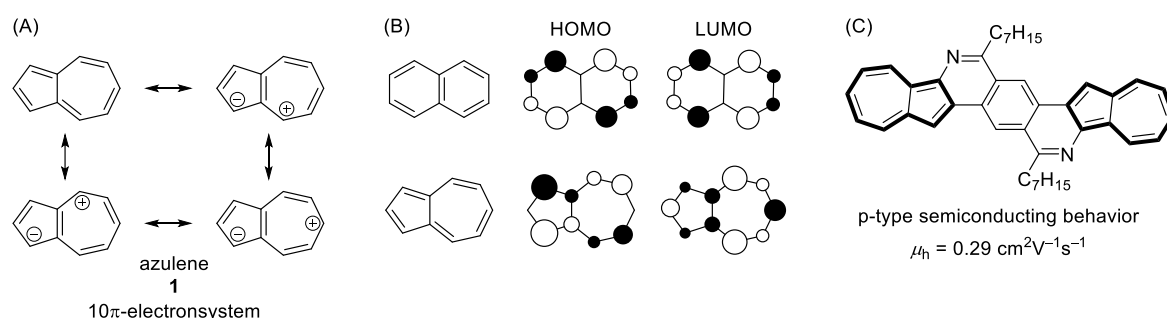

Figure 5. (A) Canonical structures of azulene **1**. (B) Frontier molecular orbitals of azulene and naphthalene calculated by the Hückel theory. (C) Example of azulene based material for electronic device.

Heptalene **2** consists of two fused cycloheptatrienes with 12π electrons (Figure 6A). In comparison to other nonalternant hydrocarbons, the most notable feature of **2** is its twisted molecular geometry with negative curvature, leading to a non-aromatic character, regardless of its $4n\pi$-system. In 1961, the first synthesis of the pristine heptalene **2** was reported as a thermally unstable compound, which readily decomposed by self-polymerization at localized double bonds. The introduction of electron-withdrawing groups enhanced the stability of **2**; the derivatives with dimethoxycarbonyl (**2a**) were isolated in crystal forms (Figure 6B).[10] Due to its nonplanar geometry, **2** possesses four isodynamic structures that are interconvertible via ring inversion and/or bond shift in a dynamic equilibrium with one another (Figure 6C).[11] The study of both dynamic processes has provided insights into their transition states, in which heptalene **2** assumes a planar geometry with an enhanced $4n\pi$-character. However, heptalene derivatives with a planar structure have not been

3

reported so far. Therefore, the experimental investigations of the physical properties of a planar heptalene, such as their antiaromaticity, have remained unexplored.
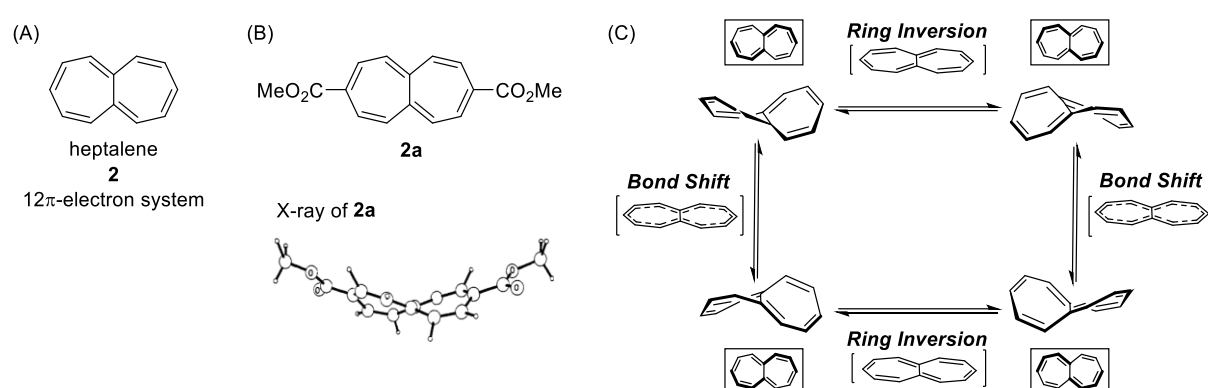

Figure 6. (A) Structure of heptalene **2**. (B) Crystal form of heptalene derivative **2a**. (C) Dynamic process of heptalene **2**.

Pentalene **3**, due to its 8π-antiaromatic nature, readily dimerizes above -196 °C.[12] The 1,3,5-tri-*tert*-butyl derivative **3a** is kinetically stabilized to be isolated.[13] Its molecular geometry shows a remarkable bond length alternation (BLA) in the ground state: NMR studies indicated that the energy barrier between two valence isomers of **3a**-I and **3a**-II is about 4 kcal/mol with the delocalized 8π-antiaromatic structure **3a**-III located at the transition state of the interconversion (Figure 7).
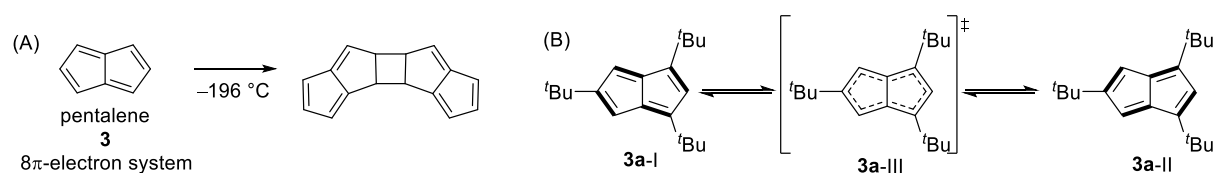

Figure 7. (A) Dimerization of pentalene **3**. (B) Interconversion of **3a** between the two valence isomers.

A fusion of benzenoid hexagon(s) to the pentalene core dramatically changes the properties of pentalene itself. For example, the benzo-annulated pentalenes, benzopentalene **4**[14] and dibenzo[*a,e*]pentalene **5**[15], have been well-known for a long time and many derivatives have been synthesized as stable compounds (Figure 8A). Contrarily, dibenzo[*a,f*]pentalene **6a**, a structural isomer of dibenzo[*a,e*]pentalene **5**, had been an unknown molecule until recently due to its instability (Figure 8B). Considering the resonance structures of **6a**, one can notice that the [*a,f*]-type dibenzo-annulation to the pentalene skeleton provides the following electronic features in the ground state (Figure 8C): (1) the enhancement of the peripheral 16π-delocalization (**6a**-III), given by the resonance of the *o*-quinoidal substructure with the loss of a local 6π-aromatic stabilization, and (2) the appearance of the singlet open-shell character (**6a**-IV) induced by the trimethylenemethane (TMM) subunit with the recovery of an extra benzenoid ring. These two features are never shared by dibenzo[*a,e*]pentalene **5**, in which the two aromatic rings remain stable and all π-electrons

4

are strongly coupled in the closed-shell singlet ground state.

In 2017, Konishi, Yasuda and co-wokers performed the first syntheses of the dibenzon[*a*,*f*]pentalene derivatives **6b**/**6c** and experimentally investigated the effects of the [*a*,*f*]-type dibenzo-annulation at the pentalene core on the electronic properties.[16] The syntheses of **6b**/**6c**, in which bulky mesityl groups were introduced to kinetically protect the reactive sites, are shown in Figure 8B. The interconversion of quinoidal units between the two equivalent structures realizes the coexistence of antiaromaticity and open-shell properties (**6a**-I and **6a**-II in Figure 8C).
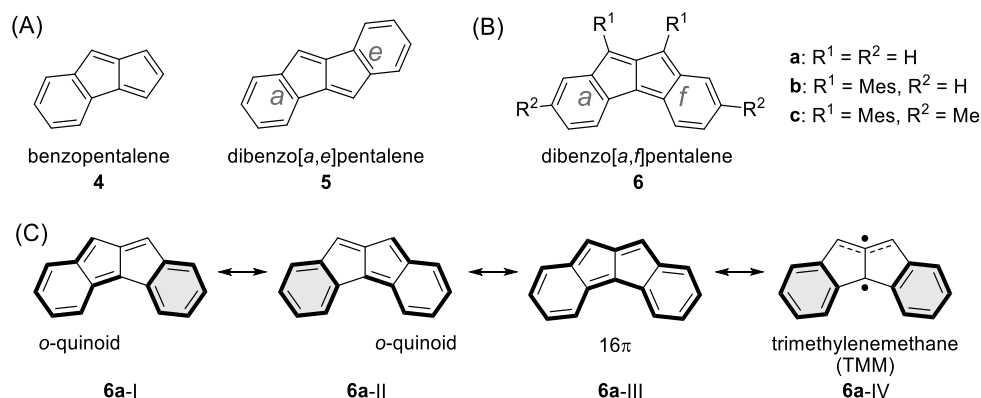

Figure 8. (A) Benzo-annulated pentalenes **4**/**5**. (B) Structures of Dibenzo[a,*f*]pentlane derivatives **6a**-**c**. (C) Resonace structures of **6a**.

On the basis of these background from the studies of non-alternant hydrocarbons, the author focused on the molecular symmetry and the embedded quinoidal structure(s) of non-alternant hydrocarbons. In this thesis, the author investigated the physical properties of bicyclic non-alternant hydrocarbons incorporating quinoidal units. Mainly, the author focused on the control the electronic properties induced by the quinoidal units, such as (anti)aromaticity and open-shell character. The molecules represented in the thesis, the π-extended pentalene, azulene, and heptalene, are shown in Figure 9. An overview in each chapter is summarized below.

In Chapter 1, the author describes the synthesis and characterization of [*a*,*f*]-type annulated pentalenes and unveil the interrelation between open-shell and antiaromatic character.

Chapter 2 demonstrates the synthesis and properties of dinaphtho[2,1-*a*:2,3-*f*]pentalene. The high stability of the molecule under ambient atmosphere allows the examination of the hole mobility in amorphous film measured by a SCLC (Space Charge Limited Current) method.

In Chapter 3, the author presents the synthesis of difluoreno[1,9,8-*alkj*:1',9',8'-*gfed*]heptalene, a first hydrocarbon containing a planarized heptalene core. the author evaluates the antiaromaticity induced by the planarization of heptalene scaffold and open-shell character.
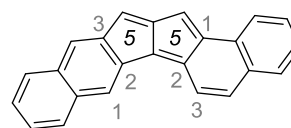
Chapter 4 shows the synthesis and characterization of bis-periazulene, which is a non-alternat isomert of pyrene. the author focuses on the physical properties originating from the embedded quinoid structures.
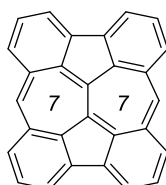
Chapter 1: Benzo[*a*]naphtho[2,3-*f*]pentalene
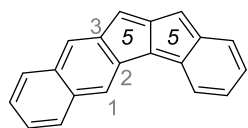
Interrelation between open-shell and antiaromatic character

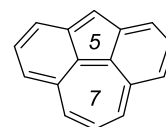**Chapter 2: Dinaphtho[2,1-*a*:2,3-*f*]pentalene**

Hole mobility in the amorphous layer

Chapter 3: Difluoreno[1,9,8-*alkj*:1',9',8'-*gfed*]heptalene

Planarized heptalene derivative with high symmetric geometry

Chapter 4: Bis-periazulene

Three aspects of the π-conjugation:
peripheral, zwitterion and open-shell π-conjugations

Figure 9. An overview of the target molecules.

Reference

(1)   Selected Reviews: (a) M. Stępień, E. Gońka, M. Żyła, N. Sprutta, Heterocyclic Nanographenes and Other Polycyclic Heteroaromatic Compounds: Synthetic Routes, Properties, and Applications, *Chem. Rev.* **2017**, *117*, 3479–3716. (b) J. Wu, W. Pisula, K. Müllen, Graphenes as Potential Material for Electronics, *Chem. Rev.* **2007**, *107*, 718–747. (c) T. M. Figueira-Duarte K. Müllen, Pyrene-Based Materials for Organic Electronics, *Chem. Rev.* **2011**, *111*, 7260–7314.

(2)   E. Clar, Polycyclic Hydrocarbons: Vol. 1 and 2, Academic Press Inc, (1964).

(3)   R. Gleiter, G. Haberhauer, Aromaticity and Other Conjugation Effects, Wiley & Sons, (1994).

(4)   A. Konishi, M. Yasuda, Breathing New Life into Nonalternant Hydrocarbon Chemistry: Syntheses and Properties of Polycyclic Hydrocarbons Containing Azulene, Pentalene, and Heptalene Frameworks, *Chem. Lett.* **2021**, *51*, 195–212.

(5)   K. Hafner, K. H. Häfner, C. Köni, M. Kreuder, G. Ploss, G. Schulz, E. Sturm, K. H. Vöpel, Fulvenes as Isomers of Benzenoid Compounds, *Angew. Chem. Int. Ed. Engl.* **1963**, *2*, 123–134.

(6)   (a) Y. Tobe, Quinodimethanes Incorporated in Non-Benzenoid Aromatic or Antiaromatic Frameworks, *Top Curr Chem.* **2018**, *376*, 12. (b) J. J. Dressler, M. M. Haley, Learning how to fine-tune diradical properties by structure refinement, *J. Phys. Org. Chem.* **2020**, *33*, e4114.

(7)   S. Ito, T. Shoji, N. Morita, Recent Advances in the Development of Methods for the Preparation of Functionalized Azulenes for Electrochromic Applications, *Synlett* **2011**, 2279–2298.

(8)   (a) H. Mori, T. Tanaka, A. Osuka, Fused porphyrinoids as promising near-infrared absorbing dyes, *J. Mater. Chem. C* **2013**, *1*, 2500–2519. (b) T. D. Lash, Out of the Blue! Azuliporphyrins and Related Carbaporphyrinoid Systems, *Acc. Chem. Res.* **2016**, *49*, 471–482.

(9)   (a) H. Xin, X. Gao, Application of Azulene in Constructing Organic Optoelectronic Materials: New Tricks for an Old Dog, *ChemPlusChem* **2017**, *82*, 945–956. (b) H. Nishimura, N. Ishida, A. Shimazaki, A. Wakamiya, A. Saeki, L. T. Scott, Y. Murata, Hole-Transporting Materials with a Two-Dimensionally Expanded π-System around an Azulene Core for Efficient Perovskite Solar Cells, *J. Am. Chem. Soc.* **2015**, *137*, 15656–15659. (c) Y. Yamaguchi, M. Takubo, K. Ogawa, K. Nakayama, T. Koganezawa, H. Katagiri, Terazulene Isomers: Polarity Change of OFETs through Molecular Orbital Distribution Contrast, *J. Am. Chem. Soc.* **2016**, *138*, 11335–11343. (d) H. Xin, C. Ge, X. Yang, H. Gao, X. Yang, X. Gao, Biazulene diimides: a new building block for organic electronic materials, *Chem. Sci.* **2016**, *7*, 6701–6705. (e) H. Xin, C. Ge, X. Jiao, X. Yang, K. Rundel, C. R. McNeill, X. Gao, Incorporation of 2,6-Connected Azulene Units into the Backbone of Conjugated Polymers: Towards High-Performance Organic Optoelectronic Materials, *Angew. Chem. Int. Ed.* **2018**, *57*, 1322–1326.

(10)   J. Stegemann, H. J. Lindner, The crystal and molecular structure of dimethyl-3,8-heptalene-dicarboxylate, *Tetrahedron Lett.* **1977**, *18*, 2515–2516.

(11)   K. Hafner, G. L. Knaup, H. J. Lindner, Syntheses and Dynamic Behavior of Chiral Heptalenes, *Bull. Chem. Soc. Jpn.* **1988**, *61*, 155–163.

(12)   (a) K. Hafner, H. U. Süss, 1,3,5-Tri-tert-Butylpentalene. A Stabilized Planar 8π-Electron System *Angew. Chem., Int. Ed.* **1973**, *12*, 575–577.
        (b) T. Bally, S. Chai, M. Neuenschwander, Z. Zhu, Pentalene: Formation, Electronic, and Vibrational Structure, *J. Am. Chem. Soc.* **1997**, *119*, 1869–1875.

(13)   K. Hafner, H. U. Süss, 1,3,5-Tri-tert-Butylpentalene. A Stabilized Planar 8π-Electron System *Angew. Chem., Int. Ed.* **1973**, *12*, 575–577.

(14)   P. Rivera-Fuentes, M. von W. Rekowski, W. B. Schweizer, J. P. Gisselbrecht, C. Boudon, F. Diederich, Cascade Carbopalladation Reaction between Alkynes and gem-Dibromoolefins: Facile Access to Monoannelated Pentalenes *Org. Lett.* **2012**, *14*, 4066–4069.

(15)   M. Saito, Synthesis and Reactions of Dibenzo[*a*,*e*]pentalenes *Symmetry* **2010**, *2*, 950–969.

(16)   A. Konishi, Y. Okada, M. Nakano, K. Sugisaki, K. Sato, T. Takui, M. Yasuda, Synthesis and Characterization of Dibenzo[*a*,*f*]pentalene: Harmonization of the Antiaromatic and Singlet Biradical Character *J. Am. Chem. Soc.* **2017**, *139*, 15284–15287.
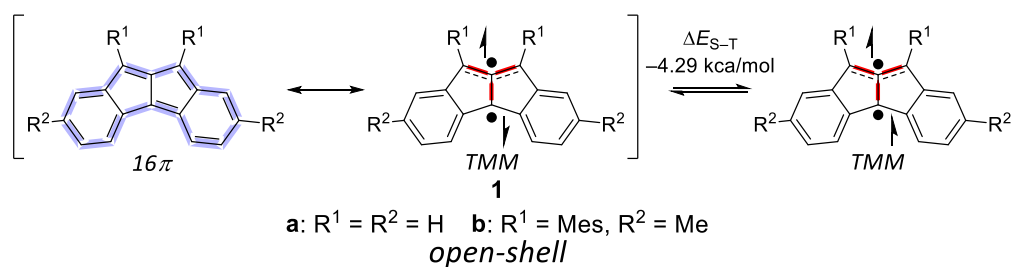
6

Chapter 1

Synthesis and Properties of Benzo[*a*]naphtho[2,3-*f*]pentalene with a Localized *o*-Benzoquinoidal Moiety: Interrelation between Open-shell and Antiaromatic Characters Governed by Fashion of Quinoidal Subunit and Molecular Symmetry
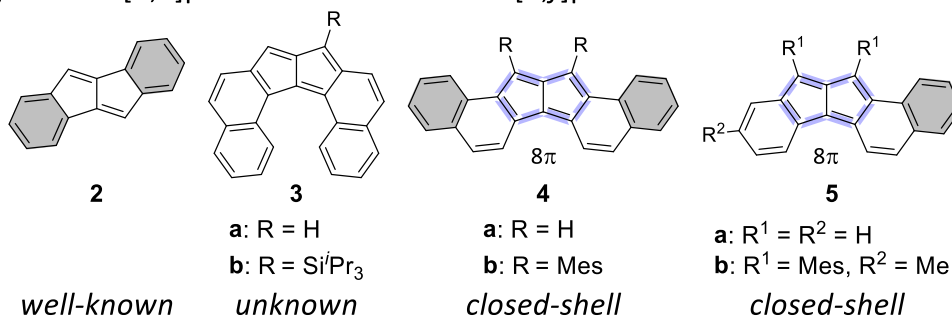
1-1. Introduction

For a decade, singlet open-shell molecules[1–6] have been intensively investigated using both experimental and theoretical approaches because their unique electronic structures are scientifically intriguing, as well as potential for applications as organic optoelectronic materials,[7] such as field-effect transistors,[8–14] nonlinear optics,[15–17] and singlet fissions.[18–20] Singlet open-shell character, which often inhabits *o*- or *p*-quinoidal subunits in polycyclic hydrocarbons,[6,21–24] is frequently associated with aromatic or antiaromatic nature because of an inherently small HOMO–LUMO gap.[25–27] Understanding the interrelation between open-shell and antiaromatic characters is one of the important subjects to describe a nature of unique π-conjugations.[28–31] In many neutral $4n\pi$-systems, however, open-shell and antiaromatic characters are incompatible in the same molecule.[29,32,33] π-Extended polycyclic antiaromatic systems reveal a tendency to assume an aromatic nature with the occurrence of an open-shell singlet ground state, in which the open-shell resonance structure relieves the $4n\pi$-antiaromatic conjugation in the closed-shell resonance structure.[9,34–36] In view of the inescapable fact, it is a major challenge to establish the rational design guide for a suitable molecular series possessing both open-shell and antiaromatic characters. This most troublesome problem is a major barrier to advance understanding and scrutinizing the interrelation between open-shell and antiaromatic characters.[37,38]

Recently, Konishi, Yasuda and cowokers have investigated dibenzo[*a,f*]pentalene **1**[39,40] that displays different properties from its long-known and well-studied structural isomer, dibenzo[*a,e*]pentalene **2** (Figures 1A and B).[41–44] Whereas **2** is a closed-shell molecule that consists of the weak paratropic pentalene core with two aromatic benzene rings, the isomer **1** exhibits a singlet open-shell character with a small singlet–triplet energy gap ($\Delta E_{S–T}$) and a peripheral 16π-antiaromatic character. Their dibenzo[*a,f*]pentalene framework, in which antiaromatic and open-shell characters are harmonized, is an acceptable model to systematically investigate the interrelation between the two characters through chemical modifications of the framework.[40] The large antiaromatic nature in the singlet ground state of **1** generates interest in the triplet aromaticity and proposed the potential use as novel chromophores for singlet fission photovoltaics.[45]

(A) Dibenzo[*a,f*]pentalene **1**

a: R^1 = R^2 = H   **b**: R^1 = Mes, R^2 = Me

open-shell

(B) Dibenzo[*a,e*]pentalene **2** and diareno[*a,f*]pentalenes

2

well-known

3
a: R = H
b: R = Si^{i}Pr$_3$

unknown

4
a: R = H
b: R = Mes

closed-shell

5
a: R^1 = R^2 = H
b: R^1 = Mes, R^2 = Me

closed-shell

(C) ***This work***: Benzo[*a*]naphtho[2,3-*f*]pentalene **6**

a: R^1 = R^2 = R^3 = H
b: R^1 = Mes, R^2 = R^3 = Me
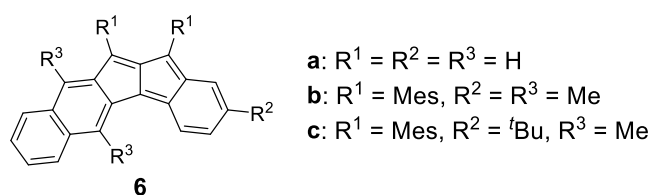**c**: R^1 = Mes, R^2 = ^{t}Bu, R^3 = Me

6

Figure 1. (A) Resonance structures of dibenzo[*a,f*]pentalene **1**. (B) Molecular structures of dibenzo[*a,e*]pentalene **2** and diarenopentalenes **3–5**. (C) Molecular structure of benzo[*a*]naphtho[2,3-*f*]pentalene **6**. Hexagons with 6π-benzenoid character are colored in gray. The main 4nπ-conjugations and trimethylenemethane (TMM)-subunit are colored in blue and red, respectively.

Using the dibenzo[*a,f*]pentalene framework, Yasuda group in recent years has focused on controlling both antiaromaticity and open-shell character through additional annulations of one or two benzene rings into the framework.[46,47] As a theoretical work by Baranac-Stojanović suggested,[48,49] the manner of the π-extension to the framework significantly impacts on the electronic properties in the resulting systems. Recent experimental efforts have been evidencing the effect of π-extensions on the electronic structures of **1** (Figure 1B). A synthetic attempt toward dinaphtho[1,2-*a*:2,1-*f*]pentalene **3** was reported by the Diederich's group, but the high reactivity of the derivative **3b** toward Diels-Alder additions hampered the isolation and characterization.[50] The authors successfully synthesized the derivatives of dinaphtho[2,1-*a*:1,2-*f*]pentalene **4**, and benzo[*a*]naphtho[1,2-*f*]pentalene **5** and characterized these molecules as closed-shell molecules in which the global paratropicity of **1** is mainly shifted to the localized 8π-pentalene core.[46]
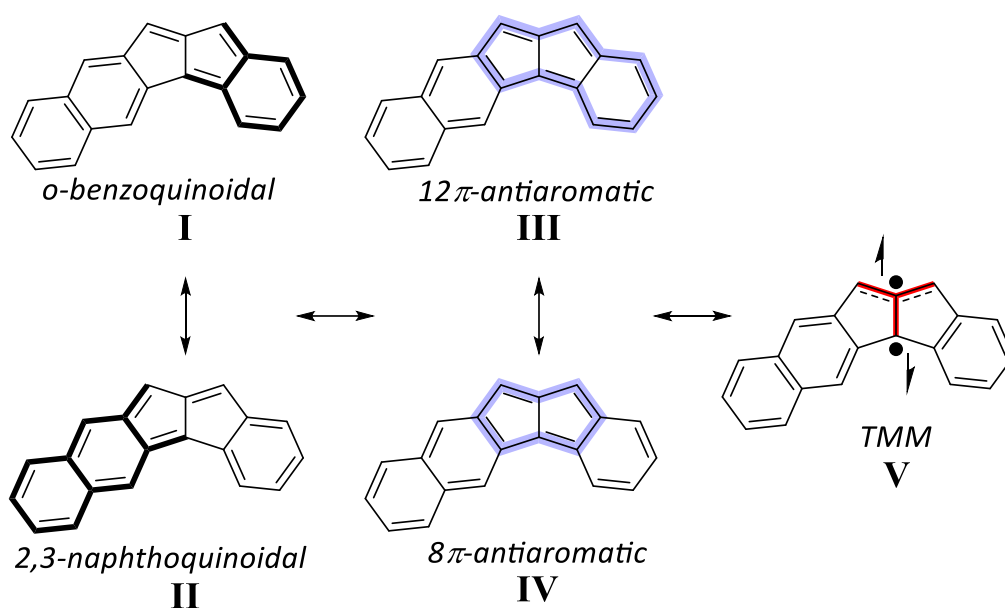
**Figure 2.** Selected resonance structures of **6a** in the singlet state.

Herein, the authors describe the synthesis and characterization of benzo[*a*]naphtho[2,3-*f*]pentalene **6**, a new member in diareno[*a,f*]pentalenes (Figure 1C). The inequivalent ring-annulation of **6** invokes the contributions of several resonance structures to the ground state. Selected representative resonance structures, quinoidal (**I/II**) 4*n*π-antiaromatic (**III/IV**) and TMM-based open-shell (**V**) structures, are depicted in Figure 2. Our experimental and theoretical investigations sufficiently describe the electronic structures of **6**. In contrast to its structural isomer **5** with singlet closed-shell ground state, the molecular **6** has an appreciable singlet open-shell character as well as a semi-global 12π-antiaromatic character. A ring fusion of a naphthalene ring at the 2,3-positions into the central pentalene illuminates a localized *o*-benzoquinoidal moiety that brings its open-shell and antiaromatic characters in the inequivalent ring-annulated network. The elucidation of behaviors between the open-shell and antiaromatic characters in our pentalenes empathizes the importance of the fashion of the quinoidal moiety and the formal molecular symmetry in governing the two characters.

1-2. Results and Discussion

Synthesis.

The syntheses of **6b** and **6c**, in which bulky mesityl groups were introduced to kinetically protect the head carbons on the pentagons, are summarized in Scheme 1. To standardize the substituent effect on the NMR signals with those of our previously reported molecules, a methyl group was introduced into the benzene ring of **6b**. A *tert*-butyl group of **6c** was introduced to improve the thermal stability in the solid state. The inequivalent ring-annulation of **6** was constructed by the consecutive introduction of naphthyl and phenyl

9

groups using palladium-catalyzed Suzuki-Miyaura cross-coupling reactions. Commercially available diethyl 2-oxomalonate was transformed into dibromoalkene **7** with CBr$_4$ and PPh$_3$.[51,52] Under the palladium-catalyzed Suzuki-Miyaura cross-coupling conditions,[52] coupling of **7** with 1,4-dimethyl-2-naphthalene boronic acid[53] furnished **8** in 60% yield. Subsequent coupling of **8** with phenylboronic acid derivatives under the same condition afforded diester **9**.[52] Reduction of ester groups of **9** with ^{i}Bu$_2$AlH afforded diol **10**, and subsequent oxidation gave dialdehyde **11**. Treatment of **11** with mesitylmagnesium bromide afforded diol **12**. Intramolecular cyclization of **12** was carried out under acidic conditions to afford dihydrogenated hydrocarbon **13** (Figure S1). The two methyl groups on the naphthyl moiety of **12** perfectly directed the cyclization at the 2,3-bond of the naphthalene ring. The oxidation of **13** was conducted through the dianion **6**$^{2-}$. The dianion **6**$^{2-}$ was cleanly generated by the treatment of **13** with nBuLi in THF at room temperature.[54] Without the isolation of **6**$^{2-}$, after confirming by NMR measurements, the subsequent two-electron oxidation of **6**$^{2-}$ with p-chloranil furnished **6** as a reddish-brown solid. Under ambient conditions, the obtained **6** was immediately decomposed to give the oxygen-adduct, as confirmed by mass spectroscopy.
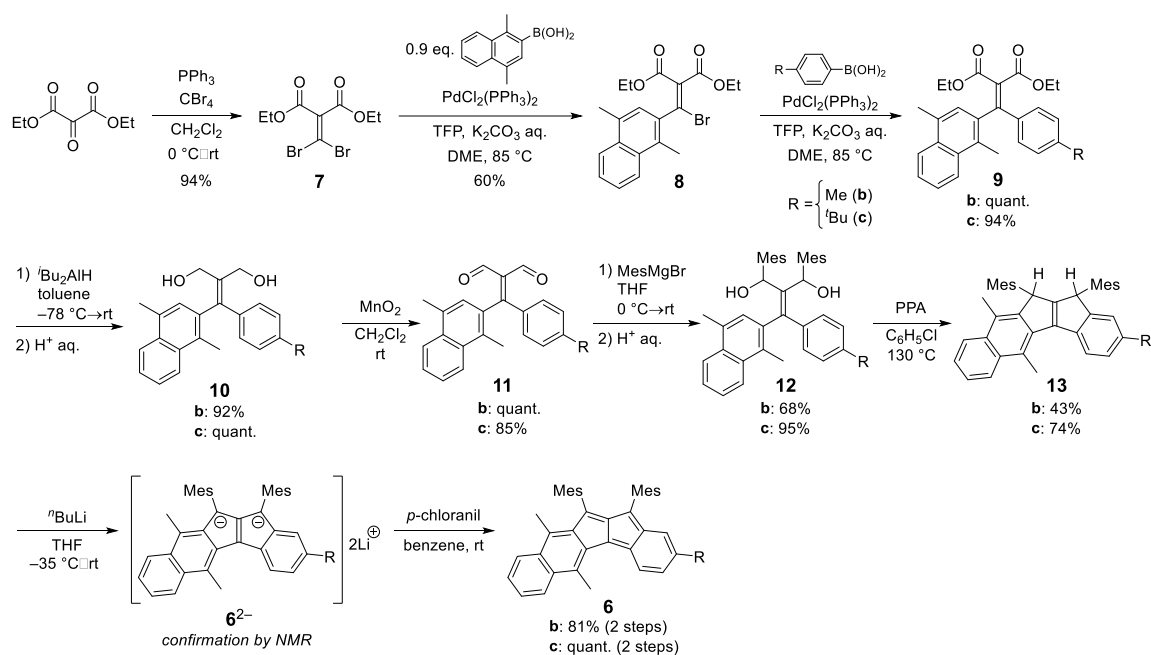

Scheme 1. Synthetic route for **6**.^{a}

X-ray Crystallographic Analysis and Bond Length Analysis.

The molecular geometry was confirmed by X-ray crystallographic analysis of **6c** (Figure 3 and S2). The high solubility of **6b/c** in common organic solvents hampered the recrystallization from the solution phases, but the molten solids of **6c** was cooled from around 200 °C to room temperature in the degassed sealed tube to finally give single crystals. Two crystallographically independent molecules of **6c** (hereafter, molecule A and B) were present in the asymmetric unit (Figure 3A). The largest difference between the two molecules

is the dihedral angles between two mesityl groups (12.1° for molecule A and 6.9° for molecule B). No other features distinguished the two molecules of **6c**; therefore, the mean values of the two structures are reported in the following discussion (Figure S3). The main core of **6c** is almost planar and the mesityl groups formed large dihedral angles (ca. 73°) with the main core. The observed bond lengths are summarized in Figure 3B. The outmost hexagon (ring *C*) in the naphthalene moiety exhibits small bond length alternation (BLA) (1.355(11)–1.420(10) Å, ave. 1.397 Å), suggesting the preservation of a local 6π-aromatic character. Contrarily, the large BLA was observed in the 5-5-6 ring (ring *A-A'-B'*) system in a direction toward the fused benzene ring, which is reminiscence of the structural contribution of a localized *o*-benzoquinoidal structure[55,56] (**6a-I**) rather than that of a naphthoquinoidal structure (**6a-II**). These observed geometric features of **6c** were supported by the harmonic oscillator model of the aromaticity (HOMA) values,[57,58] which index the degree of bond alternation[59] (Figure 3C, HOMA values for ring *A*: –0.25; ring *B*: 0.36; ring *C:* 0.85; ring *A'*: 0.10; ring *B'*: 0.30). Notably, the degree of BLA in the pentagons (1.377(9)–1.476(9) Å) lies between those of the open-shell **1b** (1.409(3)−1.458(3) Å)[40] and the closed-shell **5b** (1.362(6)−1.502(6) Å).[46] The observed molecular geometry was supported by the theoretically optimization (Figure S17) and agree with that predicted previously.[49] The calculated electrostatic potential map indicated that the contribution of the polarized structure induced by the inequivalent structure is negligible (Figure S18A).

The reactivity attributable to the *o*-quinoidal moiety was investigated. The authors heated a toluene-d_8 solution of **6c** with dienophiles (1,4-benzoquinone, fumaronitrile, and maleic anhydride) at 100 °C, but no consumption of **6c** was observed by NMR measurements (Figures S14–16). The bulky mesityl groups effectively suppresses the intermolecular reactions, such as dimerizations and cycloadditions, which are typical reactions of π-extended *o*-quinodimethanes.[21,24,50,60]

(A) Oretp drawings of **6c**

molecule A   molecule B
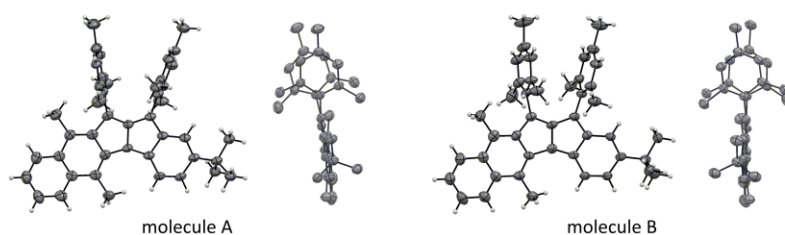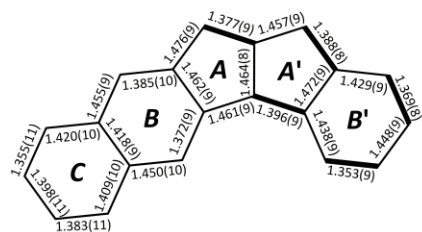
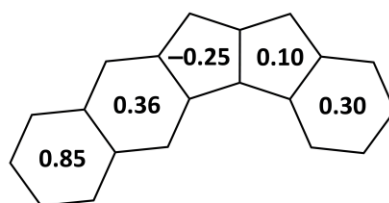(B) Averaged bond lenghts of **6c**   (C) HOMA values of **6c**

Figure 3. X-ray structures of two crystallographically independent molecules of **6c**. Thermal ellipsoids are drawn at the 50% probability level. (B) Averaged bond lengths (Å) of **6c** with the representations of each

ring. (C) HOMA values of **6c** calculated on the basis of the determined bond lengths by X-ray analysis.

Antiaromaticity on the Basis of ^{1}H NMR Spectroscopy, NICS(1), and GIMIC Calculations.

The ^{1}H NMR spectrum of **6b**, recorded at 20 °C in THF-d_8, showed line broadening. Cooling the sample was accompanied by progressive line sharpening and a well-resolved spectrum was obtained at −60 °C (Figure S5). Antiaromatic character was investigated by the comparison of the ^{1}H NMR spectra of **6b** and **6b**$^{2−}$. As the authors previously demonstrated, the upfield shift in the H^1 proton signals upon two-electron oxidation of the dianion to the corresponding neutral pentalene was a suitable indicator to assess the shielding effects of the pentalene moiety.[46] The corresponding upfield shift in the H^1 proton signals of **6b**$^{2−}$/**6b** ($\Delta\delta$(H^1)) was −1.87 ppm (Figure 4A), which was smaller than those of **1b**$^{2−}$/**1b** ($\Delta\delta$(H^1) = −2.47 ppm), **4b**$^{2−}$/**4b** ($\Delta\delta$(H^1) = −2.44 ppm), and **5b**$^{2−}$/**5b** ($\Delta\delta$(H^1) = −1.89 and −1.99 ppm).[46] The smallest upfield shift in the H^1 proton signal of **6** among the reported analogues illustrates the appearance of paratropic nature of **6** on the pentalene subunit is considerably suppressed. The NICS(1) values calculated at the GIAO-(U)B3LYP/6-311+G* level clearly supported the observed trends (Figure 4B); the smallest values were estimated in the pentagons of **6a** (+14.1 and +20.4) among the analogues (**1a**: +23.8, +27.2; **4a**: +29.5, +30.6; **5a**: +18.0, +20.4).[49] The localized o-quinoidal structure of **6** suppresses the appearance of paratropic character. The anisotropy of the induced current density (AICD) plots[61] reveal that the anticlockwise ring currents flow on the pentagons (rings A and A') and the adjacent hexagon (ring B') (Figures 4C and S20).

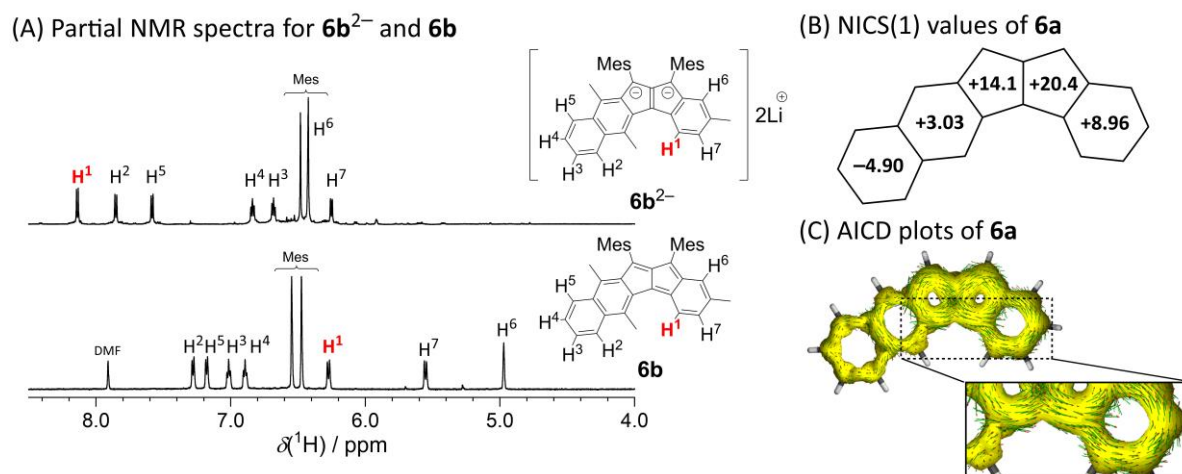**Figure 4.** (A) Partial ^{1}H NMR spectra (THF-d_8) of **6b** (−60 °C, 600 MHz) and **6b**$^{2−}$ (rt, 600 MHz). DMF was a residual solvent, which was used for washing the crude products. (B) NICS(1) values of **6a** calculated at the GIAO-UB3LYP/6-311+G*//RB3LYP-D3/6-311G* level. (C) AICD plots (isovalue surface: 0.035) of **6a** calculated at the CSGT-UB3LYP/6-311+G*//RB3LYP-D3/6-311G* level.

To get a deeper insight into the antiaromatic nature of **6**, the magnetically induced current densities of **6a^{2-}/6a** are calculated using the gauge-including magnetically induced current (GIMIC) method (Figure 5).[62–66] In the same way as **1a^{2-}**, **4a^{2-}**, and **5a^{2-}**,[46] the dianion **6a^{2-}** behaves as a global aromatic system with uniform diatropic (clockwise) ring currents of ca. +10 to +14 nA/T flowing along the peripheral pathway (Figure 5A). The ring current patterns of the neutral systems distinguish **6a** clearly from our previously systems **1a**, **4a**, and **5a** (Figures S21−22). In the fused naphthalene moiety of **6a**, whilst the inner hexagon (ring *B*) shows no significant ring current, the outmost hexagon (ring *C*) exhibits diatropic ring currents, retaining the local 6π-aromatic character (Figure 5B). The paratropic (anticlockwise) ring current of **6a** spreads toward the ring *A*-*A*'-*B*' system (−22.6 to −10.4 nA/T). The feature indicates that the antiaromatic nature of **6a** is induced by a semi-global 12π-antiaromatic system (**6a-III**), which is sharply contrast to a global 16π-system of **1**[40] and local 8π-systems of **4** and **5**.[46] The paratropic ring current strengths on the pentalene core of **6a** (−22.6 to −16.5 nA/T) are smallest among our reported systems (**1a**, **4a** and **5a**, Figures S21−22), supporting the weakened antiaromatic character of **6** in the agreement of the NICS(1) calculations. Notably, the difference in the main 4*n*π-systems between **5** and **6** depends on the direction of a naphtho-annulation into the pentalene core despite preserving the aromatic character in the outermost hexagons of the annulated naphthalene in the both molecules. Whilst the 2,1-naphtho-annulation in **5** isolates an 8π-pentalene subunit from the global π-conjugation,[46] the 2,3-naphtho-annulation in **6** shifts the main 4*n*π-conjugation into a 12π-benzopentalene subunit (**6a-III**) rather than the 8π-pentalene core (**6a-IV**). The experimentally determined or theoretically optimized molecular geometry of **6** suggests that a main canonical structure of **6** in the ground state should be described as a combination of *o*-benzoquinoidal and napththalene subunits (**6a-I**) with no 4*n*π-conjugated network. However, under magnetic field perturbations, the 12π-benzopentalene subunit (**6a-III**) would be reluctantly adopted as a main 4*n*π-conjugated network of **6** by the presence of the localized *o*-quinoidal structure.
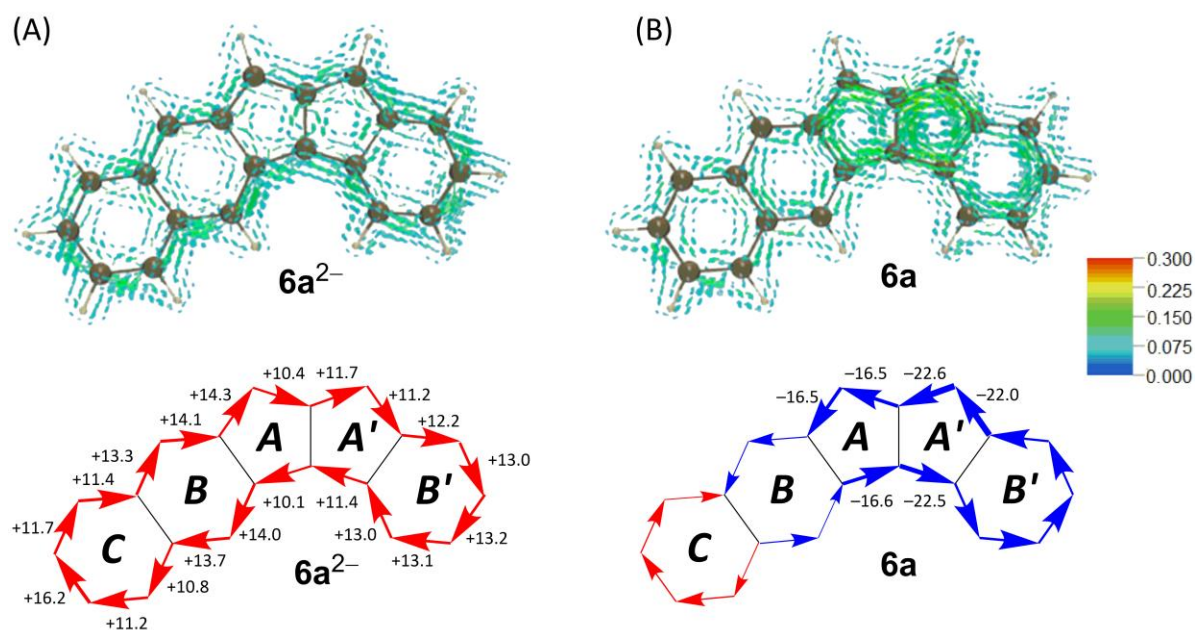
Figure 5. (Top) Magnetically-induced current (MIC) density and (Bottom) Current strength (nA/T) for the peripheral C−C bonds of for (A) **6a**$^{2-}$ and (B) **6a** calculated at the GIAO-(R/U)B3LYP/6-311+G* level. Current strength is evaluated by integrating numerically the MIC densities on the bisection plane of each bond. Diatropic currents rotate clockwise, while the paratropic ones do anticlockwise. The values in the color bar are given in a.u.

Open-shell Character Induced by a Localized *o*-Benzoquinoidal Moiety.

The line-broadening of NMR signals of **6b** at room temperature is a common feature for singlet open-shell molecules, indicating **6** has a singlet open-shell ground state (Figure S5). The line-sharpening in the NMR spectrum of **6b** was accomplished at −60 °C, which was much higher temperature than that of **1b**. For **1b**, the line sharpening was insufficient even at −100 °C.[40] Notably, the difference in the line-sharpening behaviors implies that the population of thermally excited triplet species of **6** is less than that of **1** at recorded temperatures.[49] Thermally excited triplet species of **6** was clearly observed in the ESR measurements. Solid samples of **6c** displayed signals typical of triplet species at 420 K with zero field splitting parameters ($|D|$ = 0.0398 cm^{-1} and $|E|$ = 0.0039 cm^{-1}) (Figures 6 and S7). The relatively large D value of **6** strongly suggests the occurrence of a TMM-based spin structure in the triplet state (**6a-V** in Figure 2B and Figure S18C), which is a shared feature with that previously demonstrated in **1**.[40] The smaller zero field splitting parameters of **6c** than those of **1b** ($|D|$ = 0.0561 cm^{-1} and $|E|$ = 0.0052 cm^{-1})[40] agree with the larger π-conjugation of **6** than that of **1**. ESR signal intensities of **6c** decreased with temperature decreased, indicating occurrence of a singlet ground state in **6** (Figure 6A). The Bleaney−Bowers fit[67] to the intensity change in the forbidden $\Delta M = \pm 2$ half-field signal of **6c** as a function of temperature gave a singlet−triplet energy gap (ΔE_{S-T}) of −2980 K (−5.91 kcal/mol) (Figure 6B). The expanded ΔE_{S-T} value of **6c** than that of **1b** (−4.29 kcal/mol) is supported

14

by the observed larger BLA of the pentalene core for **6c** than that of **1b**. The smaller diradical index (y_0) for **6a** ($y_0 = 0.185$) than that of **1a** ($y_0 = 0.228$) calculated at the LC-UBLYP ($\mu = 0.33$ bohr^{-1})/6-311G* level also supports the idea. For **6b**, the disappearance of the triplet signals was observed at around 420 K, failing to determine the ΔE_{S-T} value of **6b** (Figure S10). The mass spectroscopy of the annealed sample of **6b** indicated the decomposition via abstractions of hydrogen atoms.
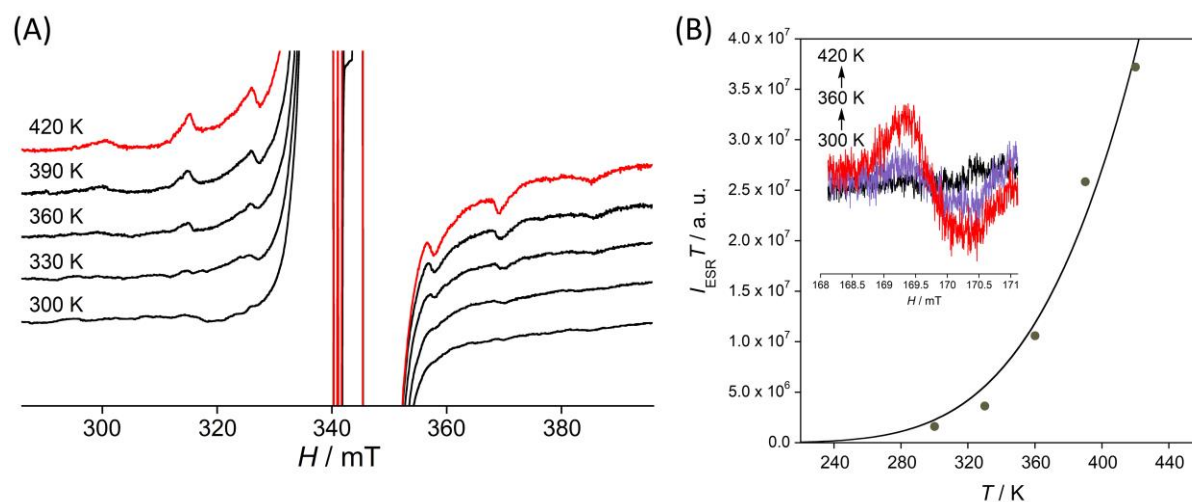

Figure 6. (A) ESR spectra of the solid sample of **6c**. (B) The change in ESR signal intensity with temperature (●) based on the half-field ESR signals (inset) and the Bleaney–Bowers fit (—).

Optoelectronic Properties.

   The optoelectronic properties of **6b** were investigated using electronic absorption spectroscopy and cyclic voltammetry. The electronic absorption spectrum of **6b** in CH$_2$Cl$_2$ gave a weak and broad longest absorption band that ranges from 700–1500 nm (Figure 7). The weak and broad longest absorption of **6b** is a shared feature with those of **1b**, **4b**, and **5b** and is typical characteristics of pentalene-based molecules (Figure S12). Time-dependent (TD)-DFT calculation at the B3LYP/6-311+G* level indicated that the absorption band is ascribed to the forbidden HOMO–LUMO transition (Tables S8–9). The cyclic voltammogram of **6b** displayed two reversible and two irreversible redox waves ($E_2^{ox, pa} = +0.67$ V, $E_1^{ox} = -0.018$ V, $E_1^{red} = -1.45$ V, and $E_2^{red, pc} = -2.23$ V vs Fc/Fc$^+$, Figure S13 and Table S5). The difference between the first oxidation and reduction potentials was used to determine the electrochemical HOMO−LUMO gap of 1.43 eV for **6b**, which ranks between those the open-shell **1b** (1.34 eV) and the closed-shell **5b** (1.68 eV).
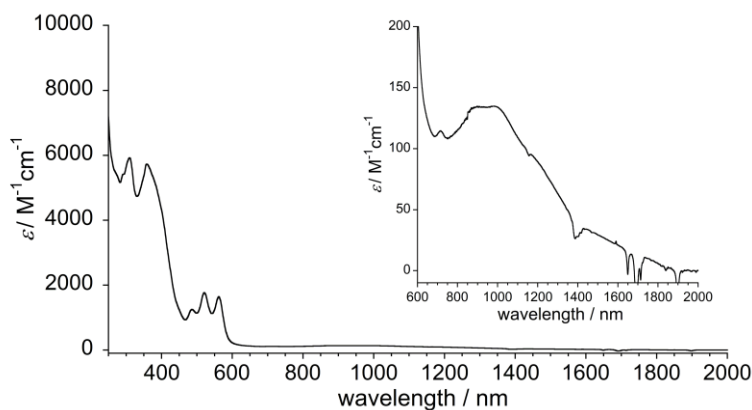
15

Figure 7. UV/vis/NIR absorption spectra of **6b** in CH_2Cl_2. The inset shows a magnified view.

Interrelation between Open-shell and Antiaromatic Characters in a Series of Diareno[*a*,*f*]pentalenes.

The elucidations of the molecular geometry and electronic structures of **6** unveil the interrelation between open-shell and antiaromatic characters in a series of our diareno[*a*,*f*]pentalenes. The authors found the regularities of the behaviors of open-shell features (y_0) against antiaromatic features (the difference of the proton chemical signal ($\Delta\delta(H^1)$) or NICS(1)) in our diareno[*a*,*f*]pentalenes **1**, **4**, **5**, and **6** (Figure S25). The plots of y_0 against $\Delta\delta(H^1)$ and of y_0 against NICS(1) are represented in Figure 8. Herein, larger y_0 ($0 < y_0 < 1$) indicates more enhanced open-shell character and more negative $\Delta\delta(H^1)$ or positive NICS(1) value indicates more larger antiaromatic character. Figure 8 clearly explains the importance in the fashion of quinoidal unit and the formal molecular symmetry in determining the interrelation between open-shell and antiaromatic characters.

The antiaromatic characters in four pentalenes considerably depend on the formal molecular symmetry (● vs ◆; see the horizontal axis direction in Figure 8). The C_{2v} symmetric pentalenes **1** and **4** show more negative $\Delta\delta(H^1)$ values, indicating their larger antiaromatic characters (Figure 8A). Their resonance structures aid in the understanding the importance of their higher symmetric structures in the antiaromaticity (Figure 9). For the two pentalenes, the resonance or interconversion between the two equivalent quinoidal (*o*-benzoquinoid for **1** and 1,2-naphthoquinoid for **4**) structures in the closed-shell resonance structures, which relieved the frustrations of the quinoidal instability derived from the loss of an aromatic ring, encourages the formal $4n\pi$-electron delocalization, resulting in their enhanced antiaromatic characters (16π-system: **1a**-**A**/**A'**; 8π-system: **4a**-**A**/**A'**). On the other hand, the C_s symmetric pentalenes **5** and **6** exhibit the weakened antiaromatic characters. Their lower symmetric structures enable the appearance of the local aromatic character on the outmost hexagons. The sufficient preservation of the local aromatic character causes the suppression of the $4n\pi$-electron delocalization and localizes the inequivalent quinoidal unit (**5a**-**A**/**B** and **6a**-**A**/**B**).
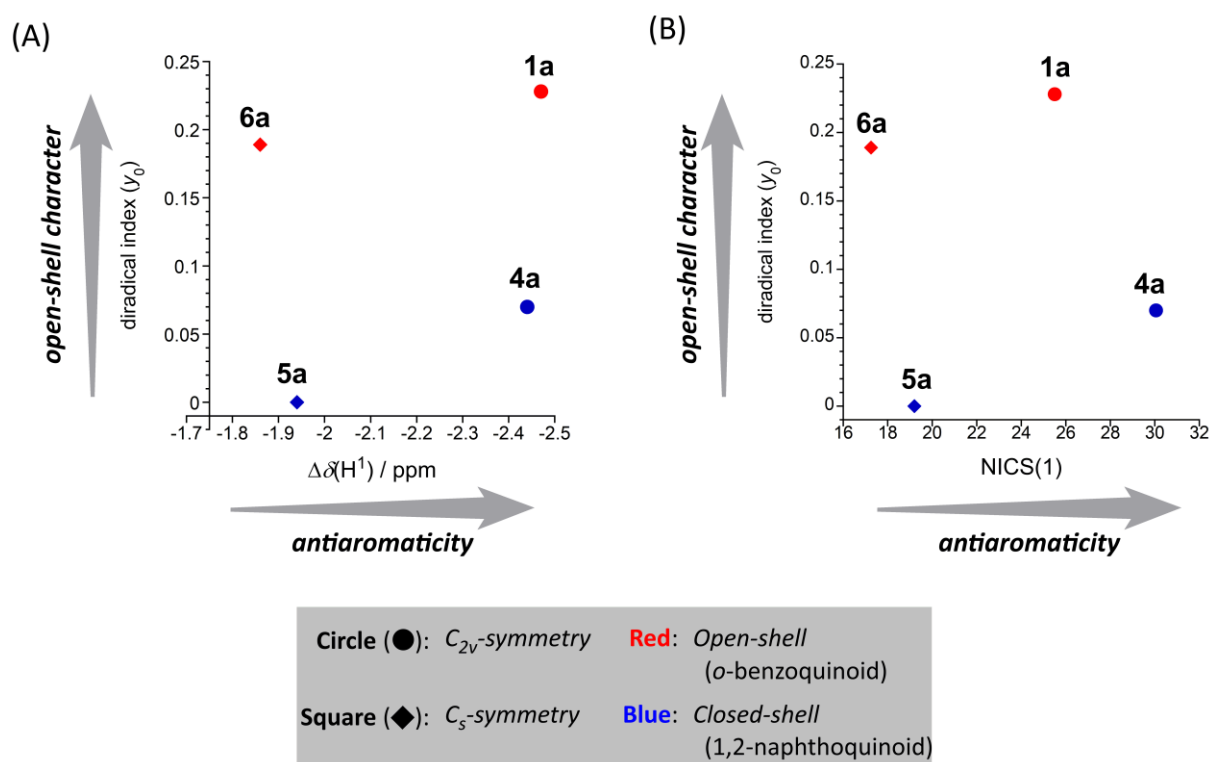
Figure 8. Plots of the behaviors of (A) y_0 against $\Delta\delta(H^1)$ and (B) y_0 against NICS(1) for our pentalenes **1** and **4–6**. The diradical index (y_0) was calculated at the LC-UBLYP (μ = 0.33 bohr^{-1})/6-311G* level. The difference in the proton chemical shift ($\Delta\delta(H^1)$) was based on the ^{1}H NMR measurements for the dianion/neutral pentalenes. The NICS(1) values of calculated at the GIAO-(U)B3LYP/6-311+G* level. The averaged NICS(1) values of two pentagons were plotted.

The difference in the paratropic character between **6** and **5** might be associated with the difference in the main $4n\pi$-conjugated circuit: the 12π-system of **6** shows the less antiaromatic character than the 8π-system of **5**. Interestingly, the paratropic behavior for the symmetry of the ring fusions evokes the similarity to Nakagawa's studies. Through the detailed NMR studies on benzenoid-annulated $[4n+2]\pi$-dehydroannulenes, Nakagawa found that diatropic characters were enhanced in the annulenes with equivalent quinoidal structures.[68] Notably, our finding expands Nakagawa's concept of annulated aromatic systems toward that of annulated antiaromatic systems.[69] $4n\pi$-Conjugated systems generally disfavor the π-electron delocalization due to their antiaromatic instability,[70] but the controlled incorporation of quinoidal units into a pentalene core realizes the tunable $4n\pi$-electron delocalization in our system.
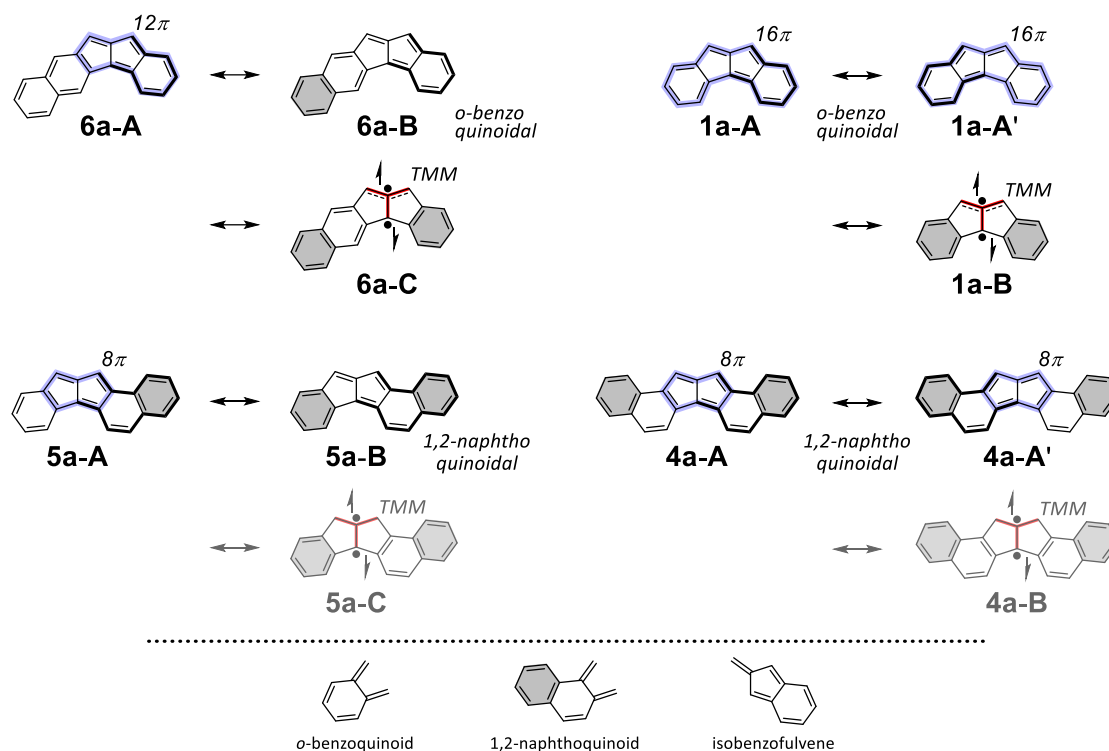
Figure 9. Resonance structures of **1** and **4–6** and the structures of key subunits. The hexagonal rings in gray denote benzenoid rings. The main $4n\pi$-conjugated circuits, quinoidal subunits and TMM-subunits are highlighted in blue, black, and red bold lines, respectively.

Contrarily, the appearance of the open-shell characters in four pentalenes depends on the presence or absence of an *o*-benzoquinoidal moiety rather than the molecular symmetry (red vs blue; see the vertical axis direction in Figure 8). A good example is the comparison between **5** and **6** because the both molecules assume C_s symmetries with the suppressed antiaromatic characters. Whilst the closed-shell pentalene **5** possesses an incorporated 1,2-naphthoquinoidal unit (**5a-B**), the open-shell pentalene **6** has a large contribution of an *o*-benzoquinoidal unit (**6a-B**). The same trend can be seen in the comparison between **1** and **4**. A 1,2-naphthoquinoidal unit has an already-existing aromatic hexagon (see the structure of 1,2-naphthoquinoid in Figure 9), which would tend to show no open-shell character (negligible contributions of **4a-B** and **5a-C**). A reason for the closed-shell electron configurations of **4** and **5** is that the number of the aromatic hexagon does not change when the closed-shell structure is transformed into an open-shell structure (see the number of the gray colored hexagons; **4a-A/A'**→**4a-B** and **5a-B**→**5a-C**). On the other hand, an additional aromatic hexagon is gained from an *o*-benzoquinoidal unit in the open-shell structures of **1** and **6** (**1a-B** and **6a-C**). For **1** and **6**, it should be noted that incorporating an *o*-benzoquinoidal unit into a pentalene core (to create an isobenzofulvene core) is more essential to exhibit their open-shell characters. According to a recent theoretical study,[71] isobenzofulvene itself has no singlet open-shell character and ring expansions of the

isobenzofulvene core are imperative for the emergence of open-shell characters. In our pentalene systems, however, the embedment of the isobenzofulvene unit into a planar pentalene skeleton facilitates access to the singlet open-shell ground state. Herein, two cooperative effects realize the small ΔE_{S-T} values of **1** and **6**. The singlet ground states (**1a**-**A/A'** and **6a**-**A**) are energetically destabilized by the induced antiaromatic natures. Concurrently, the triplet excited states are stabilized by non-disjoint TMM subunits appearing in the open-shell structures (**1a**-**B** and **6a**-**C**) on the isobenzofulvene framework. The structural harmony between a pentalene core and an *o*-benzoquinoidal moiety accomplishes of occurrences of appreciable open-shell characters for the pentalene systems.

The $\Delta\delta(H^1)$ values on the horizontal axis in Figure 8A are replaceable with the average NICS(1) values on the pentagons. The behaviors of y_0 against NICS(1) values are nearly identical to those of y_0 against $\Delta\delta(H^1)$ (Figure 8B). The antiaromatic character of **4** estimated by the NICS calculation is slightly pronounced compared to that based on the NMR measurements, which would be caused by the estimated difference in the diatropic effects of the adjacent hexagons. The applicability of the combination of the theoretical parameters (y_0 and NICS(1)) to evaluate the interplay of open-shell and antiaromatic characters promises the rational design guide for novel open-shell $4n\pi$-polycyclic molecules. Our findings shed light on the basal factors that governs the π-bond natures in the $4n\pi$-carbocycles. Two simple structural features, the fashion of *o*-quinoidal unit and the formal molecule symmetry, are important principles. The fashion of the quinoidal unit determines the electron configurations that vary from closed-shell to open-shell states. Concurrently, the formal molecule symmetry is crucial for the degree of π-electron delocalization, which is directly transcribed into the strength of the antiaromatic character. It should be noted that our diareno[*a,f*]pentalene framework harmonizes the two features, enabling us to logically access the interplay of open-shell and antiaromatic characters in polycyclic $4n\pi$-systems as a molecular design strategy.

1-3. Conclusion

The authors successfully synthesized and characterized **6**, a new member of diareno[*a,f*]pentalene family and a structural isomer of **5**. A 2,3-naphthoannulation in **6** localizes an *o*-benzoquinoidal moiety that triggers the appearance of the appreciable open-shell and antiaromatic characters. Through our experimental and theoretical investigations of **6**, the authors unveil the interrelation between open-shell and antiaromatic characters in a series of diareno[*a,f*]pentalenes. The fashion of the incorporated quinoidal moiety is deeply involved in showing open-shell character and the formal molecular symmetry introduced by the ring fusions manages the $4n\pi$-antiaromatic character. Notably, the inherent harmonization of the open-shell character with $4n\pi$-antiaromaticiy within **1**, pristine diareno[*a,f*]pentalene framework, enables the systematic assessment of the interrelation between open-shell and antiaromatic characters. The comparison among the four diareno[*a,f*]pentalenes derives the two simple principles, the fashion of an *o*-quinoidal moiety and the formal molecular symmetry, as main factors in determining the balance between open-shell and antiaromatic

19

characters. The conclusion could be easily broadened to other open-shell $4n\pi$-conjugated systems. The present study emphasizes the importance of topologically design for open-shell $4n\pi$ hydrocarbons and shows the tunability of the interrelation between open-shell and antiaromatic characters.

1-4. Experimental Section
General Information

NMR spectra were recorded on JEOL-AL400, JEOL-ECS400 (400 MHz for ^{1}H, and 100 MHz for ^{13}C) and Bruker AVANCE III spectrometers (600 MHz for ^{1}H, and 150 MHz for ^{13}C) with TMS as an internal standard. ^{1}H and ^{13}C NMR signals of compounds were assigned using HMQC, HSQC, HMBC, COSY, NOESY, and ^{13}C off-resonance techniques. ESR spectra were recorded on a Bruker EMXmicro spectrometer. Positive FAB and EI mass spectra were recorded on a JEOL JMS-700 and a Shimadzu GCMS-QP2010 Ultra, respectively. IR spectra were recorded as thin films or as solids in KBr pellets on a JASCO FT/IR 6200 spectrophotometer. UV-vis-NIR spectra were recorded on a JASCO V-670 spectrophotometer. Cyclic voltammetric measurements were performed with an ALS-600C electrochemical analyzer using a glassy carbon working electrode, a Pt counter electrode, and an Ag/AgNO$_3$ reference electrode at room temperature in CH$_2$Cl$_2$ containing 0.1 M Bu$_4$NClO$_4$ as the supporting electrolyte. Data collection for X-ray crystal analysis was performed on Rigaku/XtaLAB Synergy-S/Cu (CuK$_\alpha$ λ = 1.54187 Å) diffractometers. All non-hydrogen atoms were refined with anisotropic displacement parameters and hydrogen atoms were placed at calculated positions and refined "riding" on their corresponding carbon atoms by Olex2[72] program.

Materials

Anhydrous dichloromethane, THF, acetonitrile, diethylether, toluene and hexane were purchased and used as obtained. All reagents were obtained from commercial suppliers and used as received except for p-chloranil. p-Chloranil was recrystallized from hot toluene before use. All reactions were carried out under nitrogen. Syntheses of dianions $6\mathbf{b}^{2-}$/$\mathbf{c}^{2-}$ and pentalenes $6\mathbf{b}$/$\mathbf{c}$ were performed in a nitrogen-filled glove b

Computational Method

All calculations were conducted using the Gaussian 09 program[73]. The geometries of neutral and dianionic singlet species of $6\mathbf{a}$ and $6\mathbf{c}^{2-}$ were optimized with the RB3LYP-D3 functional and 6-311G* basis set. In previous studies, local minimum structures of fused-ring hydrocarbons exhibiting small-medium diradical characters were shown to be predicted well by using the spin-restricted RB3LYP-D3 functional.[40] The obtained RB3LYP-D3 geometry of neutral $6\mathbf{a}$ was employed for the calculations of the other properties. We also performed geometry optimization of triplet species by using the broken-symmetry approach with the UB3LYP-D3 functional. In each case, frequency analysis calculations were performed in order to confirm the local minimum structures.

During the calculations of $6\mathbf{b}$ and $6\mathbf{c}$, bulky -Mes groups were replaced by -Ph groups in order to reduce the computational efforts (referring to the model molecules as $6\mathbf{b'}$ and $6\mathbf{c'}$). For $6\mathbf{c'}$, we found two types of conformers during the geometry optimizations where the rotation angle of tBu group is different. From the comparison of total energy at the SF-TDDFT PBE50/6-311G* level with ZPVE correction at the R- or UB3LYP-D3/6-311G* level, conformation 2 (see Figure S23) is predicted to be ~1.7 kcal/mol more stable than conformation 1 in the singlet state. In the triplet state, conformation 1 is more stable, but the difference of their ZPVE corrected total energy was smaller than 0.2 kcal/mol. We should note that such a conformational change does not affect the BLA features of the main part of the compounds. Because of the steric repulsion between the substituent groups and H atoms, the systems with substituents tend to have slightly non-planar structures. Dihedral angle $D(a\text{-}b\text{-}c\text{-}d)$ and $D(b\text{-}c\text{-}d\text{-}e)$ for conformation 1/2 in the singlet state are found to be 16.2°/16.3° and 1.0°/0.9°, respectively.

NICS(1) values of neutral and dianionic species of $6\mathbf{a}$ and $6\mathbf{c}^{2-}$ were calculated at the GIAO-R(U)B3LYP/6-311+G* method

using these optimized structures. For neutral **6a**, NICS(1) values were calculated at the GIAO-UB3LYP/6-311+G* method, since the RDFT approach is considered to give very different feature of magnetic response properties of open-shell singlet systems compared with the broken-symmetry UDFT results.[25,26] We also employed gauge-including magnetically induced current (GIMIC) method[62,63,65,74] to evaluate magnetically induced current (MIC) density, which is a current-based criterion for aromaticity. The unperturbed and magnetically-perturbed electron densities necessary for GIMIC calculations were evaluated at the same level of approximation as those for NICS(1) calculations. The external magnetic field was applied to the direction perpendicular to the molecular plane. The MIC densities was evaluated by using GIMIC version 2.1.4 and Gaussian2gimic.py programs.[62,63,65,74] DrawMol application was used for the visualizations of molecular modelling and spatial distributions of MOs and MIC density.[75] Aromatic natures for each ring evaluated by NICS and GIMIC are in good agreement with each other.

AICD plot of **6a** was calculated by using the method developed by Herges[61] and only π-electrons are considered at the CSGT-UB3LYP/6-311+G*//RB3LYP-D3/6-311G* level. The magnetic field is perpendicular to the molecular plane of **6a**. Yellow surface is the isosurface of the induced current density under the magnetic field. Green allows with red head indicate the induced current density vectors. The clockwise and counterclockwise density vectors indicate diamagnetic and paramagnetic ring currents, respectively.

Diradical character (y_0) were obtained from the occupation number of LUNO ($y = n_L$) at the LC-UBLYP ($\mu = 0.33$ bohr^{-1})/6-311G* level. Adiabatic ΔE_{ST} values were calculated by the spin-flip noncolinear time-dependent density functional theory (SF-NC-TDDFT) method with the PBE50 exchange-correlation functional and 6-311G* basis set (denoted as SF-TDDFT PBE50/6-311G*)[76–79] In the ΔE_{ST} calculations, total energies of the singlet and triplet states, E_S and E_T, were evaluated at the SF-TDDFT PBE50/6-311G* level using the optimized geometries. We have also estimated the zero-point vibrational energy (ZPVE) corrections to the ΔE_{ST} values on the basis of the frequency analysis calculations at the R(U)B3LYP-D3/6-311G* level. SF-NC-TDDFT calculations were performed using Q-Chem 5 program package,[80] while the others were done using Gaussian 09 program package. In the adiabatic S–T energy gaps, we have added zero-point vibrational energy (ZPVE) corrections which were estimated from the frequency analysis calculations at the R- and UB3LYP-D3/6-311G* levels.

Symmetry-adapted molecular orbitals of **6a** were evaluated at the RB3LYP/6-311+G* level. Electronic excitation properties of **6a** were evaluated by the TDDFT method R(U)B3LYP and 6-311+G* basis set.

Synthesis and Characterization

Diethyl 2-(dibromomethylene)malonate 7
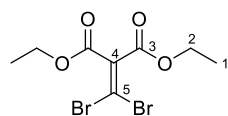
Under nitrogen atmosphere, CBr$_4$ (6.80 g, 20.5 mmol) was added to a solution of PPh$_3$ (10.6 g, 40.4 mmol) in CH$_2$Cl$_2$ (20 mL) at 0 °C. After 1 h at 0 °C, diethyl 2-oxomalonate (1.55 ml, 9.96 mmol) was added. The mixture was warmed to room temperature and stirred for 19 h, then added to pentane (35 mL), stirred for 30 min, filtered and concentrated. The crude residue was purified by flash chromatography (hexane/ethyl acetate = 75:25), yielding the product (pale yellow oil, 3.16 g, 94 %).

bp 171.0 °C /6.9 Torr; IR (neat) 2984 (s), 1735 (s), 1653 (w), 1586 (s), 1559 (m), 1465 (m), 1446 (m), 1391 (m), 1368 (s), 1218 (s), 1173 (m), 1115 (w), 1081 (s), 1021 (s), 912 (w), 869 (s), 806 (w), 778 (w), 764 (w), 724 (s), 612 (w), 567 (m) cm^{-1}; ^{1}H NMR (400 MHz, CDCl$_3$) 4.31 (q, $J = 7.2$ Hz, 4H, 2-H), 1.33 (t, $J = 7.2$ Hz, 6H, 1-H); ^{13}C NMR (100 MHz, CDCl$_3$) 162.6 (s, C-3), 134.3 (s), 107.5 (s), 62.8 (t, C-2), 14.3 (q, C-1); MS (EI$^+$, 70eV) m/z 332 ([M+4]$^+$, 9), 330 ([M+2]$^+$, 17), 328 (M$^+$, 9), 285 (100, –OEt), 257 (59); HRMS (EI$^+$, 70 eV) Calculated: (C$_8$H$_{10}$Br$_2$O$_4$) 327.8946 (M$^+$), Found: 327.8944; Analysis C$_8$H$_{10}$Br$_2$O$_4$ (329.97) Calculated: C, 29.12; H, 3.05; Br, 48.43; O, 19.39, Found: C, 29.81; H, 3.31.

Diethyl 2-(bromo(1,4-dimethylnaphthalen-2-yl)methylene)malonate 8
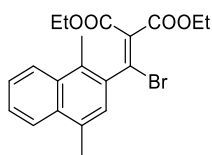
Under nitrogen atmosphere, PdCl$_2$(PPh$_3$)$_2$ (0.299 g, 0.426 mmol) was added to a solution of **7** (2.81 g, 8.52 mmol), (1,4-dimethylnaphthalen-2-yl)boronic acid[53] (1.490 g, 7.45 mmol) and tri(2-furyl)phosphine (0.306 g, 1.318 mmol) in DME (10 mL) and aqueous 2 M K$_2$CO$_3$ (10 mL) at room temperature. The mixture was heated to 85 °C for 24 h. After cooled to room temperature, aqueous 1 M HCl was added to the mixture. The products were extracted with CHCl$_3$ three times. The combined organic layers were washed with water and brine, and then were dried over MgSO$_4$. After filtration, the obtained solutions were evaporated in vacuum. The obtained residue was purified by a silica-gel column chromatography (hexane/ethyl acetate = 90:10), to give **8** as pale yellow oil (1.80 g, 60 %).

IR (neat) 3454 (w), 3071 (w), 2982 (s), 1736 (s), 1709 (s), 1629 (m), 1511 (w), 1445 (m), 1388 (m), 1367 (m), 1296 (s), 1236 (s), 1204 (s), 1071 (s), 1021 (m), 901 (m), 869 (m) cm^{-1}; ^{1}H NMR (400 MHz, CDCl$_3$) 8.08–8.06 (m, 1H), 8.00–7.98 (m, 1H), 7.57–7.54 (m, 2H), 7.14 (s, 1H), 4.42 (q, J = 7.0 Hz, 2H), 3.93 (q, J = 7.0 Hz, 2H), 2.66 (s, 3H), 2.62 (s, 3H), 1.41 (t, J = 7.0 Hz, 3H), 0.860 (t, J = 7.0 Hz, 3H); ^{13}C NMR: (100 MHz, CDCl$_3$) 164.2, 161.5, 139.6, 134.9, 132.8, 132.6, 132.4, 131.5, 129.3, 126.4, 126.1, 125.2, 124.8, 124.6, 62.1, 61.5, 19.3, 15.6, 14.0, 13.5; MS (EI$^+$, 70eV) m/z 406 ([M+2]$^+$, 30), 404 (M$^+$, 28), 251 (100), 207 (84), 165 (46); HRMS (EI$^+$, 70 eV) Calculated: (C$_{20}$H$_{21}$BrO$_4$) 404.0623 (M$^+$), Found: 404.0619.

Diethyl 2-((1,4-dimethylnaphthalen-2-yl)(*p*-tolyl)methylene)malonate 9b
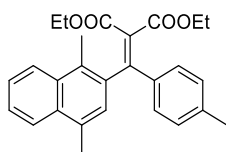
Under nitrogen atmosphere, PdCl$_2$(PPh$_3$)$_2$ (0.186 g, 0.265 mmol) was added to a solution of **8** (2.118 g, 5.23 mmol), *p*-tolylboronic acid (0.928 g, 6.82 mmol) and tri(2-furyl)phosphine (0.206 g, 0.856 mmol) in DME (20 mL) and aqueous 2 M K$_2$CO$_3$ (10 mL) at room temperature. The mixture was heated to 85 °C for 20 h. After cooled to room temperature, aqueous 1 M HCl was added to the mixture. The products were extracted with CHCl$_3$ three times. The combined organic layers were washed with water and brine, and then were dried over MgSO$_4$. After filtration, the obtained solutions were evaporated in vacuum. The obtained residue was purified by a silica-gel column chromatography (hexane/ethyl acetate = 90:10), to give **9b** as a colorless solid (2.64 g, quant.).

mp 82.3−83.1 °C; IR (KBr) 3065 (w), 2981 (w), 1732 (s), 1718 (s), 1605 (m), 1450 (w), 1389 (w), 1365 (w), 1344 (w), 1300 (m), 1269 (m), 1225 (s), 1196 (s), 1182 (s), 1117 (w), 1092 (s), 1070 (s), 1018 (w), 884 (w), 825 (w) cm^{-1}; ^{1}H NMR (400 MHz, CDCl$_3$) 8.05–8.03 (m, 1H), 8.00–7.97 (m, 1H), 7.54–7.52 (m, 2H), 7.13 (d, J = 8.4 Hz, 2H), 7.08 (d, J = 8.4 Hz, 2H), 7.06 (s, 1H), 4.18 (q, J = 7.2 Hz, 2H), 3.92 (q, J = 7.2 Hz, 2H), 2.62 (s, 3H), 2.53 (s, 3H), 2.32 (s, 3H), 1.14 (t, J = 7.2Hz, 3H), 0.79 (t, J = 7.2 Hz, 3H); ^{13}C NMR (100 MHz, CDCl$_3$) 166.7, 165.2, 156.2, 149.8, 139.6, 136.6, 132.9, 132.5, 132.1, 129.5, 129.1, 128.8, 127.2, 127.1, 125.9, 125.8, 125.1, 124.8, 61.5, 61.1, 21.5, 19.4, 16.0, 13.9, 13.6; MS (EI$^+$, 70eV) m/z 416 (M$^+$, 18), 342 (100), 270 (25), 256 (42), 239 (15); HRMS (EI$^+$, 70 eV) Calculated: (C$_{27}$H$_{28}$O$_4$) 416.1988 (M$^+$), Found: 416.1981.

Diethyl 2-((4-(*tert*-butyl)phenyl)(1,4-dimethylnaphthalen-2-yl)methylene)malonate 9c
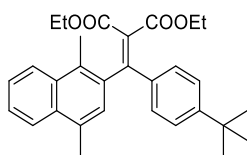
Under nitrogen atmosphere, PdCl$_2$(PPh$_3$)$_2$ (0.159 g, 0.226 mmol) was added to a solution of **8** (1.831 g, 4.52 mmol), (4-(*tert*-butyl)phenyl)boronic acid[81] (1.046 g, 5.88 mmol) and tri(2-furyl)phosphine (0.315 g, 1.356 mmol) in DME (10 mL) and aqueous 2 M K$_2$CO$_3$ (5 mL) at room temperature. The mixture was heated to 85 °C for 25 h. After cooled to room temperature, aqueous 1 M HCl was added to the mixture. The products were extracted with CHCl$_3$ three times. The combined organic layers were washed with water and brine, and then were dried over MgSO$_4$. After filtration, the obtained solutions were evaporated in vacuum. The obtained residue was purified by a silica-gel column chromatography (hexane/ethyl acetate = 90:10), to give **9c** as a colorless solid (1.95 g, 94 %).

mp 112.1–113.0 °C, IR (KBr) 3397 (w), 3069 (m), 3032 (w), 2963 (s), 2904 (s), 2867 (s), 1732 (s), 1702 (s), 1604 (s), 1509 (m), 1469 (s), 1448 (s), 1369 (s), 1344 (m), 1318 (s), 1307 (s), 1271 (s), 1245 (s), 1191 (m), 1092 (s), 1069 (s), 1016 (m), 1005 (m), 922 (w), 885 (m), 869 (m), 845 (s) cm^{-1}; ^{1}H NMR (400 MHz, CDCl$_3$) 8.06–8.03 (m, 1H), 8.00–7.97 (m, 1H), 7.54–7.52 (m, 2H), 7.28 (d, J = 8.4 Hz, 2H), 7.16 (d, J = 8.8 Hz, 2H), 7.07 (s, 1H), 4.17 (q, J = 7.2 Hz, 2H), 3.92 (q, J = 7.2 Hz, 2H), 2.63 (s, 3H), 2.54 (s, 3H), 1.28 (s, 9H), 1.06 (t, J = 7.2Hz, 3H), 0.79 (t, J = 7.2 Hz, 3H); ^{13}C NMR (100 MHz, CDCl$_3$) 166.7, 165.2, 156.1, 152.6, 136.6, 136.5, 132.9, 132.5, 132.0, 129.3, 128.5, 127.2, 127.0, 125.9, 125.8, 125.2, 125.1, 124.7, 61.5, 61.0, 34.8, 31.3, 19.4, 16.0, 13.8, 13.6; MS (EI$^+$, 70eV) m/z 458 (M$^+$, 18), 384 (100), 311 (22), 309 (22); HRMS (EI$^+$, 70 eV) Calculated: (C$_{30}$H$_{34}$O$_4$) 458.2457 (M$^+$), Found: 458.2451.

## 2-((1,4-dimethylnaphthalen-2-yl)(*p*-tolyl)methylene)propane-1,3-diol 10b
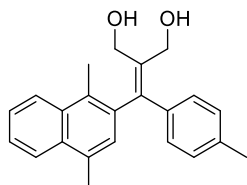
To a solution of **9b** (2.21 g, 5.30 mmol) in toluene (40 mL) was added DIBAL (26.4 mL, 1.0 M in hexane, 26.4 mmol) at −78 °C. The reaction mixture was allowed to gradually warm up to room temperature and then stirred overnight. The reaction was quenched with MeOH/EtOAc and 1 M HCl and the product was extracted with EtOAc. The organic layer was washed with water, and dried over MgSO$_4$. After filtration, the obtained solutions were evaporated in vacuum. The obtained residue was purified by a silica-gel column chromatography (hexane/ethyl acetate = 40:60), to give **10b** as a white solid (1.62 g, 92%).

mp 94.5−95.1 °C; IR (KBr) 3353 (s), 3066 (w), 3020 (w), 2940 (m), 1598 (w), 1509 (m), 1444 (m), 1409 (m), 1385 (m), 1236 (w), 1185 (s), 1038 (s), 1011 (s), 974 (m), 827 (m) cm^{-1}; ^{1}H NMR (400 MHz, CDCl$_3$) 8.06–8.04 (m, 1H), 8.00–7.97 (m, 1H), 7.56–7.53 (m, 2H), 7.16 (d, J = 8.0 Hz, 2H), 7.10 (d, J = 8.0 Hz, 2H), 7.03 (s, 1H), 4.53 (s, 2H), 4.20 (d, J = 3.2 Hz, 2H), 2.61 (s, 3H), 2.55 (s, 3H), 2.32 (s, 3H); ^{13}C NMR (100 MHz, CDCl$_3$) 142.3, 137.5, 137.3, 135.2, 133.1, 132.3, 132.1, 129.34, 129.31, 128.9, 128.2, 125.93, 125.92, 125.5, 125.1, 124.7, 64.4, 63.1, 21.3, 19.5, 15.9; MS (EI$^+$, 70eV) m/z 332 (M$^+$, 65), 299 (100), 129 (20); HRMS (EI$^+$, 70 eV) Calculated: (C$_{23}$H$_{24}$O$_2$) 332.1776 (M$^+$), Found: 332.1778.

2-((4-(*tert*-butyl)phenyl)(1,4-dimethylnaphthalen-2-yl)methylene)propane-1,3-diol 10c
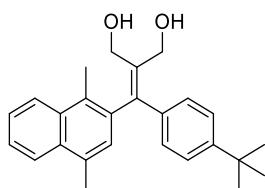
To a solution of **9c** (0.672 g, 1.47 mmol) in toluene (15 mL) was added DIBAL (7.5 mL, 1.0 M in hexane, 7.5 mmol) at –78 °C. The reaction mixture was allowed to gradually warm up to room temperature and then stirred overnight. The reaction was quenched with MeOH/EtOAc and 1 M HCl and the product was extracted with EtOAc. The organic layer was washed with water, and dried over MgSO$_4$. After filtration, the obtained solutions were evaporated in vacuum. The obtained residue was purified by a silica-gel column chromatography (hexane/ethyl acetate = 40:60), to give **10c** as a white solid (0.582 g, quant.). mp 173.2−174.1 °C; IR (KBr) 3556 (s), 3325 (s), 3065 (w), 3032 (w), 2962 (s), 2865 (s), 1599 (w), 1571 (w), 1507 (m), 1387 (s), 1362 (s), 1295 (w), 1267 (m), 1233 (m), 996 (s), 940 (w), 836 (m) cm^{-1}; ^{1}H NMR (400 MHz, CDCl$_3$) 8.07–8.05 (m, 1H), 8.01–7.98 (m, 1H), 7.57–7.53 (m, 2H), 7.31 (d, *J* = 8.4 Hz, 2H), 7.21 (d, *J* = 8.8 Hz, 2H), 7.07 (s, 1H), 4.53 (s, 2H), 4.18 (d, *J* = 3.6 Hz, 2H), 2.62 (s, 3H), 2.56 (s, 3H), 1.30 (s, 9H); ^{13}C NMR (100 MHz, CDCl$_3$) 150.3, 142.2, 137.5, 137.1, 135.2, 133.0, 132.2, 132.1, 129.2, 129.0, 128.2, 125.9, 125.5, 125.04, 125.01, 124.7, 64.1, 62.8, 34.6, 31.4, 19.5, 15.9; MS (EI$^+$, 70eV) *m/z* 374 (M$^+$, 76), 299 (100), 255 (21), 57 (66); HRMS (EI$^+$, 70 eV) Calculated: (C$_{26}$H$_{30}$O$_2$) 374.2246 (M$^+$), Found: 374.2249.

2-((1,4-dimethylnaphthalen-2-yl)(*p*-tolyl)methylene)malonaldehyde 11b
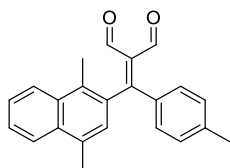
To a solution of **10b** (1.51 g, 4.54 mmol) in CHCl$_3$ (40 mL) was added MnO$_2$ (18.1 g, 209 mmol) at room temperature. The reaction mixture was stirred at the temperature 41 h. The MnO$_2$ was removed by filtration through a celite pad. The filtrate was evaporated and the residue obtained was purified by column chromatography on silica gel (hexane/ethyl acetate 8:2) to give **11b** as a yellow solid (2.02 g, quant.). mp 119.8−120.3 °C; IR (KBr) 3072 (w), 2992 (w), 2922 (w), 2843 (m), 2741 (w), 1686 (s), 1656 (s), 1604 (s), 1563 (m), 1445 (m), 1339 (m), 1305 (m), 1265 (m), 1184 (m), 1164 (w), 1002 (w), 848 (s), 829 (m) cm^{-1}; ^{1}H NMR (400 MHz, CDCl$_3$) 9.77 (d, *J* = 2.4 Hz, 1H), 9.43 (d, *J* = 1.6 Hz, 1H), 8.11–8.08 (m, 1H), 8.07–8.04 (m, 1H), 7.66–7.61 (m, 2H), 7.23 (d, *J* = 7.6 Hz, 2H), 7.15 (d, *J* = 8.0 Hz, 2H), 7.00 (s, 1H), 2.65 (s, 3H), 2.48 (s, 3H), 2.42 (s, 3H); ^{13}C NMR (100 MHz, CDCl$_3$) 190.5, 190.1, 171.5, 143.15, 143.09, 135.1, 134.3, 133.7, 133.3, 133.0, 132.3, 131.6, 129.6, 127.9, 127.1, 126.9, 125.4, 125.0, 21.8, 19.5, 16.6; MS (EI$^+$, 70eV) *m/z* 328 (M$^+$, 17), 313 (100), 299 (23), 285 (13); HRMS (EI$^+$, 70 eV) Calculated: (C$_{23}$H$_{20}$O$_2$) 328.1463 (M$^+$), Found: 328.1458.

2-((4-(*tert*-butyl)phenyl)(1,4-dimethylnaphthalen-2-yl)methylene)malonaldehyde 11c
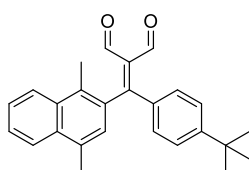
To a solution of **10c** (0.914 g, 2.44 mmol) in CHCl$_3$ (40 mL) was added MnO$_2$ (6.32 g, 72.6 mmol) at room temperature. The reaction mixture was stirred at the temperature 14 h. The MnO$_2$ was removed by filtration through a celite pad. The filtrate was evaporated and the residue obtained was purified by column chromatography on silica gel (hexane/ethyl acetate 8:2) to give **11c** as a yellow solid (0.767 g, 85%).

mp 176.5−177.1 °C; IR (KBr) 3073 (m), 2962 (s), 2844 (s), 1729 (s), 1699 (s), 1661 (s), 1505 (m), 1195 (m), 1166 (m), 1127 (w), 982 (m), 854 (s), 804 (s) cm^{-1}; ^{1}H NMR (400 MHz, CDCl$_3$) 9.78 (d, J = 2.4 Hz, 1H), 9.43 (d, J = 2.4 Hz, 1H), 8.11–8.09 (m, 1H), 8.07–8.05 (m, 1H), 7.65–7.62 (m, 2H), 7.43 (d, J = 8.8 Hz, 2H), 7.20 (d, J = 8.8 Hz, 2H), 7.02 (s, 1H), 2.66 (s, 3H), 2.49 (s, 3H), 1.34 (s, 9H); ^{13}C NMR (100 MHz, CDCl$_3$) 190.6, 190.1, 171.3, 156.0, 135.2, 134.1, 133.7, 133.3, 132.9, 132.8, 132.1, 131.5, 127.8, 127.1, 126.8, 125.8, 125.4, 125.0, 35.2, 31.2, 19.5, 16.5; MS (EI$^+$, 70eV) m/z 370 (M$^+$, 13), 355 (100), 313 (15), 156 (11); HRMS (EI$^+$, 70 eV) Calculated: (C$_{26}$H$_{26}$O$_2$) 370.1933 (M$^+$), Found: 370.1931; Analysis C$_{26}$H$_{26}$O$_2$ (370.49) Calculated: C, 84.29; H, 7.07; O, 8.64, Found: C, 83.98; H, 6.89.

### 2-((1,4-dimethylnaphthalen-2-yl)(*p*-tolyl)methylene)-1,3-dimesitylpropane-1,3-diol 12b
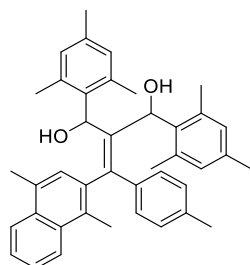
A solution of mesitylmagnesium bromide (25.6 mmol) in THF (20 mL) was added to a solution of **11b** (1.295 g, 3.94 mmol) in THF (40 mL) at 0 °C and the mixture was stirred for 2.5 h at room temperature and quenched with saturated aqueous NH$_4$Cl. The product was extracted with ethyl acetate. The organic layer was washed with water and dried over MgSO$_4$. The filtrate was evaporated and the residue was purified by column chromatography on silica gel (hexane, then hexane/ethyl acetate 80:20) to give two fractions (fractions A and B) of **11b** as pale yellow solids (1.56 g (fractions A/B = 14:1), 68%). Each fraction consisted of inseparable diastereo mixture and all spectroscopic data for each fraction were recorded using the mixture. Because of the diastereo mixture, NMR spectra were not analyzed except for signal picking.

fraction A: R_f = 0.47 (EtOAc/hexane = 1:4); mp 107.5−108.2 °C; IR (KBr) 3517 (m), 3351 (m), 3066 (m), 2953 (s), 2919 (s), 2859 (s), 2728 (w), 1610 (s), 1572 (w), 1508 (s), 1444 (s), 1383 (s), 1261 (m), 1234 (m), 1113 (w), 1077 (w), 1041 (s), 946 (w), 912 (m), 825 (s) cm^{-1}; ^{1}H NMR (400 MHz, CDCl$_3$) 7.94 (d, J = 8.4 Hz), 7.90 (d, J = 8.0 Hz), 7.81–7.79 (m), 7.76–7.73 (m), 7.51–7.48 (m), 7.45 (d, J = 8.8 Hz), 7.42–7.36 (m), 7.29 (s), 6.99 (d, J = 8.4 Hz), 6.94 (s), 6.89 (d, J = 8.8 Hz), 6.78 (s), 6.75 (d, J = 4.8 Hz), 6.72 (d, J = 8.4 Hz), 6.68 (s), 6.60 (s), 6.35 (s), 6.34 (s), 6.23 (s), 6.09 (s), 6.07 (s), 5.94 (s), 5.83 (s), 4.19 (d, J = 6.8 Hz), 2.84 (s), 2.72 (s), 2.68 (s), 2.41 (s), 2.38 (s), 2.36 (s), 2.34 (s), 2.28 (s), 2.27 (s), 2.23 (s), 2.20 (s), 2.19 (s), 2.17 (s), 2.15 (s), 2.13 (s), 2.12 (s), 2.09 (s), 2.03 (s), 1.95 (s), 1.79 (s); ^{13}C NMR (100 MHz, CDCl$_3$) 144.6, 140.0, 139.8, 139.5, 139.4, 139.0, 138.9, 138.4, 138.3, 138.1, 137.6, 137.2, 137.1, 136.9, 136.8, 136.6, 136.5, 136.4, 136.34, 136.27, 136.2, 136.03, 135.99, 135.89, 135.0, 134.8, 134.0, 133.1, 132.83, 132.80, 131.8, 131.5, 131.0, 130.7, 130.6, 130.4, 130.0, 129.8, 129.7, 129.5, 129.2, 129.0, 128.4, 128.1, 128.03, 127.97, 127.7, 127.3, 126.2, 125.3, 125.1, 125.0, 124.9, 124.8, 124.7, 124.6, 124.3, 124.2, 123.9, 85.5, 85.0, 74.1, 73.9, 73.3, 22.3, 21.8, 21.5, 21.3, 21.14, 21.09, 21.05, 21.00, 20.9, 20.80, 20.75, 20.7, 20.4, 20.0, 19.3, 19.22, 19.18, 16.9, 15.8; HRMS (ESI) Calculated: (C$_{41}$H$_{44}$O$_2$Na) 591.32335 ([M+Na]$^+$), Found: 591.32358.

fraction B: R_f = 0.23 (EtOAc/hexane = 1:4); mp 68.1−69.0 °C; IR (KBr) 3347 (m), 3067 (w), 2919 (s), 2858 (m), 1645 (s), 1609 (m), 1571 (w), 1508 (m), 1479 (m), 1446 (s), 1383 (m), 1343 (w), 1258 (w), 1139 (w), 1076 (w), 1041 (s), 1011 (m), 849 (m), 825 (m) cm^{-1}; ^{1}H NMR (400 MHz, CDCl$_3$) 7.94 (d, J = 8.8 Hz), 7.80–7.78 (m), 7.75–7.73 (m), 7.47–7.41 (m), 7.39–7.37 (m), 7.28 (s), 7.13 (s), 6.99 (d, J = 8.0 Hz), 6.81 (d, J = 8.0 Hz), 6.78 (s), 6.72 (d, J = 8.0 Hz), 6.68 (s), 6.60 (s), 6.44 (d, J = 4.8 Hz), 6.35 (s), 6.33 (s), 6.23 (s), 6.09 (s), 6.06 (s), 5.93 (s), 5.82 (s), 4.17 (d, J = 7.2 Hz), 2.84 (s), 2.73 (s), 2.40 (s), 2.38 (s),

2.36 (s), 2.27 (s), 2.26 (s), 2.27 (s), 2.19 (s), 2.18 (s), 2.17 (s), 2.11 (s), 2.09 (s), 2.02 (s), 1.95 (s), 1.90 (s), 1.87 (s), 1.78 (s); ^{13}C NMR (100 MHz, CDCl$_3$) 144.6, 139.8, 139.5, 139.4, 139.0, 138.9, 138.2, 137.2, 137.1, 136.9, 136.8, 136.6, 136.5, 136.4, 136.4, 136.33, 136.28, 136.2, 136.03, 135.99, 135.96, 135.9, 134.8, 133.0, 132.8, 131.8, 131.5, 131.0, 130.9, 130.8, 130.7, 130.0, 129.8, 129.7, 129.57, 129.52, 129.4, 129.3, 129.2, 129.1, 128.4, 128.1, 128.02, 127.97, 127.7, 126.2, 126.0, 125.3, 125.0, 124.9, 124.8, 124.7, 124.19, 124.17, 123.9, 74.1, 73.9, 73.3, 22.3, 21.50, 21.45, 21.3, 21.1, 21.0, 20.80, 20.75, 20.73, 20.68, 20.4, 20.13, 20.10, 19.4, 19.3, 19.2, 19.0, 16.9; HRMS (ESI) Calculated: (C$_{41}$H$_{44}$O$_2$Na) 591.32335 ([M+Na]$^+$), Found: 591.32292.

2-((4-(*tert*-butyl)phenyl)(1,4-dimethylnaphthalen-2-yl)methylene)-1,3-dimesitylpropane-1,3-diol 12c
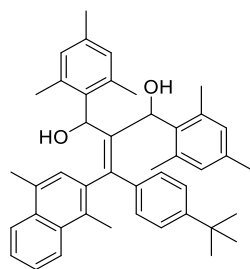

A solution of mesitylmagnesium bromide (6.53 mmol) in THF (10 mL) was added to a solution of **11c** (0.374 g, 1.01 mmol) in THF (10 mL) at 0 °C and the mixture was stirred for 2.5 h at room temperature and quenched with saturated aqueous NH$_4$Cl. The product was extracted with ethyl acetate. The organic layer was washed with water and dried over MgSO$_4$. The filtrate was evaporated and the residue was purified by column chromatography on silica gel (hexane, then hexane/ethyl acetate 75:25) to give two fractions (fractions A and B) of the target molecules as pale yellow solids (0.588 g (fractions A/B = 60:40), 95%). Each fraction consisted of inseparable diastereo mixture and all spectroscopic data for each fraction were recorded using the mixture. Because of the diastereo mixture, NMR spectra were not analyzed except for signal picking.

fraction A: R_f = 0.42 (EtOAc/hexane = 17:83); mp 74.1−74.5 °C; IR (KBr) 3521 (s), 3357 (s), 3068 (s), 2920 (s), 2729 (w), 1650 (w), 1610 (s), 1573 (m), 1507 (s), 1446 (s), 1269 (s), 1200 (m), 1153 (w), 1077 (w), 1013 (s), 932 (w), 880 (s), 847 (s) cm^{-1}; ^{1}H NMR (400 MHz, CDCl$_3$) 7.99 (d, J = 8.4 Hz), 7.85–7.83 (m), 7.78–7.74 (m), 7.52–7.44 (m), 7.43–7.40 (m), 7.26 (s), 7.25 (s), 7.17 (d, J = 8.4 Hz), 6.99 (s), 6.92 (d, J = 8.8 Hz), 6.84 (d, J = 7.6 Hz), 6.76 (s), 6.60 (s), 6.42 (s), 6.36 (s), 6.24 (s), 6.17 (s), 6.15 (d, J = 6.4 Hz), 5.98 (s), 5.91 (s), 4.22 (d, J = 7.2 Hz), 2.91 (s), 2.76 (s), 2.73 (s), 2.49 (s), 2.40 (s), 2.38 (s), 2.36 (s), 2.27 (s), 2.21 (s), 2.16 (s), 2.14 (s), 2.11 (s), 2.01 (s), 1.86 (s), 1.28 (s), 1.26 (s), 1.22 (s); ^{13}C NMR (100 MHz, CDCl$_3$) 149.4, 148.8, 143.9, 139.45, 139.37, 139.3, 139.1, 138.8, 138.3, 137.6, 137.4, 136.9, 136.8, 136.7, 136.6, 136.4, 136.24, 136.20, 136.0, 135.9, 135.1, 133.0, 132.8, 131.7, 131.5, 131.0, 130.5, 130.1, 130.0, 129.8, 129.5, 129.25, 129.18, 128.1, 127.7, 127.2, 126.1, 125.3, 125.1, 125.0, 124.9, 124.8, 124.7, 124.2, 124.1, 124.0, 76.6, 74.4, 73.7, 73.5, 34.4, 34.3, 31.8, 31.4, 31.3, 31.2, 22.1, 21.4, 21.1, 20.9, 20.8, 20.7, 20.4, 19.3, 19.1, 16.8, 16.7; HRMS (ESI) Calculated: (C$_{44}$H$_{50}$O$_2$Na) 633.37030 ([M+Na]$^+$), Found: 633.37104.

fraction B: R_f = 0.23 (EtOAc/hexane = 17:83); mp 184.2−185.1 °C; IR (KBr) 3328 (s), 3068 (w), 2962 (s), 2918 (s), 2865 (s), 1611 (m), 1507 (m), 1479 (m), 1461 (s), 1424 (m), 1381 (m), 1362 (m), 1269 (m), 1200 (w), 1138 (w), 1044 (s), 1028 (s), 877 (w), 847 (s) cm^{-1}; ^{1}H NMR (400 MHz, CDCl$_3$) 7.97 (d, J = 8.4 Hz), 7.82–7.80 (m), 7.75 (d, J = 8.8 Hz), 7.50–7.44 (m), 7.42–7.38 (m), 7.22 (d, J = 7.6 Hz), 7.14 (d, J = 8.0 Hz), 6.89 (d, J = 8.4 Hz), 6.81 (d, J = 6.0 Hz), 6.74 (s), 6.58 (s), 6.40 (s), 6.34 (s), 6.21 (s), 6.15 (s), 5.96 (s), 5.89 (s), 4.14 (d, J = 6.8 Hz), 3.95 (s), 3.56 (s), 2.88 (s), 2.46 (s), 2.38 (s), 2.34 (s), 2.24 (s), 2.18 (s), 2.14 (s), 2.11 (s), 2.08 (s), 1.99 (s), 1.83 (s), 1.24 (s), 1.18 (s); ^{13}C NMR (100 MHz, CDCl$_3$) 149.4, 148.8, 143.9, 139.5, 139.4, 139.3, 139.1, 138.8, 137.6, 137.4, 137.0, 136.8, 136.7, 136.6, 136.5, 136.32, 136.29, 136.1, 136.0, 135.1, 133.1,

132.8, 131.7, 131.5, 131.0, 130.6, 130.2, 130.1, 129.8, 129.6, 129.3, 129.2, 128.1, 127.7, 126.1, 125.3, 125.0, 124.9, 124.8, 124.7, 124.2, 124.1, 124.0, 76.7, 74.4, 73.8, 73.5, 34.5, 34.3, 31.4, 31.3, 22.1, 21.4, 21.2, 20.9, 20.8, 20.7, 20.4, 19.4, 19.2, 16.8, 16.7; HRMS (ESI) Calculated: (C$_{44}$H$_{50}$O$_2$Na) 633.37030 ([M+Na]$^+$), Found: 633.37116.

11,12-Dimesityl-2,5,10-trimethyl-11,12-dihydrobenzo[5,6]pentaleno[1,2-*b*]naphthalene 13b
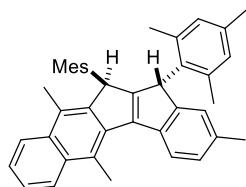
To a solution of **12b** (1.53 g, 2.69 mmol) in chlorobenzene (20 mL) was added polyphosphoric acid (two medicine spoons, ~6 g) at room temperature and the mixture was heated at 130 °C for 35 h. After cooling to room temperature, the organic layer was decanted and evaporated. The residue obtained was purified by column chromatography on silica gel (hexane, then hexane/ethyl acetate 97:3), to give **13b** of a single diastereoisomer as a colorless solid (0.624 g, 43%). Single crystals suitable for X-ray crystallographic analysis were obtained from a solution of CH$_2$Cl$_2$/hexane.

mp 253.4−254.2 °C; IR (KBr) 3068 (m), 3001 (s), 2963 (s), 2912 (s), 2857 (s), 2733 (m), 2400 (w), 1883 (w), 1750 (w), 1719 (w), 1610 (s), 1573 (m), 1474 (s), 1379 (s), 1362 (m), 1351 (m), 1141 (w), 1077 (w), 1027 (m), 988 (m), 928 (m), 847 (s), 809 (s) cm^{-1}; ^{1}H NMR (400 MHz, CDCl$_3$) 8.22 (d, *J* = 8.4 Hz, 1H), 8.08 (d, *J* = 8.0 Hz, 1H), 7.96 (d, *J* = 8.4 Hz, 1H), 7.54 (t, *J* = 7.4 Hz, 1H), 7.47 (t, *J* = 7.8 Hz, 1H), 7.21 (d, *J* = 8.0 Hz, 1H), 6.99 (s, 1H), 6.83 (s, 1H), 6.78 (s, 1H), 6.70 (s, 1H), 6.60 (s, 1H), 5.00 (s, 1H), 4.67 (s, 1H), 3.28 (s, 3H), 2.33 (s, 3H), 2.28 (s, 3H), 2.24 (s, 3H), 2.23 (s, 3H), 1.683 (s, 3H), 1.679 (s, 3H), 1.49 (s, 3H), 1.36 (s, 3H); ^{13}C NMR (100 MHz, CDCl$_3$) 162.9, 152.1, 146.8, 146.2, 138.6, 138.1, 138.0, 137.52, 137.50, 136.6, 136.3, 135.9, 134.7, 133.2, 133.1, 132.4, 131.4, 130.3, 130.0, 129.2, 128.8, 127.5, 127.3, 125.1, 125.0, 124.7, 124.6, 124.1, 123.2, 122.1, 47.6, 47.1, 21.3, 21.0, 20.9, 20.6 (two signals are overlapped.), 18.8, 18.6, 18.3, 14.4; MS (EI$^+$, 70eV) *m/z* 532 (M$^+$, 58), 517 (100), 266 (11); HRMS (EI$^+$, 70 eV) Calculated: (C$_{41}$H$_{40}$) 532.3130 (M$^+$), Found: 532.3125.

## 2-(*tert*-Butyl)-11,12-dimesityl-5,10-dimethyl-11,12-dihydrobenzo[5,6]pentaleno[1,2-*b*]naphthalene 13c
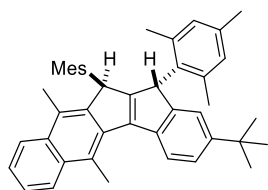
To a solution of **12c** (1.56 g, 2.55 mmol) in chlorobenzene (23 mL) was added polyphosphoric acid (three medicine spoons, ~9 g) at room temperature and the mixture was heated at 130 °C for 20 h. After cooling to room temperature, the organic layer was decanted and evaporated. The residue obtained was purified by column chromatography on silica gel (hexane, then hexane/ethyl acetate 98:2), to give **13c** of a single diastereoisomer as a pale brown solid (1.47 g, 74%).

mp 161.2−162.0 °C; IR (KBr) 3070 (w), 2961 (s), 2914 (s), 2863 (s), 2733 (w), 1610 (m), 1572 (w), 1477 (s), 1458 (m), 1378 (m), 1362 (m), 1255 (w), 1026 (w), 923 (w), 887 (w), 849 (m), 815 (m) cm^{-1}; ^{1}H NMR (400 MHz, CDCl$_3$) 8.22 (d, *J* = 8.4 Hz, 1H), 8.14 (d, *J* = 8.4 Hz, 1H), 7.96 (d, *J* = 8.4 Hz, 1H), 7.54 (t, *J* = 7.4 Hz, 1H), 7.49–7.43 (m, 2H), 7.17 (s, 1H), 6.83 (s, 1H), 6.79 (s, 1H), 6.69 (s, 1H), 6.59 (s, 1H), 4.98 (s, 1H), 4.72 (s, 1H), 3.29 (s, 3H), 2.28 (s, 3H), 2.23 (s, 6H), 1.66 (s, 6H), 1.45 (s, 3H) , 1.36 (s, 3H), 1.29 (s, 9H); ^{13}C NMR (100 MHz, CDCl$_3$) 163.3, 152.1, 148.1, 146.8, 146.1, 144.0, 138.6, 138.1, 137.9, 137.5, 136.6, 136.1, 135.9, 133.1, 133.0, 132.3, 131.4, 130.2, 130.0, 129.2, 128.8, 127.4, 125.0, 124.7, 124.6, 124.1, 123.4, 123.2, 121.8, 121.1, 48.0, 47.1, 34.7, 31.7, 21.0, 20.9, 20.7, 20.6, 18.8, 18.5, 18.4, 14.4; MS (EI$^+$, 70eV) *m/z* 574 (M$^+$, 87), 559

(100), 503 (19), 287 (13); HRMS (EI⁺, 70 eV) Calculated: ($C_{44}H_{46}$) 574.3600 (M⁺), Found: 574.3596.

11,12-Dimesityl-2,5,10-trimethylbenzo[5,6]pentaleno[1,2-*b*]naphthalene dianion 6b²⁻
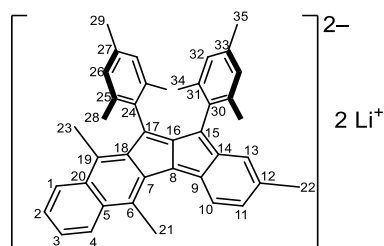
In a nitrogen-filled glove box, to a solution of **13b** (0.0248 g, 0.0465 mmol) in THF (0.15 ml) was added ⁿBuLi (0.059 mL, 0.0946 mmol, 1.6 M in hexane) at –35 °C. The reaction mixture was further stirred for 15 h at room temperature, to afford as a deep-green solution of **6b²⁻**. The dianion was subsequently oxidized without isolation. According to the NMR monitoring, the dianion was generated quantitatively.

¹H NMR (600 MHz, THF-d_8) 8.14 (d, *J* = 7.8 Hz, 1H, 10-H), 7.85 (d, *J* = 8.4 Hz, 1H, 4-H), 7.58 (d, *J* = 8.4 Hz, 1H, 1-H), 6.84 (t, *J* = 7.2 Hz, 1H, 2-H), 6.68 (t, *J* = 7.2 Hz, 1H, 3-H), 6.48 (s, 2H, 32-H2), 6.42 (s, 1H, 13-H), 6.42 (s, 2H, 26H), 6.25 (d, *J* = 7.8 Hz, 1H, 11-H), 3.55 (s, 3H, 32-H), 2.34 (s, 3H, 22-H), 2.26 (s, 3H, 23-H), 2.18 (s, 3H, 35-H), 2.17 (s, 3H, 29-H), 1.88 (s, 6H, 34-H), 1.87 (s, 6H, 28-H); ¹³C NMR (150 Hz, THF-d_8) 146.4 (s), 143.1 (s, C-24), 139.8 (s, C-30), 138.5 (s, C-25), 138.1 (s, C-31), 137.9 (s, C-18), 137.8 (s), 130.6 (s, C-33), 130.1 (s, C-27), 129.5 (s, C-7), 127.4 (s, C-20), 127.0 (d, C-32), 126.5 (d, C-26), 123.2 (s, C-5), 121.9 (s, C-9), 121.8 (d, C-4), 120.8 (s, C-12), 120.3 (d, C-1), 117.5 (d, C-2), 115.9 (d, C-10), 113.8 (d, C-13), 112.9 (d, C-3), 110.9 (s, C-6), 110.7 (d, C-11), 106.0 (s, C-19), 101.9 (s), 90.9 (s, C-15), 88.9 (s, C-17), 22.6 (q, C-22), 22.4 (q, C-28), 22.0 (q, C-34), 21.21 (q, C-29), 21.17 (q, C-35), 19.9 (q, C-21), 15.5 (q, C-23); ⁷Li{¹H} NMR (155 MHz, THF-d_8) (LiCl in THF-d_8 as external standard) –1.41.

2-(*tert*-butyl)-11,12-dimesityl-5,10-dimethylbenzo[5,6]pentaleno[1,2-*b*]naphthalene dianion 6c²⁻
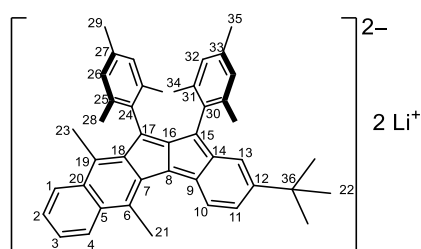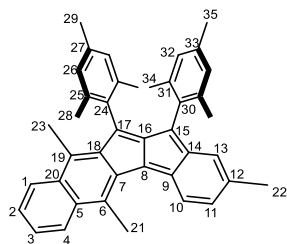

In a nitrogen-filled glove box, to a solution of **13c** (0.0235 g, 0.0409 mmol) in THF (0.15 ml) was added ⁿBuLi (0.059 mL, 0.0946 mmol, 1.6 M in hexane) at –35 °C. The reaction mixture was further stirred for 15 h at room temperature, to afford as a deep-green solution of **6c²⁻**. The dianion was subsequently oxidized without isolation. According to the NMR monitoring, the dianion was generated quantitatively.

¹H NMR (600 MHz, THF-d_8) 8.18 (d, *J* = 7.8 Hz, 1H, 10-H), 7.85 (d, *J* = 8.4 Hz, 1H, 4-H), 7.58 (d, *J* = 8.4 Hz, 1H, 1-H), 6.84 (t, *J* = 7.2 Hz, 1H, 2-H), 6.70 (s, 1H, 13-H), 6.68 (t, *J* = 7.5 Hz, 1H, 3-H), 6.51 (d, *J* = 8.4 Hz, 1H, 11-H), 6.47 (s, 2H, 32-H), 6.42 (s, 2H, 26-H), 3.56 (s, 3H, 21-H), 2.26 (s, 3H, 23-H), 2.18 (s, 3H, 35-H), 2.17 (s, 3H, 29-H), 1.89 (s, 6H, 34-H), 1.86 (s, 6H, 28-H), 1.33 (s, 9H, 22-H); ¹³C NMR (150 MHz, THF-d_8) 146.2 (s, C-16), 143.0 (s, C-24), 139.8 (s, C-30), 138.5 (s, C-25), 137.99 (s, C-31), 137.95 (s, C-18), 137.9 (s, C-14), 134.9 (s, C-12), 130.5 (s, C-33), 130.1 (s, C-27), 129.4 (s, C-7), 127.6 (s, C-20), 127.1 (d, C-32), 126.6 (d, C-26), 123.3 (s, C-5), 121.9 (s, C-9), 121.8 (d, C-4), 120.3 (d, C-1), 117.6 (d, C-2), 115.9 (d, C-10), 113.0 (d, C-3), 110.8 (s, C-6), 110.0 (d, C-13), 107.2 (d, C-11), 105.8 (s, C-19), 101.32 (s, C-8), 91.8 (s, C-15), 88.8 (s, C-17), 34.7 (s, C-36), 33.0 (q, C-22), 22.4 (q, C-28), 22.1 (q, C-34), 21.23 (s, C-29), 21.20 (q, C-35), 19.9 (q, C-21), 15.5 (q,

C-23); $^7Li\{^1H\}$ NMR (233 MHz, THF-d_8) (LiCl in THF-d_8 as external standard) –0.21, –1.19.

11,12-dimesityl-2,5,10-trimethylbenzo[5,6]pentaleno[1,2-*b*]naphthalene 6b

In a nitrogen-filled glove box, a solution of *p*-chloranil (0.1 mmol) in toluene (2 mL) was added to a solution of fresh **6b**$^{2-}$ in THF-d_8. The reaction mixture was stirred for 1 h at room temperature and the solvent was removed in vacuum. Dichloromethane and hexane were added to the residue and insoluble materials were removed by filtration through a cotton. The filtrate was evaporated to remove the solvent to give **6b** as a reddish-brown solid (0.040 g, 81%).

mp 120.3–120.7 °C (decomposed); IR (KBr) 3067 (w), 2923 (s), 2852 (m), 1701 (w), 1610 (w), 1457 (m), 1377 (w), 1261 (w), 1094 (w), 1032 (w), 849 (w), 804 (w) cm^{-1}; ^1H NMR (600 MHz, THF-d_8, –60 °C) 7.28 (d, J = 8.4 Hz, 1H, 4-H), 7.18 (d, J = 7.8 Hz, 1H, 1-H), 7.02 (t, J = 7.5 Hz, 1H, 3-H), 6.89 (t, J = 7.5 Hz, 1H, 2-H), 6.55 (s, 2H, 26-H), 6.48 (s, 2H, 32-H), 6.27 (d, J = 9.6 Hz, 1H, 10-H), 5.55 (d, J = 9.6 Hz, 1H, 11-H), 4.97 (s, 1H, 13-H), 2.14 (s, 3H, 21-H), 2.11 (s, 6H, 28-H), 2.10 (s, 3H, 29-H), 2.09 (s, 6H, 34-H), 2.07 (s, 3H, 35-H), 1.51 (s, 3H, 22-H), 1.47 (s, 3H, 23-H); ^{13}C NMR (150 Hz, THF-d_8, –60 °C) 157.8 (s), 156.6 (s), 154.7 (s), 146.7 (s, C-18), 138.2 (s, C-5), 137.6 (s, C-9), 137.5 (s, C-27), 137.1 (s, C-31), 136.8 (s), 136.7 (s, C-12), 136.3 (s, C-20), 135.9 (s, C-33), 135.8 (s, C-7), 134.61 (s, C-25), 134.56 (s, C-19), 133.3 (d, C-11), 132.7 (s, C-24), 130.1 (s, C-30), 129.0 (d, C-3), 128.1 (d, C-26), 127.6 (d, C-32), 127.0 (d, C-10), 126.7 (two signals are overlapped, d, C-1, C-2), 125.61 (s, C-15), 125.56 (d, C-4), 125.0 (s, C-6), 123.7 (d, C-13), 21.0 (q, C-22), 20.9 (q, C-35), 20.6 (q, C-34), 20.2 (q, C-29), 19.9 (q, C-28), 17.4 (q, C-21), 11.9 (q, C-23); MS (EI$^+$, 70 eV) *m/z* 528 (M$^+$, 100), 126 (24), 112 (21), 48 (9); HRMS (EI$^+$, 70 eV) Calculated: (C$_{41}$H$_{38}$) 530.2974 (M$^+$), Found: 530.2956.

2-(*tert*-butyl)-11,12-dimesityl-5,10-dimethylbenzo[5,6]pentaleno[1,2-*b*]naphthalene 6c
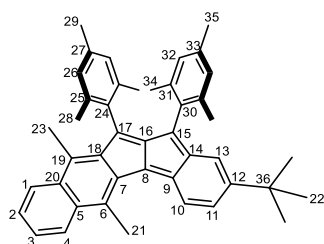
In a nitrogen-filled glove box, a solution of *p*-chloranil (0.09 mmol) in toluene (2 mL) was added to a solution of fresh **6c**$^{2-}$ in THF-d_8. The reaction mixture was stirred for 1 h at room temperature and the solvent was removed in vacuum. Toluene (2 mL) and hexane (3 mL) were added to the residue and insoluble materials were removed by filtration through a cotton. The filtrate was evaporated to remove the solvent. The filtrate was evaporated to remove the solvent to give **6c** as a reddish-brown solid (0.047 g, quant.).

mp 93.7–94.2 °C (decomposed); IR (KBr) 3072 (w), 2953 (s), 2923 (s), 2852 (s), 1611 (w), 1563 (m), 1459 (w), 1376 (w), 1261 (w), 1094 (w), 1023 (w), 846 (w), 802 (w) cm^{-1}; ^1H NMR (600 MHz, THF-d_8, –60 °C) 7.28 (d, J = 6.0 Hz, 1H, 4-H), 7.19 (d, J = 6.0 Hz, 1H, 1-H), 7.07–6.99 (m, 1H, 3-H), 6.94–6.86 (m, 1H, 2-H), 6.54 (s, 2H, 26-H), 6.46 (s, 2H, 32-H), 6.31 (d, J = 9.0 Hz, 1H, 10-H), 5.87 (d, J = 9.0 Hz, 1H, 11-H), 5.06 (s, 1H, 13-H), 2.15 (s, 3H, 21-H), 2.14–2.05 (m, 12H, 28-H, 29-H, 34-H, 35-H), 1.49 (s, 3H, 23-H), 0.91 (s, 9H, 22-H); ^{13}C NMR (150 Hz, THF-d_8, –60 °C) 157.6 (s), 156.6 (s), 154.3 (s), 148.8

(s, C-12), 146.7 (s, C-18), 138.2 (s, C-5), 137.5 (s, C-9), 137.0 (s, C-31), 136.8 (s, C-7), 136.2 (s, C-20), 135.9 (s, C-33), 135.2 (s), 134.6 (s, C-25), 134.5 (s, C-19), 132.7 (s, C-24), 130.5 (d, C-11), 130.0 (s, C-30), 129.0 (d, C-3), 128.1 (d, C-26), 127.7 (d, C-32), 126.93 (d, C-10), 126.86 (s, C-15), 126.7 (two signals are overlapped, d, C-1, C-2), 125.5 (d, C-4), 124.8 (s, C-6), 119.2 (s), 119.1 (d, C-13), 33.8 (s, C-36), 20.98 (q, C-35), 20.93 (q, C-29), 20.7 (q, C-34), 20.2 (q, C-28), 17.3 (q, C-21), 14.8 (q, C-22), 12.0 (q, C-23); MS (EI$^+$, 70 eV) m/z 572 (M$^+$, 100), 286 (10), 111 (11), 57 (16); HRMS (EI$^+$, 70 eV) Calculated: (C$_{44}$H$_{44}$) 572.3443 (M$^+$), Found: 572.3439.

Supporting Information

11,12-dimesityl-2,5,10-trimethyl-11,12-dihydrobenzo[5,6]pentaleno[1,2-*b*]naphthalene   13b   (CCDC 2069160)
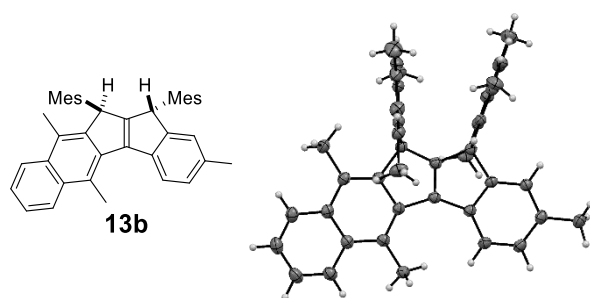

Figure S1. ORTEP drawings of **13b** at the 50% probability level. Recrystallization of **13b** from a hexane–CH$_2$Cl$_2$ solution gave single crystals for one of the diastereomers of **13b**.

Empirical Formula	C$_{44}$H$_{40}$	Space Group	*P*-1 (#2)
Formula Weight	532.73	*Z* value	2
Crystal Color, Habit	translucent intense colorless, block	D_{calc}	1.169 g/cm^3
		F_{000}	572.0
Crystal Dimensions	$0.177 \times 0.111 \times 0.073$ mm	μ(CuK$_\alpha$)	0.491 mm^{-1}
Crystal System	triclinic	Temperature	123 K
Lattice Type	Primitive	Data/restraints/parameters	6085/0/379
Lattice Parameters	$a = 10.9926(4)$ Å	Residuals: *R*1 ($I > 2.00\sigma(I)$)	0.0465
	$b = 11.1960(3)$ Å	Residuals: *wR*2 (*all data*)	0.1324
	$c = 14.1753(6)$ Å	Goodness of Fit Indicator	1.054
	$\alpha = 70.062(3)$ °		
	$\beta = 76.447(3)$ °		
	$\gamma = 68.407(3)$ °		
	$V = 1513.07(10)$ Å^3		

2-(*tert*-butyl)-11,12-dimesityl-5,10-dimethylbenzo[5,6]pentaleno[1,2-*b*]naphthalene 6c (CCDC 2069161)
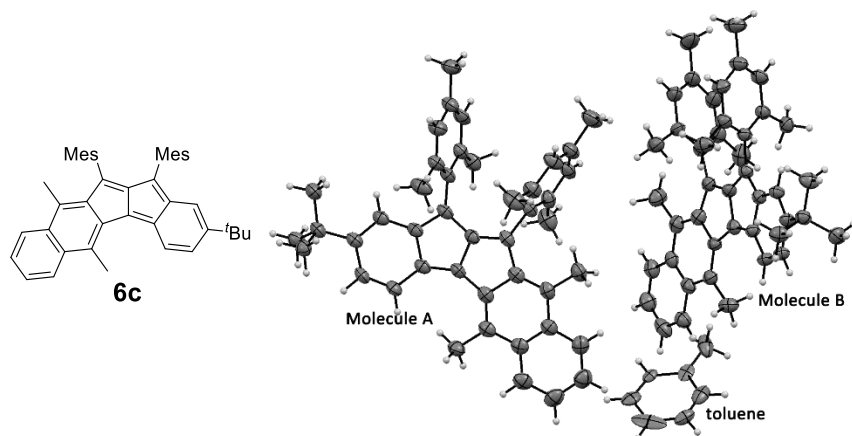

Figure S2. ORTEP drawings of **6c** at the 50% probability level.

A toluene solution of **6c** was poured into a quartz tube (external diameter: 3 mm) connected with a Pyrex glass neck. The solvent was evaporated under vacuum and the Pyrex part was sealed. The residual solids were heated at above 200 ℃ by a heatgun to be melted. The melted the solids were cooled to room temperature, to afford single crystals.

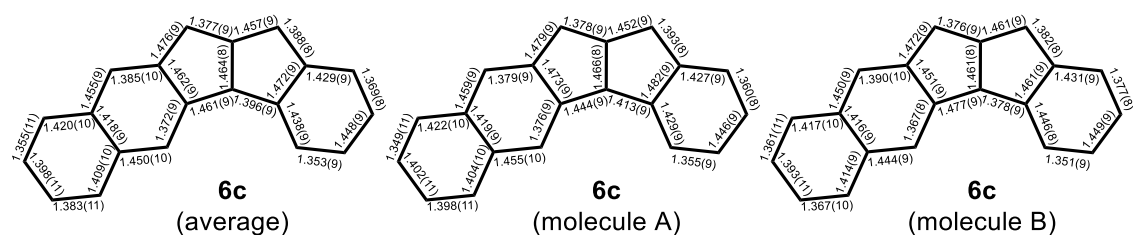|			
Empirical Formula	$C_{183}H_{184}$	Space Group	$P2_12_12_1$ (#19)
Formula Weight	2383.29	Z value	2
Crystal Color, Habit	translucent intense red needle	D_{calc}	1.099 g/cm^3
		F_{000}	2564.0
Crystal Dimensions	0.138 × 0.051 × 0.033 mm	μ(CuK$_\alpha$)	0.460 mm^{-1}
Crystal System	orthorhombic	Temperature	123 K
Lattice Type	Primitive	Data/restraints/parameters	14108/0/879
Lattice Parameters	$a = 8.2217(3)$ Å	Residuals: $R1$ ($I > 2.00\sigma(I)$)	0.0765
	$b = 29.1994(15)$ Å	Residuals: $wR2$ (*all data*)	0.2473
	$c = 30.0025(15)$ Å	Goodness of Fit Indicator	0.999
	$V = 7202.7(6)$ Å^3		

Figure S3. Summary for the observed bond lengths (Å) of the main core of **6c**.
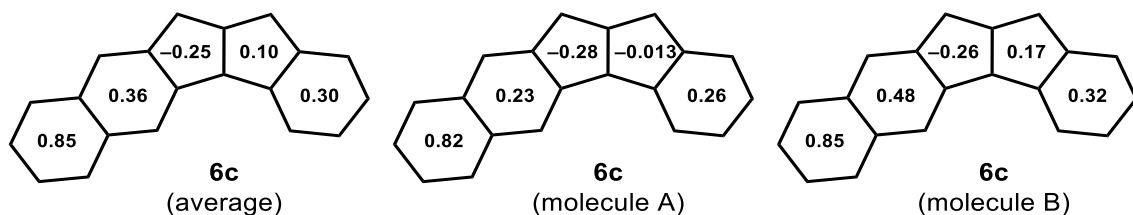

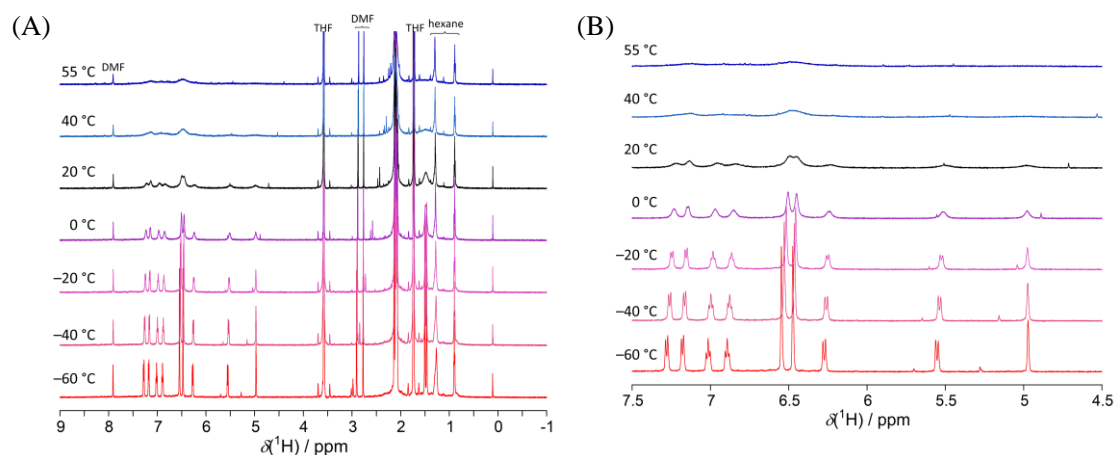**Figure S4**. Summary for the HOMA values of the main core of **6c**.

31

Figure S5. Temperature-dependent ^{1}H NMR (600 MHz) spectra of **6b** in THF-d_8. (A) total and (B) aromatic region. DMF and hexane were residual solvents, which were used for washing the crude products.
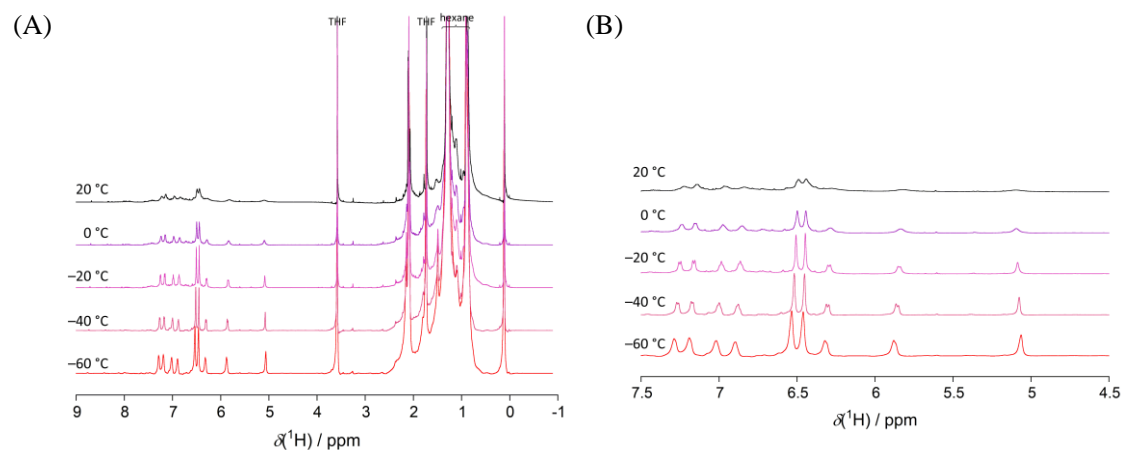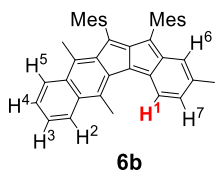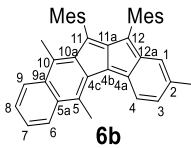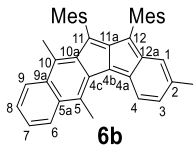

Figure S6. Temperature-dependent ^{1}H NMR (600 MHz) spectra of **6c** in THF-d_8. (A) total and (B) aromatic region.

Table S1. ^{1}H NMR chemical shifts of the main core of **6b** and **6b**$^{2-}$.

	6b $\delta(^1$H)/ppm	**6b**$^{2-}$ $\delta(^1$H)/ppm	$\Delta\delta(^1$H) / ppm [a]
H^1	6.27	8.14	−1.87
H^2	7.28	7.85	−0.57
H^3	7.02	6.68	0.34
H^4	6.89	6.84	0.05
H^5	7.18	7.58	−0.40
H^6	4.97	6.42	−1.45
H^7	5.55	6.25	−0.70

a) $\Delta\delta(^1$H) = $\delta(^1$H)(**6b**) − $\delta(^1$H)(**6b**$^{2-}$), n.d. = not determined.

Table S2. ^{13}C NMR chemical shifts of the main core of **6b** and **6b**$^{2-}$.

	6b $\delta(^{13}\text{C})$/ppm	**6b**$^{2-}$ $\delta(^{13}\text{C})$/ppm	$\Delta\delta(^{13}\text{C})$ / ppm ^{a}		**6b** $\delta(^{13}\text{C})$/ppm	**6b**$^{2-}$ $\delta(^{13}\text{C})$/ppm	$\Delta\delta(^{13}\text{C})$ / ppm ^{a}
C^1	123.7	113.8	9.90	C^7	129.0	112.9	16.1
C^2	136.7	120.8	15.9	C^8	126.7	117.5	9.20
C^3	133.3	110.7	22.6	C^9	126.7	120.3	6.40
C^4	127.0	115.9	11.1	C^{9a}	136.3	127.4	8.90
C^{4a}	137.6	121.9	15.7	C^{10}	134.56	106.0	28.6
C^{4b}	n.d.	n.d.	–	C^{10a}	146.7	137.9	8.80
C^{4c}	135.8	129.5	6.30	C^{11}	n.d.	88.9	–
C^5	125.0	110.9	14.1	C^{11a}	n.d.	n.d.	–
C^{5a}	138.2	123.2	15.0	C^{12}	125.61	90.9	34.7
C^6	125.56	121.8	3.76	C^{12a}	n.d.	n.d.	–

a) $\Delta\delta(^{13}\text{C}) = \delta(^{13}\text{C})(\textbf{6b}) - \delta(^{13}\text{C})(\textbf{6b}^{2-})$, n.d. = not determined.

Table S3. ^{1}H NMR chemical shifts of the main core of **6c** and **6c**$^{2-}$.

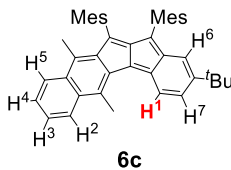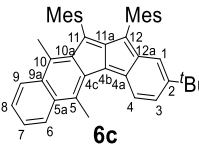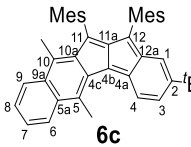|	**6c** $\delta(^1\text{H})$/ppm	**6c**$^{2-}$ $\delta(^1\text{H})$/ppm	$\Delta\delta(^1\text{H})$ / ppm $^{a)}$
H^1	6.31	8.18	−1.87
H^2	7.28	7.85	−0.57
H^3	7.03	6.68	0.35
H^4	6.90	6.84	0.06
H^5	7.19	7.58	−0.39
H^6	5.06	6.70	−1.64
H^7	5.87	6.51	−0.64

a) $\Delta\delta(^1\text{H}) = \delta(^1\text{H})(\textbf{6c}) - \delta(^1\text{H})(\textbf{6c}^{2-})$, n.d. = not determined.

Table S4. ^{13}C NMR chemical shifts of the main core of **6c** and **6c**$^{2-}$.

	6c $\delta(^{13}\text{C})$ /ppm	**6c**$^{2-}$ $\delta(^{13}\text{C})$ /ppm	$\Delta\delta(^{13}\text{C})$ / ppm ^{a}		**6c** $\delta(^{13}\text{C})$ /ppm	**6c**$^{2-}$ $\delta(^{13}\text{C})$ /ppm	$\Delta\delta(^{13}\text{C})$ / ppm ^{a}
C^1	119.1	110.0	9.10	C^7	129.0	113.0	16.0
C^2	148.8	134.9	13.9	C^8	126.7	117.6	9.10
C^3	130.5	107.2	23.3	C^9	126.7	120.3	6.40
C^4	126.93	115.9	11.0	C^{9a}	136.2	127.6	8.60
C^{4a}	137.5	121.9	15.6	C^{10}	134.5	105.8	28.7
C^{4b}	n.d.	101.32	–	C^{10a}	146.7	137.95	8.75

33

C^{4c}	136.8	129.4	7.40	C^{11}	n.d.	88.8	–
C^5	124.8	110.8	14.0	C^{11a}	n.d.	146.2	–
C^{5a}	138.2	123.3	14.9	C^{12}	126.86	91.8	35.1
C^6	125.5	121.8	3.70	C^{12a}	n.d.	137.9	–

a) $\Delta\delta(^{13}C) = \delta(^{13}C)(\mathbf{6c}) - \delta(^{13}C)(\mathbf{6c}^{2-})$, n.d. = not determined.
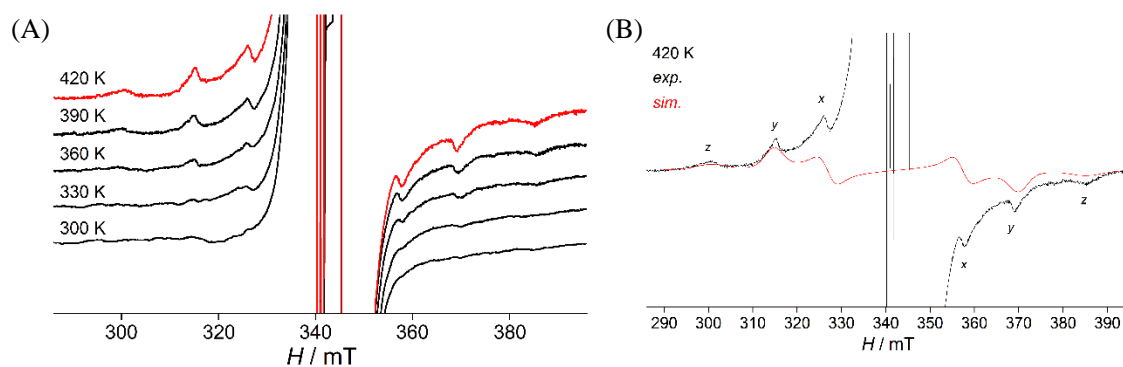

Figure S7. ESR spectra of a solid sample of **6c**. (A) Temperature-dependent ESR spectra. (B) simulated (red) and observed (black) spectra ($\Delta M_s = \pm 1$) at 420 K. The microwave frequency used was 9.60730 GHz. The zero field splitting parameters and *g*-value were determined as $|D| = 42.6$ mT $= 0.0398$ cm^{-1}, $|E| = 4.13$ mT $= 0.00386$ cm^{-1} and $|E/D| = 0.0970$, and *g*-value $= 2.002$ (line width parameters; $x = 3.5$ mT, $y = 4.0$ mT, $z = 6.5$ mT) by the spectral simulation.
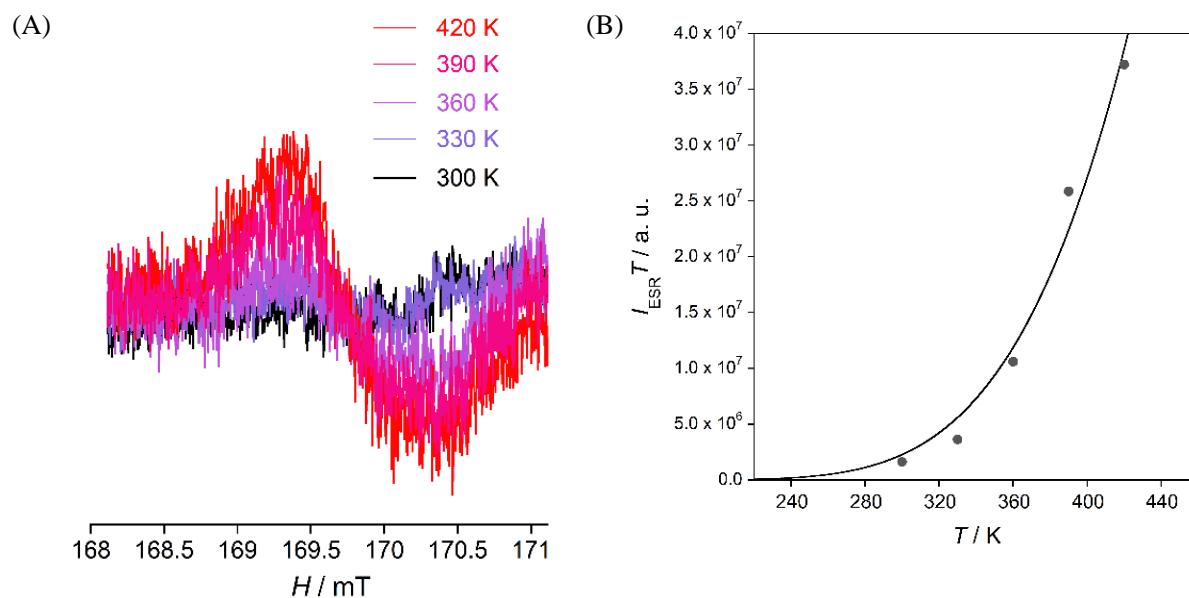

Figure S8. ESR spectra of the solid sample of **6c**. (A) Temperature-dependent ESR spectra ($\Delta M_s = \pm 2$). (B) The change in ESR signal intensity with temperature (○) and the Bleaney–Bowers fit (—).

(A) ESR spectrum plot, x-axis labeled H / mT ranging 339 to 345.

(B) plot, y-axis labeled $I_{ESR}T$ / Normalized ranging 1.0 to 2.0, x-axis labeled T / K ranging 200 to 360.
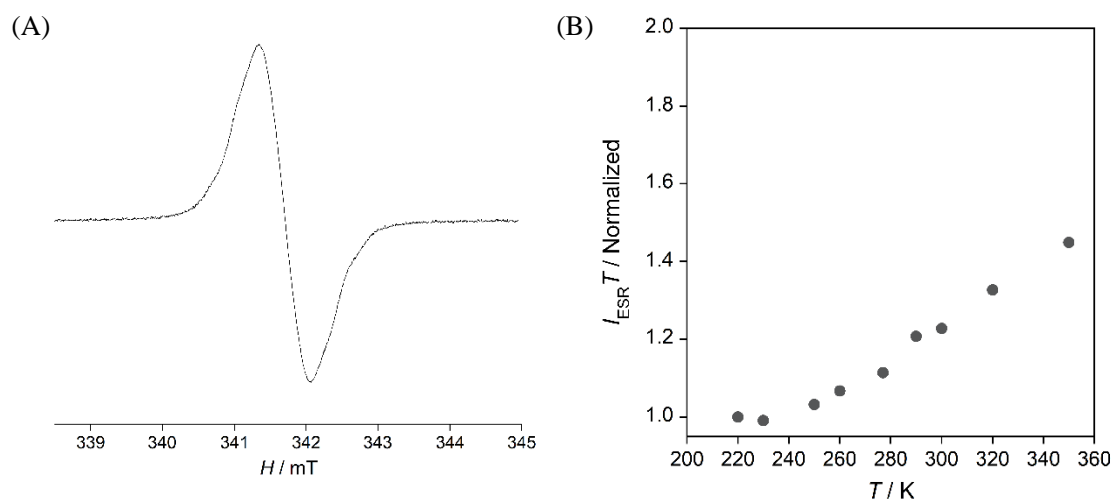
Figure S9. (A) ESR spectrum of a toluene solution of **6c**. 9.57726 GHz, g-value = 2.00263, Gain = 5000, sweep time = 5 min, modulation amplitude = 0.05 mT. (B) The temperature dependency of the ESR signal intensities in the fluid toluene solution.
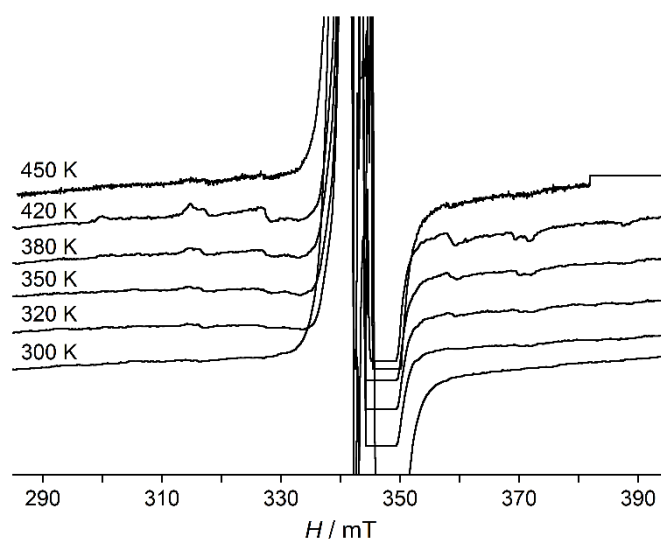

ESR spectra at 450 K, 420 K, 380 K, 350 K, 320 K, 300 K; x-axis labeled H / mT ranging 290 to 390.

Figure S10. ESR spectra of a solid sample of **6b**. Above 420 K, the signals of thermally excited species of **6b** disappeared and never recovered after re-cooling because of its thermodecomposition. At 450 K, the recording the signals was stopped at 380 mT since no fine structure was observed.
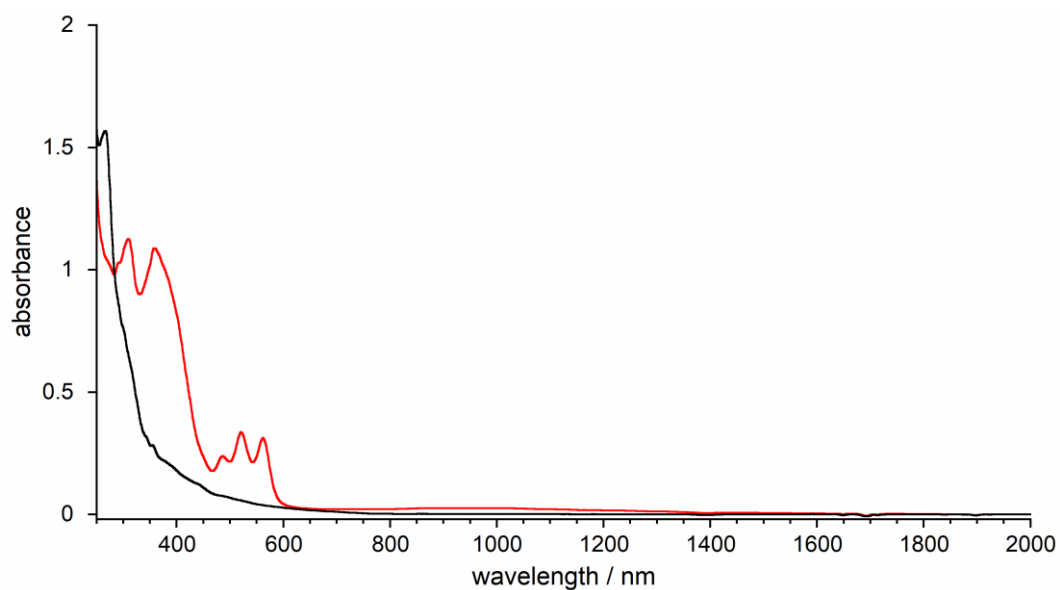
Figure S11. Electronic absorption spectra of **6b** in CH_2Cl_2 under N_2 atmosphere (red) and after 5 min of exposure to air (black).
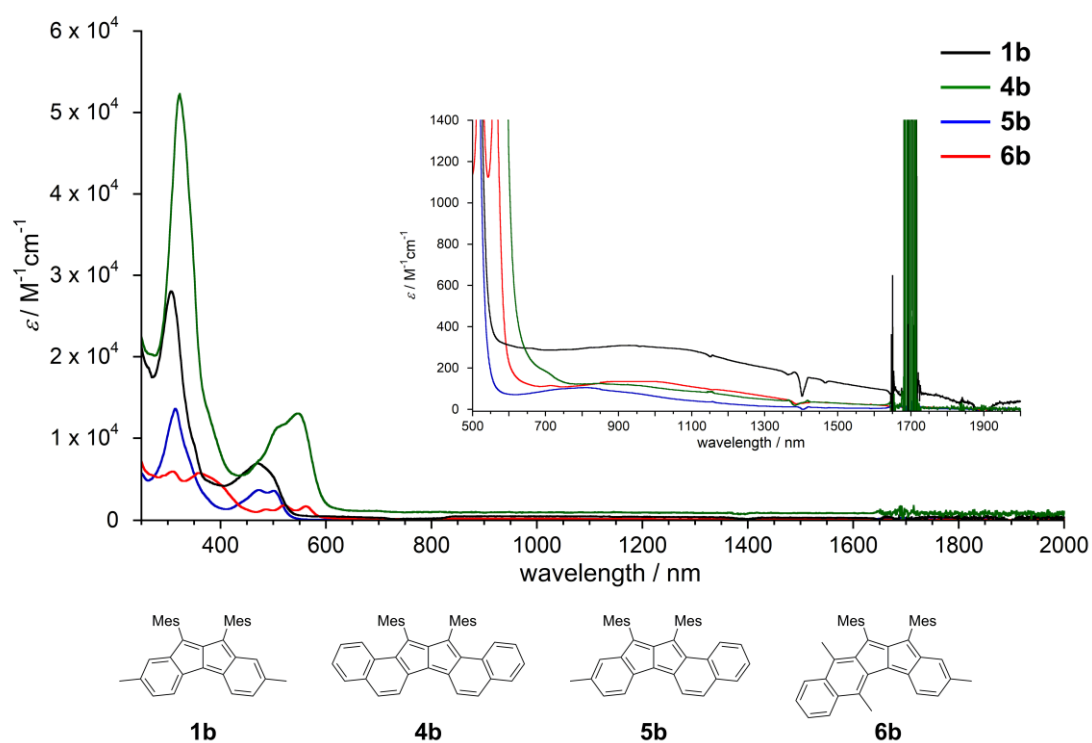

Figure S12. UV/vis/NIR absorption spectra of **1b** (black), **4b** (green), **5b** (blue), and **6b** (red) in CH_2Cl_2. The inset shows a magnified view. The background signals at 1700 nm arose from an overtone of the C−H vibrations of the solvent.
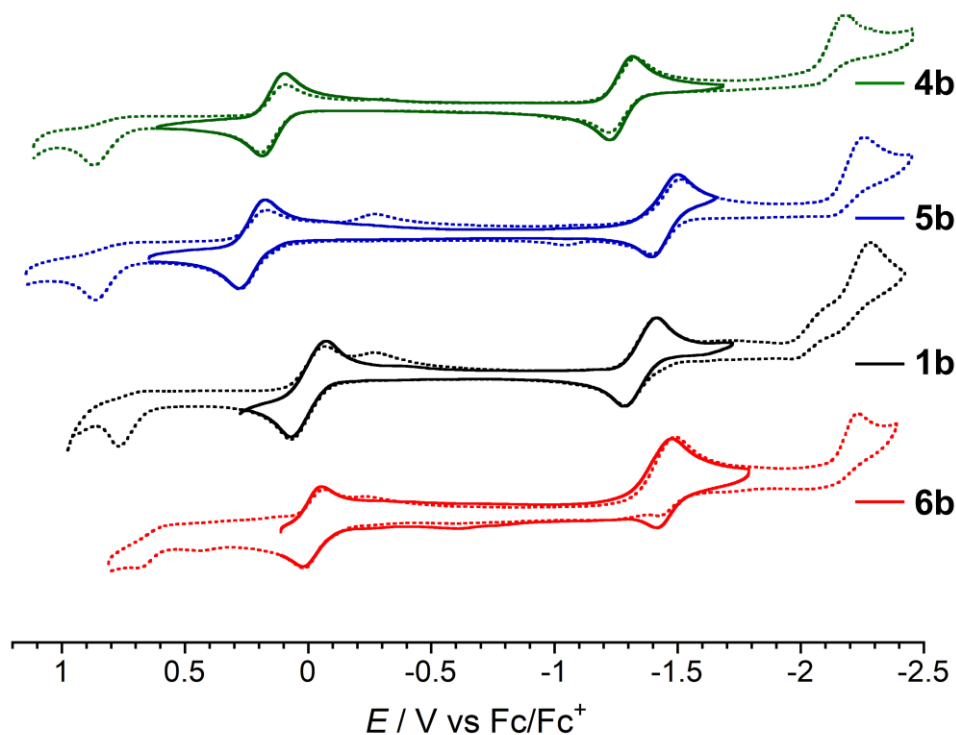
Figure S13. Cyclic voltammograms of **1b** (black), **4b** (green), **5b** (blue), and **6b** (red) (V vs Fc/Fc⁺, in 0.1 M nBu$_4$NClO$_4$/CH$_2$Cl$_2$, scan rate = 100 mV/s, room temperature).

**Table S5**. Summary of the Optoelectronic Properties of **1b**, **4b**, **5b**, and **6b**

comp.	optical[a]		electrochemical[b]				
	λ_{max} / nm	ΔE_{gap}	$E_2^{ox, pa}$	E_1^{ox}	E_1^{red}	$E_2^{red, pc}$	$\Delta^{redox} E_1$
	(ε / M^{-1} cm^{-1})	/ eV	/ V	/ V	/ V	/ V	/ eV
1b	965 (306)	1.28	+0.77	0.0	−1.34	−2.28	1.34
4b	925 (120)	1.53	+0.87	+0.13	−1.28	−2.18	1.41
5b	808 (105)	1.34	+0.86	+0.23	−1.45	−2.26	1.68
6b	983 (135)	1.26	+0.67	−0.018	−1.45	−2.23	1.43

a) The optical gap ΔE_{gap} is estimated from $\Delta E_{gap} = 1240/\lambda_{max}$. *b*) All potentials given versus the Fc/Fc⁺ couple used as internal standard. $\Delta^{redox} E_1 = E_1^{ox} - E_1^{red}$.
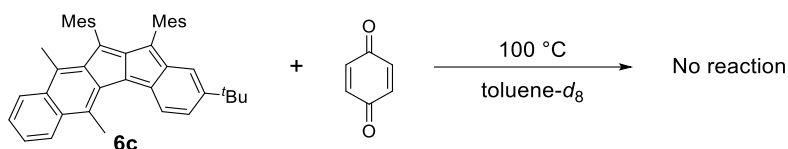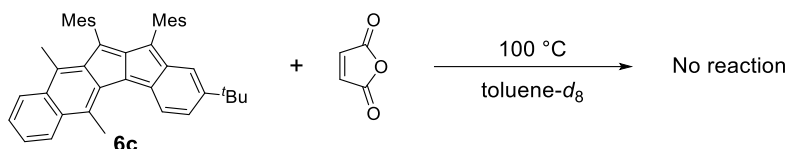
In a nitrogen-filled glove box, to a solution of **6c** (10 mg, 0.017 mmol) in toluene-d_8 (0.4 mL) was added 1,4-benzoquinone (0.017 mmol) at room temperature. The reaction mixture was loaded with a NMR tube with a J.YOUNG valve and was heated at 100 ℃. Periodical ^{1}H NMR monitoring of the reaction mixture indicated no consumption of **6c**.

Figure S14. ^{1}H NMR spectra (400 MHz, toluene-d_8, rt) of the reaction mixture of **6c** and 1,4-benzoquinone.
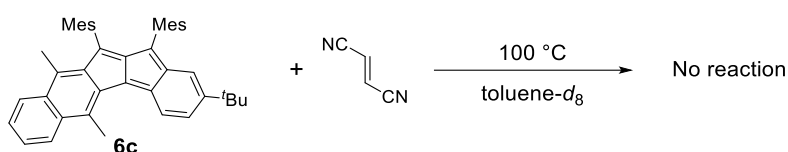
In a nitrogen-filled glove box, to a solution of **6c** (10 mg, 0.017 mmol) in toluene-d_8 (0.4 mL) was added fumaronitrile (0.017 mmol) at room temperature. The reaction mixture was loaded with a NMR tube with a J.YOUNG valve and was heated at 100 ℃. Periodical ^{1}H NMR monitoring of the reaction mixture indicated no consumption of **6c**.

Figure S15. ^{1}H NMR spectra (400 MHz, toluene-d_8, rt) of the reaction mixture of **6c** and fumaronitrile.

In a nitrogen-filled glove box, to a solution of **6c** (10 mg, 0.017 mmol) in toluene-d_8 (0.4 mL) was added maleic anhydride (0.017 mmol) at room temperature. The reaction mixture was loaded with a NMR tube with a J.YOUNG valve and was heated at 100 ℃. Periodical ^{1}H NMR monitoring of the reaction mixture indicated no consumption of **6c**.

Figure S16. ^{1}H NMR spectra (400 MHz, toluene-d_8, rt) of the reaction mixture of **6c** and maleic anhydride.
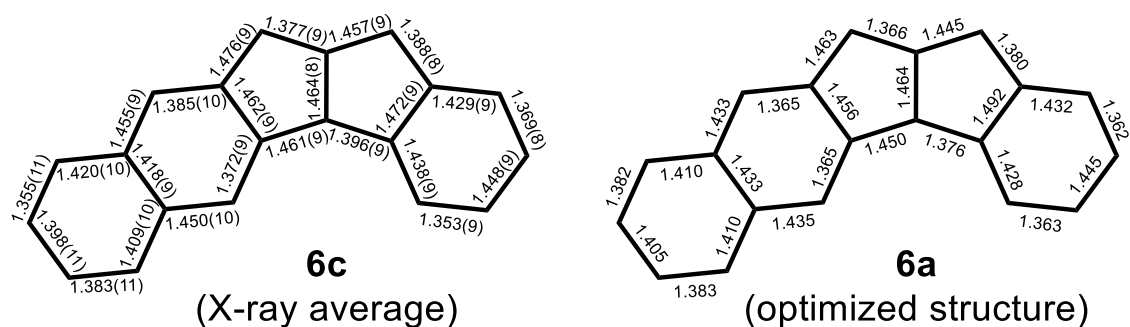
Theoretical calculations

Figure S17. Summary for the bond lengths (Å) of the main core of **6c** and computationally optimized structure of **6a** at the RB3LYP-D3/6-311G* level.
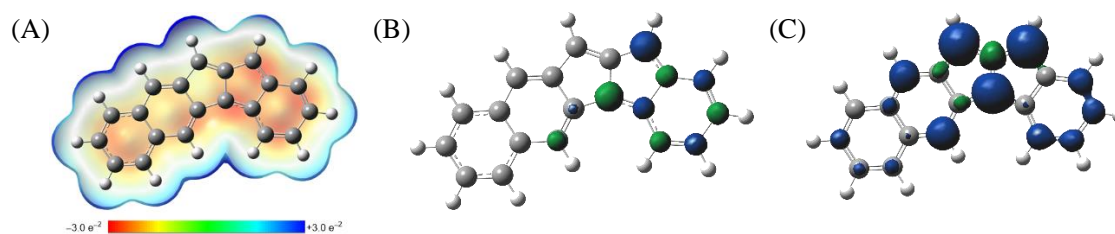
Figure S18. (A) Electrostatic potential map of **6a** drawn at the contour level of 0.0015 / Å^3 calculated at the (BS)-UB3LYP-D3/6-311G* level. Spin density distribution (the contour level of 0.003 / Å^3) of the (B) singlet and (C) triplet state of **6a** calculated by the (BS)-UB3LYP-D3/6-311G* level. Positive (blue) and negative (green) spin densities are shown.
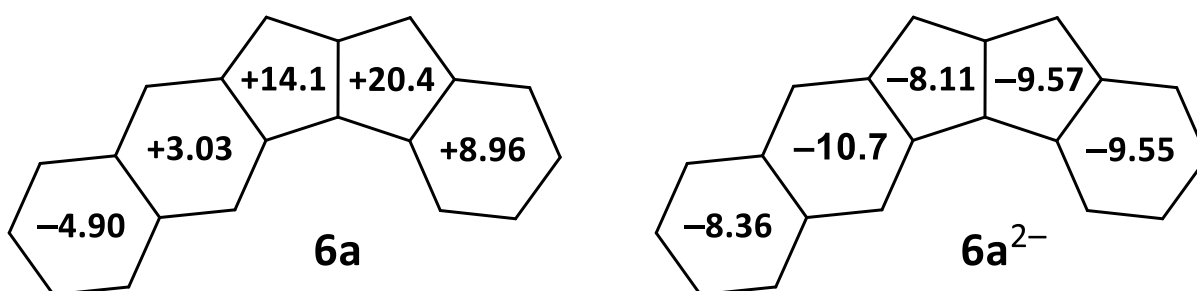
Figure S19. Summary for NICS(1) values for **6a** and **6a**$^{2-}$ calculated at the GIAO-(R/U)B3LYP/6-311+G*//RB3LYP-D3/6-311G* level.
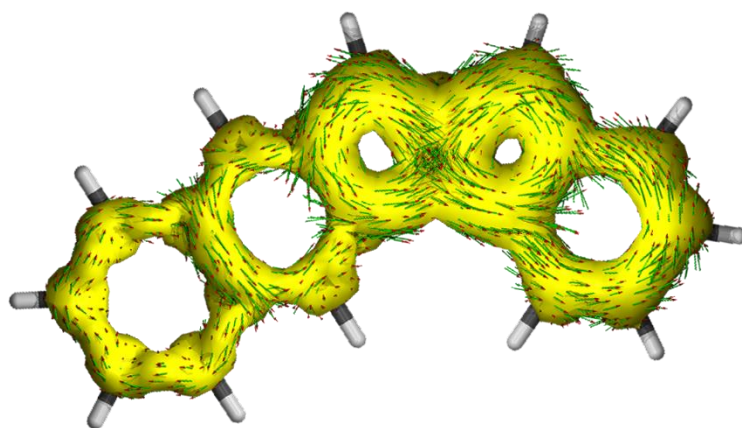
Figure S20. Summary for AICD plots (isovalue surface: 0.035) of **6a** calculated at the CSGT-UB3LYP/6-311+G*//RB3LYP-D3/6-311G* level.
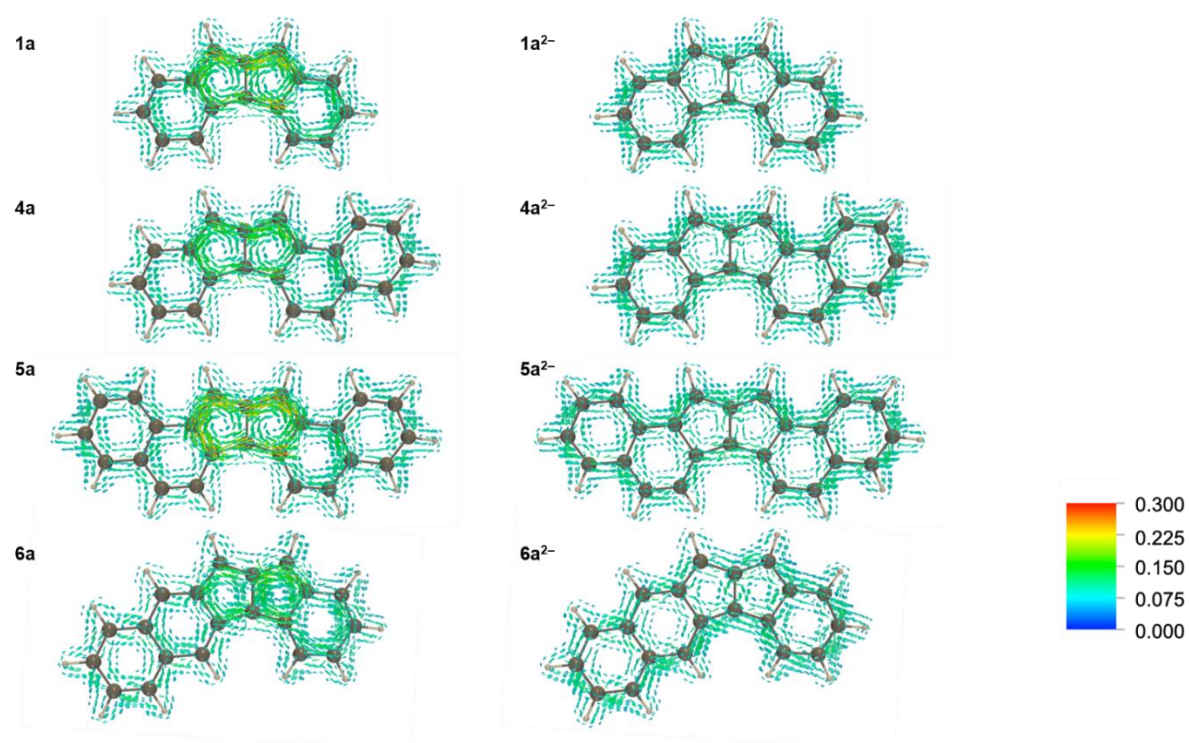
Figure S21. Magnetically-induced current density for **1a**, **4a**, **5a**, **6a** and their dianions calculated at the GIAO-(R/U)B3LYP/6-311+G* level. Diatropic currents rotate clockwise, while the paratropic ones do anticlockwise. The values in the color bar are given in a.u. The current vectors are scaled with a factor of 3 Å a.u.$^{-1}$, where 1 a.u. = 100.63 nA T^{-1} Å^{-2}. The results for **1a**, **4a** and **5a** are taken from our previous paper.[46]
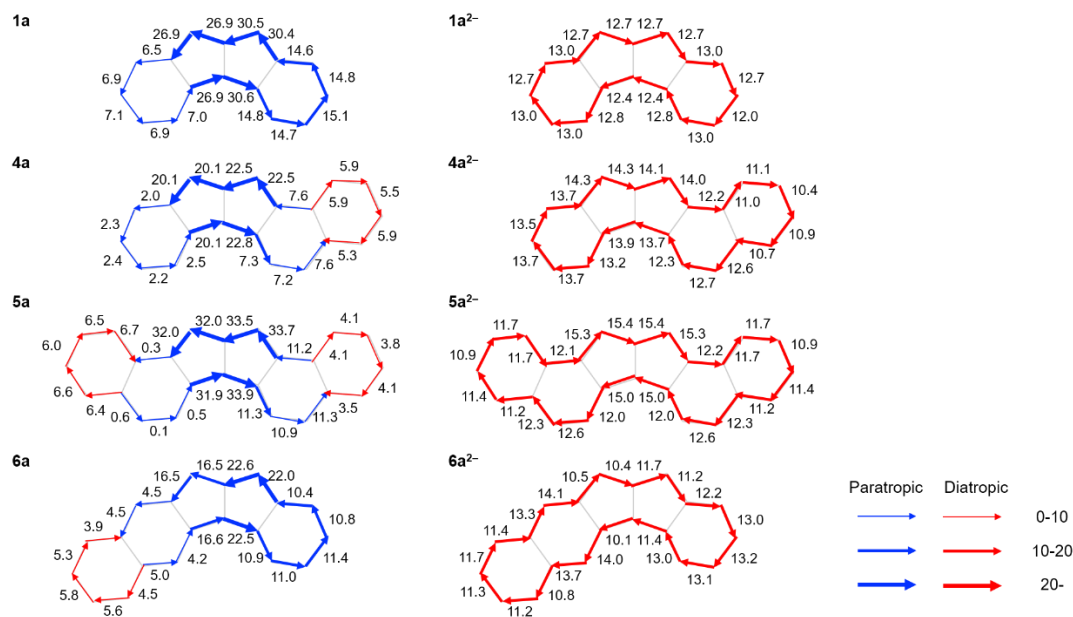
Figure S22. Current strength [nA T^{-1}] for the peripheral C–C bonds of each system. Current strength is evaluated by integrating numerically the MIC densities on the bisection plane of each bond. Diatropic currents rotate clockwise, while the paratropic ones do anticlockwise. The results for **1a**, **4a** and **5a** are taken from our previous paper.[46]

Table S6. Singlet-Triplet energy gaps of **6a**, **6b'** and **6c'**. Single point total energies were calculated at the SF-NC-TDDFT PBE50/6-311G*//(R/U)B3LYP-D3/6-311G* level. Zero-point vibrational energy (ZPVE) correction was estimated from the frequency analysis at the (R/U)B3LYP-D3/6-311G* level.

	6a	**6b'**	**6c'**	
			Conformer 1	**Conformer 2**
E(S)@S [hartree] [a]	−768.640228	−1348.196758	−1466.036723	−1466.039527
E(T)@S [hartree] [a]	−768.621018	−1348.179310	−1466.022839	−1466.022111
E(S)@S +ZPVE [hartree]	−768.389999	−1347.700970	−1465.455631	−1465.458372
E(T)@T [hartree] [a]	−768.638314	−1348.194840	−1466.037420	−1466.037013
E(T)@T +ZPVE [hartree]	−768.389538	−1347.700262	−1465.457128	−1465.456844
Vertical ΔE_{ST} [kcal/mol]	‑12.1	‑10.9	‑8.71	‑10.9
Adiabatic ΔE_{ST} (+ZPVE) [kcal/mol]	‑0.29	‑1.86	‑0.78 [b]	

[a]E(X)@Y represents the total energy of spin state X (Singlet or Triplet) for a local minimum geometry of spin state Y (Singlet or Triplet). [b]Energy difference between the red-colored values.

Conformer 1 Singlet
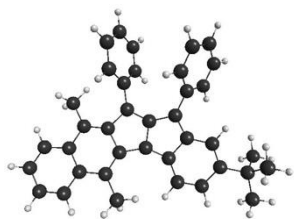
Conformer 2 Singlet
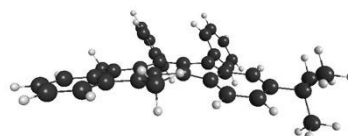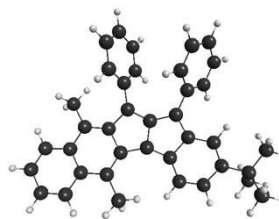
Conformer 1 Triplet

Conformer 2 Triplet
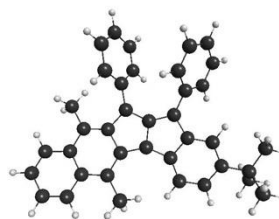
Figure S23. Geometries of conformers of **6c'** obtained from the geometry optimizations.
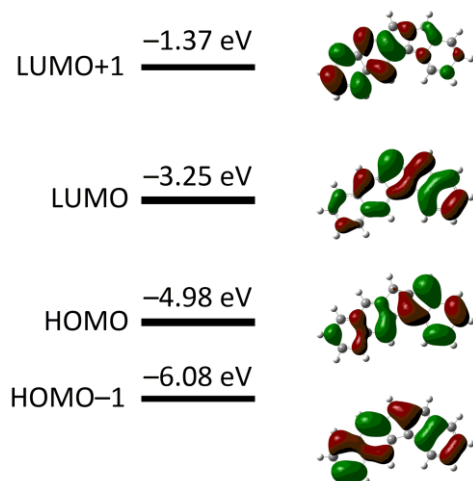
Figure S24. Calculated orbital energy diagram of HOMO–1, HOMO, LUMO, LUMO+1 for **6a** at the RB3LYP/6-311+G* level. Green and red meshes represent the isosurfaces with contour values of +0.02/–0.02 a.u., respectively.

Table S7. Summary of the calculated orbital energies of HOMO–1, HOMO, LUMO, LUMO+1 for **1a**,[46] **4a**,[46] **5a**,[46] and **6a** calculated at the RB3LYP/6-311+G* level
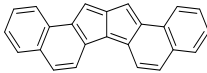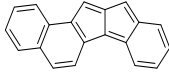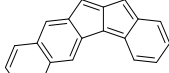
comp.	HOMO–1 / eV	HOMO / eV	LUMO / eV	LUMO+1 / eV	$\Delta E_{\text{HOMO–LUMO}}$ / eV
1a	–6.29	–5.01	–3.31	–0.60	1.70
4a	–5.86	–5.02	–3.28	–1.20	1.74
5a	–6.05	–5.14	–3.15	–1.14	1.99
6a	–6.08	–4.98	–3.25	–1.37	1.73

Table S8. Excitation energies of **6a** calculated at the TD-UB3LYP/6-311+G*//RB3LYP-D3/6-311G* level. [a)]

Excited state number	Excitation energy / eV (wavelength / nm)	Excitation amplitudes		Oscillator strength
2	1.06 (1164)	0.729	(HOMOβ – LUMOβ)	0.0089
($<S^2>$ = 0.016)		–0.681	(HOMOα – LUMOα)	
4	2.36 (525)	0.634	(HOMO-2α – LUMOα)	0.0090
($<S^2>$ = 1.914)		–0.572	(HOMO-2β – LUMOβ)	
		–0.281	(HOMO-1α – LUMOα)	
		–0.247	(HOMOβ – LUMO+1β)	
5	2.42 (511)	0.652	(HOMO-1β – LUMOβ)	0.1406
($<S^2>$ = 0.103)		0.585	(HOMO-1α – LUMOα)	
		0.294	(HOMOβ – LUMO+1β)	
		–0.266	(HOMOα – LUMO+1α)	

a) $<S^2>$ of S_0 state at the UB3LYP/6-311G(d) level is calculated to be 0.0415.

Table S9. Excitation energies of **6a** calculated at the TD-RB3LYP/6-311+G*//RB3LYP-D3/6-311G* level.

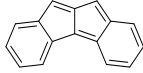| Excited state number	Excitation energy / eV (wavelength / nm)	Excitation amplitudes		Oscillator strength
1	1.06 (1169)	0.708	(HOMO – LUMO)	0.0091
2	2.42 (512)	0.634	(HOMO-1 – LUMO)	0.1522
		–0.289	(HOMO – LUMO+1)	
3	2.90 (427)	0.695	(HOMO-2 – LUMO)	0.0005
4	3.42 (363)	0.623	(HOMO – LUMO+1)	0.7071
		0.259	(HOMO-1 – LUMO)	
		0.149	(HOMO – LUMO+2)	
5	3.72 (333)	0.468	(HOMO – LUMO+2)	0.0061
		0.440	(HOMO-3 – LUMO)	
		0.219	(HOMO-4 – LUMO)	
		0.121	(HOMO-1 – LUMO+1)	
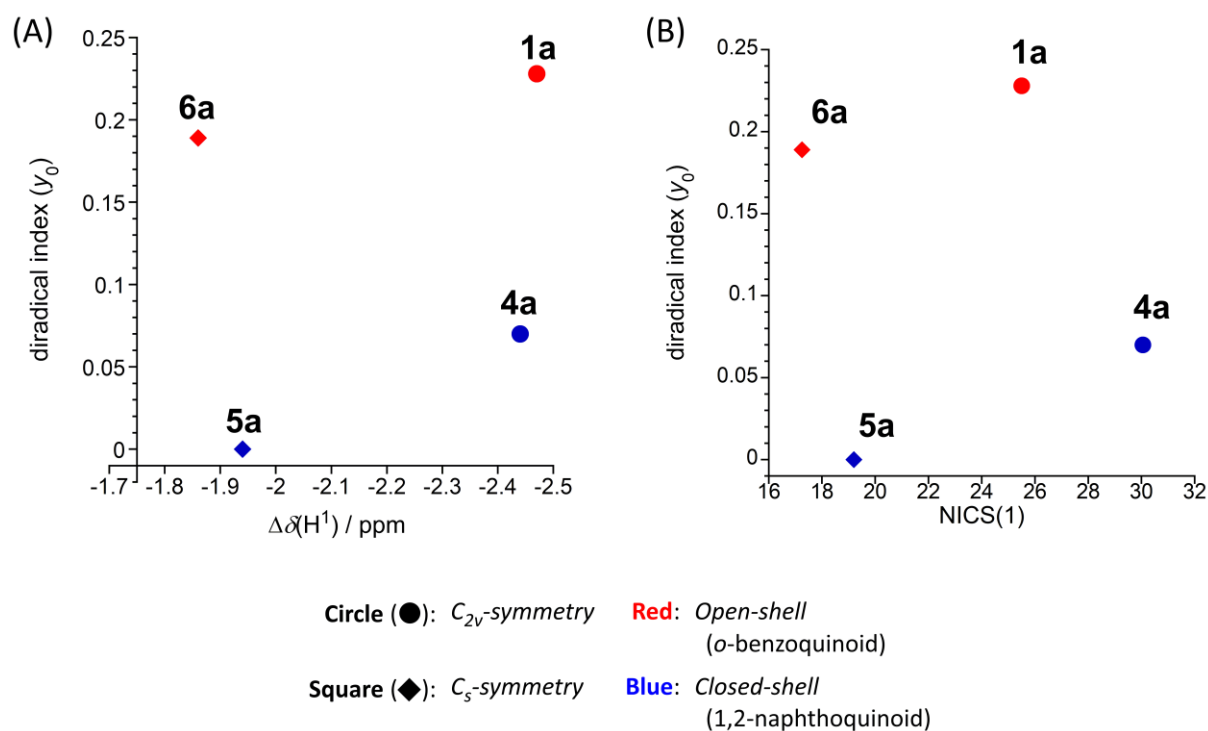
Figure S25. Plot of the behaviors of open-shell features (y_0 or ΔE_{S-T}) against antiaromatic features ($\Delta\delta(H^1)$ or NICS(1)) for our pentalenes **1** and **4–6**. Plots for (A) y_0–$\Delta\delta(H^1)$ and (B) y_0–NICS(1). The diradical index (y_0) was calculated at the LC-UBLYP ($\mu = 0.33$ bohr^{-1})/6-311G* level. The difference in the proton chemical shift ($\Delta\delta(H^1)$) was based on the ^{1}H NMR measurements for the dianion/neutral pentalenes. The NICS(1) values of calculated at the GIAO-UB3LYP/6-311+G* level. The averaged values of two pentagons were plotted.

Table S10. Calculated Singlet–Triplet energy gaps of **1a/6a** and **4a/5a**. Single point total energies were calculated at the SF-NC-TDDFT PBE50/6-311G*//(R/U)B3LYP-D3/6-311G* level. Zero-point vibrational energy (ZPVE) correction was estimated from the frequency analysis at the (R/U)B3LYP-D3/6-311G* level.

	1a	**6a**	**4a**	**5a**
Vertical ΔE_{ST} @ singlet geometry [kcal/mol]	‑10.4	‑12.1	‑16.0	‑19.6
Relaxation energy for triplet state [kcal/mol]	12.9	10.9	9.9	12.4
Adiabatic ΔE_{ST} (w/o ZPVE) [kcal/mol]	+2.5	‑1.2	‑6.1	–8.2
Adiabatic ΔE_{ST} (w/ ZPVE) [kcal/mol]	+3.2	‑0.3	‑5.3	‑7.3

Triplet PES

Relaxation energy for Triplet

Singlet PES

Vertical ΔE_{ST}

Adiabatic ΔE_{ST} w/o ZPVE

Adiabatic ΔE_{ST} w/ ZPVE
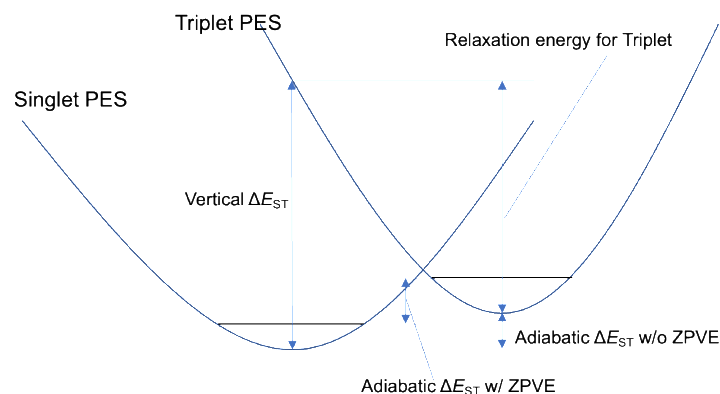
1-5. Reference

(1)   Borden, W. T. *Diradicals*; Borden, W. T., Ed.; Wiley-Interscience: New York, 1982.

(2)   Sun, Z.; Ye, Q.; Chi, C.; Wu, J. Low Band Gap Polycyclic Hydrocarbons: From Closed-Shell Near Infrared Dyes and Semiconductors to Open-Shell Radicals. *Chem. Soc. Rev.* **2012**, *41*, 7857–7889.

(3)   Sun, Z.; Zeng, Z.; Wu, J. Benzenoid Polycyclic Hydrocarbons with an Open-Shell Biradical Ground State. *Chem. Asian J.* **2013**, *8*, 2894–2904.

(4)   Abe, M. Diradicals. *Chem. Rev.* **2013**, *113*, 7011–7088.

(5)   Kubo, T. Recent Progress in Quinoidal Singlet Biradical Molecules. *Chem. Lett.* **2015**, *44*, 111–122.

(6)   Konishi, A.; Kubo, T. Benzenoid Quinodimethanes. *Top. Curr. Chem.* **2017**, *375*, 83.

(7)   Nakano, M. Open-Shell-Character-Based Molecular Design Principles: Applications to Nonlinear Optics and Singlet Fission. *Chem. Rec.* **2017**, *17*, 27–62.

(8)   Koike, H.; Chikamatsu, M.; Azumi, R.; Tsutsumi, J.; Ogawa, K.; Yamane, W.; Nishiuchi, T.; Kubo, T.; Hasegawa, T.; Kanai, K. Stable Delocalized Singlet Biradical Hydrocarbon for Organic Field-Effect Transistors. *Adv. Funct. Mater.* **2016**, *26*, 277–283.

(9)   Rudebusch, G. E.; Zafra, J. L.; Jorner, K.; Fukuda, K.; Marshall, J. L.; Arrechea-Marcos, I.; Espejo, G. L.; Ponce Ortiz, R.; Gómez-García, C. J.; Zakharov, L. N.; Nakano, M.; Ottosson, H.; Casado, J.; Haley, M. M. Diindeno-Fusion of an Anthracene as a Design Strategy for Stable Organic Biradicals. *Nat. Chem.* **2016**, *8*, 753–759.

(10)   Zeidell, A. M.; Jennings, L.; Frederickson, C. K.; Ai, Q.; Dressler, J. J.; Zakharov, L. N.; Risko, C.; Haley, M. M.; Jurchescu, O. D. Organic Semiconductors Derived from Dinaphtho-Fused s -Indacenes: How Molecular Structure and Film Morphology Influence Thin-Film Transistor Performance. *Chem. Mater.* **2019**, *31*, 6962–6970.

(11)   Hsieh, Y.; Wu, C.-F.; Chen, Y.-T.; Fang, C.; Wang, C.; Li, C.; Chen, L.; Cheng, M.; Chueh, C.; Chou, P.; Wu, Y. 5,14-Diaryldiindeno[2,1-*f*:1′,2′-*j*]Picene: A New Stable [7]Helicene with a Partial Biradical Character. *J. Am. Chem. Soc.* **2018**, *140*, 14357–14366.

(12)   Jousselin-Oba, T.; Mamada, M.; Marrot, J.; Maignan, A.; Adachi, C.; Yassar, A.; Frigoli, M. Excellent Semiconductors Based on Tetracenotetracene and Pentacenopentacene: From Stable Closed-Shell to Singlet Open-Shell. *J. Am. Chem. Soc.* **2019**, *141*, 9373–9381.

(13)   Melidonie, J.; Dmitrieva, E.; Zhang, K.; Fu, Y.; Popov, A. A.; Pisula, W.; Berger, R.; Liu, J.; Feng, X. Dipyrene-Fused Dicyclopenta[*a,f*]Naphthalenes. *J. Org. Chem.* **2020**, *85*, 215–223.

(14)   Jousselin-Oba, T.; Mamada, M.; Okazawa, A.; Marrot, J.; Ishida, T.; Adachi, C.; Yassar, A.; Frigoli, M. Modulating the Ground State, Stability and Charge Transport in OFETs of Biradicaloid Hexahydro-Diindenopyrene Derivatives and a Proposed Method to Estimate the Biradical Character. *Chem. Sci.* **2020**, *11*, 12194–12205.

(15)   Nakano, M.; Kubo, T.; Kamada, K.; Ohta, K.; Kishi, R.; Ohta, S.; Nakagawa, N.; Takahashi, H.; Furukawa, S. I.; Morita, Y.; Nakasuji, K.; Yamaguchi, K. Second Hyperpolarizabilities of Polycyclic Aromatic Hydrocarbons Involving Phenalenyl Radical Units. *Chem. Phys. Lett.* **2006**, *418*, 142–147.

(16)   Zeng, Z.; Lee, S.; Son, M.; Fukuda, K.; Burrezo, P. M.; Zhu, X.; Qi, Q.; Li, R.-W.; Navarrete, J. T. L.; Ding, J.; Casado, J.; Nakano, M.; Kim, D.; Wu, J. Push–Pull Type Oligo(*N*-Annulated Perylene)Quinodimethanes: Chain Length and Solvent-Dependent Ground States and Physical Properties. *J. Am. Chem. Soc.* **2015**, *137*, 8572–8583.

(17)   Nakano, M.; Champagne, B. Theoretical Design of Open-Shell Singlet Molecular Systems for Nonlinear Optics. *J. Phys. Chem. Lett.* **2015**, *6*, 3236–3256.

(18)   Smith, M. B.; Michl, J. Singlet Fission. *Chem. Rev.* **2010**, *110*, 6891–6936.

(19)   Minami, T.; Nakano, M. Diradical Character View of Singlet Fission. *J. Phys. Chem. Lett.* **2012**, *3*, 145–150.

(20)   Wen, J.; Havlas, Z.; Michl, J. Captodatively Stabilized Biradicaloids as Chromophores for Singlet Fission. *J. Am. Chem. Soc.* **2015**, *137*, 165–172.

(21)   Miyoshi, H.; Nobusue, S.; Shimizu, A.; Hisaki, I.; Miyata, M.; Tobe, Y. Benz[*c*]Indeno[2,1-*a*]Fluorene: A 2,3-Naphthoquinodimethane Incorporated into an Indenofluorene Frame. *Chem. Sci.* **2014**, *5*, 163–168.

(22)   Hacker, A. S.; Pavano, M.; Wood, J. E.; Hashimoto, H.; D'Ambrosio, K. M.; Frederickson, C. K.; Zafra, J. L.; Gómez-García, C. J.; Postils, V.; Ringer McDonald, A.; Casanova, D.; Frantz, D. K.; Casado, J. Fluoreno[2,1-*a*]Fluorene: An *Ortho* -Naphthoquinodimethane-Based System with Partial Diradical Character. *Chem. Commun.* **2019**, *55*, 14186–14189.

(23)   Frederickson, C. K.; Rose, B. D.; Haley, M. M. Explorations of the Indenofluorenes and Expanded Quinoidal Analogues. *Acc. Chem. Res.* **2017**, *50*, 977–987.

(24)   Sahara, K.; Abe, M.; Zipse, H.; Kubo, T. Duality of Reactivity of a Biradicaloid Compound with an *o*-Quinodimethane Scaffold. *J. Am. Chem. Soc.* **2020**, *142*, 5408–5418.

(25) Motomura, S.; Nakano, M.; Fukui, H.; Yoneda, K.; Kubo, T.; Carion, R.; Champagne, B. Size Dependences of the Diradical Character and the Second Hyperpolarizabilities in Dicyclopenta-Fused Acenes: Relationships with Their Aromaticity/Antiaromaticity. *Phys. Chem. Chem. Phys.* **2011**, *13*, 20575–20583.

(26) Nagami, T.; Fujiyoshi, J.; Tonami, T.; Watanabe, K.; Yamane, M.; Okada, K.; Kishi, R.; Nakano, M.; Champagne, B.; Liégeois, V. Evaluation of Aromaticity for Open-Shell Singlet Dicyclopenta-Fused Acenes and Polyacenes Based on a Magnetically Induced Current. *Chem. Eur. J.* **2018**, *24*, 13457–13466.

(27) Benkyi, I.; Staszewska-Krajewska, O.; Gryko, D. T.; Jaszuński, M.; Stanger, A.; Sundholm, D. Interplay of Aromaticity and Antiaromaticity in N-Doped Nanographenes. *J. Phys. Chem. A* **2020**, *124*, 695–703.

(28) Allen, A. D.; Tidwell, T. T. Antiaromaticity in Open-Shell Cyclopropenyl to Cycloheptatrienyl Cations, Anions, Free Radicals, and Radical Ions. *Chem. Rev.* **2001**, *101*, 1333–1348.

(29) Zeng, Z.; Shi, X.; Chi, C.; López Navarrete, J. T.; Casado, J.; Wu, J. Pro-Aromatic and Anti-Aromatic π-Conjugated Molecules: An Irresistible Wish to Be Diradicals. *Chem. Soc. Rev.* **2015**, *44*, 6578–6596.

(30) Yoshida, T.; Takahashi, K.; Ide, Y.; Kishi, R.; Fujiyoshi, J.; Lee, S.; Hiraoka, Y.; Kim, D.; Nakano, M.; Ikeue, T.; Yamada, H.; Shinokubo, H. Benzonorcorrole NiII Complexes: Enhancement of Paratropic Ring Current and Singlet Diradical Character by Benzo-Fusion. *Angew. Chem. Int. Ed.* **2018**, *57*, 2209–2213.

(31) Konishi, A.; Horii, K.; Shiomi, D.; Sato, K.; Takui, T.; Yasuda, M. Open-Shell and Antiaromatic Character Induced by the Highly Symmetric Geometry of the Planar Heptalene Structure: Synthesis and Characterization of a Nonalternant Isomer of Bisanthene. *J. Am. Chem. Soc.* **2019**, *141*, 10165–10170.

(32) Shimizu, A.; Kishi, R.; Nakano, M.; Shiomi, D.; Sato, K.; Takui, T.; Hisaki, I.; Miyata, M.; Tobe, Y. Indeno[2,1-*b*]Fluorene: A 20-π-Electron Hydrocarbon with Very Low-Energy Light Absorption. *Angew. Chem. Int. Ed.* **2013**, *52*, 6076–6079.

(33) Dressler, J. J.; Cárdenas Valdivia, A.; Kishi, R.; Rudebusch, G. E.; Ventura, A. M.; Chastain, B. E.; Gómez-García, C. J.; Zakharov, L. N.; Nakano, M.; Casado, J.; Haley, M. M. Diindenoanthracene Diradicaloids Enable Rational, Incremental Tuning of Their Singlet-Triplet Energy Gaps. *Chem* **2020**, *6*, 1353–1368.

(34) Miyoshi, H.; Miki, M.; Hirano, S.; Shimizu, A.; Kishi, R.; Fukuda, K.; Shiomi, D.; Sato, K.; Takui, T.; Hisaki, I.; Nakano, M.; Tobe, Y. Fluoreno[2,3-*b*]Fluorene vs Indeno[2,1-*b*]Fluorene: Unusual Relationship between the Number of π Electrons and Excitation Energy in *m*-Quinodimethane-Type Singlet Diradicaloids. *J. Org. Chem.* **2017**, *82*, 1380–1388.

(35) Tobe, Y. Quinodimethanes Incorporated in Non-Benzenoid Aromatic or Antiaromatic Frameworks. *Top. Curr. Chem.* **2018**, *376*, 12.

(36) Dressler, J. J.; Haley, M. M. Learning How to Fine-tune Diradical Properties by Structure Refinement. *J. Phys. Org. Chem.* **2020**, *33*, 1–13.

(37) Di Giovannantonio, M.; Eimre, K.; Yakutovich, A. V.; Chen, Q.; Mishra, S.; Urgel, J. I.; Pignedoli, C. A.; Ruffieux, P.; Müllen, K.; Narita, A.; Fasel, R. On-Surface Synthesis of Antiaromatic and Open-Shell Indeno[2,1-*b*]Fluorene Polymers and Their Lateral Fusion into Porous Ribbons. *J. Am. Chem. Soc.* **2019**, *141*, 12346–12354.

(38) Dressler, J. J.; Barker, J. E.; Karas, L. J.; Hashimoto, H. E.; Kishi, R.; Zakharov, L. N.; MacMillan, S. N.; Gomez-Garcia, C. J.; Nakano, M.; Wu, J. I.; Haley, M. M. Late-Stage Modification of Electronic Properties of Antiaromatic and Diradicaloid Indeno[1,2-*b*]Fluorene Analogues via Sulfur Oxidation. *J. Org. Chem.* **2020**, *85*, 10846–10857.

(39) Baker, W.; McOmie, J. F. W.; Parfitt, S. D.; Watkins, D. A. M. Attempts to Prepare New Aromatic Systems. Part VI. 1 : 2-5 : 6-Dibenzopentalene and Derivatives. *J. Chem. Soc.* **1957**, 4026–4037.

(40) Konishi, A.; Okada, Y.; Nakano, M.; Sugisaki, K.; Sato, K.; Takui, T.; Yasuda, M. Synthesis and Characterization of Dibenzo[*a,f*]Pentalene: Harmonization of the Antiaromatic and Singlet Biradical Character. *J. Am. Chem. Soc.* **2017**, *139*, 15284–15287.

(41) Saito, M. Synthesis and Reactions of Dibenzo[*a,e*]Pentalenes. *Symmetry* **2010**, *2*, 950–969.

(42) Hopf, H. Pentalenes-From Highly Reactive Antiaromatics to Substrates for Material Science. *Angew. Chem. Int. Ed.* **2013**, *52*, 12224–12226.

(43) Kawase, T.; Nishida, J. π-Extended Pentalenes: The Revival of the Old Compound from New Standpoints. *Chem. Rec.* **2015**, *15*, 1045–1059.

(44) Konishi, A.; Yasuda, M. Breathing New Life into Nonalternant Hydrocarbon Chemistry: Syntheses and Properties of Polycyclic Hydrocarbons Containing Azulene, Pentalene, and Heptalene Frameworks. *Chem. Lett.* **2021**, *50*, 195–212.

(45) El Bakouri, O.; Smith, J. R.; Ottosson, H. Strategies for Design of Potential Singlet Fission Chromophores Utilizing a Combination of Ground-State and Excited-State Aromaticity Rules. *J. Am. Chem. Soc.* **2020**, *142*, 5602–5617.

(46) Konishi, A.; Okada, Y.; Kishi, R.; Nakano, M.; Yasuda, M. Enhancement of Antiaromatic Character via Additional Benzoannulation into Dibenzo[*a,f*]Pentalene: Syntheses and Properties of Benzo[*a*]Naphtho[2,1-*f*]Pentalene and Dinaphtho[2,1-*a,f*]Pentalene. *J. Am. Chem. Soc.* **2019**, *141*, 560–571.

(47) Konishi, A.; Satake, S.; Yasuda, M. Catalytic Cycloisomerization of Conjugated Bisbutatrienes into Pentalene Skeletons: Synthesis and Properties of Bisbutatrienes with an Acenaphthene Backbone. *Chem. Lett.* **2020**, *49*, 589–592.

(48) Baranac-Stojanović, M.; Stojanović, M. The Effect of Two Types of Dibenzoannulation of Pentalene on Molecular Energies and Magnetically Induced Currents. *Phys. Chem. Chem. Phys.* **2019**, *21*, 3250–3263.

(49) Baranac-Stojanović, M. A DFT Study of the Modulation of the Antiaromatic and Open-Shell Character of Dibenzo[*a,f*]Pentalene by Employing Three Strategies: Additional Benzoannulation, BN/CC Isosterism, and Substitution. *Chem. – A Eur. J.* **2019**, *25*, 9747–9757.

(50) London, G.; Rekowski, M. v. W.; Dumele, O.; Schweizer, W. B.; Gisselbrecht, J.-P.; Boudon, C.; Diederich, F. Pentalenes with Novel Topologies: Exploiting the Cascade Carbopalladation Reaction between Alkynes and Gem-Dibromoolefins. *Chem. Sci.* **2014**, *5*, 965–972.

(51) Vu, V. A.; Marek, I.; Knochel, P. Stereoselective Preparationof Functionalized Unsaturated Lactones and Esters via FunctionalizedMagnesium Carbenoids. *Synthesis* **2003**, *8*, 1797–1802.

(52) Cardinal, S.; Voyer, N. Preparation of 2,3,3-Triarylacrylic Acid Esters Using Suzuki–Miyaura Coupling Reactions. *Synthesis* **2016**, *48*, 1202–1216.

(53) Harvey, R. G.; Dai, Q.; Ran, C.; Penning, T. M. Synthesis of the *o*-Quinones and Other Oxidized Metabolites of Polycyclic Aromatic Hydrocarbons Implicated in Carcinogenesis. *J. Org. Chem.* **2004**, *69*, 2024–2032.

(54) Uyehara, T.; Honda, T.; Kitahara, Y. CATA-CONDENSED DIBENZOPENTALENYL DIANIONS. *Chem. Lett.* **1977**, *6*, 1233–1236.

(55) Shimizu, A.; Tobe, Y. Indeno[2,1-*a*]Fluorene: An Air-Stable *Ortho*-Quinodimethane Derivative. *Angew. Chem. Int. Ed.* **2011**, *50*,

6906–6910.

(56) Sato, C.; Suzuki, S.; Kozaki, M.; Okada, K. 2,11-Dibromo-13,14-Dimesityl-5,8-Dioxapentaphene: A Stable and Twisted Polycyclic System Containing the o -Quinodimethane Skeleton. *Org. Lett.* **2016**, *18*, 1052–1055.

(57) Kruszewski, J.; Krygowski, T. M. Definition of Aromaticity Basing on the Harmonic Oscillator Model. *Tetrahedron Lett.* **1972**, *13*, 3839–3842.

(58) Krygowski, T. M. Crystallographic Studies of Inter- and Intramolecular Interactions Reflected in Aromatic Character of .Pi.-Electron Systems. *J. Chem. Inf. Comput. Sci.* **1993**, *33*, 70–78.

(59) Krygowski, T. M.; Cyrański, M. K. Structural Aspects of Aromaticity. *Chem. Rev.* **2001**, *101*, 1385–1420.

(60) Kolc, J.; Michl, J. Photochemical Synthesis of Matrix-Isolated Pleiadene. *J. Am. Chem. Soc.* **1970**, *92*, 4147–4148.

(61) Geuenich, D.; Hess, K.; Köhler, F.; Herges, R. Anisotropy of the Induced Current Density (ACID), a General Method To Quantify and Visualize Electronic Delocalization. *Chem. Rev.* **2005**, *105*, 3758–3772.

(62) Jusélius, J.; Sundholm, D.; Gauss, J. Calculation of Current Densities Using Gauge-Including Atomic Orbitals. *J. Chem. Phys.* **2004**, *121*, 3952–3963.

(63) Fliegl, H.; Taubert, S.; Lehtonen, O.; Sundholm, D. The Gauge Including Magnetically Induced Current Method. *Phys. Chem. Chem. Phys.* **2011**, *13*, 20500.

(64) Sundholm, D.; Fliegl, H.; Berger, R. J. F. Calculations of Magnetically Induced Current Densities: Theory and Applications. *Comput. Mol. Sci.* **2016**, *6*, 639–678.

(65) Rauhalahti, M.; Taubert, S.; Sundholm, D.; Liégeois, V. Calculations of Current Densities for Neutral and Doubly Charged Persubstituted Benzenes Using Effective Core Potentials. *Phys. Chem. Chem. Phys.* **2017**, *19*, 7124–7131.

(66) Sundholm, D.; Berger, R. J. F.; Fliegl, H. Analysis of the Magnetically Induced Current Density of Molecules Consisting of Annelated Aromatic and Antiaromatic Hydrocarbon Rings. *Phys. Chem. Chem. Phys.* **2016**, *18*, 15934–15942.

(67) Bleaney, B.; Bowers, K. D. Anomalous Paramagnetism of Copper Acetate. *Proc. R. Soc. London. Ser. A. Math. Phys. Sci.* **1952**, *214*, 451–465.

(68) Nakagawa, M. Cyclic Acetylenes. In *The Carbon-Carbon Triple Bond: Vol. 2*; John Wiley & Sons, Ltd.: Chichester, UK, 1978; pp 635–712.

(69) Fukuda, K.; Nagami, T.; Fujiyoshi, J. Y.; Nakano, M. Interplay between Open-Shell Character, Aromaticity, and Second Hyperpolarizabilities in Indenofluorenes. *J. Phys. Chem. A* **2015**, *119*, 10620–10627.

(70) Kertesz, M.; Choi, C. H.; Yang, S. Conjugated Polymers and Aromaticity. *Chem. Rev.* **2005**, *105*, 3448–3481.

(71) Snyder, G. J. Rational Design of High-Spin Biradicaloids in the Isobenzofulvene and Isobenzoheptafulvene Series. *J. Phys. Chem. A* **2012**, *116*, 5272–5291.
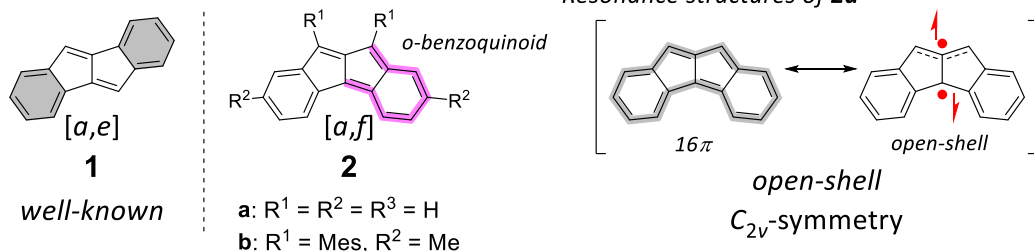
Chapter 2

Synthesis and Characterization of Dinaphtho[2,1-*a*:2,3-*f*]pentalene: A Stable Antiaromatic/Quinoidal Hydrocarbon Showing Appropriate Carrier Mobility in the Amolphous Layer
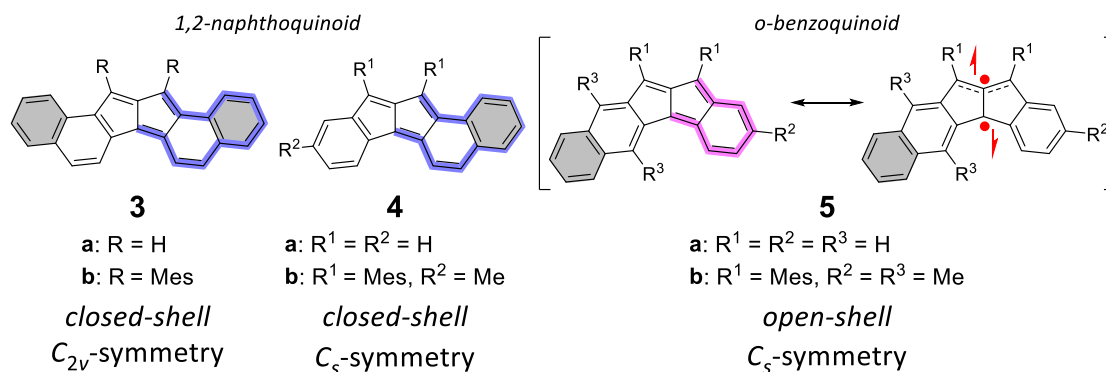
2-1. Introduction

Aromaticity and antiaromaticity are important key concepts in understanding and designing the physical and chemical properties of planar cyclic π-conjugated systems.[1–4] Antiaromatic molecules, when prepared with reasonable stability and quantity, can exhibit useful applications with distinctly different characteristics from aromatic molecules.[5] π-Extended molecules containing 4nπ-antiaromatic cores are desirable candidates for organic materials because of their fascinating properties such as narrow HOMO–LUMO energy gaps, ambipolar redox properties, low-energy absorptions, and paratropic ring currents. These unique electronic properties have attracted tremendous interest for their utility in advanced optoelectronic materials.[6,7,16–21,8–15] Among many antiaromatics, dibenzo[*a,e*]pentalene **1**, a well-known non-alternant hydrocarbon[22–26] with antiaromatic character has emerged as hot topics thanks to various types of synthetic progress (Figure 1A).[26–29] Not only the synthetic accessibilities, but also high thermal stability of various derivatives of **1** have recently received significant attractiveness as functional chromophores[26] such as organic field-effect transistors (OFETs),[30–35] organic photovoltaics (OPVs),[30,36] single-molecular wires,[37] and singlet fissions (SFs).[38–40]

Recently, the authors have focused on an structural isomer of **1**, dibenzo[*a,f*]pentalene **2**.[41,42] The isomer **2** shows an appreciable singlet open-shell character and a pronounced peripheral 16π-antiaromatic character (resonance structures in Figure 1A). These electronic features of **2** are never shared by **1** with a closed-shell and weak paratropic pentalene core. The harmonization of open-shell and antiaromatic characters of **2** allowed us to systematically address the interrelation between the two characters through additional annulations of one or two benzene rings into **2**.[43] In a series of diareno[*a,f*]pentalenes **2–5** (Figures 1A–B), the following two principles that govern the interrelation between open-shell and antiaromatic characters are derived: (1) the mode of the embedded *o*-quinoidal moiety and (2) the formal molecular symmetry of the ring-fusion pattern.[44] The open-shell/closed-shell singlet ground state is attained by the attachment of *o*-benzoquinoidal/1,2-naphthoquinoidal moiety into the pentalene skeleton, respectively. The antiaromaticity is more pronounced in the pentalenes with C_{2v}-symmetric ring-fusion patterns than those with C_s-symmetric ring-fusion patterns. The inherently narrow HOMO–LUMO energy gaps of **2–5**, originating from the open-shell and antiaromatic natures, premise potential utility for organic materials, however, the poor stability under ambient conditions (the half-lives even for closed-shell **3** and **4** are within 3 days at the most) has hampered the investigations of solid-state properties for organic devices.

(A) Dibenzopentalenes

[*a,e*]
1
well-known

a: R^1 = R^2 = R^3 = H
b: R^1 = Mes, R^2 = Me

o-benzoquinoid

[*a,f*]
2

Resonance structures of 2a

16π *open-shell*

open-shell
C_{2v}-symmetry

(B) Diareno[*a,f*]pentalenes 3–5

1,2-naphthoquinoid

3
a: R = H
b: R = Mes
closed-shell
C_{2v}-symmetry

4
a: R^1 = R^2 = H
b: R^1 = Mes, R^2 = Me
closed-shell
C_s-symmetry

o-benzoquinoid

5
a: R^1 = R^2 = R^3 = H
b: R^1 = Mes, R^2 = R^3 = Me
open-shell
C_s-symmetry

(C) *This work*: Dinaphtho[2,1-*a*:2,3-*f*]pentalene 6

1,2-naphthoquinoid

6
C_s-symmetry

a: R^1 = R^2 = H
b: R^1 = Mes, R^2 = Me

Resonance structures of 6a
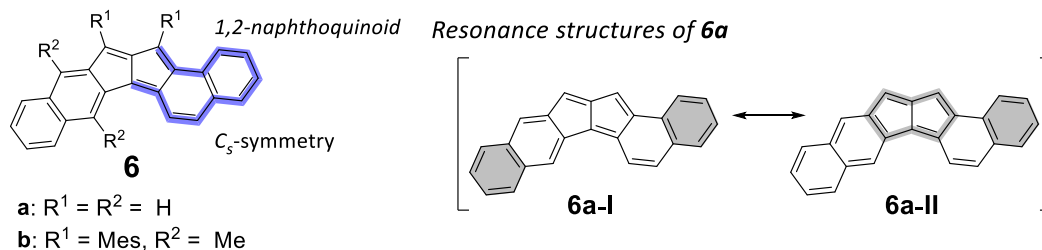
6a-I   **6a-II**

Figure 1. (A) Dibenzo[*a,e*]pentalene **1** and dibenzo[*a,f*]pentalene **2** with the resonance structures of **2a**. (B) Molecular structures of diareno[*a,f*]pentalenes **3–5**. (C) Molecular structure of dinaphtho[2,1-*a*:2,3-*f*]pentalene **6** with resonance structures of **6a**. Gray denotes hexagons with 6π-benzenoid character. Blue and pink indicate the main $4n\pi$-conjugations, 1,2-naphthoquinoid and *o*-benzoquinoid moieties, respectively.

Herein, the authors report the synthesis and characterization of unsymmetrically dinaphtho-fused pentalene, dinaphtho[2,1-*a*:2,3-*f*]pentalene **6** (Figure 1C). A reddish-purple solid of the mesityl derivative **6b** was sufficiently stable in either solid or solution state under ambient conditions. Our experimental and theoretical investigations revealed the suppressed antiaromaticity of **6** with closed-shell quinoidal structure, exhibiting a hole mobility on the order of 10^{-4} cm^2 V^{-1} s^{-1} examined by a space charge limited current (SCLC) method.

2-2. Results and Discussion

The synthetic route of **6b** is shown in Scheme 1. According to our previous study on **5**,[44] a palladium-catalyzed Suzuki-Miyaura cross-coupling of **7** with 2-naphthylboronic acid furnished diester **8** in 97% yield. Reduction of the ester moieties in **8** with iBu$_2$AlH afforded diol **9**, and subsequent oxidation gave dialdehyde **10**. Treatment of **10** with mesitylmagnesium bromide afforded diol **11**. Intramolecular cyclization of **11** was carried out under acidic conditions to afford the hydrocarbon **12** consisting of a consecutive 6-6-5-5-6-6 ring system (Figure S1). Oxidation of **12** was conducted through dianion **6b^{2-}**. Treatment of **12** with nBuLi in THF cleanly generated dianion **6b^{2-}**. Without isolating **6b^{2-}** but after confirming by NMR measurements, the subsequent two-electron oxidation of **6b^{2-}** with p-chloranil furnished **6b** as a reddish-purple solid. A dichloromethane solution of **6b** showed no decomposition for over a week upon exposure to air under room light at room temperature. The high stability is markedly different form our previous reported diareno[a,f]pentalenes **2–5**.[42–44]
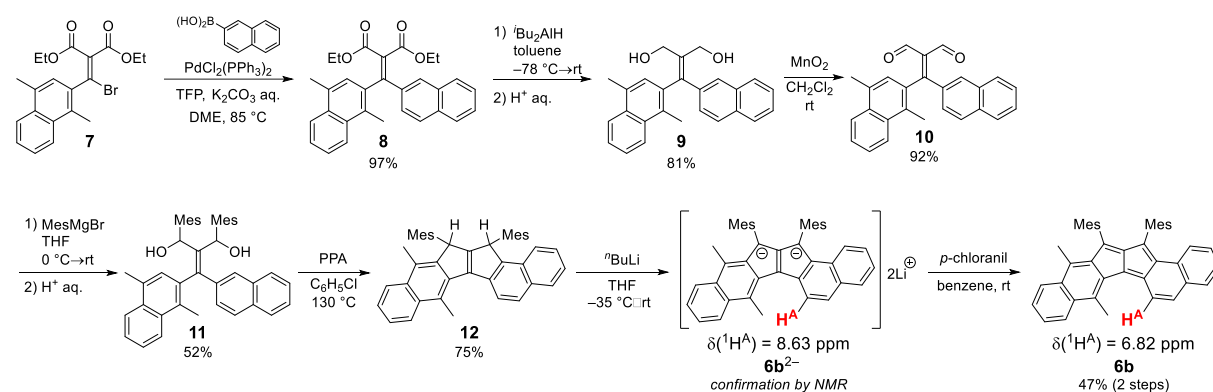
Scheme 1. Synthetic route for **6b**. TFP = tri(2-furyl)phosphine, Mes = 2,4,6-trimethylphenyl, PPA = polyphosphoric acid.

In the ¹H NMR spectrum of **6b** in THF-d_8 collected at room temperature, sharp signals attributed at the main core protons were observed, implying the closed-shell singlet ground state of **6b**. Theoretical calculation also supported the idea. No diradical character of **6b** ($y_0 = 0.00$) was estimated calculated at the LC-UBLYP ($\mu = 0.33$ bohr^{-1})/6-311G* level. Antiaromatic character of **6** was evaluated by comparing the ¹H NMR spectra between dianionic **6b^{2-}** and neutral **6b**. As the authors previously demonstrated, the upfield shift in the H^A proton signals (Scheme 1 and Figure S5) upon a two-electron oxidation of the dianion to the corresponding neutral pentalene can assess the shielding effects of the pentalene moiety.[43] The corresponding upfield shift in the H^A proton signals of **6b^{2-}/6b** ($\Delta\delta$(¹H^A)) was −1.81 ppm, which is the smallest shift among the previous analogs **2–5** (**2b^{2-}/2b**: −2.47 ppm, **3b^{2-}/3b**: −2.44 ppm, **4b^{2-}/4b**: −1.89, −1.99 ppm, **5b^{2-}/5b**: −1.87 ppm).[43,44] The NICS(1) values calculated at the GIAO-RB3LYP/6-311+G* level were consistent with the NMR observation (Figure 2A). The positive NICS values on the pentagons of **6a** (+14.3 and +10.9) were smallest among the previous analogues (**2a**: +23.8, +27.2; **3a**: +29.5, +30.6; **4a**: +18.0, +20.4; **5a**: +14.1,

51

+20.4 in Figure S11).[43,44] The anisotropy of the induced current density (AICD) plots[45] revealed the dominant 4nπ-conjugated circuit of **6a** (Figure 2B). Whilst the clockwise ring currents flowed on the outermost hexagons (rings *C* and *C'*), the flows of the anticlockwise ring current were confined into the central pentalene subunit (rings *A* and *A'*), supporting the 8π-antiaromatic nature of **6a**-**II** in Figure 1C. The isolation of a pentalene subunit is common to **3** and **4**,[43] in which the aromatic outermost hexagons isolate an 8π-conjugated system from the global π-conjugation, but the evoked paratropicity of **6** is much more suppressed than these previous analogs.
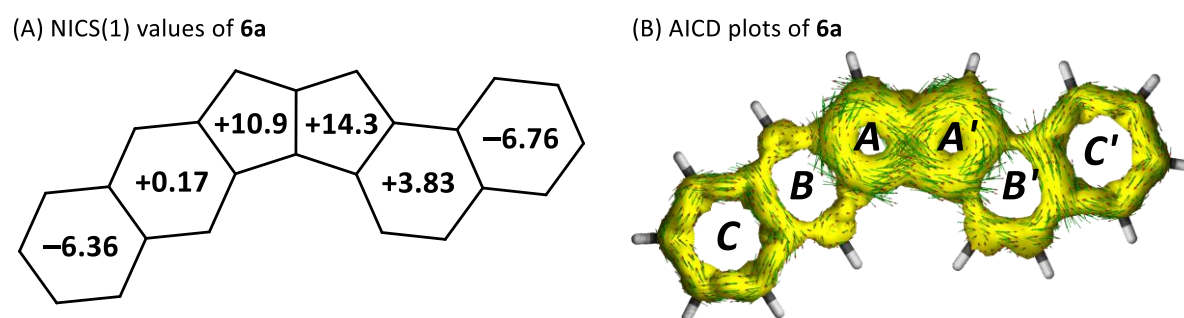

(A) NICS(1) values of **6a**

+10.9 +14.3 −6.76
+0.17 +3.83
−6.36

(B) AICD plots of **6a**

A A' C'
B B'
C

Figure 2. (A) NICS(1) values of **6a** calculated at the GIAO-RB3LYP/6-311+G*//RB3LYP-D3/6-311G* level. (B) AICD plots (isovalue surface: 0.035) of **6a** with the representations of each ring calculated at the CSGT-RB3LYP/6-311+G*//RB3LYP-D3/6-311G* level.

Molecular geometry of **6b** explained the suppressions of open-shell and antiaromatic characters. A single crystal of **6b** suitable for X-ray analysis was obtained from a hexane/diethyl ether solution. Two crystallographically independent molecules were present in the asymmetric unit, one of which is shown in Figure 3A. Because the geometries of the two molecules of **6b** are almost identical, the following discussion uses the mean values of the two structures (Figure S3). The main core of **6b** was nearly plane and the mesityl groups formed large dihedral angles with the main core (ca. 77°). The observed bond lengths and harmonic oscillator model of the aromaticity (HOMA)[46,47] values are summarized in Figures 3B and C. The C_s-symmetric main core of **6b** was characterized by two types of naphtho annulations, 1,2- and 2,3-naphtho annulations, into the pentalene core. The two outermost hexagons (rings *C* and *C'*) show small bond length alternations (BLAs) and their HOMA values are close to unity (0.86, 0.94). As demonstrated by NICS and AICD analyses, the observation reveals that the local 6π-aromatic characters are conceived in these rings. The HOMA analysis clearly shows the difference between 1,2- and 2,3-naphtho annulations; while the ring *B* in the 2,3-naphtho annulation still keeps a small BLA (0.46), the ring *B'* in the 1,2-naphtho annulation shows a large BLA (–0.069). The imbalance of BLA in the inner hexagons strongly induces the quinoidal π-bond localization on the pentalene core (ring *A* and *A'*) with a large BLA (1.372(2)–1.493(3) Å, HOMA: –0.25, –0.045). Notably, the degree of BLA of **6b** is comparable with that of the closed-shell **4b** (1.362(6)–1.502(6) Å).[43] From the observed geometry, **6b** should be described by the combination of a 1,2-

naphthoquinoid subunit and a naphthalene core in the ground state (see a canonical structure of **6a-I** in Figure 1C). The large BLA in the pentagons of **6** should cause the quinoidal closed-shell ground state with the suppressed antiaromaticity. These evaluations are in accordance with our previous study on the interrelation between open-shell and antiaromatic characters; **6** is categorized into the C_s-symmetrically fused pentalene containing a 1,2-naphthoquinoidal moiety.[44]
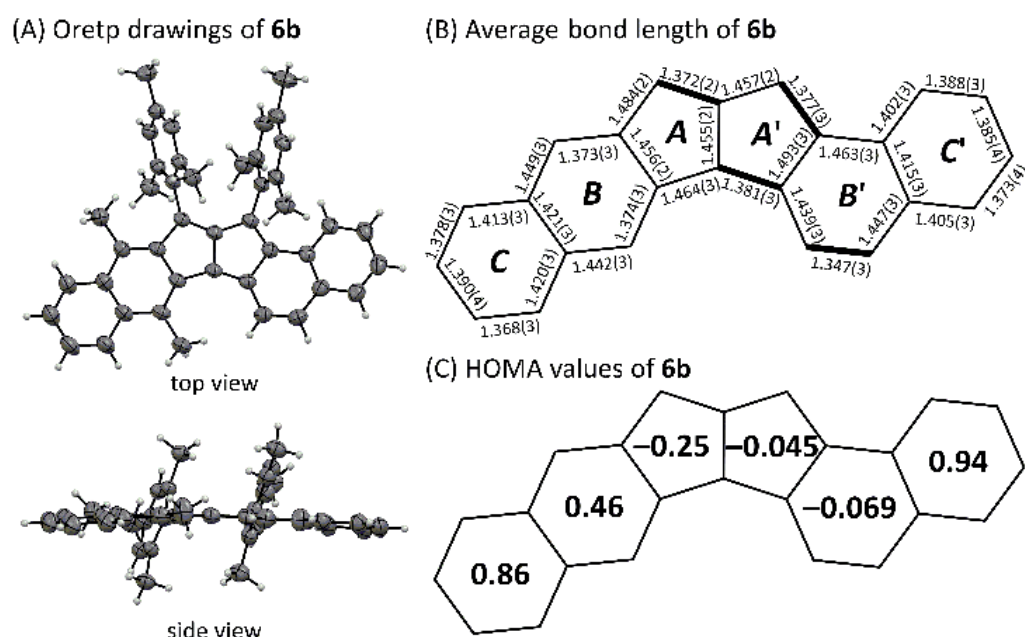

Figure 3. (A) X-ray structures of **6b** at the 50% probability level. (B) Average bond lengths (Å) of **6b** with the representations of each ring. (C) HOMA values of **6b** calculated based on the determined bond lengths by X-ray analysis.

The quinoidal characteristics of **6** with a weak antiaromaticity reflect in the optoelectronic properties (Figure 4). The cyclic voltammogram of **6b** displayed two reversible and two irreversible redox waves ($E_2^{ox, pa}$ = +0.84 V, E_1^{ox} = +0.19 V, E_1^{red} = –1.52 V, and $E_2^{red, pc}$ = –2.23 V vs Fc/Fc$^+$, Figure 4A and Table S3). The difference between the first oxidation and reduction potentials was used to determine the electrochemical HOMO–LUMO gap. The value was 1.71 eV for **6b**, which was the most expanded energy gap compared to those of **2**–**5** (Figure S9), but remains sufficiently small compared to those of the reported diareno[a,e]pentalenes (ca. 2.0 eV).[26,30,48–50] It should be noted that diareno[a,f]pentalenes contract the HOMO−LUMO energy gap more effectively than diareno[a,e]pentalenes.[43] The electronic absorption spectrum of **6b** in CH_2Cl_2 gave a low energy absorption at 755 nm (ε = 1010 M^{-1}cm^{-1}) having a long tail that extended up to 1300 nm (Figure 4B). Time-dependent (TD)-DFT calculations at the RB3LYP/6-311+G* level attributed the absorption band to the forbidden HOMO–LUMO transition (Figure S13 and Table S5).

Compared to the longest absorption of **2–5**, **6** showed the most blue-shifted (Figure S8), which caused by the smallest antiaromatic character among them.
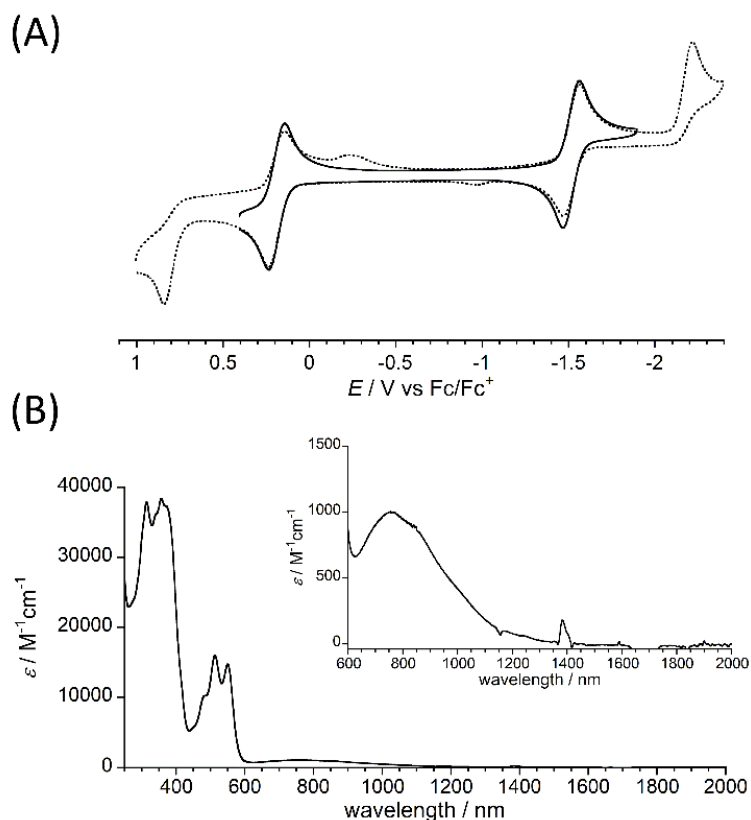

Figure 4. (A) Cyclic voltammogram of **6b** (V vs Fc/Fc$^+$, in 0.1 M nBu$_4$NClO$_4$/CH$_2$Cl$_2$, scan rate = 100 mVs^{-1}, room temperature). (B) UV/vis/NIR absorption spectra of **6b** in CH$_2$Cl$_2$. Inset shows a magnified view.

The relatively high HOMO level of **6b** (–4.90 eV estimated from the onset[51] of the first oxidation potential (+0.102 V vs Fc/Fc$^+$) from the CV measurement) prompted us to investigate the potential as hole transporter. The hole mobility (μ_h) in **6b** was examined by the space-charge-limited current (SCLC) method with a device structure of Glass/indium tin oxide (ITO)/**6b** (187 nm)/MoO$_3$ (5 nm)/Au (30 nm). The **6b** layer was spin-coated from a THF solution to give amorphous thin films (Figures S14–S15). The current density (J)–voltage (V) characteristics show clear transition to the SCLC regime ($J \propto V^2$) at a higher voltage range, from which a μ_h value of 4.37×10^{-4} cm^2 V^{-1} s^{-1} was extracted based on the Mott–Gurney expression (Figure 5A). The single crystal X-ray analysis showed that the main core of **6b** formed a herringbone-like packing associated with two nonequivalent motifs of intermolecular CH–π contacts along the b-axis direction. The corresponding transfer integrals for holes were estimated to be 21 and 16 meV, respectively (Figure 5B). These intermolecular contacts in the single crystal structure demonstrate that appreciable intermolecular interactions should be possible to form for **6b** in the solid state, despite its bulky mesityl substituents. The mobility of **6b** is moderate compared to the reported values of diareno[a,e]pentalenes.[26] However,

54

considering the high film formability and the moderate hole mobility ($\sim 10^{-4}$ cm^2 V^{-1} s^{-1}), **6b** can sufficiently show comparable performance to conventional hole transporters for organic light-emitting diodes (OLEDs) or organic photovoltaics (OPVs). It is the first study that the carrier mobility of the diareno[*a*,*f*]pentalene system has been investigated, providing the potential for applications in organic electronic devices. High-performance materials can be realized with further modifications.
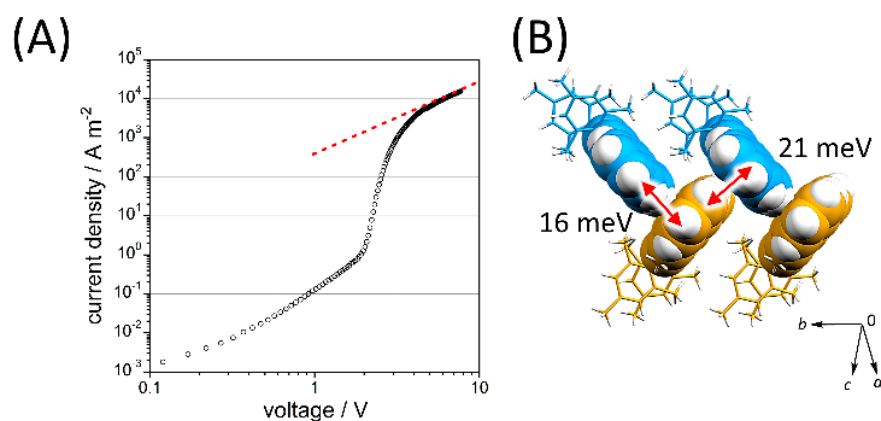

Figure 5. (A) Current density–voltage (*J*–*V*) plot of a hole-only device with **6b**. The red dashed line indicates the voltage dependence of current density with a slope of 2. (B) Transfer integrals calculated for CH–π and π–π contacts observed in the single-crystal X-ray structure. The main cores and substituents of **6b** are shown in space-filling and stick models, respectively. Symmetrically nonequivalent molecules are differentiated with blue and yellow.

2-3. Conclusion

The authors synthesized and characterized **6** as a new member of diareno[*a*,*f*]pentalene family. Unsymmetrically dinaphtho-fused structure of **6** highly localized the π-electrons on the pentalene core, which leads to a quinoidal closed-shell singlet state with a weakened antiaromatic nature. However, the π-electron localization endows **6** with sufficient stability under bench-top conditions. The stability of **6** allowed us to investigate the solid-state properties. The first charge carrier mobility for diareno[*a*,*f*]pentalenes was examined, showing a hole mobility of 4.37×10^{-4} cm^2 V^{-1} s^{-1}. Further studies on diarno[*a*,*f*]pentalenes, including chemical modifications and fabrication transistors and/or solar cells, are ongoing in our laboratories.

2-4. Experimental Section
General Information

NMR spectra were recorded on JEOL-AL400, JEOL-ECS400 (400 MHz for ^{1}H, and 100 MHz for ^{13}C) and Bruker AVANCE III spectrometers (600 MHz for ^{1}H, and 150 MHz for ^{13}C) with TMS as an internal standard. ^{1}H and ^{13}C NMR signals of compounds were assigned using HMQC, HSQC, HMBC, COSY, NOESY, and ^{13}C off-resonance techniques. Positive FAB and EI mass spectra were recorded on a JEOL JMS-700 and a Shimadzu GCMS-QP2010 Ultra, respectively. The high resolution ESI mass spectra were analyzed by using a JEOL JMS-T100LP. IR spectra were recorded as thin films or as solids in KBr pellets on a JASCO FT/IR 6200 spectrophotometer. UV-vis-NIR spectra were recorded on a JASCO V-670 spectrophotometer. Cyclic voltammetric measurements were performed with an ALS-600C electrochemical analyzer using a glassy carbon working electrode, a Pt counter electrode, and an Ag/AgNO$_3$ reference electrode at room temperature in CH$_2$Cl$_2$ containing 0.1 M nBu$_4$NClO$_4$ as the supporting electrolyte. Data collection for X-ray crystal analysis was performed on Rigaku/XtaLAB Synergy-S/Cu (CuK$_\alpha$ λ = 1.54187 Å) diffractometers. All non-hydrogen atoms were refined with anisotropic displacement parameters and hydrogen atoms were placed at calculated positions and refined "riding" on their corresponding carbon atoms by Olex2[1] program.

Materials

All reagents were obtained from commercial suppliers and used as received except for p-chloranil. p-Chloranil was recrystallized from hot toluene before use. All reactions were carried out under nitrogen. Syntheses of dianion **6b**$^{2-}$ and pentalene **6b** were performed in a nitrogen-filled glove box.

Computational Method

All calculations were conducted using the Gaussian 09 program.[2] The geometries of neutral and dianionic singlet species of **6a** and **6a**$^{2-}$ were optimized with the RB3LYP-D3 functional and 6-311G* basis set. The obtained RB3LYP-D3 geometry of neutral **6a** was employed for the calculations of the other properties. Frequency analysis calculations were performed in order to confirm the local minimum structures. NICS(1) values of neutral and dianionic species of **6a** and **6a**$^{2-}$ were calculated at the GIAO-RB3LYP/6-311+G* method using these optimized structures. AICD plot of **6a** was calculated by using the method developed by Herges[3] and only π-electrons are considered at the CSGT-RB3LYP/6-311+G*//RB3LYP-D3/6-311G* level. The magnetic field is perpendicular to the molecular plane of **6a**. Yellow surface is the isosurface of the induced current density under the magnetic field. Green allows with red head indicate the induced current density vectors. The clockwise and counterclockwise density vectors indicate diamagnetic and paramagnetic ring currents, respectively. Diradical character (y_0) were obtained from the occupation number of LUNO ($y_0 = n_L$) at the LC-UBLYP (μ = 0.33 bohr^{-1})/6-311G* level. The estimated occupation number of LUNO for **6a** was zero, thus, the diradical character of **6a** is zero at the calculation level. Symmetry-adapted molecular orbitals of **6a** were evaluated at the RB3LYP/6-311+G* level. Electronic excitation properties of **6a** were evaluated by the TDDFT method RB3LYP and 6-311+G* basis set.

Synthesis and Characterization

Diethyl 2-{bromo(1,4-dimethylnaphthalen-2-yl)methylene}malonate 7[4]
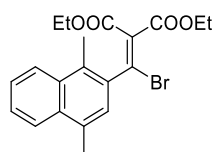
^{1}H NMR (400 MHz, CDCl$_3$) 8.08–8.06 (m, 1H), 8.00–7.98 (m, 1H), 7.57–7.54 (m, 2H), 7.14 (s, 1H), 4.42 (q, J = 7.0 Hz, 2H), 3.93 (q, J = 7.0 Hz, 2H), 2.66 (s, 3H), 2.62 (s, 3H), 1.41 (t, J = 7.0 Hz, 3H), 0.860 (t, J = 7.0 Hz, 3H); ^{13}C NMR: (100 MHz,

CDCl$_3$) 164.2, 161.5, 139.6, 134.9, 132.8, 132.6, 132.4, 131.5, 129.3, 126.4, 126.1, 125.2, 124.8, 124.6, 62.1, 61.5, 19.3, 15.6, 14.0, 13.5.


Diethyl 2-{(1,4-dimethylnaphthalen-2-yl)(naphthalen-2-yl)methylene}malonate 8
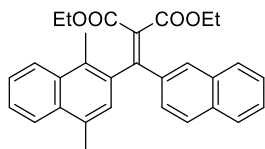
Under nitrogen, PdCl$_2$(PPh$_3$)$_2$ (0.218 g, 0.311 mmol) was added to a solution of **7**[4] (2.40 g, 5.93 mmol), 2-naphthtaleneboronic acid (1.15 g, 6.66 mmol) and tri(2-furyl)phosphine (0.225 g, 0.970 mmol) in DME (13 mL) and aqueous 2 M K$_2$CO$_3$ (10 mL) at room temperature. The mixture was heated to 85 °C for 20 h. After cooled to room temperature, aqueous 1 M HCl was added to the mixture. The products were extracted with CHCl$_3$ three times. The combined organic layers were washed with water and brine, and then were dried over MgSO$_4$. After filtration, the obtained solutions were evaporated in vacuum. The obtained residue was purified by a silica-gel column chromatography (hexane / ethyl acetate = 90:10), to give **8** as a colorless solid (2.43 g, 97%).

mp 125.2−125.4 °C; IR (KBr) 3054 (w), 2982 (m), 2904 (w), 1732 (s), 1698 (s), 1602 (m), 1503 (m), 1461 (m), 1388 (m), 1366 (m), 1300 (s), 1237 (s), 1173 (m), 1132 (w), 1095 (s), 1065 (s), 1052 (s), 1016 (m), 971 (w), 923 (w), 907 (w), 888 (w), 865 (m), 828 (m), 806 (w) cm^{-1}; ^{1}H NMR (400 MHz, CDCl$_3$) 8.07–8.05 (m, 1H), 8.02–8.00 (m, 1H), 7.80 (d, J = 8.0 Hz, 1H), 7.74 (d, J = 8.4 Hz, 1H), 7.72 (s, 1H), 7.56–7.53 (m, 2H), 7.50–7.43 (m, 2H), 7.34 (dd, J = 8.4, 1.6 Hz, 1H), 7.12 (s, 1H), 4.15 (q, J = 7.2 Hz, 2H), 3.95 (q, J = 7.0 Hz, 2H), 2.63 (s, 3H), 2.57 (s, 3H), 1.03 (t, J = 7.2Hz, 3H), 0.81 (t, J = 7.0 Hz, 3H); ^{13}C NMR (100 MHz, CDCl$_3$) 166.5, 165.2, 156.0, 137.0, 136.4, 133.5, 132.98, 132.93, 132.6, 132.2, 129.7, 128.7 (two signals are overlapped.), 128.2, 128.0, 127.8, 127.2, 127.1, 126.6, 126.1, 126.0, 125.9, 125.2, 124.8, 61.6, 61.2, 19.4, 16.2, 13.9, 13.6; MS (EI$^+$, 70eV) m/z 452 (M$^+$, 34), 378 (100), 333 (26), 305 (41), 292 (51); HRMS (EI$^+$, 70 eV) Calculated: (C$_{30}$H$_{28}$O$_4$) 452.1988 (M$^+$), Found: 452.1986.

## 2-{(1,4-Dimethylnaphthalen-2-yl)(naphthalen-2-yl)methylene}propane-1,3-diol 9
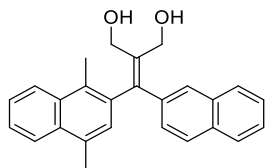
To a solution of **8** (2.70 g, 6.36 mmol) in toluene (30 mL) was added DIBAL (31.7 mL, 1.0 M in hexane, 31.7 mmol) at –78 °C. The reaction mixture was allowed to gradually warm up to room temperature and then stirred overnight. The reaction was quenched with MeOH/EtOAc and 1 M HCl and the product was extracted with EtOAc. The organic layer was washed with water, and dried over MgSO$_4$. After filtration, the obtained solutions were evaporated in vacuum. The obtained residue was purified by a silica-gel column chromatography (hexane/ethyl acetate = 20:80), to give **9** as a white solid (1.90 g, 81%).

mp 55.5−56.3 °C; IR (KBr) 3332 (bs), 3054 (s), 2938 (s), 2865 (s), 1700 (w), 1627 (w), 1598 (s), 1570 (w), 1503 (s), 1443 (s), 1408 (s), 1385 (s), 1270 (m), 1234 (m), 1199 (m), 1164 (m), 1126 (w), 1091 (w), 1058 (w), 1001 (s), 923 (w), 899 (m), 859 (s), 819 (s) cm^{-1}; ^{1}H NMR (400 MHz, CDCl$_3$) 8.08–8.06 (m, 1H), 8.01–7.99 (m, 1H), 7.81–7.78 (m, 2H), 7.76–7.73 (m, 2H), 7.58–7.53 (m, 2H), 7.47–7.44 (m, 2H), 7.37 (dd, J = 8.6, 1.8 Hz, 2H), 7.10 (s, 1H), 4.59 (s, 2H), 4.27 (d, J = 2.8 Hz, 2H), 2.62 (s, 3H), 2.60 (s, 3H), 2.13 (bs, 1H), 1.61 (bs, 1H); ^{13}C NMR (100 MHz, CDCl$_3$) 142.3, 137.7, 137.2, 136.0, 133.15, 133.07, 132.6, 132.4, 132.2, 129.6, 128.43, 128.38, 128.3, 127.71, 127.69, 127.5, 126.29, 126.26, 126.0, 125.6, 125.1, 124.8, 64.4, 63.1, 19.5, 16.0; MS (EI$^+$, 70eV) m/z 368 (M$^+$, 46), 351 (100), 289 (38), 165 (40); HRMS: (EI$^+$, 70 eV) Calculated: (C$_{26}$H$_{24}$O$_2$) 368.1776

(M[+]), Found: 368.1777.

2-{(1,4-Dimethylnaphthalen-2-yl)(naphthalen-2-yl)methylene}malonaldehyde 10
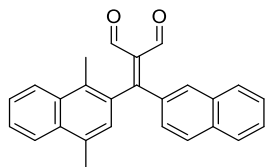
To a solution of **9** (1.896 g, 5.15 mmol) in CHCl₃ (60 mL) was added MnO₂ (13.4 g, 86.9 mmol) at room temperature. The reaction mixture was stirred at the temperature 48 h. The MnO₂ was removed by filtration through a celite pad. The filtrate was evaporated and the residue obtained was purified by column chromatography on silica gel (hexane/ethyl acetate 8:2) to give **10** as a yellow solid (1.73 g, 92%).

mp 170.0−170.3 °C; IR (KBr) 3436 (w), 3317 (w), 3053 (m), 2823 (m), 1731 (s), 1598 (m), 1559 (s), 1443 (m), 1298 (s), 1087 (w), 805 (m) cm⁻¹; ^{1}H NMR (400 MHz, CDCl₃) 9.83 (d, J = 2.0 Hz, 1H), 9.51 (d, J = 2.4 Hz, 1H), 8.13–8.10 (m, 1H), 8.09–8.06 (m, 1H), 7.89–7.85 (m, 3H), 7.83–7.82 (m, 2H), 7.66–7.57 (m, 4H), 7.05 (s, 1H), 2.65 (s, 3H), 2.54 (s, 3H); ^{13}C NMR (100 MHz, CDCl₃) 190.5, 190.1, 171.2, 135.7, 134.7, 134.5, 133.6, 133.4, 133.1, 132.8, 132.6, 132.5, 129.2, 128.72, 128.71, 128.6, 128.0, 127.5, 127.34, 127.33, 127.2, 126.9, 125.5, 125.0, 19.5, 16.7; MS (EI⁺, 70eV) m/z 364 (M⁺, 26), 349 (100), 335 (16); HRMS (EI⁺, 70 eV) Calculated: (C₂₆H₂₀O₂) 364.1463 (M⁺), Found: 364.1459.

2-{(1,4-Dimethylnaphthalen-2-yl)(naphthalen-2-yl)methylene}-1,3-dimesitylpropane-1,3-diol 11
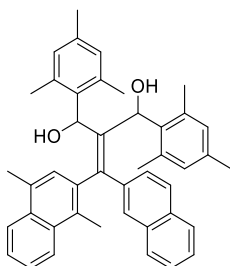
A solution of mesityl magnesium bromide (51.2 mmol) in THF (7 mL) was added to a solution of **10** (1.726 g, 4.74 mmol) in THF (10 mL) at 0 °C and the mixture was stirred for 2.5 h at room temperature and quenched with saturated aqueous NH₄Cl. The product was extracted with ethyl acetate. The organic layer was washed with water and dried over MgSO₄. The filtrate was evaporated and the residue was purified by column chromatography on silica gel (hexane, then hexane/ethyl acetate 80:20) to give two fractions (fractions A and B) of **11** as pale yellow solids (1.48 g (fractions A/B = 67:33), 52%). Each fraction consisted of inseparable diastereo mixture and all spectroscopic data for each fraction were recorded using the mixture. Because of the diastereo mixture, NMR spectra were not analyzed except for signal picking.

fraction A: R_f = 0.50 (EtOAc/hexane = 1:4)

mp 118.1−119.0 °C; IR (KBr) 3391 (w), 3054 (w), 3006 (w), 2946 (m), 2917 (m), 2860 (w), 1610 (w), 1598 (w), 1503 (w), 1480 (w), 1444 (m), 1383 (w), 1236 (w), 1130 (w), 1041 (m), 1010 (m), 909 (w), 851 (m), 819 (w) cm⁻¹; ^{1}H NMR (400 MHz, CDCl₃) 7.83 (d, J = 8.4 Hz), 7.45–7.67 (m), 7.56 (d, J = 8.8 Hz), 7.41–7.36 (m), 6.87 (s), 6.65 (s), 6.21 (d, J = 7.2 Hz), 6.14 (s), 5.93 (s), 4.19 (d, J = 7.2 Hz), 2.49 (s), 2.38 (s), 2.12 (s), 2.10 (s), 2.03 (s), 1.82 (s); ^{13}C NMR (100 MHz, CDCl₃) 144.2, 139.7, 138.5, 138.2, 136.6, 136.4, 136.2, 136.15, 136.10, 135.1, 133.1, 132.7, 132.3, 131.9, 130.7, 130.4, 130.1, 130.0, 129.6, 129.3, 128.8, 128.5, 128.0, 127.5, 126.8, 125.9, 125.8, 125.4, 125.1, 124.9, 124.2, 124.0, 76.7, 73.5, 22.2, 21.7, 21.3, 21.1,

20.6, 20.5, 19.4, 16.9; HRMS (ESI) Calculated: ($C_{44}H_{44}O_2Na$) 627.3234 ([M＋Na]$^+$), Found: 627.3226.

fraction B: R_f = 0.32 (EtOAc/hexane = 1:4);

mp 109.3−109.9 °C; IR (KBr) 3359 (w), 3054 (w), 3006 (w), 2918 (m), 2862 (w), 1610 (w), 1573 (w), 1503 (w), 1480 (w), 1446 (m), 1383 (m), 1270 (w), 1237 (w), 1130 (w), 1040 (m), 1012 (m), 965 (w), 910 (w), 876 (w), 851 (m), 813 (w) cm^{-1}; ^{1}H NMR (400 MHz, CDCl$_3$) 8.01 (d, *J* = 8.4 Hz), 7.82 (d, *J* = 8.0 Hz), 7.72 (d, *J* = 8.4 Hz), 7.57 (t, *J* = 9.0 Hz), 7.50 (t, *J* = 6.8 Hz), 7.42 (t, *J* = 7.6 Hz), 7.34–7.28 (m), 6.98 (d, *J* = 8.8 Hz), 6.86 (s), 6.65 (s), 6.46 (s), 6.39 (s), 6.29 (s), 6.15 (d, *J* = 6.4 Hz), 6.00 (s), 3.82 (s), 3.40 (s), 3.28 (s), 3.00 (s), 2.48 (s), 2.44 (s), 2.38 (s), 2.20 (s), 2.12 (s), 2.11 (s), 2.09 (s), 2.07 (s), 2.02 (s), 1.98 (s), 1.92 (s), 1.81 (s), 1.75 (s); ^{13}C NMR (100 MHz, CDCl$_3$) 139.4, 139.1, 139.0, 138.5, 137.0, 136.5, 136.3, 136.1, 136.0, 135.8, 135.2, 132.5, 132.2, 131.6, 131.2, 130.8, 130.3, 129.6, 129.3, 129.0, 128.2, 127.7, 127.4, 126.9, 126.7, 126.4, 126.1, 125.9, 125.4, 125.1, 124.7, 124.6, 124.5, 123.9, 123.7, 73.9, 72.9, 21.9, 21.4, 21.0, 20.8, 20.4, 20.1, 20.0, 19.1, 18.7, 16.6, 16.5; HRMS (ESI) Calculated: ($C_{44}H_{44}O_2Na$) 627.3234 ([M＋Na]$^+$), Found: 627.3224.

## 5,6-Dimesityl-7,12-dimethyl-5,6-dihydropentaleno[2,1-*a*:5,6-*b*′]dinaphthalene 12
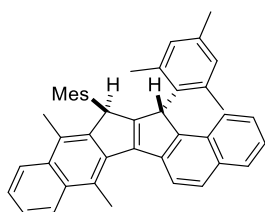
To a solution of **11** (0.198 g, 0.328 mmol) in chlorobenzene (6 mL) was added polyphosphoric acid (two medicine spoons, ~6 g) at room temperature and the mixture was heated at 130 °C for 24 h. After cooling to room temperature, the organic layer was decanted and evaporated. The residue obtained was purified by column chromatography on silica gel (hexane, then hexane/ethyl acetate 94:6), and then further purification was performed by recycle GPC, to give **12** of a single diastereoisomer as a pink solid (0.140 g, 75%). Single crystals suitable for X-ray crystallographic analysis were obtained from a solution of acetone.

mp 245.0−245.6 °C; IR (KBr) 3071 (w), 3004 (m), 2950 (m), 2916 (m), 2869 (m), 1610 (m), 1584 (w), 1540 (w), 1511 (m), 1478 (s), 1460 (s), 1478 (s), 1459 (s), 1375 (m), 1358 (m), 1221 (w), 1120 (w), 1024 (m), 1000 (w), 849 (s), 820 (s), 810 (s) cm^{-1}; ^{1}H NMR (400 MHz, CDCl$_3$) 8.46 (d, *J* = 8.8 Hz, 1H), 8.25 (d, *J* = 8.8 Hz, 1H), 7.98 (d, *J* = 8.4 Hz, 1H), 7.93 (d, *J* = 8.4 Hz, 1H), 7.88 (d, *J* = 8.0 Hz, 1H), 7.56 (t, *J* = 7.4 Hz, 1H), 7.48 (t, *J* = 7.6 Hz, 1H), 7.42 (d, *J* = 8.4 Hz, 1H), 7.32 (t, *J* = 7.6 Hz, 1H), 7.21 (t, *J* = 7.6 Hz, 1H), 6.91 (s, 1H), 6.84 (s, 1H), 6.63 (s, 2H), 5.04 (s, 1H), 5.02 (s, 1H), 3.37 (s, 3H), 2.28 (s, 3H), 2.26 (s, 6H), 1.75 (s, 3H), 1.71 (s, 3H), 1.41 (s, 3H), 1.38 (s, 3H); ^{13}C NMR (100 MHz, CDCl$_3$) 163.5, 163.4, 147.3, 146.8, 146.7, 138.7, 138.0, 137.9, 137.8, 137.7, 137.6, 137.0, 136.3, 136.0, 133.4, 133.1, 131.5, 130.8, 130.4, 130.34, 130.28, 129.31, 129.26, 128.7, 127.6, 127.4, 126.3, 125.1, 124.8, 124.7, 124.2, 124.1, 123.3, 121.8, 48.2, 47.1, 21.02, 21.97, 20.7, 19.2, 19.1, 18.7, 18.0, 14.3; MS (EI$^+$, 70eV) *m/z* 568 (M$^+$, 84), 553 (100), 284 (10); HRMS (EI$^+$, 70 eV) Calculated: ($C_{44}H_{40}$) 568.3130 (M$^+$), Found: 532.3131.

5,6-Dimesityl-7,12-dimethylpentaleno[2,1-*a*:5,6-*b*′]dinaphthalene 6b^{2-}
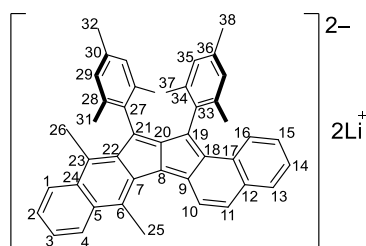
In a nitrogen-filled glove box, to a solution of **12** (0.0138 g, 0.0243 mmol) in THF (0.1 ml) was added ^{n}BuLi (0.035 mL, 0.056 mmol, 1.6 M in hexane) at –35 °C. The reaction mixture was further stirred for 24 h at room temperature, to afford as a deep-brown solution of **6b**$^{2-}$. The dianion **6b**$^{2-}$ was subsequently oxidized without isolation. According to the NMR monitoring, the dianion was generated quantitatively.

^{1}H NMR (600 MHz, THF-d_8) 8.63 (d, J = 8.4 Hz, 1H, 10-H), 7.95 (d, J = 7.8 Hz, 1H, 4-H), 7.73 (d, J = 7.8 Hz, 1H, 16-H), 7.64 (d, J = 8.4 Hz, 1H, 1-H), 7.47 (d, J = 7.8 Hz, 1H, 13-H), 6.88 (t, J = 7.5 Hz, 1H, 2-H), 6.77 (d, J = 8.4 Hz, 1H, 11-H), 6.72 (t, J = 6.9 Hz, 1H, 14-H), 6.67 (t, J = 7.2 Hz, 1H, 3-H), 6.58 (t, J = 7.8 Hz, 1H, 15-H), 6.49 (s, 2H, 35-H), 6.41 (d, 2H, 29-H), 3.64 (s, 3H, 25-H), 2.33 (s, 3H, 26-H), 2.24 (s, 3H, 38-H), 2.19 (s, 3H, 32-H), 1.86 (s, 6H, 31-H), 1.85 (s, 6H, 37-H); ^{13}C NMR (150 Hz, THF-d_8) 144.0 (s, C-20), 143.2 (s, C-27), 142.0 (s, C-33), 138.7 (s, C-28), 138.3 (s, C-34), 137.2 (s, C-22), 131.8 (s, C-36), 130.5 (s, C-30), 129.6 (s, C-12), 129.0 (s, C-17), 128.3 (s, C-7), 127.8 (s, C-18), 127.22 (d, C-35), 127.17 (s, C-24), 126.6 (d, C-13), 126.4 (d, C-29), 123.8 (d, C-16), 122.8 (d, C-4), 122.1 (s, C-5), 120.8 (d, C-10), 120.5 (d, C-1), 119.5 (d, C-15), 118.2 (d, C-2), 117.9 (d, C-14), 117.2 (s, C-9), 113.4 (s, C-6), 112.4 (d, C-3), 107.6 (d, C-11), 106.4 (s, C-23), 105.4 (s, C-8), 95.9 (s, C-19), 89.0 (s, C-21), 22.7 (q, C-27), 22.2 (q, C-33), 21.3 (two signals are overlapped, d, C-29, C-35); ^{7}Li{^{1}H} NMR (155 MHz, THF-d_8) (LiCl in THF-d_8 as external standard) –0.94.

5,6-Dimesityl-7,12-dimethylpentaleno[2,1-*a*:5,6-*b*']dinaphthalene 6b
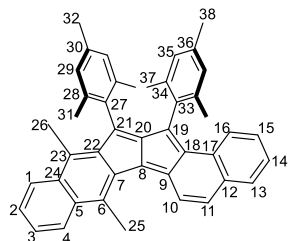
In a nitrogen-filled glove box, a solution of *p*-chloranil (0.03 mmol) in toluene (1 mL) was added to a solution of fresh **6b**$^{2-}$ in THF-d_8. The reaction mixture was stirred for 1 h at room temperature and the solvent was removed in vacuum. The residue obtained was purified by column chromatography on silica gel (hexane/toluene = 1:1) to give **6b** as a reddish-purple solid (0.0098 g, 47%).

mp 271.3−272.0 °C; IR (KBr) 3054 (w), 2916 (s), 2851 (m), 1735 (w), 1695 (w), 1611 (m), 1589 (w), 1568 (m), 1519 (w), 1468 (s), 1454 (s), 1376 (m), 1284 (w), 1258 (m), 1209 (w), 1189 (w), 1149 (w), 1097 (w), 1075 (w), 1027 (m), 890 (w), 848 (w), 804 (m) cm^{-1}; ^{1}H NMR: (600 MHz, THF-d_8) 7.53 (d, J = 7.8 Hz, 1H, 4-H), 7.40 (d, J = 8.4 Hz, 1H, 1-H), 7.14 (t, J = 7.2 Hz, 1H, 3-H), 7.03 (t, J = 7.2 Hz, 1H, 2-H), 6.91 (d, J = 7.2 Hz, 1H, 13-H), 6.85 (t, J = 6.6 Hz, 1H, 14-H), 6.82 (d, J = 10.2 Hz, 1H, 10-H), 6.59 (t, J = 7.8 Hz, 1H, 15-H), 6.55 (d, J = 7.8 Hz, 1H, 16-H), 6.51 (two signals are overlapped, s, 4H, 35-H, 29-H), 6.36 (d, J = 9.6 Hz, 1H, 11-H), 2.43 (s, 3H, 25-H), 2.141 (s, 3H, 38-H), 2.136 (s, 3H, 32-H), 2.12 (s, 6H, 31-H), 2.10 (s, 6H, 37-H), 1.69 (s, 3H, 26-H); ^{13}C NMR (150 Hz, THF-d_8) 156.4 (s), 155.0 (s), 146.1 (s, C-18), 145.6 (s, C-22), 137.32 (s, C-5), 137.26 (s, C-30), 136.6 (s, C-34), 136.5 (s, C-36), 135.8 (s, C-9), 135.73 (s, C-24), 135.68 (s, C-8), 135.4 (s), 135.0 (s, C-28), 134.8 (s, C-12), 133.7 (s, C-17), 133.3 (s, C-33), 131.9 (d, C-11), 129.31 (d, C-13), 129.26 (s), 128.6 (s, C-15), 128.2 (d, C-3), 128.1 (d, C-14), 128.04 (d, C-35), 128.98 (d, C-29), 126.4 (d, C-2), 126.2 (d, C-1), 125.51 (s, C-6), 125.47 (d, C-4), 125.1

(d, C-16), 124.9 (d, C-10), 20.93 (q, C-38), 20.86 (q, C-32), 20.5 (q, C-31), 20.4 (s, C-37), 18.0 (q, C-25), 11.8 (q, C-26); MS (EI$^+$, 70 eV) m/z 566 (M$^+$, 100), 283 (12); HRMS (EI$^+$, 70 eV) Calculated: (C$_{44}$H$_{38}$) 566.2974 (M$^+$), Found: 566.2972.

Supporting Information

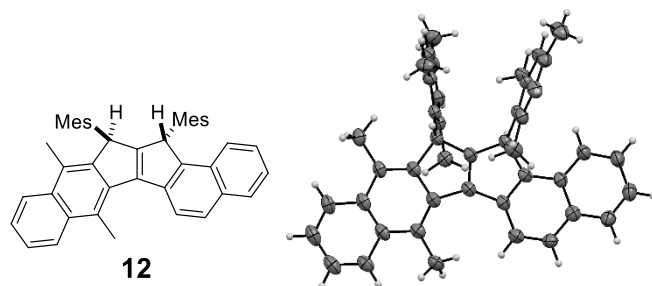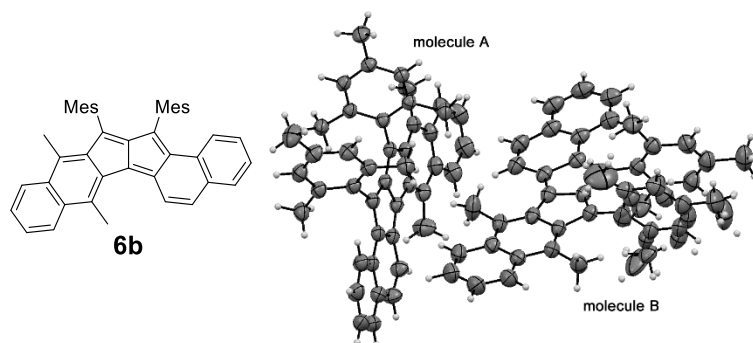### 5,6-Dimesityl-7,12-dimethyl-5,6-dihydropentaleno[2,1-*a*:5,6-*b*']dinaphthalene 12

(CCDC 2109582)

Figure S1. ORTEP drawings of **12** at the 50% probability level.

Empirical Formula	C$_{44}$H$_{40}$	Space Group	*P*-1 (#2)
Formula Weight	568.76	Z value	2
Crystal Color, Habit	translucent light colorless, block	D_{calc}	1.191 g/cm^3
	$0.13 \times 0.108 \times 0.047$ mm	F_{000}	608.0
Crystal Dimensions	triclinic	μ(CuK$_\alpha$)	0.502 mm^{-1}
Crystal System	Primitive	Temperature	123 K
Lattice Type	$a = 10.5459(2)$ Å	Data/restraints/parameters	6283/0/405
Lattice Parameters	$b = 11.5523(2)$ Å	Residuals: $R1$ ($I > 2.00\sigma(I)$)	0.0535
	$c = 14.0742(3)$ Å	Residuals: $wR2$ (*all data*)	0.1543
	$\alpha = 100.238(2)$ °	Goodness of Fit Indicator	1.054
	$\beta = 106.732(2)$ °		
	$\gamma = 97.478(2)$ °		
	$V = 1585.72(6)$ Å^3		

5,6-Dimesityl-7,12-dimethylpentaleno[2,1-*a*:5,6-*b*']dinaphthalene 6b (CCDC 2109581)
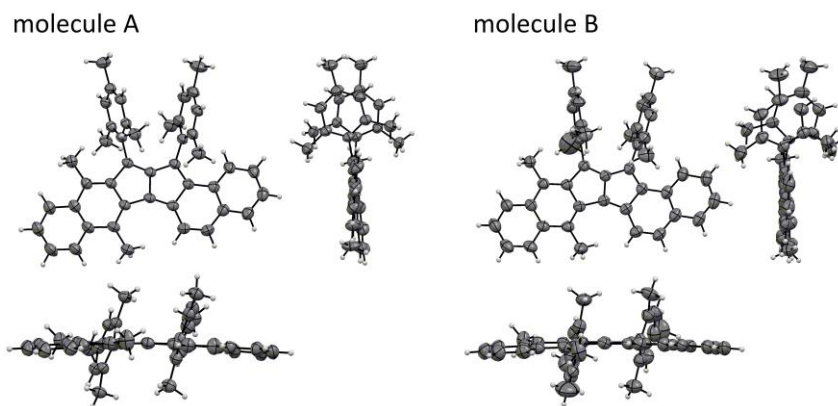
Figure S2. ORTEP drawings of **6b** at the 50% probability level.

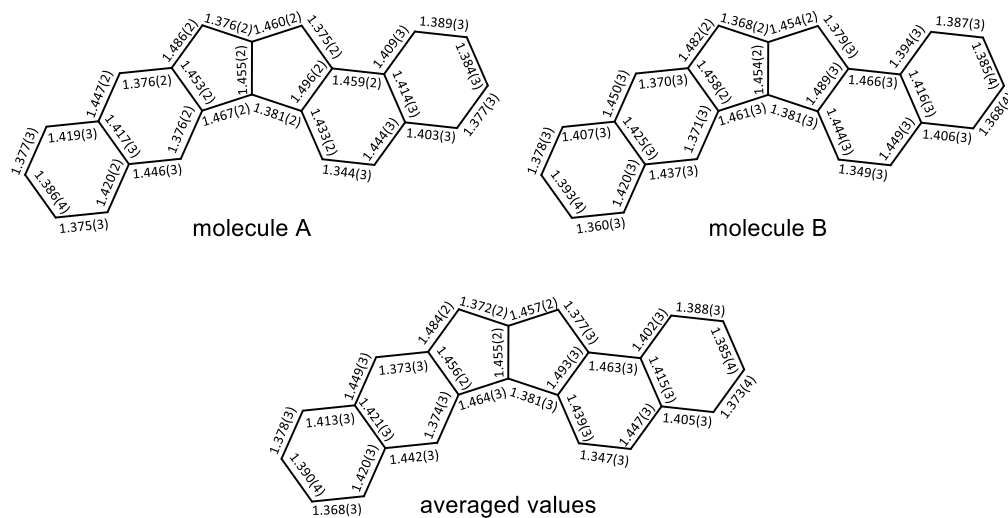|			
Empirical Formula	C₄₄H₃₈	Space Group	C2/c (#15)
Formula Weight	566.74	Z value	16
Crystal Color, Habit	metallic dark red block	D_{calc}	1.198 g/cm³
		F_{000}	4832.0
Crystal Dimensions	0.174 × 0.1 × 0.059	μ(CuK$_\alpha$)	0.507 mm⁻¹
Crystal System	monoclinic	Temperature	123 K
Lattice Type	Base-centered	Data/restraints/parameters	12594/9/894
Lattice Parameters	a = 49.5991(5) Å	Residuals: R1 (I > 2.00σ(I))	0.0571
	b = 8.20560(10) Å	Residuals: wR2 (all data)	0.1799
	c = 31.1894(3) Å	Goodness of Fit Indicator	1.028
	β = 97.9220(10) °		
	V = 12572.6(2) Å³		

Figure S3. Summary for the observed bond lengths (Å) of the main core of **6b**.
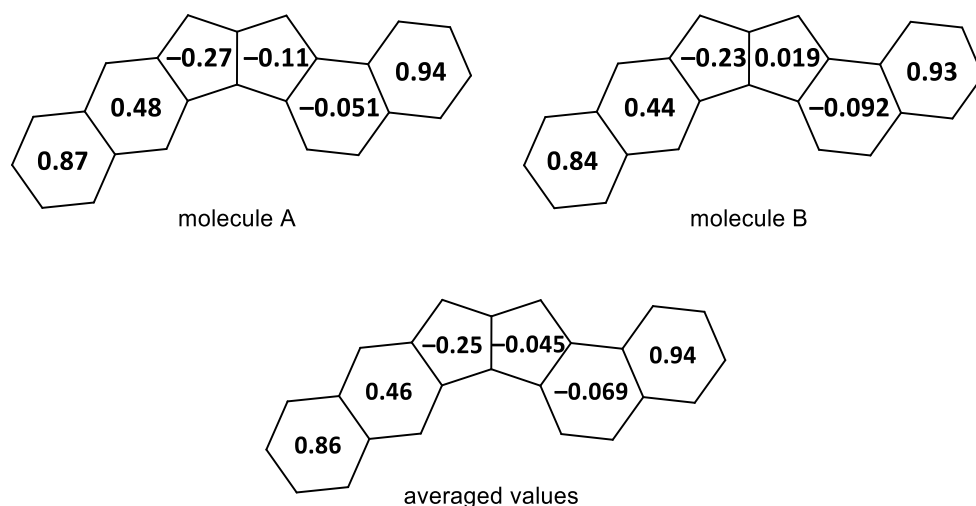
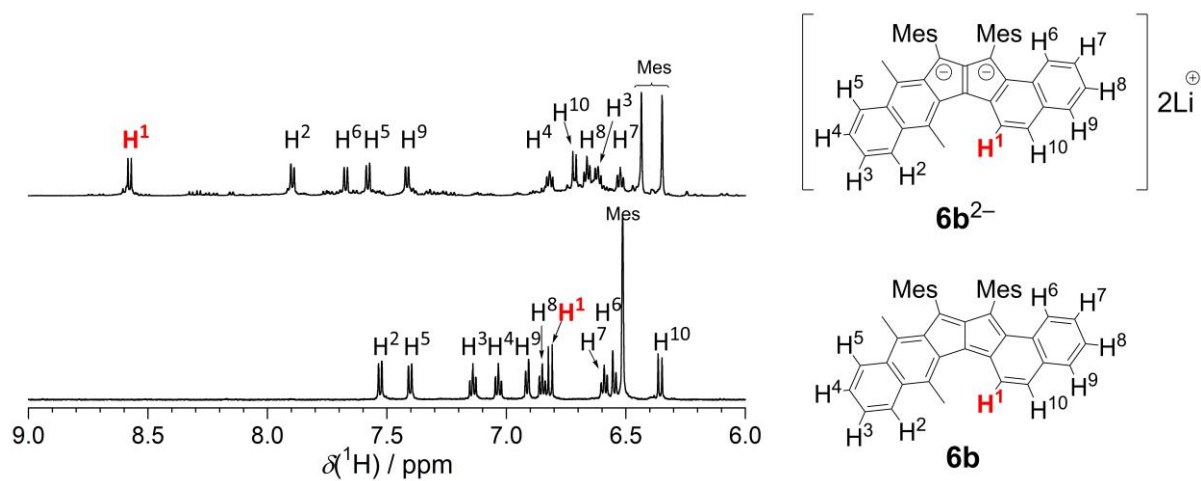**Figure S4**. Summary for the HOMA values of the main core of **6b**.
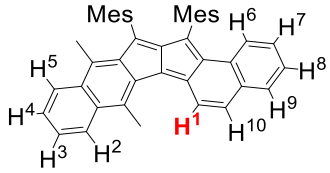
Figure S5. Partial ^{1}H NMR spectra (THF-d_8) of **6b**$^{2-}$ (rt, 600 MHz) and **6b** (rt, 600 MHz).
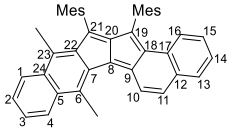
Table S1. ^{1}H NMR chemical shifts of the main core of **6b** and **6b**$^{2-}$.

	6b $\delta(^1H)$/ppm	**6b**$^{2-}$ $\delta(^1H)$/ppm	$\Delta\delta(^1H)$ / ppm $^{a)}$
H^1	6.82	8.63	−1.81
H^2	7.53	7.95	−0.42
H^3	7.14	6.67	0.47
H^4	7.03	6.88	0.15
H^5	7.40	7.64	−0.24

H^6	6.55	7.73	−1.18
H^7	6.59	6.58	0.01
H^8	6.85	6.72	0.13
H^9	6.91	7.47	−0.56
H^{10}	6.36	6.77	−0.41

a) $\Delta\delta(^1H) = \delta(^1H)(\mathbf{6b}) - \delta(^1H)(\mathbf{6b^{2-}})$, n.d. = not determined.

Table S2. ^{13}C NMR chemical shifts of the main core of **6b** and **6b^{2-}**.

	6b $\delta(^{13}C)$/ppm	**6b^{2-}** $\delta(^{13}C)$ /ppm	$\Delta\delta(^{13}C)$ / ppm ^{a}		**6b** $\delta(^{13}C)$ /ppm	**6b^{2-}** $\delta(^{13}C)$ /ppm	$\Delta\delta(^{13}C)$ / ppm ^{a}
C^1	126.2	120.5	5.70	C^{13}	129.31	126.6	2.71
C^2	126.4	118.2	8.20	C^{14}	128.1	117.9	10.2
C^3	128.2	112.4	15.8	C^{15}	128.6	119.5	9.10
C^4	125.47	122.8	2.67	C^{16}	125.1	123.8	1.30
C^5	137.32	122.1	15.2	C^{17}	133.7	129.0	4.70
C^6	125.51	113.4	12.1	C^{18}	146.1	127.8	18.3
C^7	n.d.	128.3	–	C^{19}	n.d.	95.9	–
C^8	135.68	105.4	30.3	C^{20}	n.d.	144.0	–
C^9	135.8	117.2	18.6	C^{21}	n.d.	89.0	–
C^{10}	124.9	120.8	4.10	C^{22}	145.6	137.2	8.40
C^{11}	131.9	107.6	24.3	C^{23}	n.d.	106.4	–
C^{12}	134.8	129.6	5.20	C^{24}	135.73	127.17	8.56

a) $\Delta\delta(^{13}C) = \delta(^{13}C)(\mathbf{6b}) - \delta(^{13}C)(\mathbf{6b^{2-}})$, n.d. = not determined.
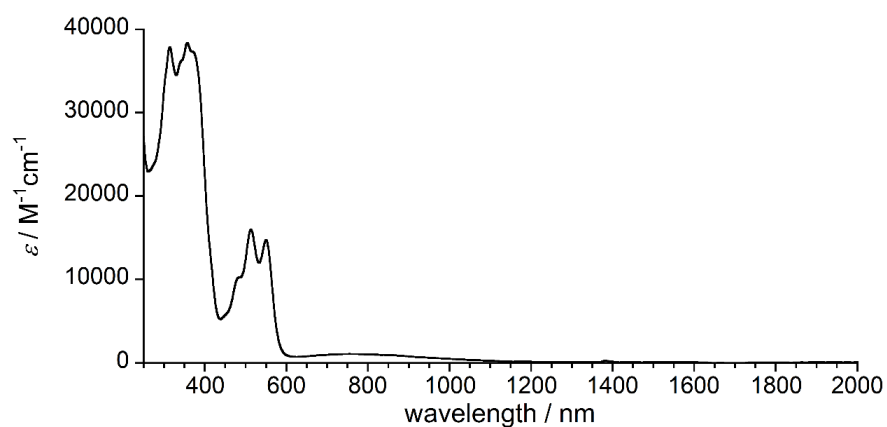

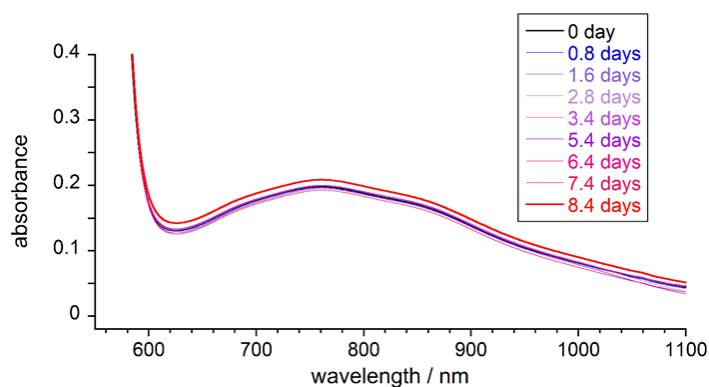**Figure S6**. Electronic absorption spectra of **6b** in CH_2Cl_2.

Figure S7. Periodical measurements of electronic absorption of **6b** in CH_2Cl_2 at lowest-energy region upon exposure to air under room light at room temperature.
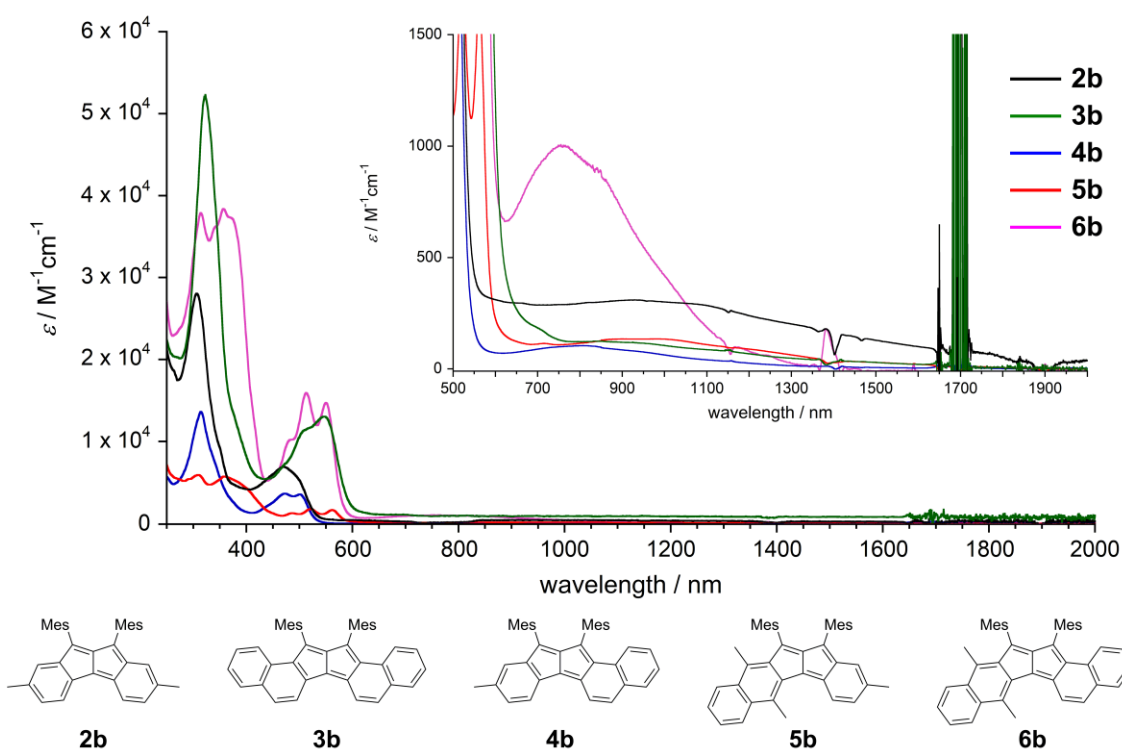

Figure S8. UV/vis/NIR absorption spectra of **2b** (black), **3b** (green), **4b** (blue), **5b** (red), and **6b** (purple) in CH_2Cl_2. The inset shows a magnified view. The background signals at 1700 nm arose from an overtone of the C−H vibrations of the solvent.

Table S3. Summary of the Optoelectronic Properties of **2b**, **3b**, **4b**, **5b**, and **6b**

comp.	optical[a]		electrochemical[b]				
	λ_{max} / nm (ε / M^{-1} cm^{-1})	ΔE_{gap} / eV	$E_2^{ox, pa}$ / V	E_1^{ox} / V	E_1^{red} / V	$E_2^{red, pc}$ / V	$\Delta^{redox} E_1$ / eV

2b	965 (306)	1.28	+0.77	0.0	−1.34	−2.28	1.34
3b	925 (120)	1.53	+0.87	+0.13	−1.28	−2.18	1.41
4b	808 (105)	1.34	+0.86	+0.23	−1.45	−2.26	1.68
5b	983 (135)	1.26	+0.67	−0.018	−1.45	−2.23	1.43
6b	755 (1010)	1.64	+0.84	+0.19	−1.52	−2.22	1.71

a) The optical gap ΔE_{gap} is estimated from $\Delta E_{gap} = 1240/\lambda_{max}$. *b*) All potentials given versus the Fc/Fc$^+$ couple used as internal standard. $\Delta^{redox} E_1 = E_1^{ox} - E_1^{red}$.
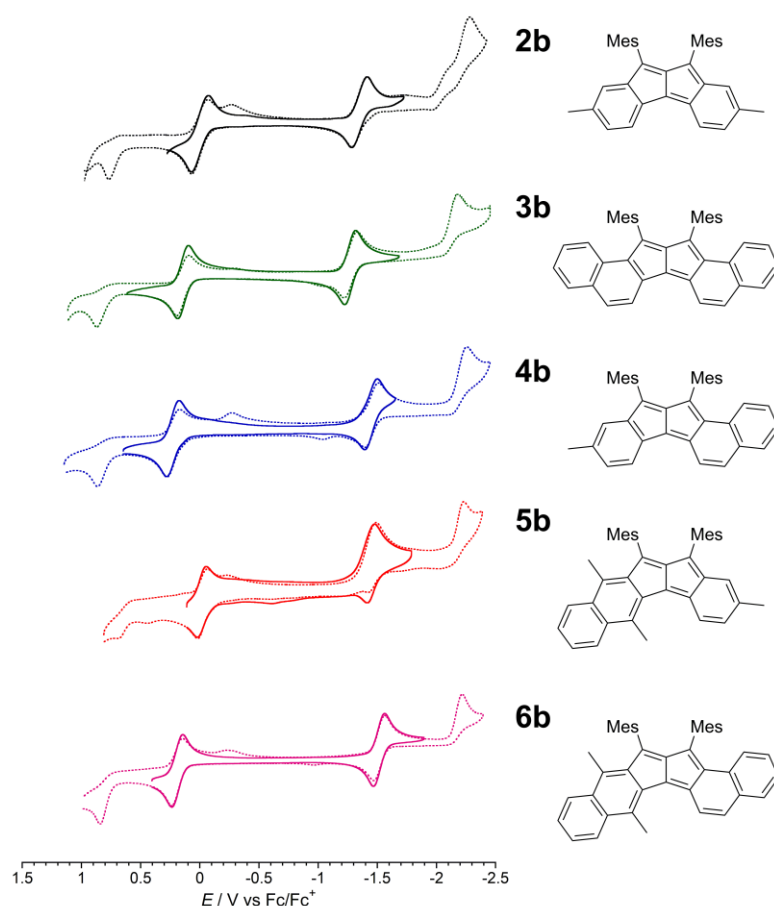

Figure S9. Cyclic voltammograms of **2b** (black), **3b** (green), **4b** (blue), **5b** (red), and **6b** (purple) (V vs Fc/Fc$^+$, in 0.1 M nBu$_4$NClO$_4$/CH$_2$Cl$_2$, scan rate = 100 mV/s, room temperature).

Table S4. Summary of the calculated orbital energies of HOMO–1, HOMO, LUMO, LUMO+1 for **2a**,[5] **3a**,[5] **4a**,[5] **5a**,[4] and **6a** calculated at the RB3LYP/6-311+G* level

comp.	HOMO–1 /eV	HOMO / eV	LUMO / eV	LUMO+1 / eV	$\Delta E_{HOMO–LUMO}$ eV
2a	−6.29	−5.01	−3.31	−0.60	1.70
3a	−5.86	−5.02	−3.28	−1.20	1.74

4a	−6.05	−5.14	−3.15	−1.14	1.99
5a	−6.08	−4.98	−3.25	−1.37	1.73
6a	−5.87	−5.12	−3.10	−1.44	2.02

Figure S10. Summary for NICS(1) values for **6a** and **6a**$^{2-}$ calculated at the GIAO-RB3LYP/6-311+G*//RB3LYP-D3/6-311G* level.
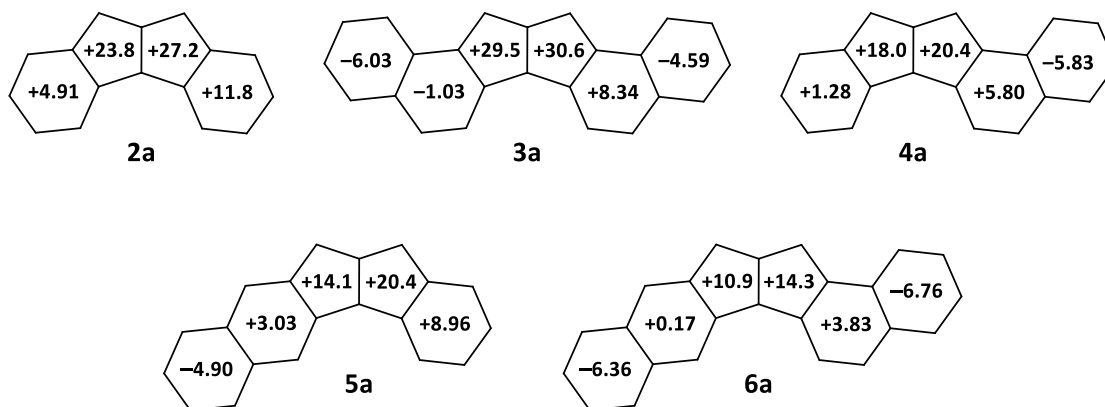

Figure S11. Summary for NICS(1) values for **2a**,[5] **3a**,[5] **4a**,[5] **5a**,[4] and **6a** calculated at the GIAO-(R/U)B3LYP/6-311+G*//RB3LYP-D3/6-311G* level.
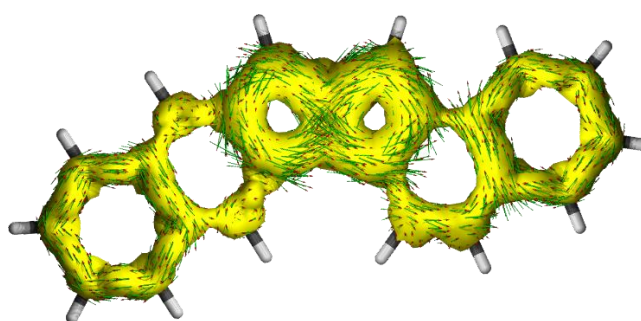

Figure S12. Summary for AICD plots (isovalue surface: 0.035) of **6a** calculated at the CSGT-RB3LYP/6-311+G*//RB3LYP-D3/6-311G* level.
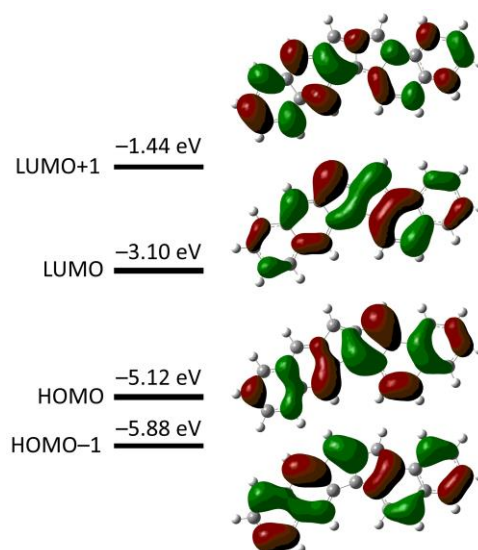
Figure S13. Calculated orbital energy diagram of HOMO–1, HOMO, LUMO, LUMO+1 for **6a** at the RB3LYP/6-311+G* level. Green and red meshes represent the isosurfaces with contour values of +0.02/–0.02 a.u., respectively.

Table S5. Excitation energies of **6a** calculated at the TD-RB3LYP/6-311+G*//RB3LYP-D3/6-311G* level. *a)*

Excited state number	Excitation energy / eV (wavelength / nm)	Excitation amplitudes		Oscillator strength
1	1.35 (921)	0.702	(HOMO – LUMO)	0.0093
2	2.42 (513)	0.647	(HOMO-1 – LUMO)	0.2643
		0.254	(HOMO – LUMO+1)	
3	2.98 (416)	0.116	(HOMO-3 – LUMO)	0.0015
		0.676	(HOMO-2 – LUMO)	
		0.106	(HOMO – LUMO+2)	
4	3.29 (377)	0.586	(HOMO-3 – LUMO)	0.0420
		−0.223	(HOMO – LUMO+1)	
		0.299	(HOMO – LUMO+2)	
5	3.41 (364)	0.146	(HOMO-4 – LUMO)	0.9233
		0.247	(HOMO-3 – LUMO)	
		−0.222	(HOMO-1 – LUMO)	
		0.582	(HOMO – LUMO+1)	
		0.131	(HOMO – LUMO+3)	

Evaluation of hole mobility

Glass/ITO substrates were cleaned by rubbing with acetone-soaked wipes, sonicating sequentially in acetone and isopropanol for 10 min each, and exposing to boiling isopropanol for 5min. The washed substrates were further treated with a UV–O$_3$ cleaner (Filgen, UV253V8) for 20 min. The substrates were transferred to a N$_2$-filled glove box, and compound **6a** was deposited by spin-coating of a THF solution (20 mg mL^{-1}) at 800 rpm for 30 s followed by thermal annealing at 100 °C for 5 min. The resulting film was 187 nm in thickness as determined using a stylus profilometer (Bruker, DektakXT). Finally, MoO$_3$ (5 nm) and Au (30 nm) were deposited at high vacuum (~10^{-5} Pa) through a shadow mask that defined an active area of 4.0 mm^2. Current–voltage characteristics of thus-prepared hole-only devices were measured using a semiconductor parameter analyzer (Agilent, 4155C) in a N$_2$-filled glove box.

The current density–voltage (*J–V*) logarithmic plots showed a slope of 2 (i.e., $J \propto V^2$) at a higher voltage range, implying that the SCLC hole mobility (μ_h) can be calculated based on the Mott–Gurney equation[6]

$$J = \frac{9}{8}\varepsilon_0\varepsilon\mu\frac{V^2}{d^3}$$

where ε_0, ε, and d represent the vacuum permittivity, dielectric constant (assumed to be 4.0), and organic film thickness, respectively. *V* is the effective voltage calculated by subtracting the built-in voltage (V_{bi}) and voltage drop (V_r) due to electrode resistance from the applied voltage (V_{app}). The μ_h value was extracted to be $(4.33 \pm 0.02) \times 10^{-4}$ cm^2 V^{-1} s^{-1} on average (6 devices) with the highest value of 4.37×10^{-4} cm^2 V^{-1} s^{-1}.
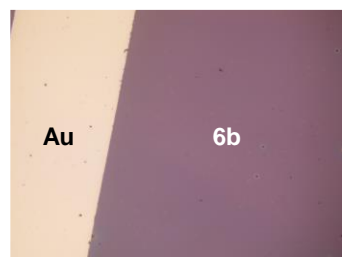

Figure S14. Photographic image of a hole-only device.

Computation of transfer integrals

Transfer integrals were calculated for single-crystal X-ray structure by the fragment orbital method with the B3LYP/DZP level of theory using the Amsterdam Density Functional (ADF) program suite.[7,8]

Film XRD analysis

Out-of-plane X-ray diffraction profiles were recorded on a Rigaku SmartLab diffractometer equipped with a rotating anode (Cu-Kα, λ = 1.5418 Å) operated at 9kW and a Rugaku D/teX Ultra silicon stlip detector. Measurements were performed in the θ–2θ mode.
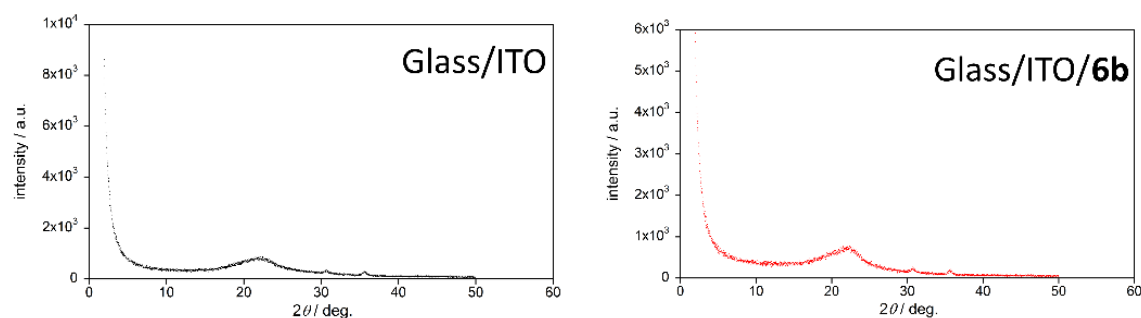

Figure S15. X-ray diffraction (XRD) patterns of (left) Glass/ITO and (right) Glass/ITO/**6b** substrates.

2-5. Reference

(1)   Garratt, P. J. *Aromaticity*; John Wiley & Sons Ltd.; New York: New York, 1986.

(2)   Breslow, R. Antiaromaticity. *Acc. Chem. Res.* **1973**, *6*, 393–398.

(3)   Minkin, V. I.; Glukhovtsev, M. N.; Simkin, B. I. A. *Aromaticity and Antiaromaticity: Electronic and Structural Aspects*; Wiley-Interscience publication; J. Wiley & Sons, 1994.

(4)   Gleiter, R.; Haberhauer, G.; Hoffmann, R. *Aromaticity and Other Conjugation Effects*; Wiley-VCH, 2012.

(5)   L. J. Karas, J. . I. W. Antiaromatic Compounds: A Brief History, Applications, and the Many Ways They Escape Antiaromaticity. In *Aromaticity Modern Computational Methods and Applications*; Fernandez, I., Ed.; Elsevier, 2021; pp 319–337.

(6)   Parkhurst, R. R.; Swager, T. M. Synthesis and Optical Properties of Phenylene-Containing Oligoacenes. *J. Am. Chem. Soc.* **2012**, *134*, 15351–15356.

(7)   Chase, D. T.; Fix, A. G.; Kang, S. J.; Rose, B. D.; Weber, C. D.; Zhong, Y.; Zakharov, L. N.; Lonergan, M. C.; Nuckolls, C.; Haley, M. M. 6,12-Diarylindeno[1,2-*b*]Fluorenes: Syntheses, Photophysics, and Ambipolar OFETs. *J. Am. Chem. Soc.* **2012**, *134*, 10349–10352.

(8)   Rudebusch, G. E.; Espejo, G. L.; Zafra, J. L.; Peña-Alvarez, M.; Spisak, S. N.; Fukuda, K.; Wei, Z.; Nakano, M.; Petrukhina, M. A.; Casado, J.; Haley, M. M. A Biradical Balancing Act: Redox Amphoterism in a Diindenoanthracene Derivative Results from Quinoidal Acceptor and Aromatic Donor Motifs. *J. Am. Chem. Soc.* **2016**, *138*, 12648–12654.

(9)   Zeng, Z.; Shi, X.; Chi, C.; López Navarrete, J. T.; Casado, J.; Wu, J. Pro-Aromatic and Anti-Aromatic π-Conjugated Molecules: An Irresistible Wish to Be Diradicals. *Chem. Soc. Rev.* **2015**, *44*, 6578–6596.

(10)   Rudebusch, G. E.; Zafra, J. L.; Jorner, K.; Fukuda, K.; Marshall, J. L.; Arrechea-Marcos, I.; Espejo, G. L.; Ponce Ortiz, R.; Gómez-García, C. J.; Zakharov, L. N.; Nakano, M.; Ottosson, H.; Casado, J.; Haley, M. M. Diindeno-Fusion of an Anthracene as a Design Strategy for Stable Organic Biradicals. *Nat. Chem.* **2016**, *8*, 753–759.

(11)   Marshall, J. L.; Uchida, K.; Frederickson, C. K.; Schütt, C.; Zeidell, A. M.; Goetz, K. P.; Finn, T. W.; Jarolimek, K.; Zakharov, L. N.; Risko, C.; Herges, R.; Jurchescu, O. D.; Haley, M. M. Indacenodibenzothiophenes: Synthesis, Optoelectronic Properties and Materials Applications of Molecules with Strong Antiaromatic Character. *Chem. Sci.* **2016**, *7*, 5547–5558.

(12)   Nishida, J.; Tsukaguchi, S.; Yamashita, Y. Synthesis, Crystal Structures, and Properties of 6,12-Diaryl-Substituted Indeno[1,2-*b*]Fluorenes. *Chem. - A Eur. J.* **2012**, *18*, 8964–8970.

(13)   Ie, Y.; Sato, C.; Yamamoto, K.; Nitani, M.; Aso, Y. A Thiazole-Fused Antiaromatic Compound Containing an *s*-Indacene Chromophore with a High Electron Affinity. *Chem. Lett.* **2018**, *47*, 1534–1537.

(14)   Yamamoto, K.; Ie, Y.; Tohnai, N.; Kakiuchi, F.; Aso, Y. Antiaromatic Character of Cycloheptatriene-Bis-Annelated Indenofluorene Framework Mainly Originated from Heptafulvene Segment. *Sci. Rep.* **2018**, *8*, 17663.

(15)   Nishinaga, T.; Ohmae, T.; Aita, K.; Takase, M.; Iyoda, M.; Arai, T.; Kunugi, Y. Antiaromatic Planar Cyclooctatetraene: A Strategy for Developing Ambipolar Semiconductors for Field Effect Transistors. *Chem. Commun.* **2013**, *49*, 5354–5356.

(16)   Zeidell, A. M.; Jennings, L.; Frederickson, C. K.; Ai, Q.; Dressler, J. J.; Zakharov, L. N.; Risko, C.; Haley, M. M.; Jurchescu, O. D. Organic Semiconductors Derived from Dinaphtho-Fused *s*-Indacenes: How Molecular Structure and Film Morphology Influence Thin-Film Transistor Performance. *Chem. Mater.* **2019**, *31*, 6962–6970.

(17)   Nakazato, T.; Takekoshi, H.; Sakurai, T.; Shinokubo, H.; Miyake, Y. Synthesis and Characterization of 16π Antiaromatic 2,7-Dihydrodiazapyrenes: Antiaromatic Polycyclic Hydrocarbons with Embedded Nitrogen. *Angew. Chemie Int. Ed.* **2021**, *60*, 13877–13881.

(18)   Shin, J.-Y.; Yamada, T.; Yoshikawa, H.; Awaga, K.; Shinokubo, H. An Antiaromatic Electrode-Active Material Enabling High Capacity and Stable Performance of Rechargeable Batteries. *Angew. Chemie Int. Ed.* **2014**, *53*, 3096–3101.

(19)   Fujii, S.; Marqués-González, S.; Shin, J.; Shinokubo, H.; Masuda, T.; Nishino, T.; Arasu, N. P.; Vázquez, H.; Kiguchi, M. Highly-Conducting Molecular Circuits Based on Antiaromaticity. *Nat. Commun.* **2017**, *8*, 15984.

(20)   Usuba, J.; Hayakawa, M.; Yamaguchi, S.; Fukazawa, A. Dithieno[*a,e*]Pentalenes: Highly Antiaromatic Yet Stable Π-Electron Systems without Bulky Substituents. *Chem. – A Eur. J.* **2021**, *27*, 1638–1647.

(21)   Ando, N.; Yamada, T.; Narita, H.; Oehlmann, N. N.; Wagner, M.; Yamaguchi, S. Boron-Doped Polycyclic π-Electron Systems with an Antiaromatic Borole Substructure That Forms Photoresponsive B–P Lewis Adducts. *J. Am. Chem. Soc.* **2021**, *143*, 9944–9951.

(22)   Hafner, K.; Häfner, K. H.; König, C.; Kreuder, M.; Ploss, G.; Schulz, G.; Sturm, E.; Vöpel, K. H. Fulvenes as Isomers of Benzenoid Compounds. *Angew. Chemie Int. Ed. English* **1963**, *2*, 123–134.

(23)   Hafner, K. Structure and Aromatic Character of Non-Benzenoid Cyclically Conjugated Systems. *Angew. Chemie Int. Ed. English* **1964**, *3*, 165–173.

(24)   Hafner, K. New Aspects of the Chemistry of Nonbenzenoid Polycyclic Conjugated π-Electron Systems. *Pure Appl. Chem.* **1982**, *54*, 939–956.

(25)   Tobe, Y. Non-Alternant Non-Benzenoid Aromatic Compounds: Past, Present, and Future. *Chem. Rec.* **2015**, *15*, 86–96.

(26)   Konishi, A.; Yasuda, M. Breathing New Life into Nonalternant Hydrocarbon Chemistry: Syntheses and Properties of Polycyclic Hydrocarbons Containing Azulene, Pentalene, and Heptalene Frameworks. *Chem. Lett.* **2021**, *50*, 195–212.

(27)   Hopf, H. Pentalenes-From Highly Reactive Antiaromatics to Substrates for Material Science. *Angew. Chemie Int. Ed.* **2013**, *52*, 12224–12226.

(28)   Saito, M. Synthesis and Reactions of Dibenzo[*a,e*]Pentalenes. *Symmetry (Basel).* **2010**, *2*, 950–969.

(29)   Kawase, T.; Nishida, J. π-Extended Pentalenes: The Revival of the Old Compound from New Standpoints. *Chem. Rec.* **2015**, *15*, 1045–1059.

(30)   Kawase, T.; Fujiwara, T.; Kitamura, C.; Konishi, A.; Hirao, Y.; Matsumoto, K.; Kurata, H.; Kubo, T.; Shinamura, S.; Mori, H.; Miyazaki, E.; Takimiya, K. Dinaphthopentalenes: Pentalene Derivatives for Organic Thin-Film Transistors. *Angew. Chemie Int. Ed.* **2010**, *49*, 7728–7732.

(31)   Li, C.; Liu, C.; Li, Y.; Zhu, X.; Wang, Z. Facile Synthesis of a Pyrrole-Fused Dibenzo[a,e]Pentalene and Its Application as a New Extended, Ladder-Type Fused Aromatic System. *Chem. Commun.* **2015**, *51*, 693–696.

(32)   Wilbuer, J.; Grenz, D. C.; Schnakenburg, G.; Esser, B. Donor- and Acceptor-Functionalized Dibenzo[*a,e*]Pentalenes: Modulation of the Electronic Band Gap. *Org. Chem. Front.* **2017**, *4*, 658–663.

(33)   Dai, G.; Chang, J.; Jing, L.; Chi, C. Diacenopentalene Dicarboximides as New N-Type Organic Semiconductors for Field-Effect Transistors. *J. Mater. Chem. C* **2016**, *4*, 8758–8764.

(34)   Hermann, M.; Wu, R.; Grenz, D. C.; Kratzert, D.; Li, H.; Esser, B. Thioether- and Sulfone-Functionalized Dibenzopentalenes as n-Channel Semiconductors for Organic Field-Effect Transistors. *J. Mater. Chem. C* **2018**, *6*, 5420–5426.

(35)   Yuan, B.; Zhuang, J.; Kirmess, K. M.; Bridgmohan, C. N.; Whalley, A. C.; Wang, L.; Plunkett, K. N. Pentaleno[1,2-*a*:4,5′]Diacenaphthylenes: Uniquely Stabilized Pentalene Derivatives. *J. Org. Chem.* **2016**, *81*, 8312–8318.

(36)   Zhang, Z.; Fan, H.; Zhu, X. Fast Construction of Dianthraceno[*a,e*]Pentalenes for OPV Applications. *Org. Chem. Front.* **2017**, *4*, 711–716.

(37)   Schmidt, M.; Wassy, D.; Hermann, M.; González, M. T.; Agräit, N.; Zotti, L. A.; Esser, B.; Leary, E. Single-Molecule Conductance of Dibenzopentalenes: Antiaromaticity and Quantum Interference. *Chem. Commun.* **2021**, *57*, 745–748.

(38)   Wu, Y.; Wang, Y.; Chen, J.; Zhang, G.; Yao, J.; Zhang, D.; Fu, H. Intramolecular Singlet Fission in an Antiaromatic Polycyclic Hydrocarbon. *Angew. Chemie Int. Ed.* **2017**, *56*, 9400–9404.

(39)   Liu, Y.; Wu, Y.; Wang, L.; Wang, L.; Yao, J.; Fu, H. Efficient Triplet Pair Separation from Intramolecular Singlet Fission in Dibenzopentalene Derivatives. *Sci. China Chem.* **2019**, *62*, 1037–1043.

(40)   El Bakouri, O.; Smith, J. R.; Ottosson, H. Strategies for Design of Potential Singlet Fission Chromophores Utilizing a Combination of Ground-State and Excited-State Aromaticity Rules. *J. Am. Chem. Soc.* **2020**, *142*, 5602–5617.

(41)   Baker, W.; McOmie, J. F. W.; Parfitt, S. D.; Watkins, D. A. M. Attempts to Prepare New Aromatic Systems. Part VI. 1 : 2-5 : 6-Dibenzopentalene and Derivatives. *J. Chem. Soc.* **1957**, 4026–4037.

(42)   Konishi, A.; Okada, Y.; Nakano, M.; Sugisaki, K.; Sato, K.; Takui, T.; Yasuda, M. Synthesis and Characterization of Dibenzo[*a,f*]Pentalene: Harmonization of the Antiaromatic and Singlet Biradical Character. *J. Am. Chem. Soc.* **2017**, *139*, 15284–15287.

(43)   Konishi, A.; Okada, Y.; Kishi, R.; Nakano, M.; Yasuda, M. Enhancement of Antiaromatic Character via Additional Benzoannulation into Dibenzo[*a,f*]Pentalene: Syntheses and Properties of Benzo[*a*]Naphtho[2,1-*f*]Pentalene and Dinaphtho[2,1-*a,f*]Pentalene. *J. Am. Chem. Soc.* **2019**, *141*, 560–571.

(44)   Konishi, A.; Horii, K.; Iwasa, H.; Okada, Y.; Kishi, R.; Nakano, M.; Yasuda, M. Characterization of Benzo[*a*]Naphtho[2,3-*f*]Pentalene: Interrelation between Open-shell and Antiaromatic Characters Governed by Mode of the Quinoidal Subunit and Molecular Symmetry. *Chem. – An Asian J.* **2021**, *16*, 1553–1561.

(45)   Geuenich, D.; Hess, K.; Köhler, F.; Herges, R. Anisotropy of the Induced Current Density (ACID), a General Method To Quantify and Visualize Electronic Delocalization. *Chem. Rev.* **2005**, *105*, 3758–3772.

(46)   Kruszewski, J.; Krygowski, T. M. Definition of Aromaticity Basing on the Harmonic Oscillator Model. *Tetrahedron Lett.* **1972**, *13*, 3839–3842.

(47)   Krygowski, T. M. Crystallographic Studies of Inter- and Intramolecular Interactions Reflected in Aromatic Character of .Pi.-Electron Systems. *J. Chem. Inf. Comput. Sci.* **1993**, *33*, 70–78.

(48)   Oshima, H.; Fukazawa, A.; Yamaguchi, S. Facile Synthesis of Polycyclic Pentalenes with Enhanced Hückel Antiaromaticity. *Angew. Chemie Int. Ed.* **2017**, *56*, 3270–3274.

(49)   Frederickson, C. K.; Zakharov, L. N.; Haley, M. M. Modulating Paratropicity Strength in Diareno-Fused Antiaromatics. *J. Am. Chem. Soc.* **2016**, *138*, 16827–16838.

(50)   Dai, G.; Chang, J.; Zhang, W.; Bai, S.; Huang, K.-W.; Xu, J.; Chi, C. Dianthraceno[*a,e*]Pentalenes: Synthesis, Crystallographic Structures and Applications in Organic Field-Effect Transistors. *Chem. Commun.* **2015**, *51*, 503–506.

(51)   Sworakowski, J.; Janus, K. On the Reliability of Determination of Energies of HOMO Levels in Organic Semiconducting Polymers from Electrochemical Measurements. *Org. Electron.* **2017**, *48*, 46–52.

Chapter 3

Appearance of Open-shell and Antiaromatic Character Induced by High Symmetric Geometry of Planar Heptalene Structure: Synthesis and Characterization of a Non-alternant Isomer of Bisanthene

3-1. Introduction

Non-alternant polycyclic hydrocarbons[1] have experienced a remarkable renaissance thanks to their unique electronic configurations and molecular orbital characteristics, which are never shared by alternant systems.[2] The π-extended non-alternant polycyclic hydrocarbons, azulene[3]-, pentalene[4]- and indacene[5]-based molecules, have recently fueled rich insights into the electronic properties of (anti)aromaticity[6] and/or open-shell character.[7] The topology of π-electron network is a primary concern that determines the ground state electronic structures of polycyclic hydrocarbons.[8–15] The transformation of naphthalene into azulene is a thought-provoking example for the topological difference in the π-conjugation with the same number of π-electrons (Figure 1A). The replacement of hexagons of naphthalene with a heptagon and a pentagon associates the structural change with the reduction of molecular symmetry from a D_{2h} to a C_{2v} symmetry, which leads to the unsymmetrically distributed frontier orbitals and unusual physical or chemical properties of azulene. Many related studies have illustrated that incorporating a non-alternant scaffold into an alternant system is a powerful strategy to impact the electronic properties of polycyclic hydrocarbons,[16,17] however, lowering the molecular symmetry upon the transformation of an alternant to a non-alternant system has been little considered despite the factor that triggers large electronic perturbations.

Our particular interest here is to investigate the crossover of ground state from the aromatic closed-shell state to the antiaromatic open-shell state in an isomeric pair of alternant and non-alternant hydrocarbons with the same molecular symmetry. The authors selected a 12π-heptalene scaffold as an antiaromatic moiety. The pristine heptalene is a twisted molecule with non-aromatic character, however, the ring fusions into the heptalene core possibly fix the geometry into a plane. The planar heptalene skeleton, which corresponds to a transition structure of the ring inversion and/or the π-bond shift (Figure 1B), provides an access to its 12π antiaromatic character.[18] As a model molecule, difluoreno[1,9,8-*alkj*:1',9',8'-*gfed*]heptalene **1**, which is a non-alternant isomer of bisnathene **2** and incorporates a planarized heptalene skeleton, was designed (Figure 1C). Bisanthene[19,20] is a benzenoid polycyclic aromatic hydrocarbon (PAH) and a smallest member of the *peri*-acene series.[21] While bisanthene possesses singlet closed-shell ground state with local aromatic character, the larger homologues, teranthene[22] and *peri*-tetracene,[23,24] have been revealed to be singlet open-shell compounds. For *peri*-tetracene, its non-alternant isomer with two azulene cores was successfully synthesized on Au(111) surface, demonstrating the appearance of open-shell character and the reduction of the HOMO–LUMO energy gap.[25]
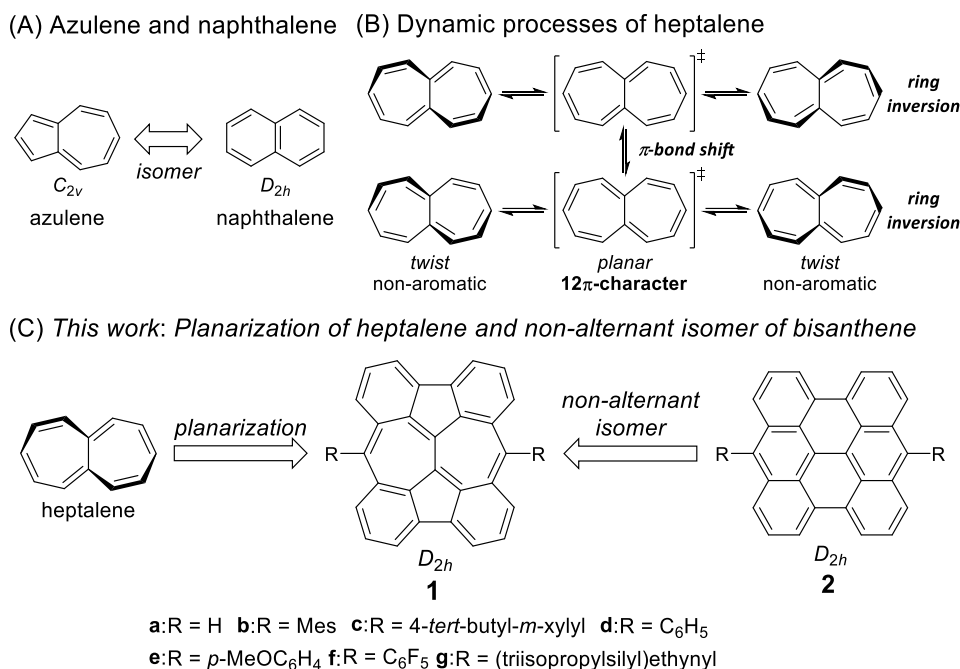
Figure 1. Molecular structures of (A) azulene and naphthalene, (B) dynamic processes of heptalene and (C) difluoreno[1,9,8-*alkj*:1',9',8'-*gfed*]heptalene **1** and bisanthene **2**. Mes = 2,4,6-trimethylphenyl.

The target molecule **1** serves as an acceptable non-alternant isomer of **2**. The D_{2h}-symmetric scaffold of **1** enables to rule out the reduction of the molecular symmetry in the non-alternant system and to directly assess the effect of the incorporated odd-membered rings. The existence of two *o*-quinoidal subunits in **1** allows to convert the aromatic/closed-shell character of **2** into the antiaromatic/open-shell character (**1a-A** in Figure 2). The central heptalene unit of **1** should induce paratropic character as a 12π-electron system (**1a-B**). In contrast to the reported heptalene derivatives,[26] the planar geometry given by the highly fused structure and the formal delocalization of *o*-quinoidal substructures would enhance the local antiaromatic character. Furthermore, the recovery of benzenoid character of the *o*-quinoidal hexagons would attain to the singlet open-shell state of **1**, pushing out the two unpaired electrons on the head carbon of the heptagons (**1a-C**).
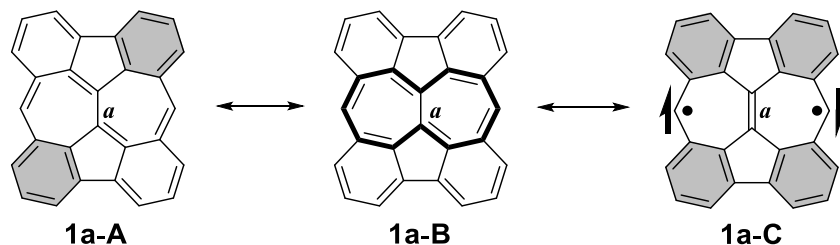

Figure 2. Resonance structures of **1a**. The hexagonal rings in gray denote benzenoid rings, and the the $4n\pi$-conjugated circuit that contributed significantly to a canonical structure is highlighted in bold lines.

3-2. Results and Discussion

The synthetic route for the derivatives **1** is shown in Scheme 1. For the construction of fully conjugated system, the less aromatic character of **1** should impede the progress of the conventional reaction,[27] such as dehydrogenation or dehydration. Thus, the authors designed the route via an aromatic dication species **1**$^{2+}$ as a key precursor. According to Haper's procedure,[28] the oxidation of fluoranthene afforded the florenone derivative **3**.
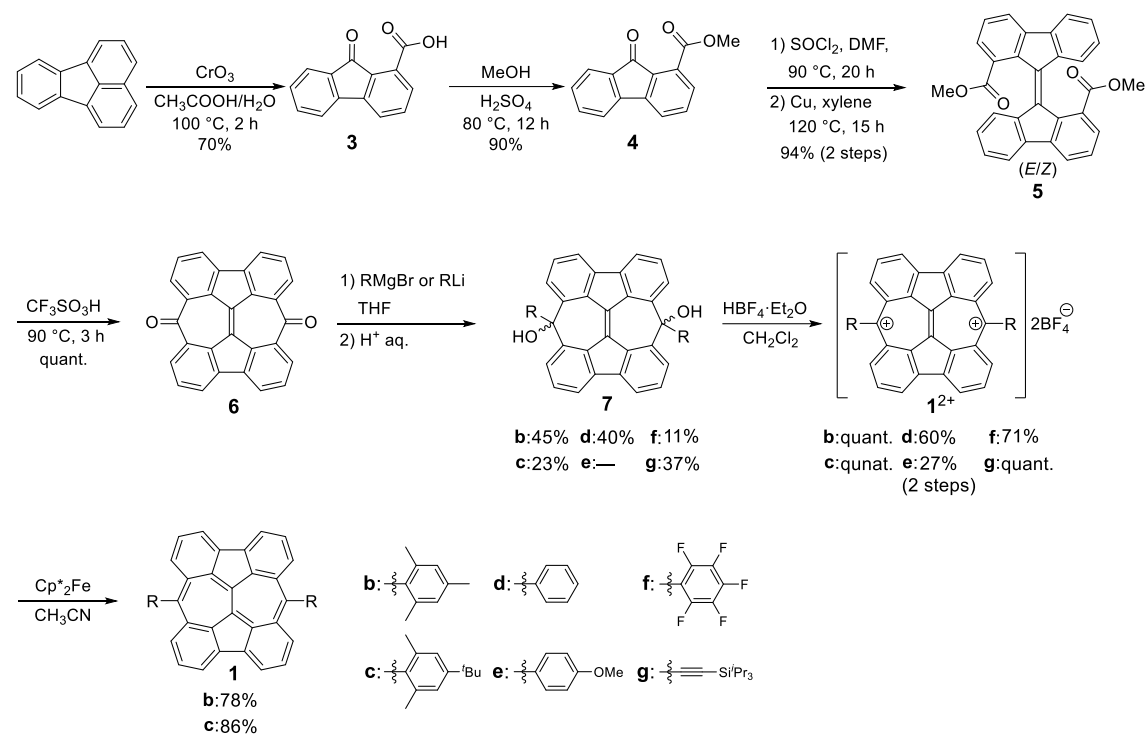
Scheme 1. Synthesis of **1**

After esterification of the carboxylic group of **3** yielded **4**,[29] the dichlorination of the carbonyl group of **4** and subsequent treatment with cupper powder gave the 9,9'-bifluorenylidene derivative **5**.[30] The cyclization was performed by the treatment of **5** with heated trifluoromethanesulfonic acid, to quantitatively yield dione **6** with two heptagons. Nucleophilic attack on the dione **6** with arylmagnesium bromides or (triisopropylsilyl)ethynyl lithiate afforded diols **7**. Except for **7e** with electron-donating groups, all diols **7** were isolated (Figure S1). The reductive dearomatization of **7** with SnCl$_2$ failed to afford complicated mixtures, presumably due to the lack of two benzene rings in **1** from **7**. Alternatively, the treatment of diols **7** with tetrafluoroboric acid diethyl ether complex in CH$_2$Cl$_2$ immediately gave dication salts **1**·2BF$_4$ as green to purple solids, which are the two-electron oxidized species of the target molecules **1**. All dications **1**·2BF$_4$ were confirmed by the spectroscopic measurements and the molecular geometry of the 4-*tert*-butyl-*m*-xylyl derivative **1c**·2BF$_4$ was determined by the X-ray crystallographic analysis (Figure S2). Two-electron reduction of **1**$^{2+}$ with decamethylferrocene furnished the mesityl derivative **1b** and the 4-*tert*-butyl-*m*-xylyl

74

derivative **1c** as greenish black solids. The reductions of the other dications **1d**–**g**$^{2+}$ were also tried, but the approaches gave unidentified mixtures presumably due to the inadequately kinetic protections of the reactive site under the reaction conditions. A CH$_2$Cl$_2$ solution of **1b** showed gradual decomposition with a half-life of 3 days upon exposure to air under room light at room temperature (Figure S13).

Careful recrystallization from a chloroform/chlorobenzene solution in a degassed sealed tube gave a single crystal of **1b** suitable for X-ray crystallographic analysis (Figure 3). X-ray crystallographic analysis of **1b** illustrated the main core of **1b** assumed a planar structure and the two mesityl groups formed a large dihedral angle (*ca.* 85°) with the main core (Figure S3). The main core of **1b** assumes an approximate D_{2h} symmetry; the observed bond lengths of the main core of **1b** is good agreement with those of theoretically optimized D_{2h} model rather than C_{2h} model of **1a** (Figure S14). When comparing the bond length alternation (BLA) of the heptagons in **1b** with that of **1c**$^{2+}$, the antiaromatic nature of **1b** was quite obvious. The dication **1c**$^{2+}$ bearing a 10π-aromatic unit exhibited the less BLA on the heptagons (1.423(3)–1.454(3) Å; Figure S4). On the other hand, the degree of the BLA of the heptagons in **1b** was increased (1.428(2)–1.470(2) Å). Although the reported heptalene derivatives exhibited twisted geometries to avoid the instability of the 4nπ-electron delocalization,[31] the highly planar and symmetric structure of **1b**, which are realized by the surrounding ring-fusions, would enhance the contribution of the 4nπ-system. The NICS(1) values for the heptagons estimated at the GIAO-(U)B3LYP/6-311+G* level also support the idea, which indicates the large positive value of +11.2 for **1a** and the negative value of –6.70 for **1a**$^{2+}$ (Figure S16). The paratropic character on the heptagons for **1a** would magnetically suppress the aromatic character of the surrounding hexagon (denoted by *A* in Figure 3; NICS(1); –0.84), which was also estimated in the π-extended pentalenes.[32]
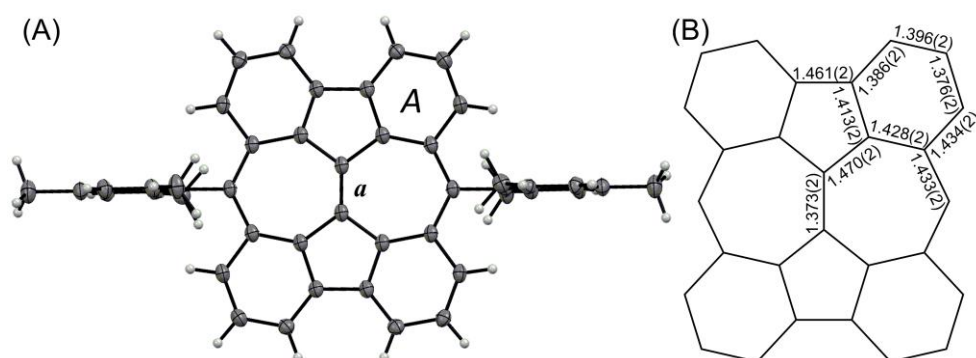

Figure 3. (A) Ortep drawing of **1b** with at the 50% probability level, and (B) bond lengths (mean values) in the main core rings of **1b**.

The observed high symmetric structure of **1b** deeply reflected the contribution of the singlet open-shell character to the ground state electronic configuration. The biradical resonance contribution was be found in a contraction of the *a* bonds due to their double-bond character. The length of the *a* bond in **1b** is 1.373(2) Å,

which is considerably shorter than length of a typical C(sp2)–C(sp2) single bond (1.467 Å). Additionally, the peripheral four hexagons sustain the high degree of benzenoid character; the harmonic oscillator model of aromaticity (HOMA) analysis[33] indicated a larger value for the hexagons (ring A; +0.80). Furthermore, these geometric features are line with the degree of the diradical character (y) estimated at the CASSCF(2,2)/6-31G* level, which indicates a large LUMO occupation number of 0.72 for **1a** in contrast to only 0.065 for **2a**. The spin densities are mainly distributed the head carbons on the heptagons (Figure S15).

The determined physical properties of **1b** supported the open-shell character. Superconducting quantum interference device (SQUID) measurement was conducted for the microcrystalline sample of **1b**. The measurement showed an increasing susceptibility above 150 K (Figure S6). From Bleaney−Bower's fitting of the observed increase, the value of the singlet−triplet energy gap ($\Delta E_{\text{S–T}}$) was determined to be –1080 K (–2.15 kcal/mol), which is reasonable to the theoretical estimation of –1370 K (–2.72 kcal/mol) calculated using a UB3LYP-D3/6-311G* method for **1a**. The experimentally determined $\Delta E_{\text{S–T}}$ of **1b** is smaller than those of teranthene (–3.82 kcal/mol)[22] and *peri*-tetracene (–2.5 kcal/mol)[24] derivatives, even though **1b** is the smallest π-conjugated system among them. This unusual trend of **1** might come from the destabilization of the singlet ground state induced by 4nπ-delocalization. The small $\Delta E_{\text{S–T}}$ indicates that **1b** is easily activated to a triplet state even at low temperature. Actually, no ^{1}H NMR signal of the main core of **1b** in THF-d_8 was observed even at –100 °C (Figure S9).[34,35] ESR measurements of **1b** clearly displayed signals typical of triplet species. A glassy toluene sample of **1b** gave a splitting pattern of $\Delta M_{\text{s}} = \pm 1$ signal and a forbidden $\Delta M_{\text{s}} = \pm 2$ half-field signal at 170–115 K (Figure S7). The signal intensity decreased upon cooling, which occurrence of a singlet ground state in **1b**.
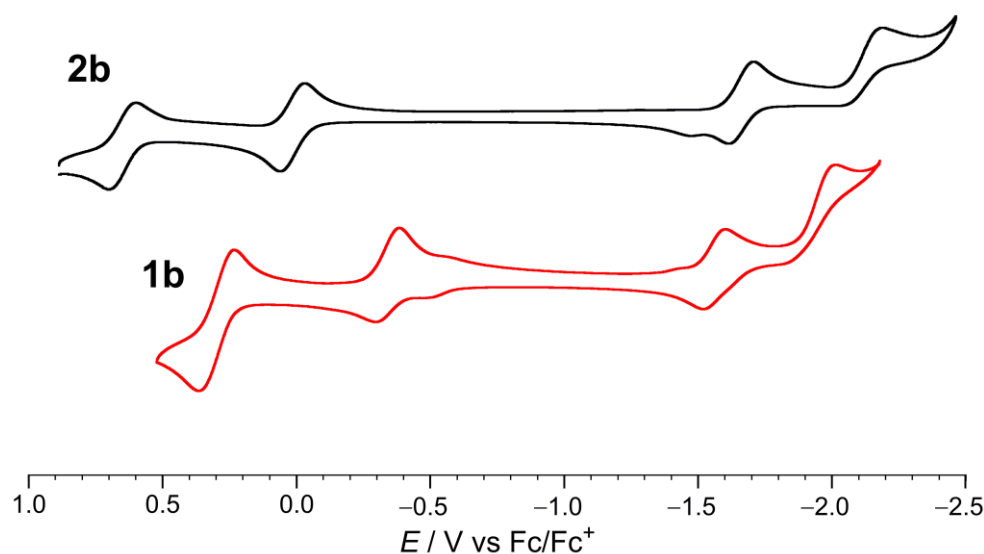

Figure 4. Cyclic voltammograms of **1b** (red) and **2b** (black) (V vs Fc/Fc$^+$, in 0.1 M nBu$_4$NClO$_4$/CH$_2$Cl$_2$, scan rate = 100 mV/s, room temperature).
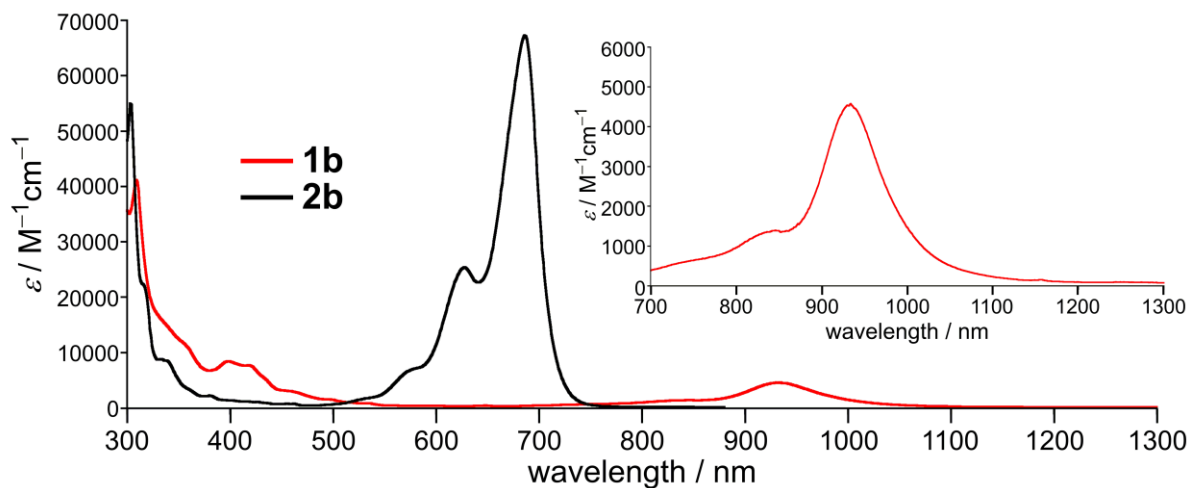
Figure 5. UV/vis/NIR absorption spectra of **1b** (red) and **2b** (black) in CH_2Cl_2. The inset shows a magnified view.

The open-shell and antiraomtic nature of **1** are featured by the small HOMO−LUMO energy gap. The cyclic voltammogram of **1b** showed three reversible and an irreversible redox waves (E_2^{ox} = +0.30 V, E_1^{ox} = –0.34 V, E_1^{red} = –1.56 V, and $E_2^{red, pc}$ = –2.01 V vs Fc/Fc$^+$, Figure 4). The electrochemical HOMO−LUMO gap of 1.22 eV, which was estimated from the difference between the first oxidation and reduction potentials, was 0.46 eV smaller than that of **2b**.[36] The electronic absorption spectrum of **1b** in CH_2Cl_2 gave a lowest-energy band (λ_{max}) at 934 nm (ε = 4579 $M^{-1}cm^{-1}$), which was significantly red-shifted compared with those of **2b** (λ_{max} = 686 nm, ε = 67300 $M^{-1}cm^{-1}$; Figure 5). Notably, the absorption intensity (*i.e.* molar absorption coefficient) of the lowest-energy band of **1b** is less than one-tenth of that of **2b**. The DFT calculation of **1a** at the UB3LYP/6-311+G* level indicated that the embedment of the odd-membered rings gave rise to the reconfiguration of the frontier orbitals of **2b**, leading to the pseudo degeneration between the LUMO and LUMO+1 level (Figure S17). The time-dependent (TD)-DFT calculations on **1a** suggest that the band at 934 nm of **1b** is ascribed to the partially allowed HOMO→LUMO+1 transition (λ = 935 nm, f = 0.021, see Figure S17 and Table S3). These orbitals associated with the transition show the disjoint feature[37] with α/β spins localized at the two head carbons on the heptagons, thus, the observed weak and lowest-energy absorption of **1b** would derive from the open-shell character of **1**.

3-3. Conclusion

The autrhors achieved a synthesis and characterization of **1**, the non-alternant isomer of bisanthene **2**. The obtained **1** displayed antiaromatic character from the central heptalene core and possessed singlet biradical features, which have not been observed in bisanthene **2**. The highly planar and symmetric geometry of **1** realizes unusual electronic properties in an unexpectedly small π-conjugated system. The present study sheds

light on the importance of the topologically design for non-alternant polycyclic hydrocarbons. Further studies on the related systems, as well as the development of the facile synthetic method, are ongoing in our group.

3-4. Experimental Section

General

NMR spectra were recorded on JEOL-AL400, JEOL-ECS400 (400 MHz for ^{1}H, and 100 MHz for ^{13}C) and Bruker AVANCE III spectrometers (600 MHz for ^{1}H, and 150 MHz for ^{13}C) with TMS as an internal standard. ^{1}H and ^{13}C NMR signals of compounds were assigned using HMQC, HMQC, HMBC, COSY, NOESY, and ^{13}C off-resonance techniques. ESR spectra were recorded on a Bruker EMXmicro spectrometer. The temperature-dependent magnetic susceptibility was measured for randomly oriented polycrystalline samples of **3c** on a Quantum Design SQUID magnetometer MPMS-XL in the temperature range of 2−300 K. Positive FAB and EI mass spectra were recorded on a JEOL JMS-700 and a Shimadzu GCMS-QP2010 Ultra, respectively. Positive ESI mass spectra were taken by using ThermoFisher Scientific LTQ ORBITRAP XL mass spectrometer. IR spectra were recorded as thin films or as solids in KBr pellets on a HORIBA FT-720 and a JASCO FT/IR 6200 spectrophotometer. UV-vis-NIR spectra were recorded on a JASCO V-670 spectrophotometer. Cyclic voltammetric measurements were performed with an ALS-600C electrochemical analyzer using a glassy carbon working electrode, a Pt counter electrode, and an Ag/AgNO$_3$ reference electrode at room temperature in CH$_2$Cl$_2$ containing 0.1 M Bu$_4$NClO$_4$ as the supporting electrolyte. Data collection for X-ray crystal analysis was performed on Rigaku/XtaLAB Synergy-S/Mo (MoKα λ = 0.71075 Å) and Rigaku/XtaLAB Synergy-S/Cu (CuK$_\alpha$ λ = 1.54187 Å) diffractometers. All calculations were performed with the observed reflections [I>2σ(I)] by the program CrystalStructure crystallographic software packages[38] except for refinement, which was performed using SHELXL-97.[39] All non-hydrogen atoms were refined with anisotropic displacement parameters and hydrogen atoms were placed at calculated positions and refined "riding" on their corresponding carbon atoms.

Materials

All reagents were obtained from commercial suppliers. All reactions were carried out under nitrogen. The florenone derivatives **3**[28] and **4**[29] and bisanthene **2b**[36] were prepared by the reported procedures. Synthesis of **1** was performed in a nitrogen-filled glove box. For the variable temperature ^{1}H NMR measurement, the solution of **1b** in THF-d_8 was degassed by a repeated freeze-pump-thaw method (5 times) and then the sample tube was sealed. For the ESR measurement of the fluid sample of **1b**, the solution of **1b** in toluene (0.49 mM) was degassed by a repeated freeze-pump-thaw method (5 times) and then the sample tube was sealed.

Computational Method

All calculations were conducted using the Gaussian 09 program.[40] The geometries of **1a**$^{2+}$ and **2a** in the singlet state were optimized with the RB3LYP-D3 functional and 6-311G* basis set, to afford the optimized structures with a D_{2h} symmetry. We performed geometry optimization of neutral **1a** by using the RB3LYP-D3 functional and the broken-symmetry (BS) approach with the UB3LYP-D3 functional. Under a D_{2h} geometry, the RB3LYP-D3 method gave a first-order saddle point with one imaginary frequency (687.82i cm^{-1}), but the UB3LYP-D3 method gave the open-shell optimized structure with a D_{2h} symmetry (<S^2> = 1.015) as a local minimum structure giving all positive vibrational frequencies. Alternatively, the RB3LYP-D3 method gave a C_{2h} geometry with closed-shell singlet state (<S^2> = 0). The C–C bond lengths of neutral **1a** with a D_{2h} symmetry calculated by UB3LYP-D3 method nicely agreed with those of **1b** determined by X-ray analysis (Figure S14). Judging from the result, we employed the UB3LYP-D3 geometry of neutral **1a** for the calculations of the other properties. NICS(1) values of **1a**$^{2+}$ were calculated at the GIAO-RB3LYP/6-311+G* method using these optimized structures. For neutral **1a**, NICS(1)

values were calculated at the GIAO-UB3LYP/6-311+G* method, since the RDFT approach is considered to give very different feature of magnetic response properties of open-shell singlet systems compared with the broken-symmetry UDFT results.[41,42] Molecular orbitals of **1a** and **2a** were evaluated at the UB3LYP/6-311+G* and the RB3LYP/6-311+G*level, respectively. Electronic excitation properties of **1a** and **2a** were evaluated by the TDDFT method U or RB3LYP and 6-311+G* basis set, respectively. We have evaluated diradical index (y) and singlet-triplet energy gap ($\Delta E_{ST} = E_S – E_T$) of **1a**. Geometry optimizations of **1a** in the singlet and triplet states were performed at the UB3LYP-D3/6-311G* level. The values of y were obtained from the occupation number of LUMO ($y = n_L$) at the CASSCF/6-31G* level.

Synthesis and Characterization

(E) or *(Z)*-Dimethyl-[9,9′-bifluorenylidene]-1,1′-dicarboxylate 5
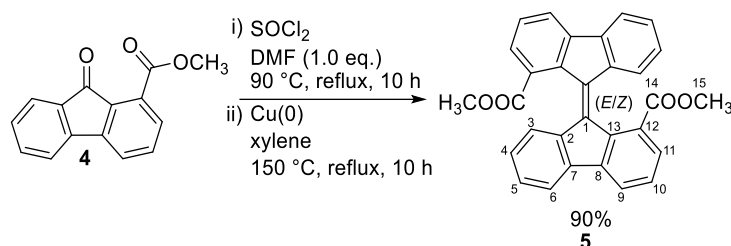

A procedure from the literature[30] was modified as follows: A mixture of **4**[29] (7.51 g, 31.5 mmol) and thionyl chloride (10 mL) with DMF (2.4 mL, 31.2 mmol) was refluxed for 10 h. After cooling to room temperature, excessive thionyl chloride and DMF were removed under vacuum and the residue was washed with dry CH_2Cl_2 (2 mL x 3). The obtained light brown solids was dissolved with dry xylene (20 mL). After copper powder (pre-dried at 150 °C for 10 h under vacuum, 10 g) was added to the mixture, the reaction mixture was heated at 150 °C for 10 h under a N_2 atmosphere. After cooling to room temperature, copper powder was removed by filtration and the obtained solution was washed with water, and dried over $MgSO_4$. The organic phase was collected by filtration and the solvents were removed under vacuum. The residue was purified by column chromatography on silica gel (hexane then hexane/ethyl acetate 8:2) to give **5** as a red solid of inseparable diastereo mixture (6.55 g (isomer A/B = 5:2), 94%).

R_f = 0.33 (EtOAc/hexane = 1:4); mp 225.1–225.3 °C; IR (KBr) ν = 3063 (w), 2943 (w), 1729 (s), 1448 (m), 1431 (m), 1412 (m), 1282 (m), 1261 (s), 1194 (m), 1143 (m), 767 (s), 730 (s) cm^{-1};

isomer A: ^{1}H NMR (400 MHz, CDCl$_3$) 7.82 (d, J = 7.6 Hz, 2H), 7.76 (d, J = 7.6 Hz, 2H), 7.68 (d, J = 8.0 Hz, 2H), 7.64 (d, J = 6.8 Hz, 2H), 7.45 (t, J = 7.4 Hz, 2H), 7.27–7.23 (m, 2H), 7.13 (t, J = 7.8 Hz, 2H), 3.22 (s, 6H, H-15); ^{13}C NMR (100 MHz, CDCl$_3$) 168.9 (s, C-14), 143.0 (s), 141.7 (s), 139.0 (s), 138.2 (s), 135.3 (s), 131.7 (s), 129.18 (d), 129.0 (d), 128.8 (d), 127.79 (d), 123.8 (d), 122.7 (d), 119.7 (d), 51.6 (q, C-15);

isomer B: ^{1}H NMR (400 MHz, CDCl$_3$) 8.47 (d, J = 7.6 Hz, 2H), 7.79 (d, J = 7.2 Hz, 2H), 7.71 (d, J = 7.6 Hz, 2H), 7.49 (d, J = 8.4 Hz, 2H), 7.38–7.28 (m, 6H), 3.00 (s, 6H, H-15); ^{13}C NMR (100 MHz, CDCl$_3$) 168.2 (s, C-14), 142.2 (s), 141.9 (s), 139.6 (s), 138.1 (s), 136.8 (s), 130.1 (s), 129.20 (d), 129.1 (d), 128.7 (d), 127.80 (d), 125.9 (d), 122.2 (d), 120.1 (d), 51.1 (q, C-15); MS (FAB$^+$, 70 eV) m/z 444.2 (M$^+$, 32), 154 (94), 136 (100) ; HRMS (FAB$^+$, 70 eV) Calculated: (C$_{30}$H$_{20}$O$_4$) 444.1362 (M$^+$), Found: 444.1364; Analysis C$_{30}$H$_{20}$O$_4$ (444.49) Calculated: C, 81.07; H, 4.54; O, 14.40, Found: C, 80.80; H, 4.48.

Heptaleno[2,1,10,9-*jklm*:4,5,6,7-*j'k'l'm'*]difluorene-7,14-dione 6
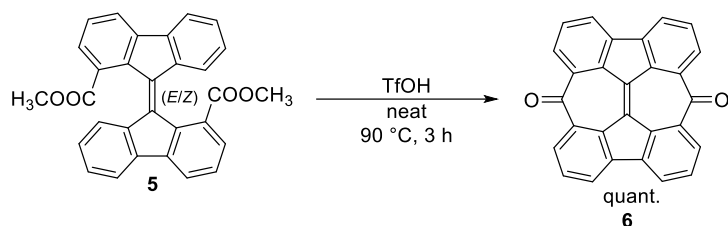
A mixture of **5** (1.00 g, 2.26 mmol) and trifluoromethanesulfonic acid (2 mL) was heated at 90 °C for 3 h and the reaction mixture was poured onto crashed ice. The precipitated solids were collected by filtration and washed with water (10 mL x 2), acetone (10 mL x 2), CHCl₃ (10 mL x 2), and hexane (10 mL x 2). The obtained solid was dried at 100 °C under vacuum for 5 h to give **6** as an insoluble green solid (0.860, quant.). The obtained product was too insoluble to record any NMR spectrum.

mp >300°C: IR (KBr) v = 3064 (w), 1634 (m), 1593 (m), 1421 (m), 1372 (w), 1257 (s), 1173 (s), 1032 (s), 827 (w), 766 (m), 715 (w), 641 (m), 580 (w), 523 (w) cm⁻¹ MS (EI⁺, 70 eV) m/z 380 (M⁺, 100), 352 (29, –CO), 322 (15, –2CO); HRMS (EI⁺, 70 eV) Calculated: (C₂₈H₁₂O₂) 380.0837 (M⁺), Found: 380.0833.

7,14-Dimesityl-7,14-dihydroheptaleno[2,1,10,9-*jklm*:4,5,6,7;*j'k'l'm'*]difluorene-7,14-diol 7b
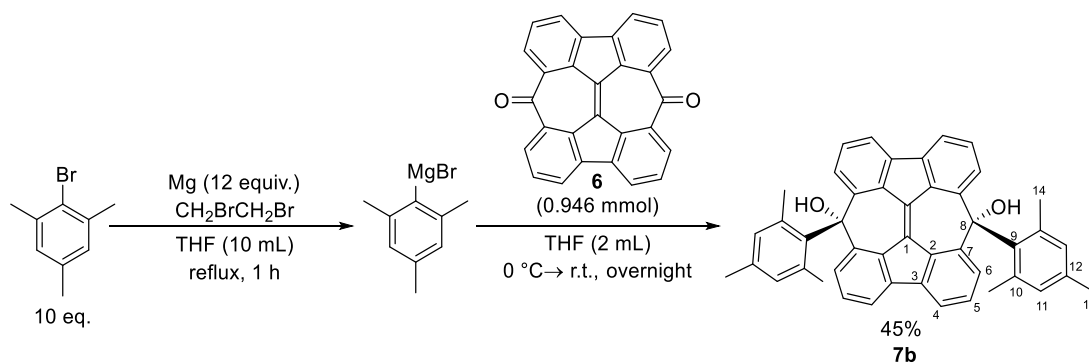
The Grignard reagent was prepared by the reaction of magnesium turnings (0.274 g, 11.4 mmol) and 2-bromomesitylene (1.43 mL, 9.46mol) in THF (10 mL) containing a small amount of 1,2-dibromoethane (0.1 mL) as the initiator. The mixture was refluxed for 1 h to give a solution of mesityl magnesium bromide in THF. A solution of mesityl magnesium bromide in THF was added to a suspension of **6** (0.360 g, 0.946 mmol) in THF (2 mL) at 0 °C. The mixture was stirred for overnight at room temperature and quenched with water. Ethyl acetate (10 mL) was added to the mixture. An insoluble solid was removed by filtration and the obtained organic layer was washed with water, and dried over Na₂SO₄. The filtrate was evaporated and the residue was washed with hexane (10 mL). The precipitated solids were collected by filtration and washed with hexane/CHCl₃ (7:3) to obtain **7b** as yellow solid of a single diastereomer (0.264 g, 45%).

The recrystallization for X-ray crystallographic analysis was performed from a solution of toluene/dichloromethane solution.

mp 258.5–260.0 °C; IR (KBr) v = 3530 (s), 2971 (w), 2920 (w), 1607 (m), 1582 (w), 1476 (w), 1455 (w), 1416 (m), 1042 (w), 1030 (w), 1004 (w), 939 (w), 851 (w), 803 (w), 770 (s), 725 (w) cm⁻¹; ¹H NMR (400 MHz, CDCl₃) 7.77 (d, J = 6.8 Hz, 4H, H-4), 7.30 (t, J = 7.8 Hz, 4H, H-5), 7.18 (d, J = 8.0 Hz, 4H, H-6), 6.90 (brs, 4H, H-11), 2.76 (brs, 2H, OH), 2.36 (s, 6H, H-13), 2.17 (s, 12H, H-14); ¹³C NMR (100 MHz, CDCl₃) 143.3 (s), 141.0 (s), 140.9 (s), 137.52 (s), 137.47 (s), 136.3 (d), 133.2 (s), 131.7 (s), 129.9 (d, C-5), 129.2 (d, C-6), 119.2 (d, C-4), 84.4 (s, C-8), 30.9 (q), 20.7 (q); MS (MALDI-TOF) m/z 621 (M+H⁺); HRMS (EI⁺, 70 eV) Calculated: (C₃₀H₂₀O₄) 620.2715 (M⁺), Found: 620.2716.

7,14-Bis(4-(*tert*-butyl)-2,6-dimethylphenyl)-7,14-dihydroheptaleno[2,1,10,9-*jklm*:4,5,6,7-*j'k'l'm'*]difluorene-7,14-diol 7c
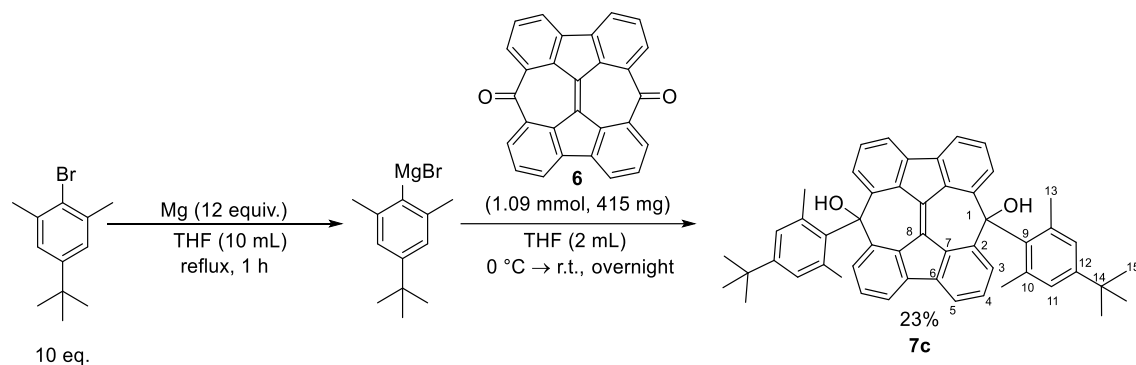
The Grignard reagent was prepared by the reaction of magnesium turnings (0.314 g, 13.1 mmol) and 2-bromo-5-(*tert*-butyl)-1,3-dimethylbenzene (2.63 g, 10.9 mmol) in THF (10 mL) containing a small amount of 1,2-dibromoethane (0.1 mL) as the initiator. The mixture was refluxed for 1 h to give a solution of (4-(*tert*-butyl)-2,6-dimethylphenyl)magnesium bromide in THF. A solution of (4-(*tert*-butyl)-2,6-dimethylphenyl)magnesium bromide in THF was added to a suspension of **6** (0.415 g, 1.09 mmol) in THF (2 mL) at 0 °C. The mixture was stirred for overnight at room temperature and quenched with water. Ethyl acetate (10 mL) was added to the mixture. An insoluble solid was removed by filtration and the obtained organic layer was washed with water, and dried over Na2SO4. The filtrate was evaporated and the residue was washed with hexane (10 mL). The precipitated solids were collected by filtration and washed with hexane/CHCl3 (7:3) to obtain **7c** as yellow solid of a single diastereomer (0.180 g, 23%).

mp 250.5 °C (decomposition); IR (KBr) ν = 3532 (s), 3426 (m), 3060 (w), 2961 (s), 2902 (w), 2865 (m), 1604 (m), 1480 (m), 1418 (m), 1225 (m), 1006 (m), 799 (m), 767 (s), 748 (m) cm^{-1}; ^{1}H NMR (400 MHz, CDCl3) 7.78 (d, J = 7.2 Hz, 4H, H-5), 7.31 (t, J = 7.8 Hz, 4H, H-4), 7.14 (d, J = 7.6 Hz, 4H, H-3), 7.08 (brs, 4H, H-11), 2.80–2.17 (m, 12H, H-13), 1.70 (brs, 2H, OH), 1.39 (s, 18H, H-15); ^{13}C NMR (100 MHz, CDCl3) 149.4 (s), 143.4 (s, C-10), 141.0 (s), 140.7 (s), 137.6 (s), 136.9 (d, C-11), 133.3 (s), 129.9 (d, C-4), 129.3 (d, C-3), 127.7 (s), 119.2 (d, C-5), 84.5 (s, C-1), 34.1 (s, C-14), 31.4 (q, C-15), 25.4 (q, C-13); MS (MALDI-TOF) m/z 703 ([M–H]$^+$); HRMS (ESI) Calculated: (C28H12O2) 1431 .7201 ([2M+Na]$^+$), Found: 1431.7187.

7,14-Dimesityl-7,14-dihydroheptaleno[2,1,10,9-*jklm*4,5,6,7-*j'k'l'm'*]difluorene-7,14-diylium tetrafluoroborate 1b·2BF4
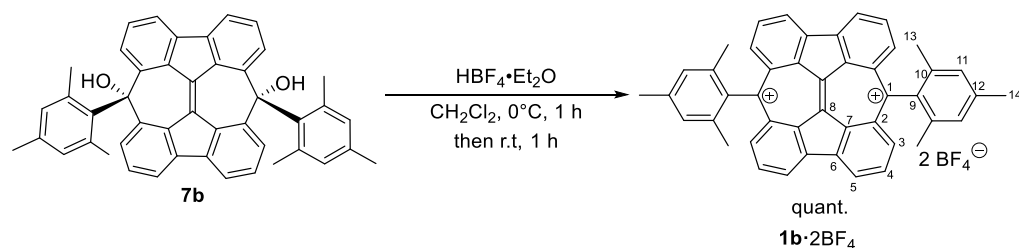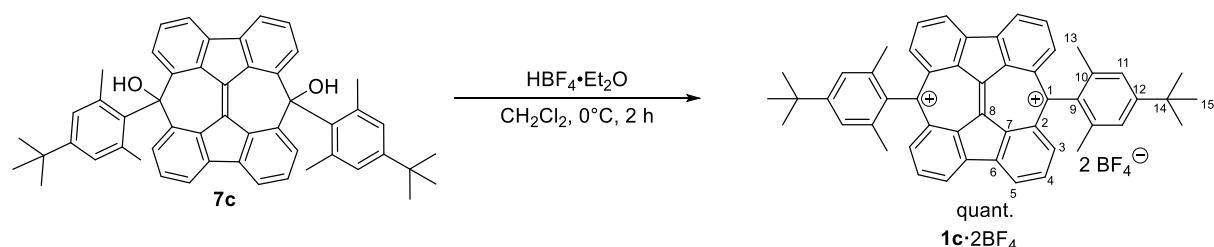

A procedure from the literature[43] was modified as follows: To a solution of **7b** (0.10 g, 0.161 mmol) in dichloromethane (2 mL) was added tetrafluoroboric acid/diethyl ether complex (50–55 % in diethylether, 0.19 mL). The reaction mixture was stirred at 0 °C for 1 h and allowed to warm to room temperature. After 1 h of stirring at room temperature, a layer of diethyl ether (15 mL) was placed on the reaction mixture. Slow stirring the mixture led to the formation of a black precipitate. The precipitate was collected by filtration washed with diethylether and dried in a vacuum to give **1b·2BF4** as a dark green solid (0.122 g, quant.).

mp 253.0 °C (decomposition); IR (KBr) ν =2966 (w), 2920 (w), 2735 (w), 2717 (w), 2561 (w), 2377 (w), 1610 (m), 1544 (m),

1463 (m), 1431 (w), 1405 (s), 1362 (w), 1305 (m), 1224 (m), 1192 (s), 1160 (m), 1082 (s), 1053 (s), 1038 (s), 917 (m), 769 (m) cm^{-1}; ^{1}H NMR (400 MHz, CDCl$_3$ (0.06% CF$_3$SO$_3$H)) 9.68 (d, J = 6.8 Hz, 4H, H-5), 9.01 (d, J = 8.4 Hz, 4H, H-3), 8.68 (t, J = 7.8 Hz, 4H, H-4), 7.32 (s, 4H, H-11), 2.62 (s, 6H, H-14), 1.82 (s, 12H, H-13); ^{13}C NMR (100 MHz, CDCl$_3$ (0.06% CF$_3$SO$_3$H)) 194.2 (s, C-1), 149.1 (s, C-8), 144.2 (d, C-3), 142.5 (s, C-12), 141.0 (s, C-6), 140.0 (d, C-5), 139.8 (s, C-7), 137.0 (s, C-2), 136.64 (s, C-10), 136.59 (d, C-4), 135.5 (s, C-9), 128.9 (d, C-11), 21.3 (q, C-14), 20.5 (q, C-13); MS (MALDI-TOF) m/z 586 (M$^+$); HRMS (EI, 70 eV) Calculated: (C$_{46}$H$_{34}$) 586.2650 (M$^+$), Found: 586.2651 (M$^+$); Analysis C$_{46}$H$_{34}$B$_2$F$_8$ (760.3852) Calculatedd: C, 72.66; H, 4.51, B, 2.84, F, 19.99, Found: C, 69.49; H, 4.85 (Due to the sensitivity to air moisture, acceptable values were not obtained.).

7,14-Bis(4-(*tert*-butyl)-2,6-dimethylphenyl)-7,14-dihydroheptaleno[2,1,10,9-*jklm*:4,5,6,7-*j'k'l'm'*]difluorene-7,14-diylium tetrafluoroborate 1c·2BF$_4$

A procedure from the literature[43] was modified as follows: To a solution of **7c** (50.0 mg, 0.071 mmol) in dichloromethane (2 mL) was added tetrafluoroboric acid/diethyl ether complex (50–55 % in diethylether, 0.10 mL) at 0 °C. The reaction mixture was stirred at 0 °C for 1 h and allowed to warm to room temperature. After 1 h of stirring at room temperature, a layer of diethyl ether (15 mL) was placed on the reaction mixture. Slow stirring the mixture led to the formation of a black precipitate. The precipitate was collected by filtration washed with diethylether and dried in a vacuum to give **1c**·2BF$_4$ as a dark green solid (0.068 g, quant.).

mp >300 °C; IR (KBr) ν = 3047 (w), 2961 (s), 2903 (m), 2869 (w), 1609 (m), 1547 (s), 1463 (s), 1408 (s), 1363 (m), 1295 (m), 1225 (m), 1188 (s), 1053 (s), 945 (s), 905 (w), 871 (w), 808 (w), 768 (m), 678 (w), 564 (m), 505 (m) cm^{-1}; ^{1}H NMR (400 MHz, CDCl$_3$ (0.06% CF$_3$SO$_3$H)) 9.68 (d, J = 6.8 Hz, 4H, H-5), 8.97 (d, J = 8.8 Hz, 4H, H-3), 8.69 (t, J = 8.0 Hz, 4H, H-4), 7.48 (s, 4H, H-11), 1.85 (s, 12H, H-13), 1.55 (s, 18H, H-15); ^{13}C NMR (100 MHz, CDCl$_3$ (0.06% CF$_3$SO$_3$H)) 194.4 (s, C-1), 155.6 (s, C-12), 149.1 (s, C-2), 144.1 (d, C-3), 141.0 (s, C-6), 139.9 (d, C-5), 139.7 (s, C-7), 137.0 (s, C-10), 136.6 (d, C-4), 136.4 (s, C-8), 135.6 (s, C-9), 125.2 (d, C-11), 35.0 (s, C-14), 31.3 (q, C-15), 20.8 (q, C-13); MS (EI$^+$, 70 eV) m/z 670 (M$^+$, 100), 613 (6); HRMS (EI$^+$, 70 eV) Calculated: (C$_{52}$H$_{46}$) 670.3589 (M$^+$), Found: 670.3592 (M$^+$); Analysis C$_{52}$H$_{46}$B$_2$F$_8$ (844.5472) Calculated: C, 73.95; H, 5.49, B, 2.56, F, 18.00, Found: C, 73.18; H, 5.55 (Due to the sensitivity to air moisture, acceptable values were not obtained.).

7,14-Dimesitylheptaleno[2,1,10,9-*jklm*:4,5,6,7-*j'k'l'm'*]difluorene 1b
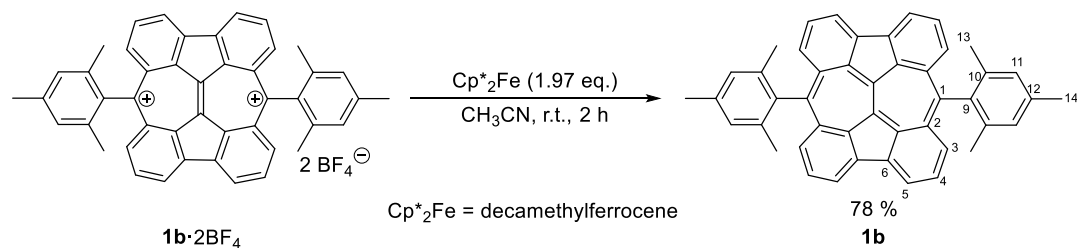
In a nitrogen-filled glove box, a solution of decamethylferrocene (49.0 mg 0.150 mmol) in CH$_3$CN (3 mL) was added to a solution of **1b**·2BF$_4$ (58.0 mg, 0.0763 mmol) in CH$_3$CN (5 mL). The mixture was stirred at room temperature for 2 h. The precipitated solids were collected by filtration and washed with CH$_3$CN until the filtrate was not green-colored. The collected solids were dissolved in benzene (10 mL) and insoluble materials were removed by filtration through a cotton. The filtrate was evaporated to obtain **1b** as a green solid (35.0 mg, 78 %). The recrystallization of **1b** from a chlorobenzene–chloroform solution in a degassed sealed tube afforded a single crystal suitable for the X-ray crystallographic analysis.

mp >300 °C; IR (KBr) ν = 2911 (w), 1579 (w), 1457 (m), 1411 (w), 1397 (w), 1374 (w), 1055 (w), 1034 (w), 918 (w), 848 (m), 787 (s), 745 (s), 720 (m) cm^{-1}; MS (EI$^+$, 70 eV) m/z 586 (M$^+$, 100), 468 (32), 350 (20); HRMS (EI$^+$, 70 eV) Calculated: (C$_{46}$H$_{34}$) 586.2661 (M$^+$), Found: 586.2651 (M$^+$).

7,14-Bis(4-(*tert*-butyl)-2,6-dimethylphenyl)-heptaleno[2,1,10,9-*jklm*:4,5,6,7-*j'k'l'm'*]difluorene 1c
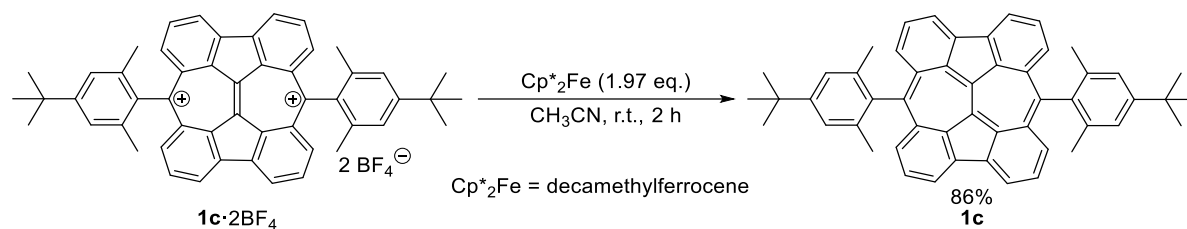
In a nitrogen-filled glove box, a solution of decamethylferrocene (33.9 mg 0.102 mmol) in CH$_3$CN (2 mL) was added to a solution of **1c**·2BF$_4$ (39.4 mg, 0.0518 mmol) in CH$_3$CN (2 mL). The mixture was stirred at room temperature for 2 h. The precipitated solids were collected by filtration and washed with CH$_3$CN until the filtrate was not green-colored. The collected solids were dissolved in benzene (10 mL) and insoluble materials were removed by filtration through a cotton. The filtrate was evaporated to obtain **1c** as a green solid (30.0 mg, 86 %).

mp >300 °C; IR (KBr) ν = 2910 (w), 1608 (w), 1578 (m), 1455 (m), 1411 (w), 1396 (m), 1372 (m), 1036 (w), 918 (m), 849 (m), 788 (s), 745 (s), 721 (w), 661 (w) cm^{-1}; MS: (EI$^+$, 70 eV) m/z 670 (M$^+$, 100), 613 (5); HRMS (EI$^+$, 70 eV) Calculated: (C$_{46}$H$_{34}$) 670.3600 (M$^+$), Found: 670.3591 (M$^+$).

Supporting Information

7,14-Dimesityl-7,14-dihydroheptaleno[2,1,10,9-*jklm*:4,5,6,7-*j'k'l'm'*]difluorene-7,14-diol 7b
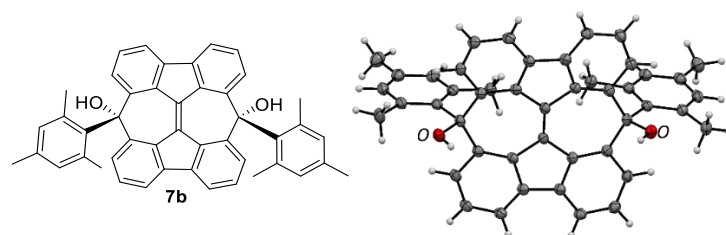

Figure S1. ORTEP drawings of **7b** at the 50% probability level.

Empirical Formula	C$_{46}$H$_{36}$O$_2$	Space Group	P-1 (#2)
Formula Weight	620.79	Z value	2
Crystal Color, Habit	Metallic light yellow, block	D_{calc}	1.336 g/cm^3
Crystal Dimensions	0.229 X 0.172 X 0.138 mm	F_{000}	656.00
Crystal System	triclinic	μ(CuK$_\alpha$)	6.183 cm^{-1}
Lattice Type	Primitive	Temperature	−150.0 °C
Lattice Parameters	a = 8.3096(2) Å	No. Observations (All reflections)	6226
	b = 13.4671(5) Å	No. Variables	435
	c = 13.8293(4) Å	Reflection/Parameter Ratio	14.31
	α = 93.309(3) °	Residuals: R1 (I > 2.00σ(I))	0.0458
	β = 91.851(2) °	Residuals: wR2 (All reflections)	0.1284
	γ = 91.515(2) °	Goodness of Fit Indicator	1.058
	V = 1543.58(8) Å^3	Max Shift/Error in Final Cycle	0.000

7,14-bis(4-(tert-butyl)-2,6-dimethylphenyl)-7,14-dihydroheptaleno[2,1,10,9-*jklm*:4,5,6,7-*j'k'l'm'*]difluorene-7,14-diylium 1c·2BF$_4$
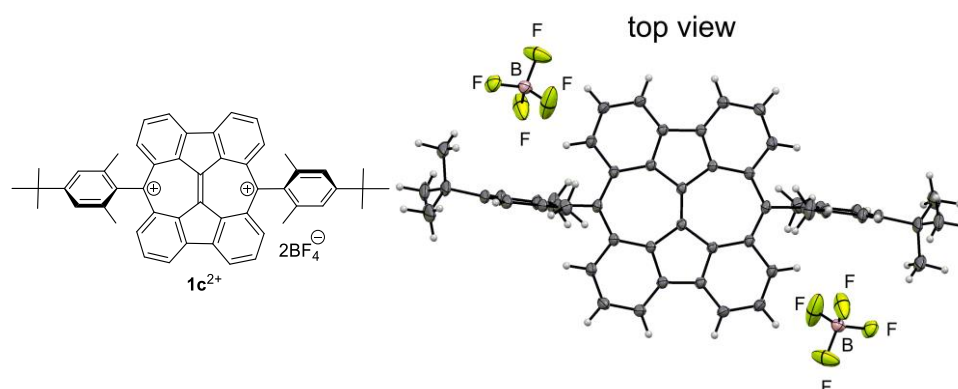

Figure S2. ORTEP drawings of **1c**·2BF$_4$ at the 50% probability level.

Empirical Formula	C$_{52}$H$_{46}$B$_2$F$_8$	D_{calc}	1.356 g/cm^3
Formula Weight	844.54	F_{000}	1760.00
Crystal Color, Habit	Metallic light purple, block	μ(MoK$_\alpha$)	1.016 cm^{-1}
Crystal Dimensions	0.404 X 0.083 X 0.067 mm	Temperature	−150.0 °C
Crystal System	monoclinic	No. Observations (All reflections)	5265
Lattice Type	I-centered	No. Variables	280
Lattice Parameters	a = 28.2664(9) Å	Reflection/Parameter Ratio	18.80
	b = 8.0077(2) Å	Residuals: R1 (I > 2.00σ(I))	0.0667
	c = 18.2814(5) Å	Residuals: wR2 (All reflections)	0.1788
	β = 90.756(3) °	Goodness of Fit Indicator	1.044
	V = 4137.6(2) Å^3	Max Shift/Error in Final Cycle	0.000
Space Group	I2/a (#15)		
Z value	4		

7,14-dimesitylheptaleno[2,1,10,9-*jklm*:4,5,6,7-*j′k′l′m′*]difluorene 1b

top view   **side view**
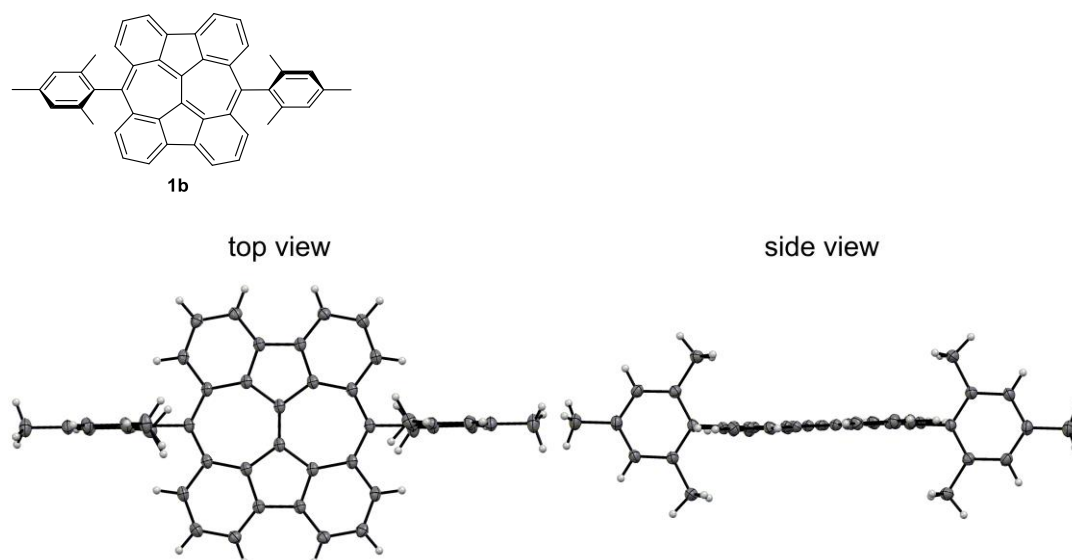
Figure S3. ORTEP drawings of **1b** at the 50% probability level.

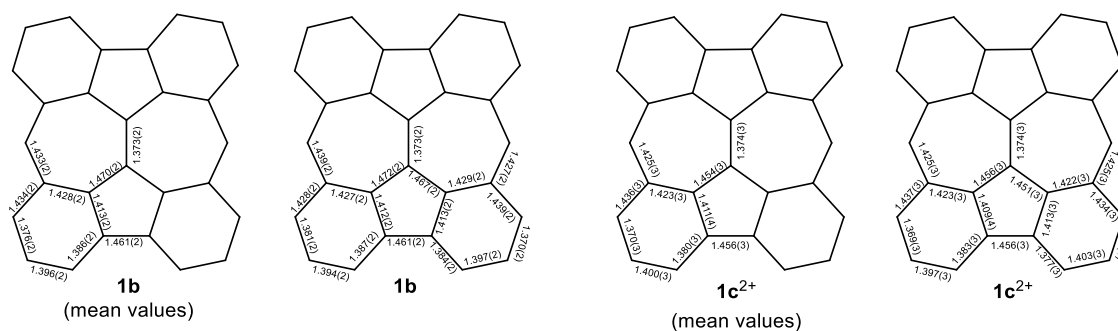|			
Empirical Formula	$C_{46}H_{34}$	D_{calc}	1.299 g/cm^3
Formula Weight	586.77	F_{000}	620.00
Crystal Color, Habit	Metallic light black, block	μ(CuK$_\alpha$)	5.545 cm^{-1}
Crystal Dimensions	0.128 X 0.102 X 0.075 mm	Temperature	−150.0 °C
Crystal System	monoclinic	No. Observations (*All reflections*)	3028
Lattice Type	Primitive	No. Variables	208
Lattice Parameters	a = 8.21746(18) Å	Reflection/Parameter Ratio	14.56
	b = 24.3054(5) Å	Residuals: $R1$ (I > 2.00σ(I))	0.0430
	c = 7.85743(16) Å	Residuals: $wR2$ (*All reflections*)	0.1082
	β = 107.053(2) °	Goodness of Fit Indicator	1.039
	V = 1500.36(6) Å^3	Max Shift/Error in Final Cycle	0.001
Space Group	$P2_1/c$ (#14)		
Z value	2		

Figure S4. Summary for the observed bond lengths (displayed to three decimal places) / Å for **1b** and **1c^{2+}**.
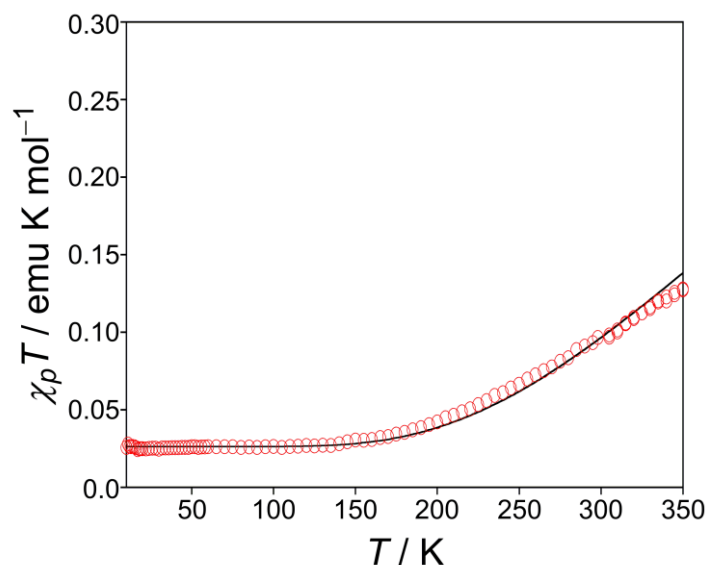
Figure S6. $\chi_p T$–T plot of the powdered **1b**. The measured data are plotted as open circles. The theoretical curve is drawn using the Bleaney–Bowers equation for the singlet–triplet model,[44] with the parameters of $2J/k$B $(= \Delta E_{S-T}) = -1080$ K, impurity spin contamination $= 7.0\%$, $g = 2.00$, diamagnetic susceptibility $= -200 \times 10^{-6}$ emu/mol.
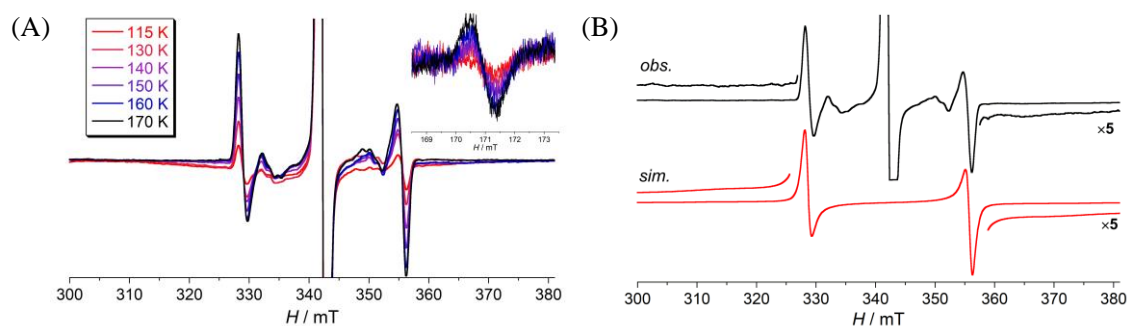

Figure S7. ESR spectra of a glassy toluene sample of **1b** at 170–115 K. (A) Temperature-dependent ESR spectra (g-value $= 2.0027$), the inset is the forbidden $\Delta M_s = \pm 2$ half-field signals and (B) simulated (red) and observed (black) spectra ($\Delta M_s = \pm 1$) at 160 K. The microwave frequency used was 9.58840 GHz. The zero field splitting parameters were determined as $|D| = 27.3$ mT $= 0.0252$ cm^{-1}, $|E| = 0$ mT $= 0$ cm^{-1} (line width parameters; $x = 1.55$ mT, $y = 0.70$ mT, $z = 13.0$ mT) by the spectral simulation.
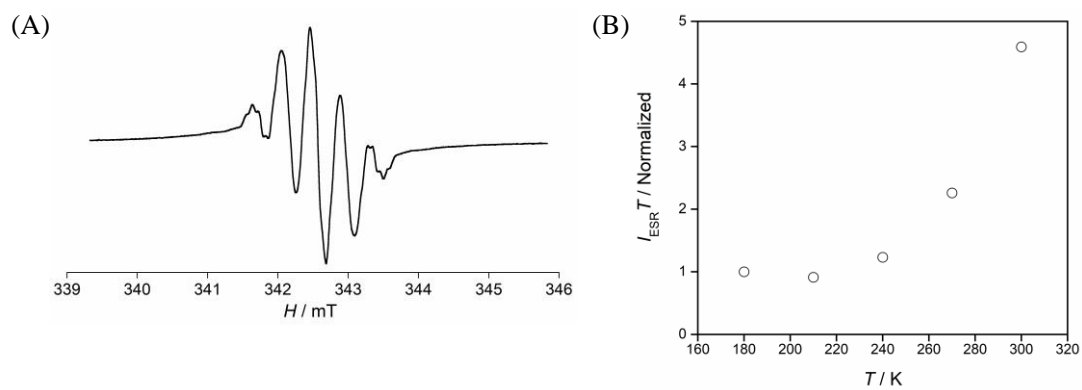
(A)

(B)

Figure S8. (A) ESR spectra of a toluene solution of **1b** at 300 K. 9.60243 GHz, g-value = 2.0027, Gain = 4480, sweep time = 5 min, modulation amplitude = 0.05 mT, and (B) the temperature dependency of the ESR signal intensities in the fluid toluene solution at 180–300 K.
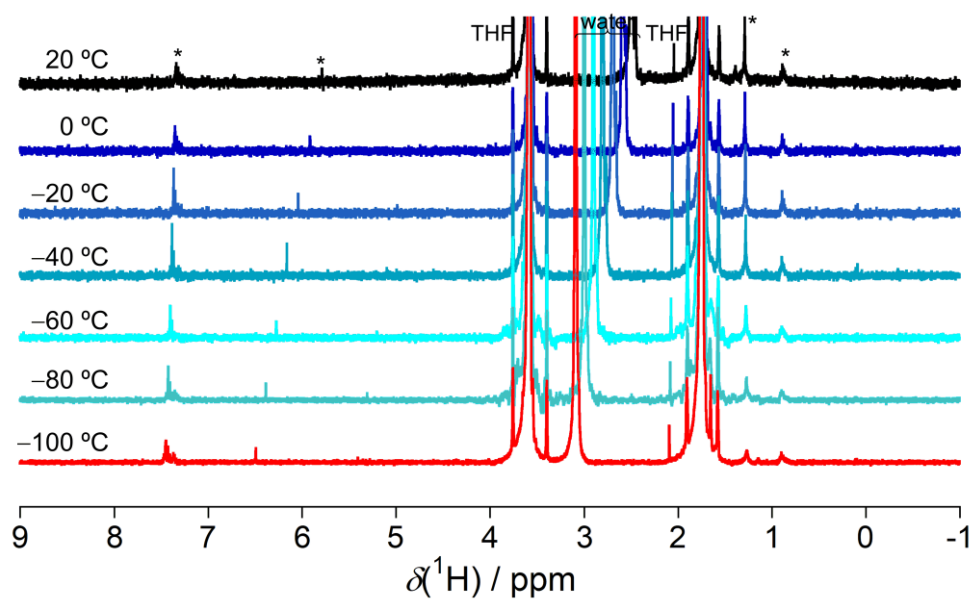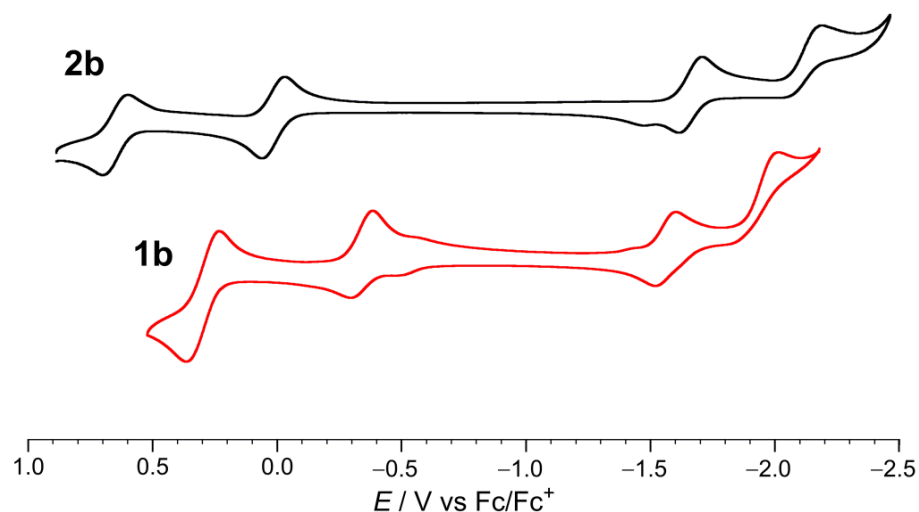

Figure S9. Temperature-dependent ^{1}H NMR (400 MHz) spectra of **1b** in THF-d_8. Small asterisk indicates a small amount of residual solvents for recrystallization.

compound	E_2^{ox} / V	E_1^{ox} / V	E_1^{red} / V	E_2^{red} / V	$\Delta_{redox}E_1$ / V
1b	+0.30	−0.34	−1.56	−2.01[a)]	1.22
2b	+0.65	+0.02	−1.66	−2.19[a)]	1.68

a) peak potential

Figure S10. Cyclic voltammograms of **1b** (red) and **2b**[36] (black) (V vs. Fc/Fc⁺, in 0.1M nBu₄NClO₄/CH₂Cl₂, scan rate = 100 mV/s, room temperature).
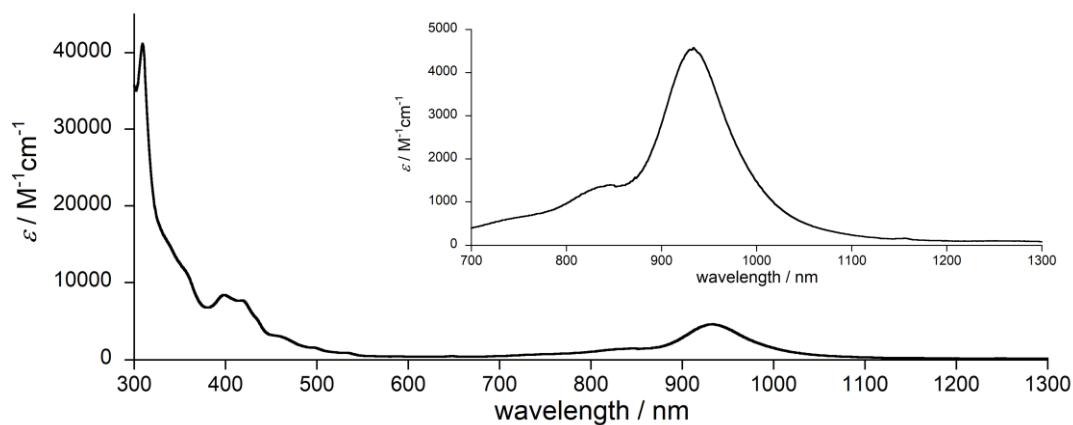

Figure S11. Electronic absorption spectrum of **1b** in CH₂Cl₂. Inset shows a magnified view.

λ / nm (ε / M⁻¹cm⁻¹) 934 (4579), 418 (7681), 398 (8388), 309 (41170).

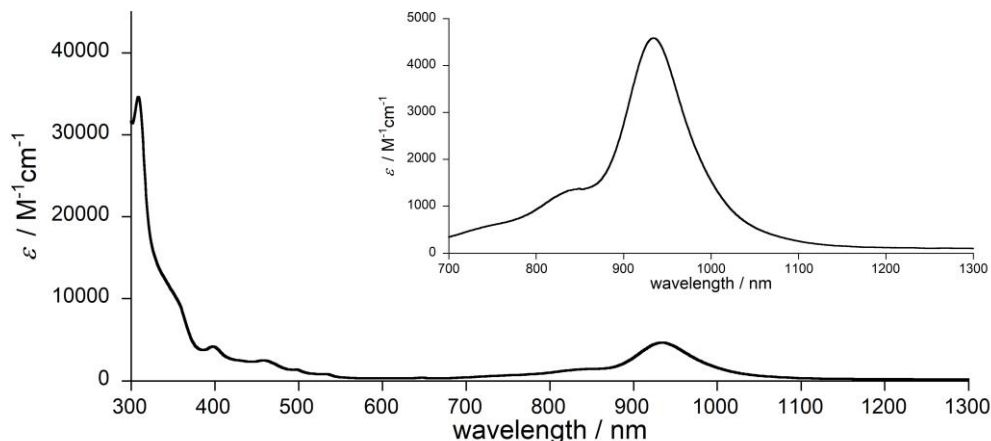**Figure S12.** Electronic absorption spectrum of **1c** in CH_2Cl_2. Inset shows a magnified view.

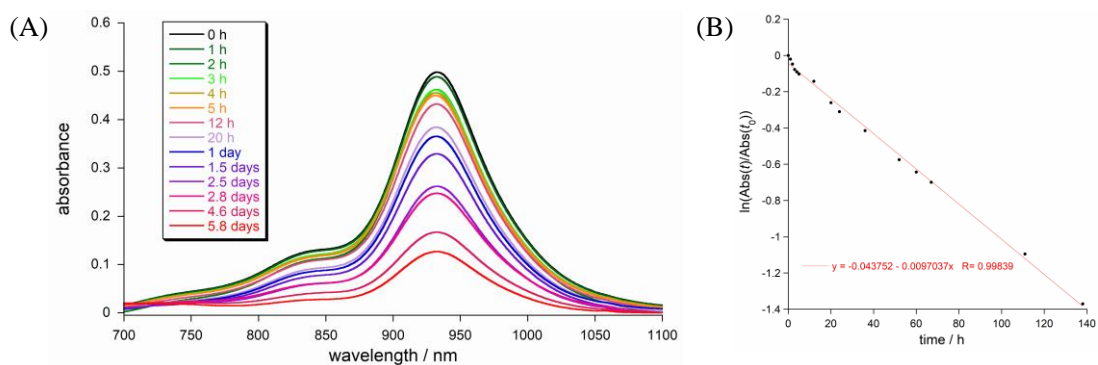λ / nm (ε / $M^{-1}cm^{-1}$) 935 (4586), 398 (4113), 309 (34604).

Figure S13. (A) Periodical measurements of electronic absorption of **1b** in CH_2Cl_2 at lowest-energy region upon exposure to air under room light at room temperature, and (B) plot of the absorbance at 934 nm with time and the half-life time was estimated to be 3 days.
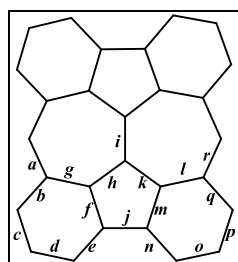
Optimization of 2a

Table S1. Summary of bond lengths of optimized structure.

bond	Observed bond length / Å	D_{2h} model of **1a**[a) bond length / Å	C_{2h} model of **1a**[b) bond length / Å	bond	Observed bond length / Å	D_{2h} model of **1a**[a) bond length / Å	C_{2h} model of **1a**[b) bond length / Å
a	1.4387(16)	1.41454	1.38145	**j**	1.4614(18)	1.46082	1.46275
b	1.4278(19)	1.42698	1.44735	**k**	1.4667(16)	1.46953	1.48218
c	1.3806(17)	1.38113	1.36232	**l**	1.4285(18)	1.41903	1.4131
d	1.3936(18)	1.40019	1.42434	**m**	1.4125(18)	1.41317	1.41225
e	1.3866(19)	1.38902	1.36734	**n**	1.3838(16)	1.38902	1.38984
f	1.4117(16)	1.41317	1.43814	**o**	1.3970(20)	1.40019	1.39573

89

g	1.4272(17)	1.41903	1.43852	**p**	1.3700(20)	1.38113	1.38491
h	1.4724(19)	1.46953	1.42175	**q**	1.4386(17)	1.42698	1.41999
i	1.3727(17)	1.37213	1.40411	**r**	1.4273(19)	1.41454	1.42984

a) The optimization was performed by the (BS)-UB3LYP-D3/6-311G* level. *b*) The optimization was performed by the RB3LYP-D3/6-311G*.
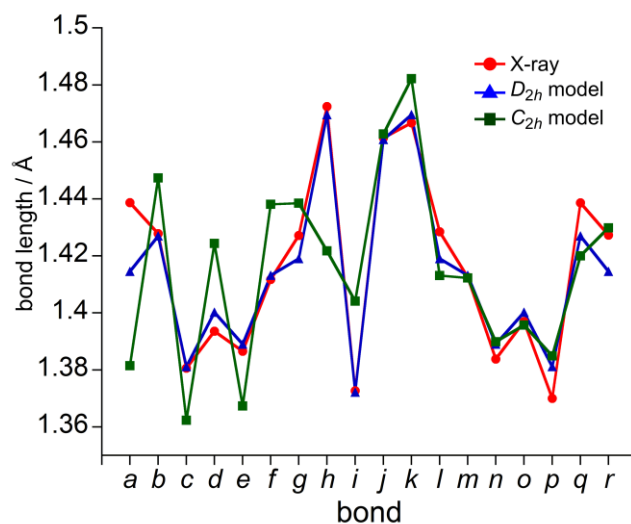

Figure S14. Comparison of bond lengths among the observed geometry of **1b** and the theoretically optimized models of **1a**.

Table S2. Calculated results of diradical index (*y*) and adiabatic

Singlet-Triplet energy gaps (ΔE_{S-T})[a] of **1a**.

	1a
CASSCF(2,2)/6-31G* *y*	0.715
ΔE_{S-T} / kcalmol^{-1}	–2.68
ΔE_{S-T} (+ZPVE) / kcalmol^{-1}	–2.79
singlet (ZPVE) /hartree $<S^2> = 1.015$	–1075.7472763 (0.3210932)
triplet (ZPVE) /hartree $<S^2> = 2.050$	–1075.745121 (0.3211829)

a) Geometry optimizations of **1a** in the singlet and triplet states were performed at the (BS)-UB3LYP-D3/6-311G* level.
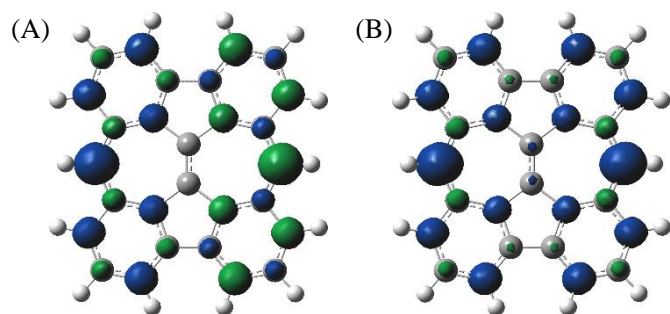
Figure S15. Spin density distribution (the contour level of 0.005 / Å³) of the (A) singlet and (B) triplet state of **1a** calculated by the (BS)-UB3LYP-D3/6-311G* level. Positive (blue) and negative (green) spin densities are shown.
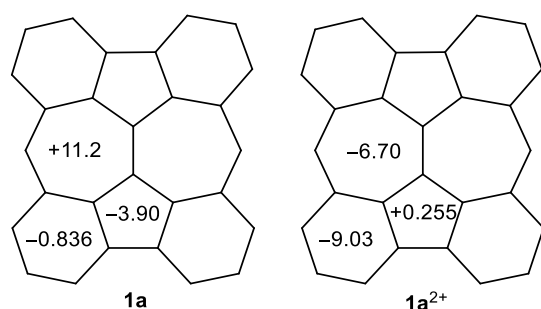

Figure S16. Summary for NICS(1) values of **1a** and **1a²⁺**. The NICS(1)values were calculated at the GIAO-(U)B3LYP/6-311+G*//(U) or (R)B3LYP-D3/6-311G* level.
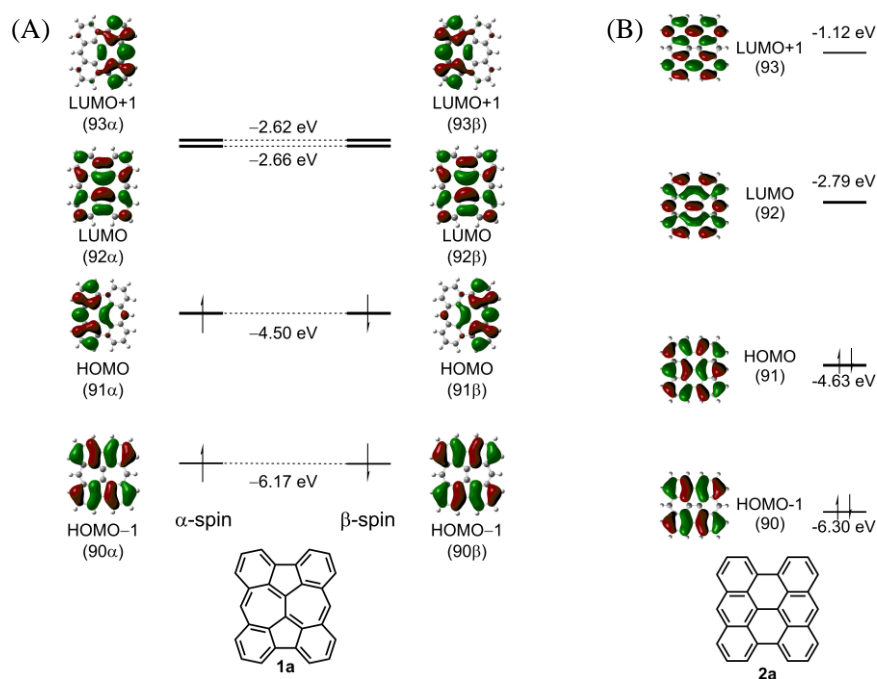

Figure S17. Calculated orbital energy diagram of HOMO–1, HOMO, LUMO, LUMO+1 (A) for **1a** at the UB3LYP-D3/6-311G* level and (B) for **2a** at the RB3LYP-D3/6-311G* level.

Table S3. Selected excitation energies of **1a** calculated at the TD-UB3LYP/6-311+G*//UB3LYP-D3/6-311G* level.

Excited state number	Excitation energy / eV (wavelength / nm)	Excitation amplitudes		Oscillator strength
1	0.929 (1335)	−0.701	(HOMOα – LUMOα)	0.0000
($<S^2>$ = 0.940)		0.701	(HOMOβ – LUMOβ)	
3	1.26 (981)	0.705	(HOMOα – LUMO+1α)	0.0000
($<S^2>$ = 0.213)		0.705	(HOMOβ – LUMO+1β)	
4	1.33 (935)	−0.704	(HOMOα – LUMO+1α)	0.0209
($<S^2>$ = 0.111)		0.704	(HOMOβ – LUMO+1β)	
7	2.49 (497)	−0.302	(HOMO-1α – LUMO+1α)	0.0000
($<S^2>$ = 0.937)		−0.601	(HOMOα – LUMO+2α)	
		0.302	(HOMO-1β– LUMO+1β)	
		0.601	(HOMOβ– LUMO+2β)	

Table S4. Selected excitation energies of **2a** calculated at the TD-B3LYP/6-311+G*//RB3LYP-D3/6-311G* level.

Excited state number	Excitation energy / eV (wavelength / nm)	Excitation amplitudes		Oscillator strength
1	1.72 (721)	0.714	(HOMO – LUMO)	0.2323
2	2.81 (442)	0.402	(HOMO-1 – LUMO)	0.0000
		0.542	(HOMO – LUMO+1)	
3	2.95 (420)	0.531	(HOMO-1 – LUMO)	0.0000
		−0.272	(HOMO – LUMO+1)	
		0.369	(HOMO – LUMO+2)	

3-5. Reference

(1)   (a) Hafner, K. Structure and Aromatic Character of Non-Benzenoid Cyclically Conjugated Systems. *Angew. Chem. Int. Ed. Engl.* **1964**, *3*, 165–173. (b) Nozoe, T. *Topics in Nonbenzenoid Aromatic Chemistry*; Wiley, 1973. (c) Hafner, K. New Aspects of the Chemistry of Nonbenzenoid Polycyclic Conjugated π-Electron Systems. *Pure Appl. Chem.* **1982**, *54*, 939–956. (d) Tobe, Y. Non-Alternant Non-Benzenoid Aromatic Compounds: Past, Present, and Future. *Chem. Rec.* **2015**, *15*, 86–96. (e) Tobe, Y. Quinodimethanes Incorporated in Non-Benzenoid Aromatic or Antiaromatic Frameworks. *Top. Curr. Chem.* **2018**, *376*, 12.

(2)   Gleiter, R.; Haberhauer, G.; Hoffmann, R. *Aromaticity and Other Conjugation Effects*; Wiley-VCH, 2012.

(3)   *For selected reports*: (a) Fukazawa, Y.; Aoyagi, M.; Itô, S. Naphtho[1,8-*ab*:4,5-*a'b'*]Diazulene, the First Nonalternant Isomer of Dibenzopyrene. *Tetrahedron Lett.* **1981**, *22*, 3879–3882. (b) Nakasuji, K.; Todo, E.; Murata, I. Azuleno[4,5,6-*cd*] Phenalene; A Novel Nonalternant Isomer of Benzo[*a*] Pyrene. *Angew. Chem. Int. Ed. Engl.* **1977**, *16*, 784–785. (c) Todo, E.; Yamamoto, K.; Murata, I. BENZO[4,5]CYCLOHEPT[1,2,3-*bc*]ACENAPHTHYLENE AND BENZO[*a*]NAPHTH[3,4,4a,5-*cde*]AZULENE. NONALTERNANT ISOMERS OF BENZO[*a*]PYRENE. *Chem. Lett.* **1979**, *8*, 537–540. (d) Hibi, D.; Kitabayashi, K.; Fujita, K.; Takeda, T.; Tobe, Y. Diindenopyrenes: Extended 1,6- and 1,8-Pyrenoquinodimethanes with Singlet Diradical Characters. *J. Org. Chem.* **2016**, *81*, 3735–3743. (e) Uehara, K.; Mei, P.; Murayama, T.; Tani, F.; Hayashi, H.; Suzuki, M.; Aratani, N.; Yamada, H. An Anomalous Antiaromaticity That Arises from the Cycloheptatrienyl Anion Equivalent. *Eur. J. Org. Chem.* **2018**, *2018*, 4508–4511.

(4)   *For selected recent reviews and reports*: (a) Hopf, H. Pentalenes-From Highly Reactive Antiaromatics to Substrates for Material Science. *Angew. Chem. Int. Ed.* **2013**, *52*, 12224–12226. (b) Saito, M. Synthesis and Reactions of Dibenzo[*a,e*]Pentalenes. *Symmetry* **2010**, *2*, 950–969. (c) Kawase, T.; Nishida, J. π-Extended Pentalenes: The Revival of the Old Compound from New Standpoints. *Chem. Rec.* **2015**, *15*, 1045–1059. (d) Levi, Z. U.; Tilley, T. D. Synthesis and Electronic Properties of Extended, Fused-Ring Aromatic Systems Containing Multiple Pentalene Units. *J. Am. Chem. Soc.* **2010**, *132*, 11012–11014. (e) Cao, J.; London, G.; Dumele, O.; Rekowski, M. v. W.; Trapp, N.; Ruhlmann, L.; Boudon, C.; Stanger, A.; Diederich, F. The Impact of Antiaromatic Subunits in [4*n*+2] π-Systems: Bispentalenes with [4*n*+2] π-Electron Perimeters and Antiaromatic Character. *J. Am. Chem. Soc.* **2015**, *137*, 7178–7188. (f) Oshima, H.; Fukazawa, A.; Yamaguchi, S. Facile Synthesis of Polycyclic Pentalenes with Enhanced Hückel Antiaromaticity. *Angew. Chem. Int. Ed.* **2017**, *56*, 3270–3274. (g) Sekine, K.; Schulmeister, J.; Paulus, F.; Goetz, K. P.; Rominger, F.; Rudolph, M.;

Zaumseil, J.; Hashmi, A. S. K. Gold-Catalyzed Facile Synthesis and Crystal Structures of Benzene-/Naphthalene-Based Bispentalenes as Organic Semiconductors. *Chem. Eur. J.* **2019**, *25*, 216–220. (h) Konishi, A.; Okada, Y.; Nakano, M.; Sugisaki, K.; Sato, K.; Takui, T.; Yasuda, M. Synthesis and Characterization of Dibenzo[*a,f*]Pentalene: Harmonization of the Antiaromatic and Singlet Biradical Character. *J. Am. Chem. Soc.* **2017**, *139*, 15284–15287.

(5)   *For selected recent reviews and reports*: (a) Frederickson, C. K.; Rose, B. D.; Haley, M. M. Explorations of the Indenofluorenes and Expanded Quinoidal Analogues. *Acc. Chem. Res.* **2017**, *50*, 977–987. (b) Dressler, J. J.; Teraoka, M.; Espejo, G. L.; Kishi, R.; Takamuku, S.; Gómez-García, C. J.; Zakharov, L. N.; Nakano, M.; Casado, J.; Haley, M. M. Thiophene and Its Sulfur Inhibit Indenoindenodibenzothiophene Diradicals from Low-Energy Lying Thermal Triplets. *Nat. Chem.* **2018**, *10*, 1134–1140. (c) Dressler, J. J.; Zhou, Z.; Marshall, J. L.; Kishi, R.; Takamuku, S.; Wei, Z.; Spisak, S. N.; Nakano, M.; Petrukhina, M. A.; Haley, M. M. Synthesis of the Unknown Indeno[1,2-*a*]Fluorene Regioisomer: Crystallographic Characterization of Its Dianion. *Angew. Chem. Int. Ed.* **2017**, *56*, 15363–15367. (d) Shimizu, A.; Tobe, Y. Indeno[2,1-*a*]Fluorene: An Air-Stable *Ortho*-Quinodimethane Derivative. *Angew. Chem. Int. Ed.* **2011**, *50*, 6906–6910. (e) Liu, J.; Ma, J.; Zhang, K.; Ravat, P.; Machata, P.; Avdoshenko, S.; Hennersdorf, F.; Komber, H.; Pisula, W.; Weigand, J. J.; Popov, A. A.; Berger, R.; Müllen, K.; Feng, X. π-Extended and Curved Antiaromatic Polycyclic Hydrocarbons. *J. Am. Chem. Soc.* **2017**, *139*, 7513–7521. (f) Shimizu, A.; Kishi, R.; Nakano, M.; Shiomi, D.; Sato, K.; Takui, T.; Hisaki, I.; Miyata, M.; Tobe, Y. Indeno[2,1-*b*]Fluorene: A 20-π-Electron Hydrocarbon with Very Low-Energy Light Absorption. *Angew. Chem. Int. Ed.* **2013**, *52*, 6076–6079. (g) Yamamoto, K.; Ie, Y.; Tohnai, N.; Kakiuchi, F.; Aso, Y. Antiaromatic Character of Cycloheptatriene-Bis-Annelated Indenofluorene Framework Mainly Originated from Heptafulvene Segment. *Sci. Rep.* **2018**, *8*, 17663. (h) Sbargoud, K.; Mamada, M.; Marrot, J.; Tokito, S.; Yassar, A.; Frigoli, M. Diindeno[1,2-*b*:2',1'-*n*]Perylene: A Closed Shell Related Chichibabin's Hydrocarbon, the Synthesis, Molecular Packing, Electronic and Charge Transport Properties. *Chem. Sci.* **2015**, *6*, 3402–3409. (i) Ma, J.; Liu, J.; Baumgarten, M.; Fu, Y.; Tan, Y.-Z.; Schellhammer, K. S.; Ortmann, F.; Cuniberti, G.; Komber, H.; Berger, R.; Müllen, K.; Feng, X. A Stable Saddle-Shaped Polycyclic Hydrocarbon with an Open-Shell Singlet Ground State. *Angew. Chem. Int. Ed.* **2017**, *56*, 3280–3284. (j) Melidonie, J.; Liu, J.; Fu, Y.; Weigand, J. J.; Berger, R.; Feng, X. Pyrene-Fused *s*-Indacene. *J. Org. Chem.* **2018**, *83*, 6633–6639. (k) Hsieh, Y.; Wu, C.-F.; Chen, Y.-T.; Fang, C.; Wang, C.; Li, C.; Chen, L.; Cheng, M.; Chueh, C.; Chou, P.; Wu, Y. 5,14-Diaryldiindeno[2,1-*f*:1',2'-*j*]Picene: A New Stable [7]Helicene with a Partial Biradical Character. *J. Am. Chem. Soc.* **2018**, *140*, 14357–14366. (l) Majewski, M. A.; Chmielewski, P. J.; Chien, A.; Hong, Y.; Lis, T.; Witwicki, M.; Kim, D.; Zimmerman, P. M.; Stępień, M. 5,10-Dimesityldiindeno[1,2-*a*:2',1'-*i*]Phenanthrene: A Stable Biradicaloid Derived from Chichibabin's Hydrocarbon. *Chem. Sci.* **2019**, *10*, 3413–3420. (m) Ma, J.; Zhang, K.; Schellhammer, K. S.; Fu, Y.; Komber, H.; Xu, C.; Popov, A. A.; Hennersdorf, F.; Weigand, J. J.; Zhou, S.; Pisula, W.; Ortmann, F.; Berger, R.; Liu, J.; Feng, X. Wave-Shaped Polycyclic Hydrocarbons with Controlled Aromaticity. *Chem. Sci.* **2019**, *10*, 4025–4031.

(6)   (a) Breslow, R. Antiaromaticity. *Acc. Chem. Res.* **1973**, *6*, 393–398. (b) Minkin, V. I.; Glukhovtsev, M. N.; Simkin, B. I. A. *Aromaticity and Antiaromaticity: Electronic and Structural Aspects*; Wiley-Interscience publication; J. Wiley & Sons, 1994. (c) Frederickson, C. K.; Zakharov, L. N.; Haley, M. M. Modulating Paratropicity Strength in Diareno-Fused Antiaromatics. *J. Am. Chem. Soc.* **2016**, *138*, 16827–16838. (d) Majzik, Z.; Pavliček, N.; Vilas-Varela, M.; Pérez, D.; Moll, N.; Guitián, E.; Meyer, G.; Peña, D.; Gross, L. Studying an Antiaromatic Polycyclic Hydrocarbon Adsorbed on Different Surfaces. *Nat. Commun.* **2018**, *9*, 1198.

(7)   (a) Abe, M. Diradicals. *Chem. Rev.* **2013**, *113*, 7011. (b) Y. Gopalakrishna, T.; Zeng, W.; Lu, X.; Wu, J. From Open-Shell Singlet Diradicaloids to Polyradicaloids. *Chem. Commun.* **2018**, *54*, 2186–2199. (c) Zeng, Z.; Shi, X.; Chi, C.; López Navarrete, J. T.; Casado, J.; Wu, J. Pro-Aromatic and Anti-Aromatic π-Conjugated Molecules: An Irresistible Wish to Be Diradicals. *Chem. Soc. Rev.* **2015**, *44*, 6578–6596. (e) Kubo, T. Recent Progress in Quinoidal Singlet Biradical Molecules. *Chem. Lett.* **2015**, *44*, 111–122. (f) Nakano, M. Open-Shell-Character-Based Molecular Design Principles: Applications to Nonlinear Optics and Singlet Fission. *Chem. Rec.* **2017**, *17*, 27–62. (g) Sun, Z.; Wu, J. Open-Shell Polycyclic Aromatic Hydrocarbons. *J. Mater. Chem.* **2012**, *22*, 4151–4160.

(8)   Clar, E. *Polycyclic Hydrocarbons: Volume 1 and 2*; Academic Press Inc, 1964.

(9)   Randić, M. Aromaticity of Polycyclic Conjugated Hydrocarbons. *Chem. Rev.* **2003**, *103*, 3449–3606.

(10)   Wu, J.; Pisula, W.; Müllen, K. Graphenes as Potential Material for Electronics. *Chem. Rev.* **2007**, *107*, 718–747.

(11)   Morita, Y.; Suzuki, S.; Sato, K.; Takui, T. Synthetic Organic Spin Chemistry for Structurally Well-Defined Open-Shell Graphene Fragments. *Nat. Chem.* **2011**, *3*, 197–204.

(12)   Hu, P.; Wu, J. Modern Zethrene Chemistry. *Can. J. Chem.* **2017**, *95*, 223–233.

(13)   Narita, A.; Wang, X.-Y.; Feng, X.; Müllen, K. New Advances in Nanographene Chemistry. *Chem. Soc. Rev.* **2015**, *44*, 6616–6643.

(14)   Narita, A.; Chen, Z.; Chen, Q.; Müllen, K. Solution and On-Surface Synthesis of Structurally Defined Graphene Nanoribbons as a New Family of Semiconductors. *Chem. Sci.* **2019**, *10*, 964–975.

(15)   Konishi, A.; Kubo, T. Benzenoid Quinodimethanes. *Top. Curr. Chem.* **2017**, *375*, 83.

(16)   (a) Hafner, K.; Fleischer, R.; Fritz, K. Pentaleno[2,1,6-*def*]Heptalene– a Non-Benzenoid Isomer of Pyrene. *Angew. Chem. Int. Ed. Engl.* **1965**, *4*, 69–70. (b) Anderson, A. G.; MacDonald, A. A.; Montana, A. F. Dicyclopenta[*ef,kl*]Heptalene (Azupyrene). *J. Am. Chem. Soc.* **1968**, *90*, 2993–2994. (c) Reel, H.; Vogel, E. Dicyclohepta[*cd,gh*]Pentalene?A New Pyrene Isomer. *Angew. Chem. Int. Ed. Engl.* **1972**, *11*, 1013–1014. (d) Reid, D. H.; Stafford, W. H.; Ward, J. P. The Fine Structure of Azulene. Part I. CycloHepta[*bc*]Acenaphthylene and Cyclohepta[*def*]Fluorene. *J. Chem. Soc.* **1955**, *84*, 1193–1201. (e) Gardner, P. D.; Wulfman, C. E.; Osborn, C. L. Cyclohepta[*klm*]Benz[*e*]Indene. Further Considerations on the Stability of Complex Polynuclear Systems. *J. Am. Chem. Soc.* **1958**, *80*, 143–148. (f) Boekelheide, V.; Langeland, W. E.; Liu, C.-T. A Study of the Synthesis and Some Properties of Acepleiadiene. *J. Am. Chem. Soc.* **1951**, *73*, 2432–2435.

(17)   (a) Yang, X.; Shi, X.; Aratani, N.; Gonçalves, T. P.; Huang, K.-W.; Yamada, H.; Chi, C.; Miao, Q. Benzo[4,5]Cyclohepta[1,2-*b*]Fluorene: An Isomeric Motif for Pentacene Containing Linearly Fused Five-, Six- and Seven-Membered Rings. *Chem. Sci.* **2016**, *7*, 6176–6181. (b) Dickens, T. K.; Mallion, R. B. Topological Ring-Currents and Bond-Currents in the Altan-[*r,s*]-Coronenes. *Chem. Commun.* **2015**, *51*, 1819–1822. (c) Rizzo, D. J.; Veber, G.; Cao, T.; Bronner, C.; Chen, T.; Zhao, F.; Rodriguez, H.; Louie, S. G.; Crommie, M. F.; Fischer, F. R. Topological Band Engineering of Graphene Nanoribbons. *Nature* **2018**, *560*, 204–208. (d) Wang, Q.; Gopalakrishna, T. Y.; Phan, H.; Herng, T. S.; Dong, S.; Ding, J.; Chi, C. Cyclopenta Ring Fused Bisanthene and Its Charged Species with Open-Shell Singlet Diradical Character and Global Aromaticity/Anti-Aromaticity. *Angew. Chem. Int. Ed.* **2017**, *56*, 11415–11419. (e) Jiang, Q.; Tao, T.; Phan, H.; Han, Y.; Gopalakrishna, T. Y.; Herng, T. S.; Li, G.; Yuan, L.; Ding, J.; Chi, C. Diazuleno-*s*-Indacene Diradicaloids: Syntheses, Properties, and Local (Anti)Aromaticity Shift from Neutral to Dicationic State. *Angew. Chem. Int. Ed.* **2018**, *57*, 16737–16741.

(18)   (a) Toyota, A.; Kataoka, M.; Koseki, S. Energy Component Analysis of the Pseudo Jahn-Teller Effect in Pentalene and Heptalene. *Chem. Lett.* **1992**, *21*, 791–794. (b) Toyota, A.; Koseki, S. Energy Component Analysis of the Pseudo-Jahn−Teller Effect in the

Bicyclic Nonalternant Hydrocarbons: The Pentalenoid and Heptalenoid Systems. *J. Phys. Chem.* **1996**, *100*, 2100–2106. (c) Kozuch, S. Heavy Atom Tunneling in the Automerization of Pentalene and Other Antiaromatic Systems. *RSC Adv.* **2014**, *4*, 21650–21656. (d) Hafner, K.; Knaup, G. L.; Lindner, H. J. Syntheses and Dynamic Behavior of Chiral Heptalenes. *Bull. Chem. Soc. Jpn.* **1988**, *61*, 155–163.

(19)   Scholl, R.; Meyer, K. Der Blaue Aromatische Grundkohlenwasserstoff Des Meso-Naphtho-Dianthrons Und Seine Überführung Durch Maleinsäure-Anhydrid in Anthro-Dianthren. *Ber. Dtsch. Chem. Ges. (A B Series)* **1934**, *67*, 1236–1238.

(20)   Clar, E. Synthesen von Benzologen Des Perylens Und Bisanthens. (Aromatische Kohlenwasserstoffe, XLVIII. Mitteil.). (Mitbearbeitet von H. Frömmel.). *Chem. Ber.* **1949**, *82*, 46–60.

(21)   (a) Jiang, D.; Sumpter, B. G.; Dai, S. First Principles Study of Magnetism in Nanographenes. *J. Chem. Phys.* **2007**, *127*, 124703. (b) Hod, O.; Barone, V.; Scuseria, G. E. Half-Metallic Graphene Nanodots: A Comprehensive First-Principles Theoretical Study. *Phys. Rev. B* **2008**, *77*, 1. (c) Moscardó, F.; San-Fabián, E. On the Existence of a Spin-Polarized State in the n-Periacene Molecules. *Chem. Phys. Lett.* **2009**, *480*, 26–30. (d) Plasser, F.; Pašalić, H.; Gerzabek, M. H.; Libisch, F.; Reiter, R.; Burgdörfer, J.; Müller, T.; Shepard, R.; Lischka, H. The Multiradical Character of One- and Two-Dimensional Graphene Nanoribbons. *Angew. Chem. Int. Ed.* **2013**, *52*, 2581–2584.

(22)   Konishi, A.; Hirao, Y.; Nakano, M.; Shimizu, A.; Botek, E.; Champagne, B.; Shiomi, D.; Sato, K.; Takui, T.; Matsumoto, K.; Kurata, H.; Kubo, T. Synthesis and Characterization of Teranthene: A Singlet Biradical Polycyclic Aromatic Hydrocarbon Having Kekulé Structures. *J. Am. Chem. Soc.* **2010**, *132*, 11021–11023.

(23)   Ajayakumar, M. R.; Fu, Y.; Ma, J.; Hennersdorf, F.; Komber, H.; Weigand, J. J.; Alfonsov, A.; Popov, A. A.; Berger, R.; Liu, J.; Müllen, K.; Feng, X. Toward Full Zigzag-Edged Nanographenes: *peri*-Tetracene and Its Corresponding Circumanthracene. *J. Am. Chem. Soc.* **2018**, *140*, 6240–6244.

(24)   Ni, Y.; Gopalakrishna, T. Y.; Phan, H.; Herng, T. S.; Wu, S.; Han, Y.; Ding, J.; Wu, J. A Peri-Tetracene Diradicaloid: Synthesis and Properties. *Angew. Chem. Int. Ed.* **2018**, *57*, 9697–9701.

(25)   Mishra, S.; Lohr, T. G.; Pignedoli, C. A.; Liu, J.; Berger, R.; Urgel, J. I.; Müllen, K.; Feng, X.; Ruffieux, P.; Fasel, R. Tailoring Bond Topologies in Open-Shell Graphene Nanostructures. *ACS Nano* **2018**, *12*, 11917–11927.

(26)   (a) Dauben, H. J.; Bertelli, D. J. HEPTALENE. *J. Am. Chem. Soc.* **1961**, *83*, 4659–4660. (b) Vogel, E.; Königshofen, H.; Wassen, J.; Müllen, K.; Oth, J. F. M. A Heptalene Synthesis from 1,6-Methano[10]Annulene; Evidence for a Fast π-Bond Shift. *Angew. Chem. Int. Ed. Engl.* **1974**, *13*, 732 *Angew. Chem. Int. Ed. Engl.* **1974**, *13*, 732734. (c) Briquet, A. A. S.; Uebelhart, P.; Hansen, H.-J. Double-Bond Shifts in [4n]Annulenes as a New Principle for Molecular Switches: First Results with Dimethyl Heptalene-1,2- and -4,5-Dicarboxylates. *Helv. Chim. Acta* **1996**, *79*, 2282 *Helv. Chim. Acta* **1996**, *79*, 2282–2315.

(27)   Iyoda, M.; Tanake, S.; Nishioka, K.; Oda, M. Synthesis and Properties of Butatrienes Containing a Bisdehydro[13]Annulene System as Terminal Groups. *Tetrahedron Lett.* **1983**, *24*, 2861–2864.

(28)   George, S. R. D.; Scott, L. T.; Harper, J. B. Synthesis of 1-Substituted Fluorenones. *Polycycl. Aromat. Compd.* **2016**, *36*, 697–715.

(29)   Hojo, M.; Ichi, T.; Shibato, K. Synthesis and Structure of a New Stable Carbocation Stabilized by Two Neighboring Sulfur Atoms. Dimethyl[9,9-Bis(Methylthio)-1-Fluorenyl]Carbenium Ion. *J. Org. Chem.* **1985**, *50*, 1478–1482.

(30)   Wawzonek, S.; Henry, J. P. Studies on the Possibility of Resolving Dicarboxy-$\Delta^{9,9'}$-Bifluorenes. *J. Org. Chem.* **1953**, *18*, 1461–1465.

(31)   (a) Lindner, H. J.; Kitschke, B. Crystal and Molecular Structure of Dimethyl 1,2-Heptalenedicarboxylate. *Angew. Chem. Int. Ed. Engl.* **1976**, *15*, 106–107. (b) Stegemann, J.; Lindner, H. J. The Crystal and Molecular Structure of Dimethyl-3,8-Heptalene-Dicarboxylate. *Tetrahedron Lett.* **1977**, *18*, 2515–2516. (c) Oshima, H.; Fukazawa, A.; Sasamori, T.; Yamaguchi, S. A Nonaromatic Thiophene-Fused Heptalene and Its Aromatic Dianion. *Angew. Chem. Int. Ed.* **2015**, *54*, 7636–7639.

(32)   Konishi, A.; Okada, Y.; Kishi, R.; Nakano, M.; Yasuda, M. Enhancement of Antiaromatic Character via Additional Benzoannulation into Dibenzo[*a,f*]Pentalene: Syntheses and Properties of Benzo[*a*]Naphtho[2,1-*f*]Pentalene and Dinaphtho[2,1-*a,f*]Pentalene. *J. Am. Chem. Soc.* **2019**, *141*, 560–571.

(33)   (a) Kruszewski, J.; Krygowski, T. M. Definition of Aromaticity Basing on the Harmonic Oscillator Model. *Tetrahedron Lett.* **1972**, *13*, 3839–3842. (b) Krygowski, T. M. Crystallographic Studies of Inter- and Intramolecular Interactions Reflected in Aromatic Character of π-Electron Systems. *J. Chem. Inf. Model.* **1993**, *33*, 70–78.

(34)   Konishi, A.; Hirao, Y.; Matsumoto, K.; Kurata, H.; Kishi, R.; Shigeta, Y.; Nakano, M.; Tokunaga, K.; Kamada, K.; Kubo, T. Synthesis and Characterization of Quarteranthene: Elucidating the Characteristics of the Edge State of Graphene Nanoribbons at the Molecular Level. *J. Am. Chem. Soc.* **2013**, *135*, 1430–1437.

(35)   (a) Miyoshi, H.; Miki, M.; Hirano, S.; Shimizu, A.; Kishi, R.; Fukuda, K.; Shiomi, D.; Sato, K.; Takui, T.; Hisaki, I.; Nakano, M.; Tobe, Y. Fluoreno[2,3-*b*]Fluorene vs Indeno[2,1-*b*]Fluorene: Unusual Relationship between the Number of π Electrons and Excitation Energy in *m*-Quinodimethane-Type Singlet Diradicaloids. *J. Org. Chem.* **2017**, *82*, 1380–1388. (b) Zeng, W.; Gopalakrishna, T. Y.; Phan, H.; Tanaka, T.; Herng, T. S.; Ding, J.; Osuka, A.; Wu, J. Superoctazethrene: An Open-Shell Graphene-like Molecule Possessing Large Diradical Character but Still with Reasonable Stability. *J. Am. Chem. Soc.* **2018**, *140*, 14054–14058.

(36)   Konishi, A.; Hirao, Y.; Matsumoto, K.; Kurata, H.; Kubo, T. Facile Synthesis and Lateral π-Expansion of Bisanthenes. *Chem. Lett.* **2013**, *42*, 592–594.

(37)   Bendikov, M.; Duong, H. M.; Starkey, K.; Houk, K. N.; Carter, E. A.; Wudl, F. Oligoacenes: Theoretical Prediction of Open-Shell Singlet Diradical Ground States. *J. Am. Chem. Soc.* **2004**, *126*, 7416–7417.

Chapter 4

Bis-periazulene as a Non-alternant Isomer of Pyrene: Synthesis and Characterization of Triaryl Derivatives

4-1. Introduction

Non-alternant hydrocarbons have recently experienced a remarkable resurgence.[1,2,11,3–10] Their unique electron configurations and molecular orbital characteristics are derived from the topological difference of the π-electron network, which is given by replacing hexagons of alternant hydrocarbons with a pair of pentagon and heptagon.[12] One seminal example of a non-alternant hydrocarbon is azulene. Its deep blue color and polarized structure have engaged many chemists' attentions[13–16] as a building block of π-extended molecules[17–20] and as a great candidate of optoelectronics.[21–24] Other vital studies include structural isomers of pyrene (Figure 1A).[5] Through pioneering works by Boekelheide,[25,26] Reid,[27] Gardner,[28] Hafner,[29] Anderson,[30] and Vogel,[31] six of the seven possible non-alternant isomers of pyrene, which contain the pair(s) of pentagon and heptagon, have been isolated and characterized as stable aromatic molecules, revealing their different optoelectronic properties from pyrene itself.

(A) Non-alternant isomer of pyrene

pyrene   Boekelheide   Reid   Gardner   Hafner   Anderson   Vogel

1a
bis-periazulene
This work
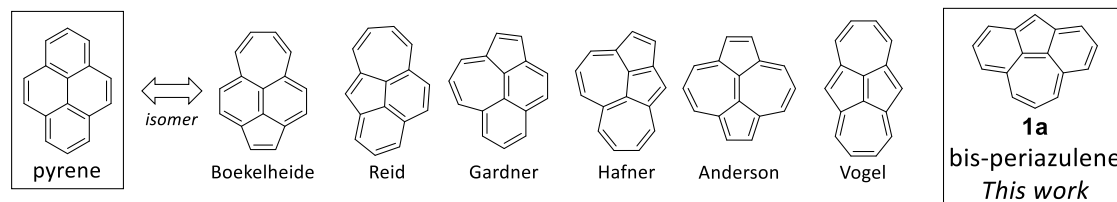
(B) Reported attempts of the synthesis of **1**

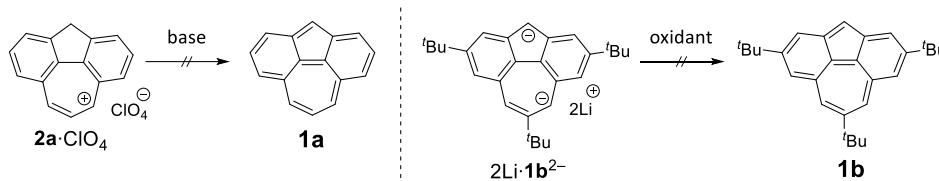**2a·ClO₄**   **1a**   2Li·**1b²⁻**   **1b**

Figure 1. (A) Molecular structures of non-alternant isomers of pyrene. (B) Synthetic attempts of bis-periazulenes **1**.

The only one unsynthesized isomer, bis-periazulene (cyclohepta[*def*]fluorene) **1**, remains elusive despite many synthetic efforts. The first synthetic attempt of **1a** was reported in 1955 from Reid's group.[27] Sutherland followed Reid's work, to synthesize the tropylium-type cation salt **2a⁺·ClO₄⁻**.[32,33] Hafner designed a kinetically protected derivative **1b** by three *tert*-butyl groups and characterized the dianion **1b²⁻** by NMR

measurements.[34] These synthetic works provided the useful precursors of **1**. However, the transformations into **1** by deprotonation or two-electron oxidation failed due to the inherent instability of **1** against oxidation and self-polymerization (Figure 1B).[33,34] Recently, Wu reported the synthetic attempt of π-extended analog but failed to undergo the Lewis-acid mediated cyclization.[35] The theoretical calculations have offered fascinating clues as to the electronic structures of **1**.[36] The previous DFT calculation predicted that **1** would have an open-shell nature with the triplet ground state that is around 2 kcal/mol lower than the lowest singlet state, even though **1** can be described by a closed-shell Kekulé structure.[37] Malrieu suggested that the lowest singlet and triplet states of **1** are nearly degenerate in their different equilibrium geometries by using both geometry-dependent Heisenberg Hamiltonian and *ab initio* methods.[38] These intriguing experimental and theoretical studies demonstrate the worth of synthesizing and characterizing **1**.

The double *peri*-benzoannulation on an azulene provides the fascinating electronic features of **1** (Figure 2). The hexagons within **1** adopt *o*-quinoidal forms in the closed-shell Kekulé structure (**1a-A**), which should peripherally delocalize the 14π-system by the equivalent resonance/interconversion.[39,40] When the quinoidal forms are transformed into the benzenoid forms, two possible structures are considered. One is the charge-separated polarized structure (**1a-B**), which is reminiscent of the contribution of the embedded azulene core.[9,41–43] The other is the open-shell diradical structure (**1a-C**), where an *m*-quinodimethane subunit, a typical non-disjoint non-Kekulé diradical,[44–46] engages in the stabilization of the triplet state. These considerations prompted us to synthesize **1** and unveil the electronic structures of **1**, including the actual ground state. In this chapter, the authors synthethized and characterized kinetically stabilized bis-periazulene derivtives.
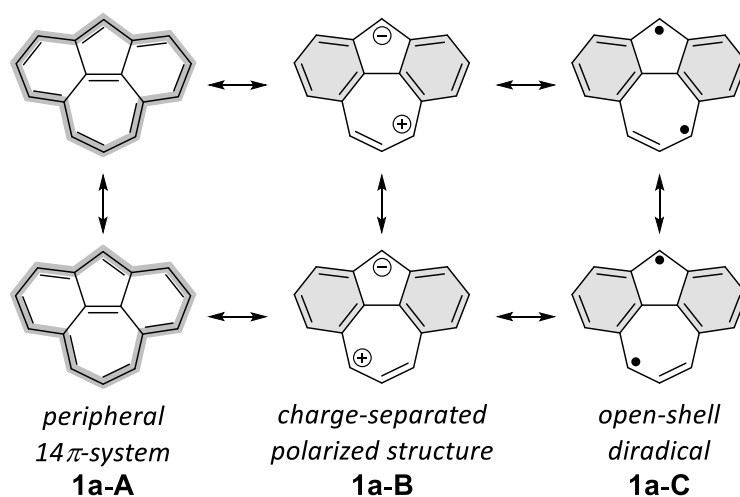

Figure 2. Resonance structures of **1a**. Hexagonal rings in gray denote benzenoid rings. Bold lines indicate the peripheral-conjugated circuit.

4-2. Results and Discussion

To improve the kinetic stability, the authors planned to introduce *ortho*-disubstituted aromatic groups into the three reactive sites of **1a** (Scheme 1). According to the reported procedures,[47,48] 9-aryl-9*H*-fluorenes **3** were synthesized. 2,4,6-Trimethylphenyl (Mes) (**c**), 2,4,6-triisopropylphenyl (Trip) (**d**), and 2,6-dichlorophenyl (Dcp) (**e**) groups were introduced into the pentagon of **3**. Formylation of **3** followed by palladium-catalyzed cross-coupling of **4** with (trimethylsilyl)acetylene afforded fluorene derivatives **5**. An intramolecular cyclization between the aldehyde and alkyne of **5** is a direct step to construct a heptagon (Table S1). Considering an affinity to both carbonyl and alkyne moieties,[49,50] the authors applied indium(III) salts as Lewis acid to the cyclization. Fortunately, treating **5** with In(OTf)$_3$ directly gave **6**. The indium(III) center would activate the carbonyl and facilitate the cyclization. Nucleophilic attack on enones **6** with mesitylmagnesium bromide afforded 1,4-addcuts **7** and oxidation by 2,3-dichloro-5,6-dicyano-*p*-benzoquinone (DDQ) gave mesityl-substituted enones **8**. Re-treatment of **8** with mesitylmagnesium bromide afforded alcohols **9** as 1,2-adducts to the carbonyls. Treating alcohols **9** with HBF$_4$·Et$_2$O immediately produced tropylium-type cation salts **2$^+$**·BF$_4^-$.[51] For the deprotonation of **2$^+$** into **1**, the choice of a suitable base was important. When the authors applied sodium hydride to the deprotonation of **2d$^+$**,[52,53] an over-reduced radical anion **1d$^{•-}$**, confirmed by X-ray analysis, was unexpectedly obtained. Alternatively, changing base into lithium hydride successfully transformed **2$^+$** into the desired molecule **1**. The obtained compounds **1** were air-sensitive dark brown solids. A THF solution of **1** gradually decomposed upon exposure to air under room light and temperature (half-lives: **1c**: 2.4 h, **1d**: 19 h, **1e**: 73 h).
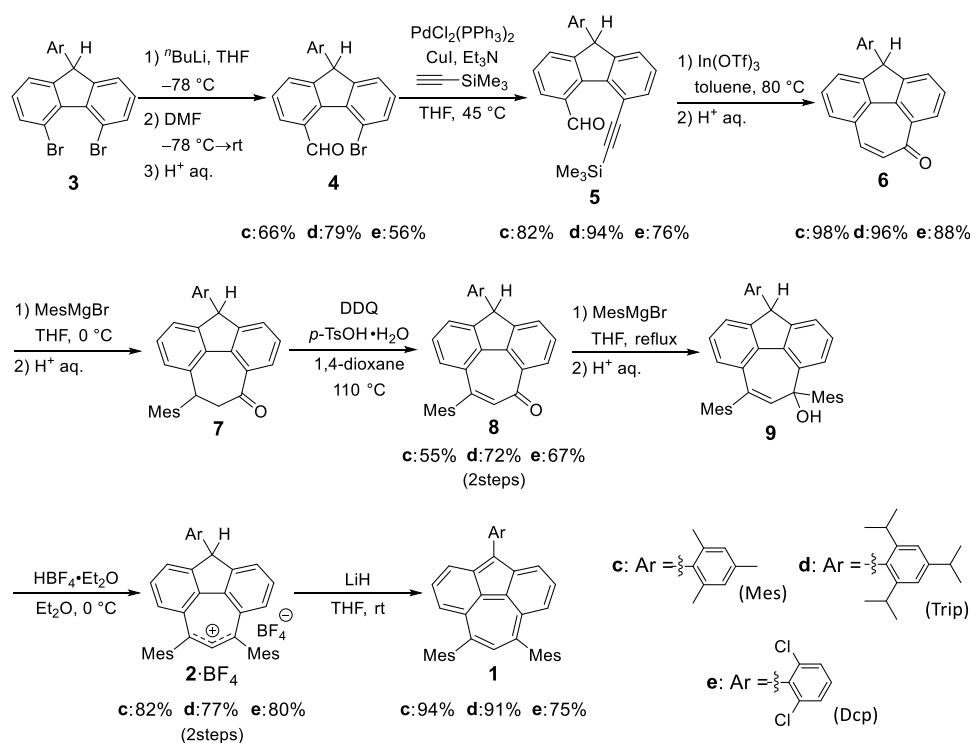
Scheme 1. Synthesis of triaryl bis-periazulenes **1**.

The redox behaviors of **1c–e** in solution were investigated with cyclic voltammetry (Figure S1 and Table S2). The cyclic voltammogram of **1c** showed two reversible and two irreversible redox waves ($E_2^{ox, pa}$ = +0.76 V, E_1^{ox} = –0.17 V, E_1^{red} = –1.31 V, and $E_2^{red, pc}$ = –2.04 V vs Fc/Fc$^+$). The electrochemical HOMO−LUMO gap of 1.14 eV, estimated from the difference between the first oxidation and reduction potentials, is comparable to Feng's nonbenzenoid nanographene (1.13 eV),[54] even though **1c** is a much smaller π-conjugated system. The observed behaviors were essentially the same as in **1c–e**. Treating **1c** with AgSbF$_6$ afforded a radical cation **1c·$^+$**, characterized by ESR spectroscopic and X-ray crystallographic analyses (Figures S2 and S9). The reduction of **1c** with potassium metal quantitatively yielded the dianion **1c^{2-}**, which was confirmed by the NMR measurements (Figure S4) and reproduced Hafner's study.[34]

Careful recrystallizations from a CH$_2$Cl$_2$/hexane (**1c** and **1d**) or THF/hexane (**1e**) solution in a nitrogen-filled glovebox gave single crystals of **1c–e** suitable for X-ray crystallographic analyses. Ortep drawing of **1d** was shown in Figure 3A (Figures S5–7 for **1c** and **e**). X-ray crystallographic analysis illustrated the main core of **1d** assumes a planar structure. The dihedral angle of the Trip group on the pentagon with the main core (65°) is smaller than that of the mesityl groups on the heptagon (ave. 82°). The main core of **1d** exhibits a slight bond length alternation (BLA) but assumes an approximate C_{2v} symmetry. These fundamental geometrical characteristics of **1d** are mostly identical to those of **1c**/**e** (Figures S11–13). To evaluate the canonical structure contributing to the observed geometry, the authors focused on the bridging bond *a* between the pentagon and heptagon (Figure 3). The bond length of the *a* bond in **1d** is 1.391(2) Å, which is considerably shorter than that of azulene (1.489 Å).[55] The double bond character of the *a* bond implies that a quinoidal form (**1a-A** in Figure 2) emerges as a dominant resonance structure. The BLA of the two hexagons is not small according to the harmonic oscillator model of aromaticity (HOMA)[56,57] analysis (ca. 0.6), which supports the quinoidal character (Figure 3B). Contrarily, the HOMA value indicates a larger value for the perimeter of the main core of **1d** (0.88), suggesting the peripheral 14π-electron delocalization is induced by the interconversion between equivalent two quinoidal forms (**1a-A**).
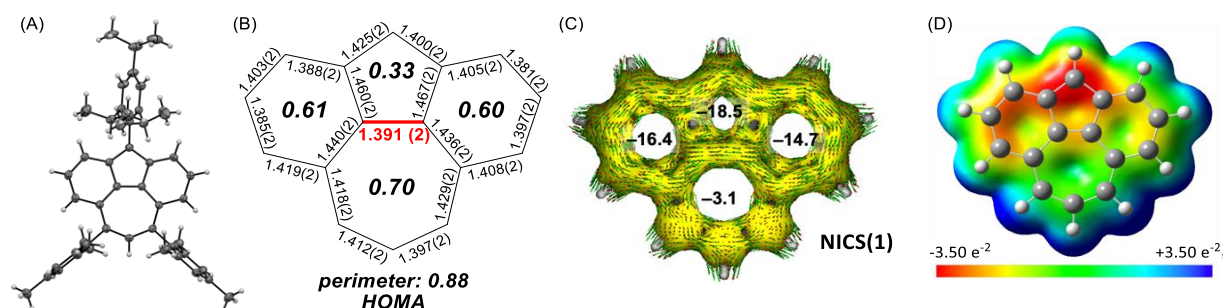

Figure 3. (A) Ortep drawing of 1d with at the 50% probability level. (B) Selected bond lengths with HOMA values (italic) of **1d**. (C) AICD plots with NICS(1) values (italic) of **1a'**. (D) ESP map of **1a'**.

The magnetic criteria for aromaticity illustrate another aspect of the π-conjugation of **1** (Figure 3C). The NICS(1) calculations of **1a'** (The substituents of the X-ray geometry of **1d** were replaced by hydrogen atoms.) at the UCAM-B3LYP/def2-SVP level reveal that the large negative values (from –14.7 to –18.5) appear on the fluorene moiety, whereas non-aromatic character (–3.1) emerges on the heptagon. The anisotropy of the induced current density (AICD)[58,59] plots clockwise manifests the diamagnetic ring currents on the 6-5-6 ring system. Additionally, the electrostatic potential (ESP) map of **1a'** indicates that the pentagon and the adjacent hexagons have a negative charge, whereas the heptagon has a relatively positive charge (Figure 3D). Judging from these magnetic/electrostatic evaluation, **1** should be described by the combination of a fluorenyl anion and an allyl cation, suggesting the charge-separated polarized structure is a non-negligible resonance structure (**1a-B** in Figure 2). Experimentally, **1** behaves as a basic hydrocarbon like azulene-based hydrocarbons.[42,60–65] **1c** was readily protonated by CF_3SO_3H to a tropylium-type cation salt $\mathbf{2c^+} \cdot OSO_2CF_3^-$ (Figure S14).

On the other hand, the determined physical properties of **1** demonstrated the open-shell character. Superconducting quantum interference device (SQUID) measurements determined the actual ground state of the triaryl-substituted bis-periazulenes **1**. The measurements for the microcrystalline sample of **1d** showed a decreasing magnetic susceptibility upon cooling from 300 K to 2 K (Figure 4A). From the Bleaney–Bowers fitting, the singlet–triplet energy gap (ΔE_{S-T}) is –454 K (–0.90 kcal/mol). Although the ground state of **1d** is determined to be singlet, contrary to the previous predictions, the determined ΔE_{S-T} of **1d** is less than half those of the related polycyclic systems with azulene cores (~ –2 kcal/mol).[40,54] Our QD-SC-NEVPT2 calculations using SA-CASSCF(4e,4o)/def2-SVP solutions support the singlet ground states of **1c–e**, 2.7–4.7 kcal/mol lower than the lowest triplet states (Table S4). Due to the small ΔE_{S-T}, no NMR signal of the main core of **1d** in THF-d_8 was observed even at –100 °C (Figure S28).[40] The electron spin resonance (ESR) measurements of **1d** clearly displayed signals typical of a triplet species (Figures 4B and S18–19). The signal intensity decreases upon cooling, supporting the singlet ground state in **1d**. The observed zero field splitting parameters ($|D| = 0.0190$ cm^{-1} and $|E| = 0.0022$ cm^{-1}) were well consistent the geometry of **1d**.
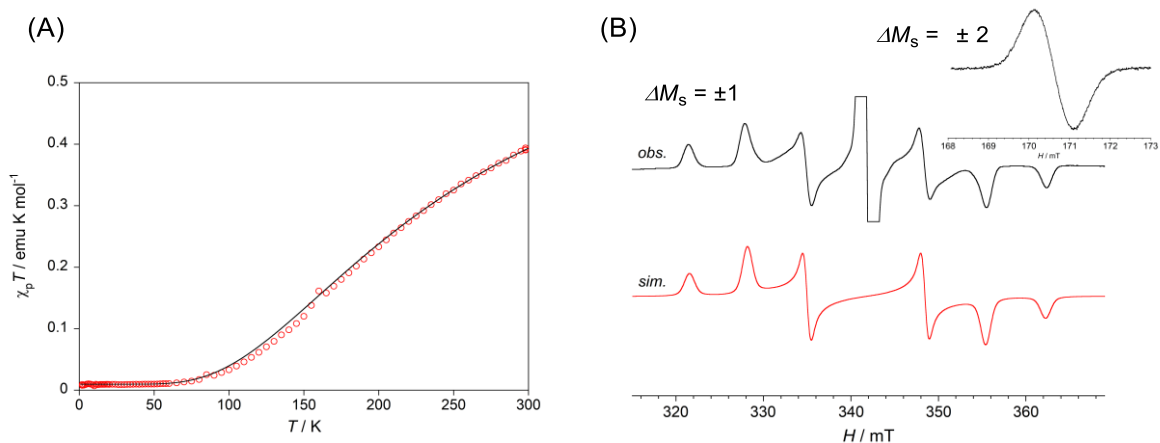
Figure 4. (A) $\chi_p T$–T Plot of the powdered **1d**. The measured data (○) and Bleaney–Bowers fit (—). (B) Observed (black) and simulated (red) ESR spectra of a glassy toluene sample of **1d** at 155 K.

At the present stage, it is unclear why the determined ground state of **1** is a singlet state, regardless of the previous theoretical studies.[36–38] The introduced aryl groups may affect the energy gap between the lowest singlet and triplet states. The SQUID and ESR measurements of **1e**, in which a Dcp group is introduced instead of the Trip group of **1d**, showed an expanded $\Delta E_{S–T}$ of around –2300 K (–4.6 kcal/mol), five times larger than that of **1d**, due to an electron-withdrawing character of Dcp (Figures S25–S26). The inductive effect of the Dcp group should stabilize the polarized negative charge, lowering the singlet energy level and strengthening the pairing of two unpaired electrons (Table S6 and Figure S44). The two impacts can qualitatively explain the expansion of the $\Delta E_{S–T}$ of **1e**, but more comprehensive investigations are required.

The three derivatives **1c–e** gave almost identical electronic absorptions. Figure 5 shows the electronic absorption spectrum of **1d** in THF. The longest absorption band of **1d** was a weak and broad band centered at around 1700 nm, reaching to over 2000 nm. No solvatochromism of **1c/e** was observed among THF, CH_2Cl_2, and benzene (Figures S32 and S37).[43,52] According to the small $\Delta E_{S–T}$, the absorption spectrum of **1d** at room temperature should be composed of absorption bands derived from triplet species as well as ground-state singlet species. The variable-temperature measurements of **1d** in THF showed the consecutive spectrum changes with isosbestic points upon cooling from 294 K to 183 K (Figure S39). The increased absorption intensities at around 1700, 700, and 500 nm can be assigned to the singlet transitions. Contrarily, the absorptions at 850 and 400 nm with reduced intensities were observed due to the triplet transitions. The DFT calculations of singlet **1c** at the CAM-B3LYP-D3/def2-SVP demonstrates that the HOMO (ψ_{149})/LUMO (ψ_{150}), regardless of the α-/β-spin, is mainly distributed on the fluorenyl/dibenzo[a, c] cycloheptenyl moiety, respectively (Figure S43). The time-dependent (TD)-DFT calculations of **1c** reveal that the lowest transition around 1700 nm is ascribed to the HOMO→LUMO transition across the pentagon to the heptagon (Table S5). Contrarily, at the triplet state, the frontier orbitals are different depending on the α-/β-spin (Figure S44). The α-orbitals ($\alpha_{150}/\alpha_{151}$) are localized on the dibenzo[a,c] cycloheptenyl moiety, whereas the β-orbitals (β_{148}/β_{149}) are localized on the fluorenyl moiety. The low-lying triplet transitions can be described by linear combinations of the local excitation for the α-/β-spin electron, resulting in a higher energy transition than the singlet (Table S6). The molecular orbital characteristics originating from the non-alternant character of **1** visualized the difference in the electronic structure between the singlet and triplet states.
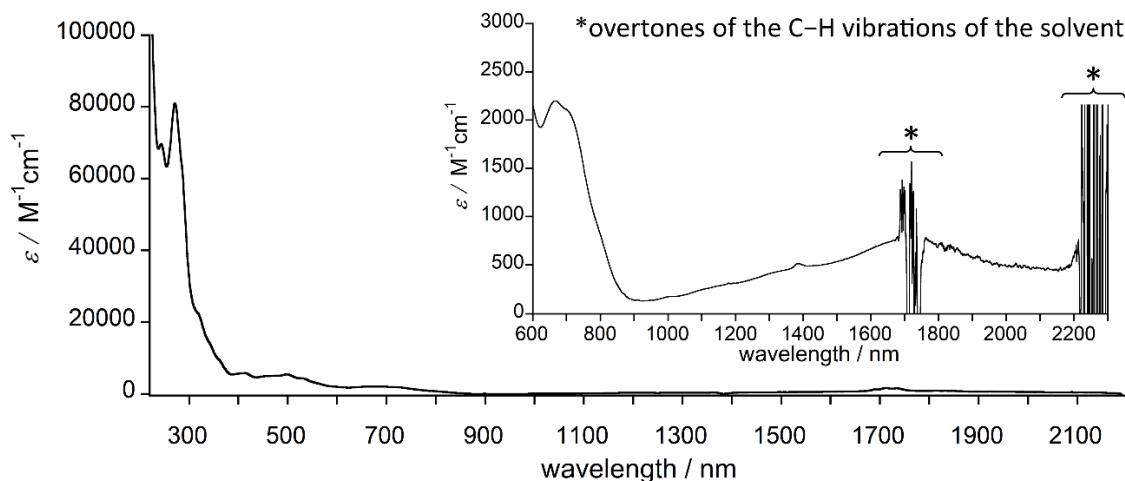
Figure 5. UV/vis/NIR absorption spectra of **1d** in THF at room temperature. Inset shows a magnified view.

4-3. Conclusion

In conclusion, the authors successfully synthesized and characterized **1**, the remaining non-alternant isomer of pyrene. Triaryl substituted **1c–e** exhibit singlet open-shell ground states, contrary to the previous theoretical predictions for **1a**. Notably, **1** contains three aspects of π-conjugation: peripheral, charge-separated, and open-shell π-conjugations. To evaluate the properties harbored by the complex electronic structure, further studies, including the actual ground state of the pristine **1a** and the substituent effects on the ΔE_{S-T} of **1**, are ongoing in our group.

4-4. Experimental Section

General Information

NMR spectra were recorded on JEOL-AL400, JEOL-ECS400 (400 MHz for ^{1}H, and 100 MHz for ^{13}C) and Bruker AVANCE III spectrometers (600 MHz for ^{1}H, and 150 MHz for ^{13}C) with TMS as an internal standard. ^{1}H and ^{13}C NMR signals of compounds were assigned using HMQC, HSQC, HMBC, COSY, and ^{13}C off-resonance techniques. ESR spectra were recorded on a Bruker EMXmicro spectrometer. The temperature-dependent magnetic susceptibility was measured for randomly oriented polycrystalline samples on a Quantum Design SQUID magnetometer MPMS-XL in the temperature range of 2−300 K (for **1d**) and 2−350 K (for **1e**). Positive FAB and EI mass spectra were recorded on a JEOL JMS-700 and a Shimadzu GCMS-QP2010 Ultra, respectively. IR spectra were recorded as thin films or as solids in KBr pellets on a JASCO FT/IR 6200 spectrophotometer. UV-vis-NIR spectra were recorded on JASCO V-670 and V-770 spectrophotometers. Cyclic voltammetric measurements were performed with an ALS-600C electrochemical analyzer using a glassy carbon working electrode, a Pt counter electrode, and an Ag/AgNO$_3$ reference electrode at room temperature in THF containing 0.1 M ^{n}Bu$_4$NClO$_4$ as the supporting electrolyte. Data collection for X-ray crystal analysis was performed on Rigaku/XtaLAB Synergy-S/Cu (CuKα λ = 1.54187 Å) diffractometers. All non-hydrogen atoms were refined with anisotropic displacement parameters and hydrogen atoms were placed at calculated positions and refined "riding" on their corresponding carbon atoms by Olex2[66] program.

Materials

All reagents were obtained from commercial suppliers and used as received. Sodium hydride was pre-washed with dried hexane before use in order to remove the dispersed oils. 4,5-Dibromo-9*H*-fluoren-9-one **S1**[47] were prepared by the reported procedures. Syntheses of **1** and the reduction/oxidation of **1c** were performed in a nitrogen-filled glove box.

Synthesis and Characterization

4,5-Dibromo-9-mesityl-9*H*-fluorene 3c
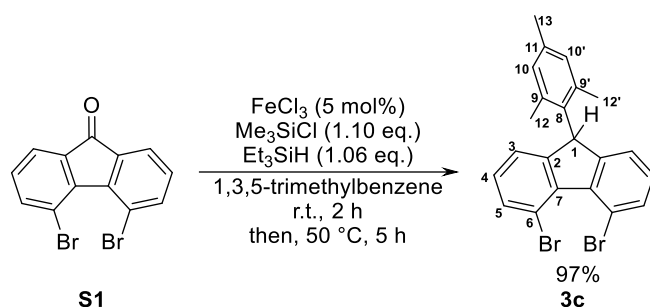
A procedure from the literature[48] was modified as follows: To a mixture of 4,5-dibromo-9*H*-fluoren-9-one **S1**[47] (3.00 g, 8.88 mmol) and iron(III) chloride (75 mg, 0.46 mmol) in mesitylene (6 mL) was added chlorotrimethylsilane (1.24 mL, 9.77 mmol) and triethylsilane (1.5 mL, 9.45 mmol) at room temperature. The reaction mixture was stirred for 2 h at room temperature, then it was heated at 50 °C for 5 h. After cooling to room temperature, the reaction was quenched with water and the product was extracted with chloroform. The organic layer was washed with water, and dried over MgSO$_4$. The solution was collected by filtration and the solvents were removed under vacuum. The residue was purified by column chromatography on silica gel (hexane) to give **3c** as a colorless solid (3.13 g, 97%).

R_f = 0.29 (hexane), 0.71 (hexane : EtOAc = 9:1); mp 140.2–141.0 °C; IR (KBr) ν = 3047 (w), 2963 (w), 2916 (w), 2858 (w), 1554 (w), 1455 (w), 1400 (m), 1102 (m), 855 (m), 753 (s) cm^{-1}; ^{1}H NMR: (400 MHz, CDCl$_3$) 7.67–7.65 (m, 2H, 5-H), 7.15–7.12 (m, 4H, 3-H, 4-H), 7.01 (s, 1H, 10′-H), 6.67 (s, 1H, 10-H), 5.50 (s, 1H, 1-H), 2.62 (s, 3H, 12′-H), 2.28 (s, 3H, 13-H), 1.09 (s, 3H, 12-H); ^{13}C NMR (100 MHz, CDCl$_3$) 151.0 (s, C-2), 139.5 (s, C-7), 137.7 (s, C-9, C-9′, two signals were overlapped.), 136.8 (s, C-11), 134.0 (d, C-5), 133.1 (s, C-8), 130.7 (d, C-10), 128.92 (d), 128.87 (d), 122.5 (d, C-4), 116.2 (s, C-6), 50.4 (s, C-1), 21.6 (q, C-12′), 20.8 (q, C-13), 18.7 (q, C-12); MS (EI, 70 eV) *m/z* 444 ([M+4]$^+$, 23), 442 ([M+2]$^+$, 45), 440 (M$^+$, 24), 361 (100), 267 (64); HRMS (EI, 70 eV) Calculated (C$_{22}$H$_{18}$Br$_2$): 439.9775 (M$^+$), Found: 439.9770; Analysis: C$_{22}$H$_{18}$Br$_2$ (442.1940) Calculated: C, 59.76; H, 4.10; Br, 36.14, Found: C, 59.82; H, 4.06.

5-Bromo-9-mesityl-9*H*-fluorene-4-carbaldehyde 4c
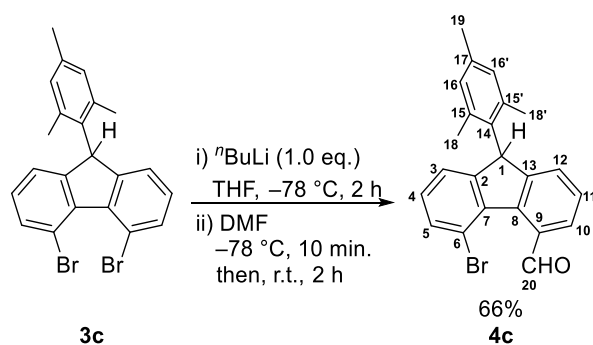
Under nitrogen atmosphere, ^{n}BuLi (1.6 M in hexane, 5.5 mL, 8.86 mmol) was added to a solution of **3c** (3.92 g, 8.86 mmol) in freshly dried THF (35 mL) at –78 °C. After stirred for 2 h at the temperature, anhydrous DMF (20 mL) was added to the

reaction mixture. The reaction mixture was stirred for 10 min at –78 °C and was allowed to gradually warm to room temperature for 2 h. The reaction was quenched by aqueous HCl (1 M) at 0 °C. After the mixture was stirred for 30 min at 0 °C, the products were extracted with chloroform. The organic layer was washed with water and dried over MgSO$_4$. After filtration of the drying agent, the solvent was removed under vacuum. The residues were purified by column chromatography on silica gel with hexane and ethyl acetate (95:5) to give **4c** as a colorless solid (2.30 g, 66%).

R_f = 0.37 (hexane : EtOAc = 9:1); mp 131.0–131.5 °C; IR (KBr) ν = 3062 (w), 2968 (w), 2858 (w), 1685 (s), 1455 (m), 1445 (m), 1380 (m), 1230 (m), 853 (m), 760 (s) cm^{-1}; ^{1}H NMR (400 MHz, CDCl$_3$) 10.99 (s, 1H, 20-H), 7.84 (d, J = 8.0 Hz, 1H, 10-H), 7.61–7.59 (m, 1H, 5-H), 7.40 (t, J = 7.2 Hz, 1H, 11-H), 7.37–7.34 (m, 1H, 12-H), 7.21–7.18 (m, 1H, 3-H), 7.17 (t, J = 6.4 Hz, 1H, 4-H), 7.03 (s, 1H, 16′-H), 6.67 (s, 1H, 16-H), 2.65 (s, 3H, 18′-H), 2.27 (s, 3H, 19-H), 1.07 (s, 3H, 18-H); ^{13}C NMR (100 MHz, CDCl$_3$) 191.6 (d, C-20), 151.2 (s, C-2), 149.0 (s, C-13), 139.9 (s, C-8), 139.3 (s, C-7), 137.7 (s, C-15′), 137.4 (s, C-15), 136.9 (s, C-17), 132.8 (d, C-5), 132.4 (s, C-9, C-14, two signals were overlapped.), 130.7 (d, C-16), 129.6 (d, C-4), 129.0 (d, C-16′), 128.1 (d, C-11), 127.8 (d, C-12), 127.2 (d, C-10), 123.4 (d, C-3), 117.5 (s, C-6), 50.4 (d, C-1), 21.6 (q, C-18′), 20.8 (q, C-19), 18.6 (q, C-18); MS (EI, 70 eV) m/z 392 ([M+2]$^+$, 4), 390 (M$^+$, 4), 311 (100); HRMS (EI, 70 eV) Calculated (C$_{23}$H$_{19}$BrO): 390.0619 (M$^+$), Found: 390.0613; Analysis C$_{23}$H$_{19}$BrO (391.3080) Calculated: C, 70.60; H, 4.89; Br, 20.42; O, 4.09, Found: C, 70.81; H, 4.77.

9-Mesityl-5-((trimethylsilyl)ethynyl)-9*H*-fluorene-4-carbaldehyde 5c
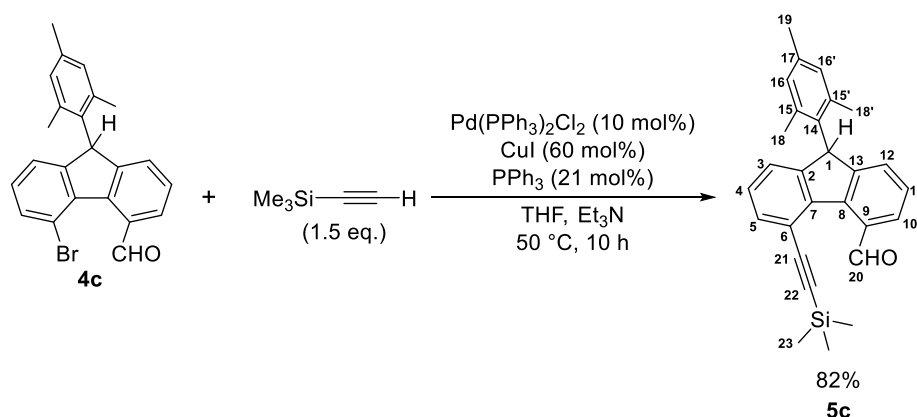
Under nitrogen atmosphere, PdCl$_2$(PPh$_3$)$_2$ (0.430 g, 0.588 mmol) was added to a mixture of **4c** (2.30 g, 5.88 mmol), CuI (0.675 g, 3.53 mmol) and PPh$_3$ (0.323 g, 1.23 mmol) in freshly dried THF (100 mL) and anhydrous Et$_3$N (40 mL) at room temperature. The mixture was heated to 50 °C and stirred for 10 h at the temperature. The reaction was quenched by saturated aqueous NH$_4$Cl at 0 °C and the products were extracted with chloroform. The organic layer was washed with water and dried over MgSO$_4$. After filtration of the drying agent, the solvent was removed under vacuum. The residues were purified by column chromatography on silica gel with hexane and ethyl acetate (95:5) to give **5c** as a colorless solid (1.98 g, 82%).

R_f = 0.51 (hexane : EtOAc = 9:1); mp 157.0–158.0 °C; IR (KBr) ν = 3062 (w), 2963 (m), 2864 (w), 2146 (m), 1688 (s), 1389 (m), 1249 (s), 848 (s), 762 (s) cm^{-1}; ^{1}H NMR (400 MHz, CDCl$_3$) 11.32 (s, 1H, 20-H), 7.92 (dd, J = 6.8 Hz, 2.0 Hz 1H, 10-H), 7.61 (d, J = 7.6 Hz, 1H, 5-H), 7.41–7.36 (m, 2H, 11-H, 12-H), 7.28 (t, J = 7.4 Hz, 1H, 4-H), 7.21 (d, J = 7.2 Hz, 3-H), 7.03 (s, 1H, 16′-H), 6.67 (s, 1H, 16-H), 5.47 (s, 1H, 1-H), 2.66 (s, 3H, 18′-H), 2.28 (s, 3H, 19-H), 1.07 (s, 3H, 18-H), 0.32 (s, 9H, 23-H); ^{13}C NMR (100 MHz, CDCl$_3$) 192.1 (d, C-20), 149.1 (s, C-2), 149.0 (s, C-13), 140.9 (s, C-8), 139.7 (s, C-7), 137.7 (s, C-15′), 137.5 (s, C-15), 136.8 (s, C-17), 134.1 (d, C-5), 132.64 (s, C-14), 132.58 (s, C-9), 130.7 (d, C-16), 129.0 (d, C-16′), 128.0 (d), 127.9 (d), 127.8 (d), 126.6 (d, C-10), 124.6 (d, C-3), 119.0 (s, C-6), 105.0 (s, C-21), 99.3 (s, C-22), 49.7 (d, C-1), 21.7 (q, C-18′), 20.8 (q, C-19), 18.7 (q, C-18), –0.51 (q, C-23); MS (CI, 70 eV) m/z 409 ([M+H]$^+$, 100), 393 (7); HRMS (CI, 70 eV) Calculated (C$_{28}$H$_{29}$OSi): 409.1982 ([M+H]$^+$), Found: 409.1985; Analysis C$_{28}$H$_{28}$OSi (408.6160) Calculated: C, 82.30; H, 6.91; O, 3.92; Si, 6.87, Found: C, 81.95; H, 7.07.

4-Mesitylcyclohepta[*def*]fluoren-8(4*H*)-one 6c
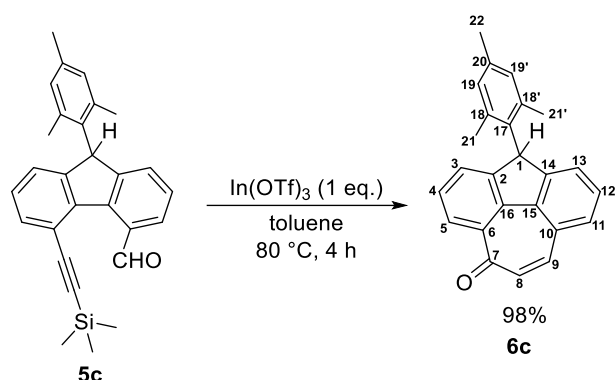
Under nitrogen atmosphere, In(OTf)₃ (2.62 g, 4.67 mmol) was added to a solution of **5c** (1.90 g, 4.66 mmol) in toluene (80 mL) at room temperature. The mixture was heated to 80 °C and stirred for 4 h at the temperature. The reaction was quenched by aqueous HCl (1 M) at 0 °C and the products were extracted with chloroform. The organic layer was washed with water and dried over MgSO₄. After filtration of the drying agent, the solvent was removed under vacuum. The residues were purified by column chromatography on silica gel with hexane and ethyl acetate (95:5) to give **6c** as a colorless solid (1.53 g, 98%).

R_f = 0.20 (hexane : EtOAc = 9:1); mp 173.0–174.0 °C; IR (KBr) ν = 3015 (w), 2963 (w), 2911 (w), 1624 (s), 1589 (s), 1413 (m), 1335 (m), 778 (m), 738 (m) cm⁻¹; ¹H NMR (400 MHz, CDCl₃) 8.46–8.43 (m, 1H, 5-H), 7.62–7.52 (m, 4H), 7.49 (t, *J* = 7.4 Hz, 1H, 12-H), 7.41 (d, *J* = 8.0 Hz, 1H, 13-H), 7.06 (s, 1H, 19′-H), 6.94 (d, *J* = 12.4 Hz, 1H, 8-H), 6.65 (s, 1H, 19-H), 5.64 (s, 1H, 1-H), 2.71 (s, 3H, 21′-H), 2.29 (s, 3H, 22-H), 0.97 (s, 3H, 21-H); ¹³C NMR (100 MHz, CDCl₃) 187.3 (s, C-7), 148.6 (s), 148.0 (s), 140.3 (d, C-9), 140.02 (s), 139.97 (s), 137.8 (s, C-18′), 137.5 (s, C-18), 136.8 (s, C-20), 133.3 (s, C-6), 133.2 (d, C-8), 132.6 (s, C-17), 131.2 (s,C-10), 130.6 (d, C-19), 130.0 (d), 129.0 (d, C-19′), 128.6 (d), 128.4 (d), 127.9 (d, C-5), 127.8 (d, C-3), 125.3 (d, C-13), 49.5 (d, C-1), 21.8 (q, C-21′), 20.8 (q, C-22), 18.7 (q, C-21); MS (EI, 70 eV) *m/z* 336 (M⁺, 100); HRMS (EI, 70 eV) Calculated (C₂₅H₂₀O): 336.1514 (M⁺), Found: 336.1509.

4,10-Dimesitylcyclohepta[*def*]fluoren-8(4*H*)-one 8c
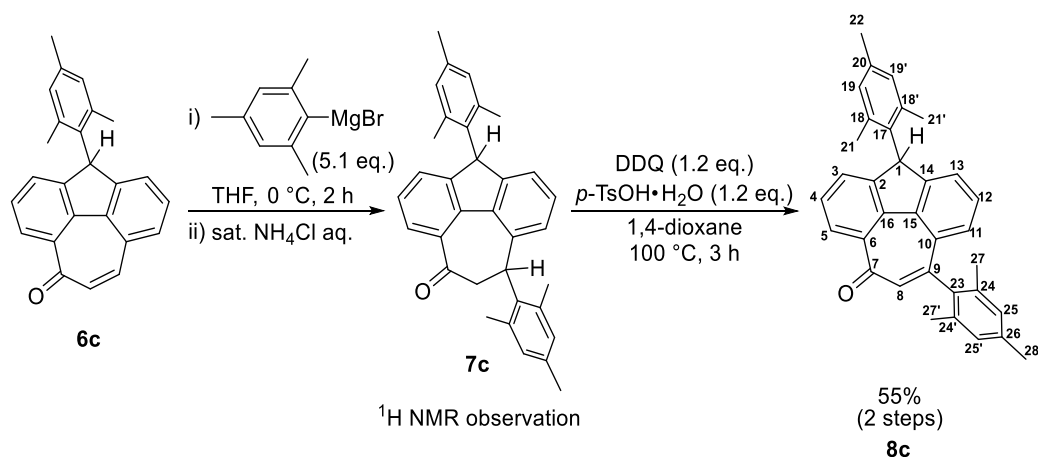
The Grignard reagent was prepared by the reaction of magnesium turnings (0.513 g, 21.1 mmol) and 2-bromomesitylene (2.90 mL, 19.3 mmol) in THF (10 mL) containing a small amount of 1,2-dibromoethane (0.1 mL) as the initiator. The mixture was refluxed for 1 h to give a solution of mesityl magnesium bromide in THF. Under nitrogen atmosphere, a solution of mesityl magnesium bromide in THF was added to a solution of **6c** (1.26 g, 3.76 mmol) in THF (10 mL) at 0 °C and stirred for 2 h at the temperature. The reaction was quenched by saturated aqueous NH₄Cl at 0 °C and the products were extracted with

chloroform. The organic layer was washed with water and dried over MgSO₄. After filtration of the drying agent, the solvent was removed under vacuum. The residues were purified by column chromatography on silica gel with hexane and ethyl acetate (95:5) to give **7c** as colorless solids of diastereo mixture (*isomer A/B* = 1:1). After the confirmation of the products by ^{1}H NMR measurement, the diastereo mixture was subsequently oxidized without further purification. To a mixture of **7c** and 2,3-dichloro-5,6-dicyano-*p*-benzoquinone (DDQ) (1.03 g, 4.51 mmol) in 1,4-dioxane (15 mL) was added *p*-toluenesulfonic acid monohydrate (0.863 g, 4.53 mmol) at room temperature. The mixture was heated to 100 °C and stirred for 3 h at the temperature. After cooling to room temperature, the reaction was quenched by water and the products were extracted with chloroform. The organic layer was washed with water and dried over MgSO₄. After filtration of the drying agent, the solvent was removed under vacuum. The residues were purified by column chromatography on silica gel with hexane and ethyl acetate (90:10) to give **8c** as a colorless solid (0.939 g, 55% in two steps).

4,10-Dimesityl-9,10-dihydrocyclohepta[*def*]fluoren-8(4*H*)-one 7c

^{1}H NMR (400 MHz, in CDCl₃) 7.98 (t, J = 7.4 Hz, 2H), 7.45–7.32 (m, 4H), 7.16–7.07 (m, 4H), 7.05 (s, 1H), 7.03 (s, 1H), 6.95 (s, 2H), 6.93 (s, 2H), 6.73–6.66 (m, 4H), 5.63 (s, 1H), 5.51 (s, 1H), 5.03 (d, J = 7.6 Hz, 1H), 5.00 (d, J = 8.4 Hz, 1H), 3.97 (t, J = 12.4 Hz, 1H), 3.83 (t, J = 12.2 Hz, 1H), 3.09 (d, J = 12.8 Hz, 1H), 3.02 (d, J = 12.4 Hz, 1H), 2.69 (s, 6H), 2.33–2.28 (m, 18H), 2.07 (s, 6H), 1.28–1.26 (m, 3H), 0.98 (s, 3H); MS (EI, 70 eV) m/z 456 (M⁺, 68), 336 (100), 310 (81); HRMS (EI, 70 eV) Calculated (C₃₄H₃₂O): 456.2453 (M⁺), Found: 456.2457.

4,10-Dimesitylcyclohepta[*def*]fluoren-8(4*H*)-one 8c

R_f = 0.32 (hexane : EtOAc = 9:1); mp 259.0–260.0 °C; IR: (KBr) v = 3052 (w), 3006 (w), 2916 (w), 1613 (s), 1588 (s), 1330 (m), 849 (m), 776 (m), 739 (m) cm⁻¹; ^{1}H NMR (400 MHz, CDCl₃) 8.50–8.48 (m ,1H, 5-H), 7.65–7.60 (m, 2H, 3-H, 4-H), 7.40 (d, J = 8.0 Hz, 1H, 13-H), 7.31 (t, J = 7.6 Hz, 1H, 12-H), 7.09 (d, J = 7.6 Hz, 1H, 11-H), 7.07 (s, 1H, 19′-H), 7.00 (s, 2H, 25-H, 25′-H), 6.94 (s, 1H, 8-H), 6.68 (s, 1H, 19-H), 5.71 (s, 1H, 1-H), 2.73 (s, 3H, 21′-H), 2.39 (s, 3H, 28-H), 2.30 (s, 3H, 22-H), 2.09 (s, 3H, 27′-H), 2.05 (s, 3H, 27-H), 1.03 (s, 3H, 21-H); ¹³C NMR (100 MHz, CDCl₃) 187.2 (s, C-7), 150.5 (s, C-9), 148.5 (s, C-2, C-14, two signals were overlapped.), 140.3 (s, C-16), 140.0 (s, C-15), 138,6 (s, C-23), 137.7 (s, C-18′), 137.5 (s, C-18), 137.1 (s, C-26), 136.7 (s, C-20), 135.11 (s), 135.08 (s), 135.02 (d, C-8), 133.2 (s, C-6), 132.8 (s, C-17), 131.6 (s, C-10), 130.7 (d, C-19), 129.1 (d, C-19′), 128.6 (d, C-3). 128.41 (d), 128.35 (d, C-25, C-25′, two signals were overlapped.), 128.3 (d), 127.8 (d, C-4), 127.6 (d, C-5), 125.3 (d, C-13), 49.4 (d, C-1). 21.7 (q, C-21′), 21.1 (q, C-28), 20.8 (q, C-22), 19.9 (q, C-27, C-27′, two signals were overlapped.) 18.7 (q, C-21); MS (EI, 70 eV) m/z 454 (M⁺, 100), 439 (4); HRMS (EI, 70 eV) Calculated (C₃₄H₃₀O): 454.2297 (M⁺), Found: 454.2290.

4,8,10-Trimesityl-4,8-dihydrocyclohepta[*def*]fluoren-8-ylium tetrafluoroborate 2c·BF₄
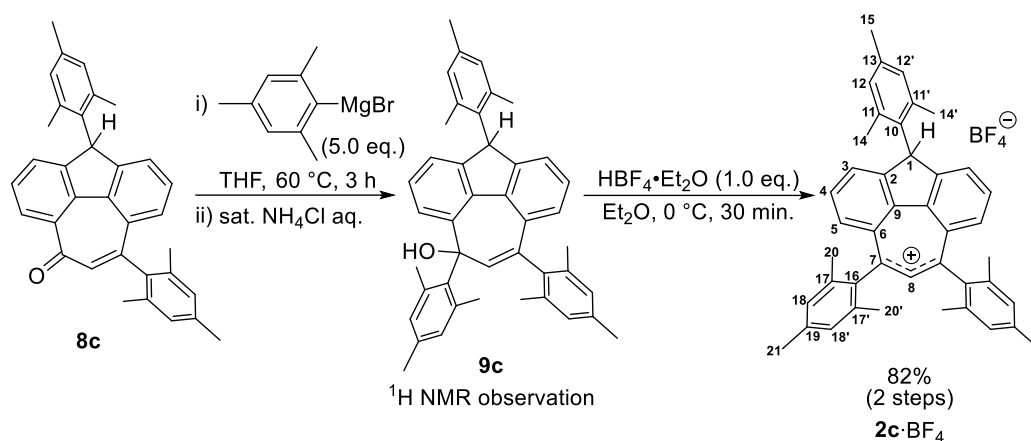
The Grignard reagent was prepared by the reaction of magnesium turnings (0.294 g, 12.1 mmol) and 2-bromomesitylene (1.48 mL, 9.85 mol) in THF (10 mL) containing a small amount of 1,2-dibromoethane (0.1 mL) as the initiator. The mixture was refluxed for 1 h to give a solution of mesityl magnesium bromide in THF. Under nitrogen atmosphere, a solution of mesityl magnesium bromide in THF was added to a solution of **8c** (0.896 g, 1.97 mmol) in THF (2 mL) at 0 °C and stirred for 3 h at 60 °C. The reaction was quenched by saturated aqueous NH₄Cl at 0 °C and the products were extracted with ethyl acetate. The organic layer was washed with water and dried over Na₂SO₄. After filtration of the drying agent, the solvent was removed under vacuum. The residue was filtered through a pad of alumina eluting with hexane/ethyl acetate (95:5) to give **9c** as a pale yellow solid. After the confirmation by ¹H NMR measurement, the product was subsequently treated by acid without further purification. A procedure from the literature[51] was modified as follows: To a solution of **9c** in diethyl ether (15 mL) was added HBF₄·Et₂O (0.26 mL, 1.89 mmol). The reaction mixture was stirred at 0 °C for 2 h and allowed to warm to room temperature. The red precipitate was collected by filtration washed with diethyl ether and dried in a vacuum to give **2c**·BF₄ as a red solid (1.04 g, 82% in two steps).

### 4,8,10-Trimesityl-4,8-dihydrocyclohepta[*def*]fluoren-8-ol 9c

¹H NMR (400 MHz, CDCl₃) 7.20–7.17 (m, 2H), 7.10 (t, *J* = 7.6 Hz, 1H), 7.06–7.04 (m, 2H), 6.95 (s, 1H), 6.89–6.78 (m, 4H), 6.68 (s, 1H), 6.10 (s, 1H), 5.95 (s, 1H), 5.60 (s. 1H), 2.70–2.69 (m, 6H), 2.34–2.27 (m, 12H), 2.02 (s, 3H), 1.89–1.84 (m, 3H), 1.18–1.16 (m, 3H); MS (EI, 70 eV) *m/z* 574 (M⁺,3), 556 ([M–18]⁺, 100); HRMS: (EI, 70 eV) Calculated (C₄₃H₄₂O): 574.3236 (M⁺), Found: 574.3222.

4,8,10-Trimesityl-4,8-dihydrocyclohepta[*def*]fluoren-8-ylium tetrafluoroborate 2c·BF₄

mp > 300 °C; ¹H NMR (600 MHz, CDCl₃) 8.47 (s, 1H, 8-H), 8.42 (d, *J* = 7.2 Hz, 2H, 3-H), 8.29 (t, *J* = 7.8 Hz, 2H, 4-H), 8.19 (d, *J* = 8.4 Hz, 2H, 5-H), 7.18 (s, 1H, 12′-H), 7.12 (s, 2H, 18′-H), 7.11 (s, 2H, 18-H), 6.70 (s, 1H, 12-H) , 6.40 (s, 1H, 1-H) , 2.87 (s, 3H, 14′-H) , 2.43 (s, 6H, 21-H), 2.33 (s, 3H, 15-H), 1.96 (s, 6H, 20′-H), 1.95 (s, 6H, 20-H), 0.83 (s, 3H, 14-H); ¹³C NMR (150 MHz, CDCl₃) 178.3 (s, C-7), 152.6 (s, C-2), 147.5 (s, C-9), 140.3 (s, C-19), 140.1 (d, C-8), 139.3(s), 139.2 (s), 138.2 (s, C-13), 137.9 (s, C-16), 136.7 (s, C-11), 136.5 (s, C-6), 134.7 (s, C-17), 134.3 (d, C-4), 134.1 (d, C-3), 133.7 (s, C-17′), 131.9 (d, C-5), 130.8 (d, C-12), 130.0 (d, C-12′), 129.4 (d, C-18), 129.0 (d, C-18′) , 49.8 (d, C-1), 21.9 (q, C-14′), 21.2 (q, C-21), 20.9 (q, C-15), 20.4 (q), 20.3 (q), 18.9 (q, C-14); ¹¹B{¹H} NMR (127 MHz, CDCl₃, BF₃·Et₂O in CDCl₃ as standard) – 1.45 ppm; ¹⁹F NMR (372 MHz, CDCl₃, BF₃·Et₂O in CDCl₃ as standard) –154.5 ppm; IR: (KBr) *ν* = 3099 (w), 3010 (w), 2916 (w), 1608 (m), 1552 (m), 1488 (s), 1461 (s), 1405 (s), 1063 (s) cm⁻¹; MS (EI, 70 eV) *m/z* 557 (M⁺, 100), 541 (6); HRMS (EI, 70 eV) Calculated (C₄₃H₄₁⁺): 557.3203 (M⁺), Found: 557.3215; Analysis C₄₃H₄₁BF₄ (644.6046) Calculated: C, 80.12; H, 6.41;

B, 1.68; F, 11.79, Found: C, 80.22; H, 6.42.

4,8,10-Trimesitylcyclohepta[*def*]fluorene 1c
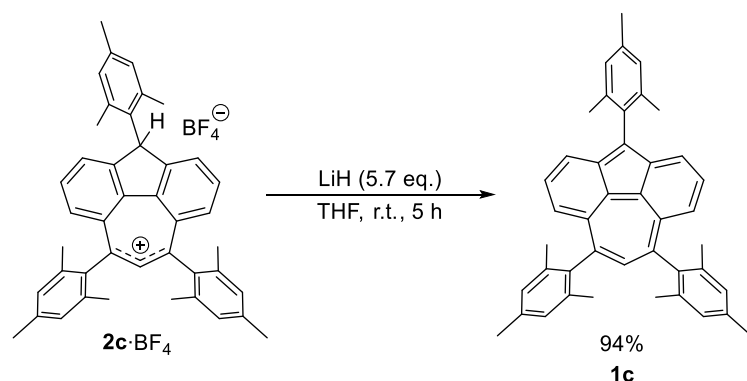
In a nitrogen-filled glove box, LiH (4.1 mg, 0.52 mmol) was added to a solution of **2c·BF₄** (58.9 mg, 0.091 mmol) in freshly dried THF (8 mL). The mixture was stirred at room temperature for 3 h. After insoluble materials were removed by filtration, the solvent was removed under vacuum. The residues were dissolved in hexane and insoluble materials were removed by filtration. The filtrate was evaporated to give **1c** as dark blown solid (47.7 mg, 94%). The recrystallization of **1c** from a dichloromethane–hexane solution in a glove box afforded a single crystal suitable for the X-ray crystallographic analysis.

mp 189.5–190.0 °C; IR (KBr) v = 3047 (w), 2959 (s), 2923 (s), 2866 (m), 1608 (m), 1560 (w), 1459 (m), 1429 (m), 1380 (m), 1361 (m), 1055 (w), 849 (m), 797 (w) cm⁻¹; MS (EI⁺, 70 eV) m/z 556 (M⁺, 84), 541 (7); HRMS (EI⁺, 70 eV) Calculated (C₄₃H₄₀): 556.3130 (M⁺), Found: 556.3137 (M⁺).

4,5-Dibromo-9-(2,4,6-triisopropylphenyl)-9*H*-fluorene 3d
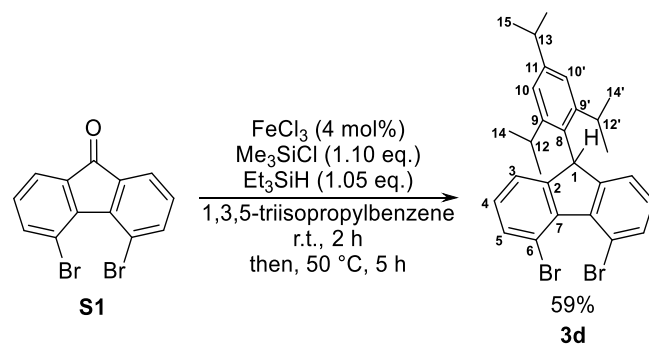
A procedure from the literature[48] was modified as follows: To a mixture of **S1**[47] (1.29 g, 3.81 mmol) and iron(III) chloride (25 mg, 0.154 mmol) in 1,3,5-triisopropylbenzene (2.5 mL) was added chlorotrimethylsilane (0.54 mL, 4.25 mmol) and triethylsilane (0.64 mL, 4.03 mmol) at room temperature. The reaction mixture was stirred for 2 h at room temperature, then it was heated at 50 °C for 5 h. After cooling to room temperature, the reaction was quenched with water and the product was extracted with chloroform. The organic layer was washed with water, and dried over MgSO₄. The solution was collected by filtration and the solvents were removed under vacuum. The residue was purified by column chromatography on silica gel (hexane) to give **3d** as a colorless solid (1.18 g, 59%).

R_f = 0.33 (hexane), 0.91 (hexane : EtOAc = 9:1); mp 158.0–159.0 °C; IR (KBr) v = 3062 (w), 2953 (s), 2924 (m), 2864 (m), 1557 (w), 1455 (s), 1410 (s), 1400 (s), 1382 (w), 1361 (w), 1160 (m), 1104 (s), 882 (m), 847 (w), 762 (s), 685 (m) cm⁻¹; ¹H NMR (400 MHz, CDCl₃) 7.65 (td, J = 4.6 Hz, 0.8 Hz, 2H, 4-H), 7.13 (d, J = 5.2 Hz, 4H, 3-H, 5-H), 7.11 (d, J = 1.6 Hz, 1H. 10′-H), 6.85 (d, J = 2.4 Hz, 1H, 10-H), 5.55 (s, 1H, 1-H), 3.47 (sep, J = 6.7 Hz, 1H, 12′-H), 2.89 (sep, J = 6.9 Hz, 1H, 13-H),

1.46 (sep, J = 6.8 Hz, 1H, 12-H), 1.40 (d, J = 6.7 Hz, 6H, 14′-H), 1.26 (d, J = 6.9 Hz, 6H, 15-H), 0.43 (d, J = 6.8 Hz, 6H, 14-H); ^{13}C NMR (100 MHz, CDCl$_3$) 153.0 (s, C-2), 148.8 (s, C-9), 147.93 (s), 147.88 (s), 138.8 (s, C-7), 133.8 (d, C-4), 130.2 (s, C-8), 128.7 (d, C-5), 123.1 (d, C-10), 122.6 (d, C-3), 120.9 (d, C-10′), 116.2 (s, C-6), 49.1 (d, C-1), 34.0 (d, C-13), 30.9 (d, C-12′), 28.9 (d, C-12), 24.7 (q, C-14′), 23.9 (q, C-15), 23.3 (q, C-14); MS (EI, 70 eV) m/z 528 ([M+4]$^+$, 41), 526 ([M+2]$^+$, 81), 524 (M$^+$, 40), 447 (100), 445 (98); HRMS (EI, 70 eV) Calculated (C$_{28}$H$_{30}$Br$_2$): 524.0714 (M$^+$), Found: 524.0718.

5-Bromo-9-(2,4,6-triisopropylphenyl)-9*H*-fluorene-4-carbaldehyde 4d
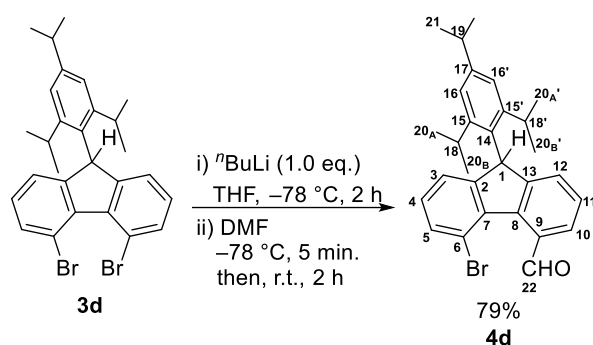
Under nitrogen atmosphere, ^{n}BuLi (1.6 M in hexane, 5.95 mL, 9.51 mmol) was added to a solution of **3d** (5.01 g, 9.51 mmol) in freshly dried THF (40 mL) at –78 °C. After stirred for 2 h at the temperature, anhydrous DMF (20 mL) was added to the reaction mixture. The reaction mixture was stirred for 5 min at –78 °C and was allowed to gradually warm to room temperature for 2 h. The reaction was quenched by the addition of aqueous HCl (1 M) at 0 °C. After the mixture was stirred for 30 min at 0 °C, the products were extracted with chloroform. The organic layer was washed with water and dried over MgSO$_4$. After filtration of the drying agent, the solvent was removed under vacuum. The residues were purified by column chromatography on silica gel with hexane and ethyl acetate (95:5) to give **4d** as a colorless solid (3.56 g, 79%).

R_f = 0.49 (hexane : EtOAc = 9:1); mp 167.0–168.0 °C; IR: (KBr) ν = 3062 (w), 2957 (s), 2866 (m), 1692 (s), 1589 (w), 1573 (w), 1456 (m), 1383 (m), 1362 (w), 1290 (w), 1230 (m), 1167 (w), 881 (w), 837 (w), 766 (m), 754 (m), 704 (w) cm^{-1}; ^{1}H NMR (400 MHz, CDCl$_3$) 11.03 (s, 1H, 22-H), 7.85 (dd, J = 7.0 Hz, 1.4 Hz, 1H, 10-H), 7.61 (dd, J = 7.4 Hz, 1.8 Hz, 1H, 5-H), 7.42 (t, J = 7.2 Hz, 1H, 11-H), 7.40–7.38 (m, 1H, 12-H), 7.22–7.20 (m, 1H, 3-H), 7.18 (t, J = 7.4 Hz, 1H, 4-H), 7.14 (d, J = 2.0 Hz, 1H, 16′-H), 6.86 (d, J = 2.0 Hz, 1H, 16-H), 5.60 (s, 1H, 1-H), 3.51 (sep, J = 6.7 Hz, 1H, 18′-H), 2.89 (sep, J = 6.9 Hz, 1H, 19-H), 1.43 (d, J = 6.7 Hz, 3H, 20′-H), 1.42 (d, J = 6.7 Hz, 3H, 20′-H), 1.38 (sep, J = 6.2 Hz, 1H, 18-H), 1.27 (d, J = 6.9 Hz, 6H, 21-H), 0.44 (d, J = 6.2 Hz, 3H, 20-H), 0.42 (d, J = 6.2 Hz, 3H, 20-H); ^{13}C NMR (100 MHz, CDCl$_3$) 191.7 (d, C-22), 153.2 (s, C-2), 151.2 (s, C-13), 148.7 (s, C-15), 148.1 (s, C-17), 147.9 (s, C-15′), 139.3 (s, C-8), 138.7 (s, C-7), 132.63 (d, C-5), 132.56 (s, C-9), 129.5 (s, C-14), 129.4 (d, C-3), 127.9 (d), 127.8 (d), 126.9 (d, C-10), 123.5 (d, C-4), 123.1 (d, C-16), 121.0 (d, C-16′), 117.5 (s, C-6), 49.2 (d, C-1), 34.0 (d, C-19), 31.0 (d, C-18′), 28.8 (d, C-18), 24.8 (q, C-20′), 24.6 (q, C-20′), 23.9 (q, C-21), 23.4 (q, C-20), 23.3 (q, C-20); MS (EI, 70 eV) m/z 476 ([M+2]$^+$, 12), 474 (M$^+$, 12), 395 (100); HRMS (EI, 70 eV) Calculated (C$_{29}$H$_{31}$BrO): 474.1558 (M$^+$), Found: 474.1565; Analysis C$_{29}$H$_{31}$BrO, Calculated: C, 73.26; H, 6.57; Br, 16.81; O, 3.36. Found: C, 72.95; H, 6.52.

9-(2,4,6-Triisopropylphenyl)-5-((trimethylsilyl)ethynyl)-9*H*-fluorene-4-carbaldehyde 5d
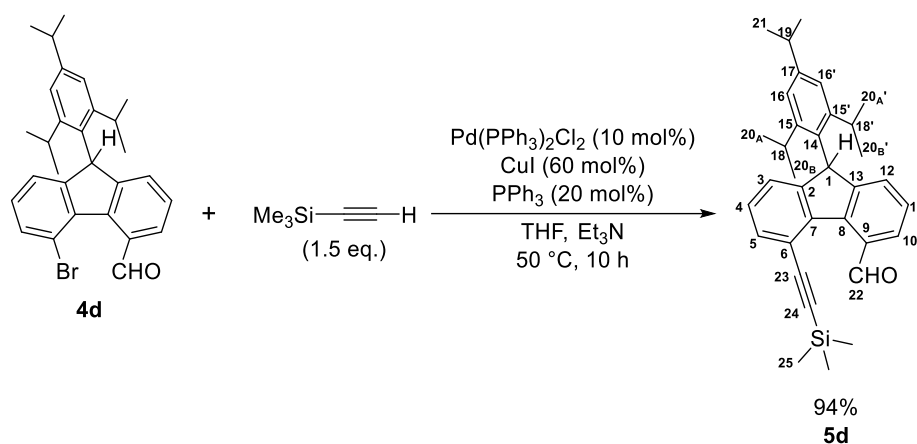
Under nitrogen atmosphere, PdCl$_2$(PPh$_3$)$_2$ (0.511 g, 0.728 mmol) was added to a mixture of **4d** (3.41g, 7.18 mmol), CuI (1.49 g, 7.45 mmol) and PPh$_3$ (0.381 g, 1.45 mmol) in freshly dried THF (100 mL) and anhydrous Et$_3$N (60 mL) at room temperature. The mixture was heated to 50 °C and stirred for 10 h at the temperature. The reaction was quenched by saturated aqueous NH$_4$Cl at 0 °C and the products were extracted with chloroform. The organic layer was washed with water and dried over MgSO$_4$. After filtration of the drying agent, the solvent was removed under vacuum. The residues were purified by column chromatography on silica gel with hexane and ethyl acetate (95:5) to give **5d** as a colorless solid (3.33 g, 94%).

R_f = 0.62 (hexane : EtOAc = 9:1), 0.06 (hexane); mp 165 0–165.1 °C; IR: (KBr) ν = 3062 (w), 2960 (s), 2869 (m), 2146 (m), 1690 (s), 1467 (m), 1386 (m), 1362 (w), 1296 (w), 1250 (m), 1235 (m), 862 (s), 846 (s), 759 (s) cm^{-1}; ^{1}H NMR (400 MHz, CDCl$_3$) 11.38 (s, 1H, 22-H), 7.93–7.89 (m, 1H, 10-H), 7.61 (d, J = 7.2 Hz, 1H, 5-H), 7.41–7.37 (m, 2H, 11-H, 12-H), 7.28 (t, J = 7.6 Hz, 1H, 4-H), 7.23 (d. J = 7.2 Hz, 1H, 3-H), 7.13 (d, J = 2.0 Hz, 1H, 16′-H), 6.86 (d, J = 1.6 Hz, 1H, 16-H), 5.51 (s, 1H, 1-H), 3.51 (sep, J = 6.9 Hz, 1H, 18′-H), 2.90 (sep, J = 6.9 Hz, 1H, 19-H), 1.42 (d, J = 6.9 Hz, 6H, 20′-H), 1.39 (sep, J = 6.7 Hz, 1H, 18-H), 1.27 (d, J = 6.9 Hz, 6H, 21-H), 0.43 (d, J = 6.7 Hz, 6H, 20-H), 0.33 (s, 9H, 25-H); ^{13}C NMR (100 MHz, CDCl$_3$) 192.4 (d, C-22), 151.3 (s, C-2), 151.1 (s), 148.8 (s, C-15), 148.02 (s, C-15′), 147.94 (s, C-17), 140.3 (s), 139.0 (s, C-7), 134.0 (d, C-5), 132.7 (s, C-9), 129.7 (s, C-14), 128.1 (d, C-12), 127.7 (d, C-4), 127.6 (d, C-11), 126.5 (d, C-10), 124.7 (d, C-3), 123.0 (d, C-16), 121.0 (d, C-16′), 119.1 (s, C-6), 105.2 (s, C-23), 99.3 (s, C-24), 48.5 (d, C-1), 34.0 (d, C-19), 31.0 (d, C-18′), 28.8 (d, C-18), 24.72 (q, C-20′), 24.67 (q, C-20′), 24.0 (q, C-21), 23.5 (q, C-20), 23.4 (q, C-20), –0.49 (q, C-25); MS (EI, 70 eV) *m/z* 492 (M$^+$, 5), 477 (100), (CI, 70 eV) *m/z* 493 ([M+H]$^+$, 100), 492 (M$^+$, 3), HRMS (CI, 70 eV) Calculated (C$_{34}$H$_{41}$OSi): 493.2927 ([M+H]$^+$), Found: 493.2928.
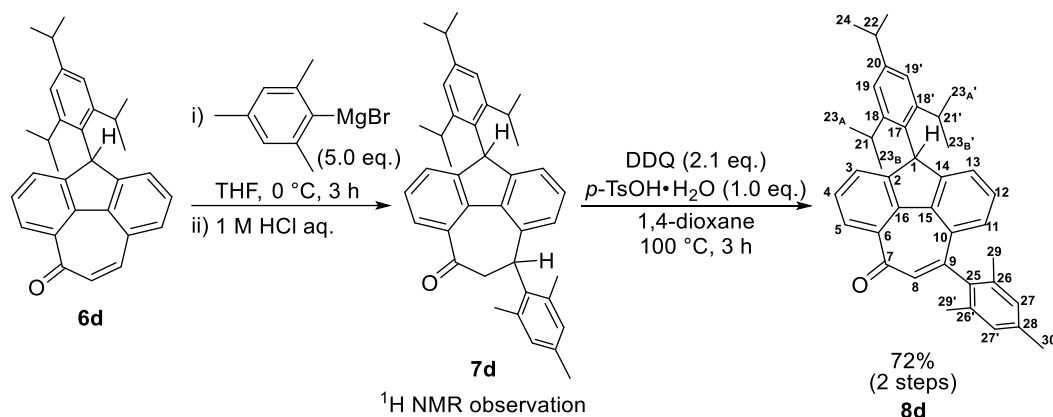
4-(2,4,6-Triisopropylphenyl)cyclohepta[*def*]fluoren-8(4*H*)-one 6d
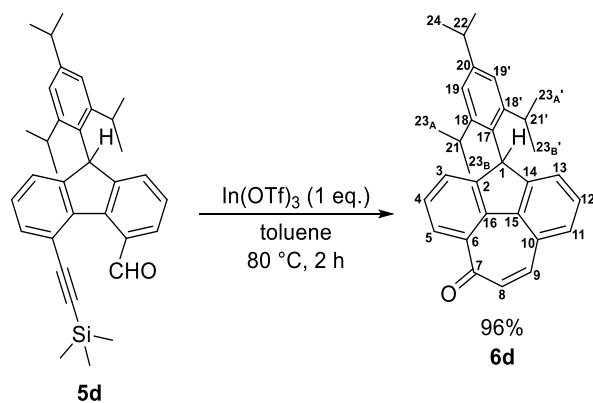
Under nitrogen atmosphere, In(OTf)$_3$ (1.88 g, 3.35 mmol) was added to a solution of **5d** (1.65g, 3.35 mmol) in toluene (55 mL) at room temperature. The mixture was heated to 80 °C and stirred for 2 h at the temperature. The reaction was quenched by aqueous HCl (1 M) at 0 °C and the products were extracted with chloroform. The organic layer was washed with water and dried over MgSO$_4$. After filtration of the drying agent, the solvent was removed under vacuum. The residues were purified by column chromatography on silica gel with hexane and ethyl acetate (95:5) to give **6d** as a colorless solid (1.35 g, 96%).

R_f = 0.32 (hexane : EtOAc = 9:1); mp 230.0–230.1 °C (Sublimation); IR (KBr) v = 3062 (w), 2958 (m), 2867 (w), 1625 (s), 1590 (s), 1467 (w), 1411 (w), 1335 (w), 1215 (w), 855 (w), 770 (w), 736 (m) cm^{-1}; ^{1}H NMR (400 MHz, CDCl$_3$) 8.48–8.43 (m, 1H, 5-H), 7.62–7.54 (m, 4H), 7.49 (t, J = 7.4 Hz, 1H, 12-H), 7.44 (d, J = 7.6 Hz, 1H, 13-H), 7.17 (s, 1H, 19′-H), 6.97 (d, J = 12.8 Hz, 1H, 8-H), 6.86 (s, 1H, 19-H), 5.69 (s, 1H, 1-H), 3.59 (sep, J = 6.8 Hz, 1H, 21′-H), 2.91 (sep, J = 6.8 Hz, 1H, 22-H), 1.47 (d, J = 6.8 Hz, 6H, 23′-H), 1.33–1.24 (m, 7H, 24-H, 21-H), 0.365 (d, J = 6.8 Hz, 3H, 23-H), 0.358 (d, J = 6.8 Hz, 3H, 23-H); ^{13}C NMR (100 MHz, CDCl$_3$) 187.4 (s, C-7), 150.7 (s), 150.2 (s), 148.9 (s, C-18), 148.0 (s, C-18′), 147.9 (s, C-20), 140.4 (d, C-9), 139.4 (s, two signals were overlapped.), 133.5 (s), 133.3 (d, C-8), 131.4 (s, C-10), 129.7 (d, C-17), 129.6 (s), 128.4 (d), 128.2 (d), 127.73 (d), 127.67 (d), 125.3 (d), 123.0 (d, C-19), 121.0 (d, C-19′), 48.4 (d, C-1), 34.0 (d, C-22), 31.0 (d, C-21′), 28.8 (d, C-21), 24.74 (q, C-23′), 24.68 (q, C-23′), 23.9 (q, C-24), 23.40 (q, C-23), 23.36 (q, C-23); MS (EI, 70 eV) m/z 420 (M$^+$, 100); HRMS (EI, 70 eV) Calculated (C$_{31}$H$_{32}$O): 420.2453 (M$^+$), Found: 420.2447.

10-Mesityl-4-(2,4,6-triisopropylphenyl)cyclohepta[*def*]fluoren-8(4*H*)-one 8d

6d

i) mesityl—MgBr (5.0 eq.)
THF, 0 °C, 3 h
ii) 1 M HCl aq.

7d
^{1}H NMR observation

DDQ (2.1 eq.)
p-TsOH•H$_2$O (1.0 eq.)
1,4-dioxane
100 °C, 3 h

72%
(2 steps)
8d

The Grignard reagent was prepared by the reaction of magnesium turnings (0.385 g, 15.8 mmol) and 2-bromomesitylene (2.15 mL, 14.3 mmol) in THF (15 mL) containing a small amount of 1,2-dibromoethane (0.1 mL) as the initiator. The mixture was refluxed for 1 h to give a solution of mesityl magnesium bromide in THF. Under nitrogen atmosphere, a solution of mesityl magnesium bromide in THF was added to a solution of **6d** (1.20 g, 2.85 mmol) in THF (15 mL) at 0 °C and stirred for 3 h at the temperature. The reaction was quenched by aqueous HCl (1 M) at 0 °C and the products were extracted with chloroform. The organic layer was washed with water and dried over MgSO$_4$. After filtration of the drying agent, the solvent was removed under vacuum. The residues were purified by column chromatography on silica gel with hexane and ethyl acetate (95:5) to give **7d** as colorless solids of diastereo mixture (*isomer A/B* = 5:4). After the confirmation of the products by ^{1}H NMR measurement, the diastereo mixture was subsequently oxidized without further purification. To a mixture of **7d** and 2,3-dichloro-5,6-dicyano-*p*-benzoquinone (DDQ) (1.36 g, 6.00 mmol) in 1,4-dioxane (2 mL) was added *p*-toluenesulfonic acid monohydrate (0.540 g, 2.84 mmol) at room temperature. The mixture was heated to 100 °C and stirred for 3 h at the temperature. After cooling to room temperature, the reaction was quenched by water and the products were extracted with chloroform. The organic layer was washed with water and dried over MgSO$_4$. After filtration of the drying agent, the solvent was removed under vacuum. The residues were purified by column chromatography on silica gel with hexane and ethyl acetate (90:10) to give **8d** as a colorless solid (1.10 g, 72% in two steps).

110

### 10-Mesityl-4-(2,4,6-triisopropylphenyl)-9,10-dihydrocyclohepta[*def*]fluoren-8(4*H*)-one 7d

[1H] NMR (400 MHz, CDCl$_3$); 8.00 (d, *J* = 7.6 Hz, 1H, *isomer A*), 7.93 (d, *J* = 7.6 Hz, 0.8H, *isomer B*), 7.47–7.44 (m, 1.8H), 7.37–7.32 (m, 1.8H), 7.18–7.05 (m, 5.4H), 6.96 (s, 1.8H), 6.93 (s, 1H, *isomer A*), 6.90 (s, 0.8H, *isomer B*), 6.86 (dd, *J* = 8.4 Hz, 2.0 Hz, 1.8H), 6.76 (d, *J* = 7.6 Hz, 0.8H, *isomer B*), 6.67–6.65 (m, 1H, *isomer A*), 5.69 (s, 1H, *isomer A*), 5.57 (s, 0.8H, *isomer B*) 5.09 (d, *J* = 11.2 Hz, 0.8H, *isomer B*), 5.02 (d, *J* = 12.4 Hz, 1H, *isomer A*), 3.98 (t, *J* = 12.6 Hz, 1H, *isomer A*), 3.76 (t, *J* = 12.0 Hz, 0.8H, *isomer B*), 3.64–3.55 (m, 1.8H), 3.15 (dd, *J* = 12.6 Hz, 1.8 Hz, 0.8H, *isomer B*), 3.04 (dd, *J* = 12.4 Hz, 0.8 Hz, 1H, *isomer A*), 2.94–2.86 (m, 1.8H), 2.37–2.32 (m, 10.8H), 2.09 (s, 3H, *isomer A*),1.99 (s, 2.4H, *isomer B*), 1.88–1.76 (m, 0.8H, *isomer B*), 1.47–1.42 (m, 10.8H), 1.29–1.18 (m, 11.8H), 0.50–0.32 (m, 10.8H).

10-Mesityl-4-(2,4,6-triisopropylphenyl)cyclohepta[*def*]fluoren-8(4*H*)-one 8d

R_f = 0.47 (hexane : EtOAc = 9:1); mp 285.0–285.1 °C; IR (KBr) ν = 3052 (w), 2958 (m), 2922 (w), 1616 (s), 1589 (s), 1461 (w), 1361 (m), 1330 (m), 738 (m) cm^{-1}; [1H] NMR: (400 MHz, CDCl$_3$) 8.50–8.48 (m, 1H, 5-H), 7.66–7.61 (m, 2H, 3-H, 4-H), 7.41 (d, *J* = 7.2 Hz, 1H, 13-H), 7.31 (t, *J* = 7.8 Hz, 1H, 12-H), 7.17 (d, *J* = 1.6 Hz, 1H, 19′-H), 7.09 (d, *J* = 7.6 Hz, 1H, 11-H), 7.00 (s, 2H, 27-H, 27′-H), 6.96 (s, 1H, 8-H), 6.86 (d, *J* = 1.6 Hz, 1H, 19-H), 5.76 (s, 1H, 1-H), 3.62 (sep, *J* = 6.8 Hz, 1H, 21′-H), 2.91 (sep, *J* = 6.8 Hz, 1H, 22-H), 2.39 (s, 3H, 30-H), 2.09 (s, 3H, 29′-H), 2.07 (s, 3H, 29-H), 1.48 (d, *J* = 6.8 Hz, 3H, 23′-H), 1.47 (d, *J* = 6.8 Hz, 3H, 23′-H), 1.40 (sep, *J* = 6.9 Hz, 1H, 21-H), 1.28 (d, *J* = 6.8 Hz, 6H, 24-H), 0.41 (d, *J* = 6.9 Hz, 3H, 23-H), 0.33 (d, *J* = 6.9 Hz, 3H, 23-H); ^{13}C NMR (100 MHz, CDCl$_3$) 187.5 (s, C-7), 150.74 (s), 150.65 (s), 150.6 (s), 148.8 (s, C-18), 148.01 (s, C-20), 147.90 (s, C-18′), 139.8 (s, C-16), 139.3 (s, C-15), 138.6 (s, C-25), 137.1 (s, C-28), 135.2 (s), 135.1 (s), 135.0 (d, C-8), 133.4 (s, C-6), 131.8 (s, C-10), 129.9 (s, C-17), 128.5 (d), 128.4 (d), 128.33 (d), 128.25 (d, C-12), 128.1 (d, C-11), 127.8 (d, C-3), 127.4 (d, C-5), 125.5 (d, C-13), 123.0 (d, C-19), 121.0 (d, C-19′), 48.2 (d, C-1), 34.0 (d, C-22), 31.0 (d, C-21′), 28.8 (d, C-21), 24.75 (q, C-23′), 24.70 (q, C-23′), 23.9 (q, C-24), 23.4 (q, C-23), 23.2 (q, C-23), 21.1 (d, C-30), 19.9 (d), 19.8 (d); MS (EI, 70 eV) *m/z* 538 (M$^+$, 100), 521(9); HRMS (EI, 70 eV) Calculated (C$_{40}$H$_{42}$O): 538.3236 (M$^+$), Found: 538.3244.

8,10-Dimesityl-4-(2,4,6-triisopropylphenyl)-4,8-dihydrocyclohepta[*def*]fluoren-8-ylium tetrafluoroborate 2d·BF$_4$
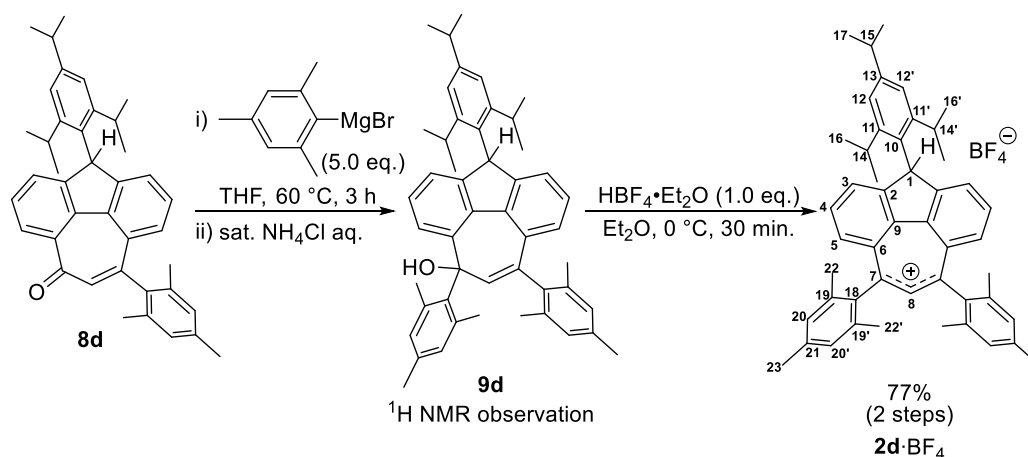
The Grignard reagent was prepared by the reaction of magnesium turnings (0.305 g, 12.5 mmol) and 2-bromomesitylene (1.50 mL, 10.21 mol) in THF (20 mL) containing a small amount of 1,2-dibromoethane (0.1 mL) as the initiator. The mixture was refluxed for 1 h to give a solution of mesityl magnesium bromide in THF. Under nitrogen atmosphere, a solution of mesityl magnesium bromide in THF was added to a solution of **8d** (1.10 g, 2.04 mmol) in THF (20 mL) at 0 °C and stirred for 3 h at 60 °C. The reaction was quenched by saturated aqueous NH$_4$Cl at 0 °C and the products were extracted with ethyl acetate. The

organic layer was washed with water and dried over Na$_2$SO$_4$. After filtration of the drying agent, the solvent was removed under vacuum. The residues were purified by column chromatography on alumina with hexane and ethyl acetate (95:5) to give **9d** as a pale yellow solid of diastereo mixture. After the confirmation of the products by ^{1}H NMR measurement, the products were subsequently treated by acid without further purification. A procedure from the literature[51] was modified as follows: To a solution of **9d** in diethyl ether (30 mL) was added HBF$_4$·Et$_2$O (0.26 mL, 1.89 mmol). The reaction mixture was stirred at 0 °C for 2 h and allowed to warm to room temperature. After the reaction, the solvent was removed under vacuum and the residues were washed by dried hexane several times, to give **2d**·BF$_4$ (1.15 g, 77% in two steps).

8,10-Dimesityl-4-(2,4,6-triisopropylphenyl)-4,8-dihydrocyclohepta[*def*]fluoren-8-ol 9d

^{1}H NMR (400 MHz, CDCl$_3$) 7.24–7.16 (m, 3H), 7.14 (s, 1H), 7.12–7.08 (m, 1H), 7.05–7.03 (m, 1H), 6.96 (s, 1H), 6.90–6.80 (m, 5H), 6.12–6.11 (m, 1H), 5.66 (s, 1H), 3.71–3.61 (m, 1H), 2.96–2.85 (m, 1H), 2.69 (s, 3H), 2.33–2.27 (m, 9H), 2.04–1.99 (m, 3H), 1.92 (s, 3H), 1.75–1.65 (m, 1H), 1.54–1.45 (m, 6H), 1.29–1.27 (m, 6H), 0.48–0.39 (m, 6H).

8,10-Dimesityl-4-(2,4,6-triisopropylphenyl)-4,8-dihydrocyclohepta[*def*]fluoren-8-ylium tetrafluoroborate 2d·BF$_4$

mp >300 °C; IR (KBr) ν = 3006 (w), 2963 (m), 2926 (w), 2869 (w), 1609 (m), 1554 (m), 1489 (m), 1458 (s), 1406 (s), 1086 (s), 1057 (s) cm^{-1}; ^{1}H NMR (400 MHz, CDCl$_3$) 8.50 (s, 1H, 8-H), 8.44 (d, J = 7.2 Hz, 2H, 3-H), 8.31 (t, J = 7.8 Hz, 2H, 4-H), 8.21 (d, J = 8.4 Hz, 2H, 5-H), 7.29 (d, J = 1.6 Hz, 1H, 12′-H), 7.14 (s, 2H, 20′-H), 7.12 (s, 2H, 20-H), 6.86 (d, J = 1.6 Hz, 1H, 12-H), 6.43 (s, 1H, 1-H), 3.73 (sep, J = 7.2 Hz, 1H, 14′-H), 2.94 (sep, J = 6.8 Hz, 1H, 15-H), 2.44 (s, 6H, 23-H), 2.00 (s, 6H, 22′-H), 1.90 (s, 6H, 22-H), 1.55 (d, J = 7.2 Hz, 6H, 16′-H), 1.30 (d, J =6.8 Hz, 6H, 17-H), 0.91 (sep, J = 6.8 Hz, 1H, 14-H), 0.24 (d, J = 6.8 Hz, 6H, 16-H); ^{13}C NMR (100 MHz, CDCl$_3$) 178.4 (s, C-7), 154.2 (s, C-2), 149.4 (s, C-13), 149.1 (s, C-11′), 148.0 (s, C-11), 147.0 (s, C-9), 140.4 (s, C-21), 140.2 (d, C-8), 137.7 (s, C-18), 136.5 (s, C-6), 134.4 (s, C-19′), 134.2 (d, C-4), 134.0 (d, C-3), 133.6 (s, C-19), 131.9 (d, C-5), 129.4 (d, C-20′), 129.0 (d, C-20), 126.9 (s, C-10), 123.1 (d, C-12), 122.2 (d, C-12′), 48.5 (d, C-1), 34.1 (d, C-15), 31.3 (d, C-14′), 29.6 (d, C-14), 24.8 (q, C-16′), 23.9 (q, C-17), 23.3 (q, C-16), 21.2 (q, C-23), 20.4 (q, C-22′), 20.0 (q, C-22); ^{11}B{^{1}H} NMR (127 MHz, CDCl$_3$, BF$_3$·Et$_2$O in CDCl$_3$ as an external standard) –1.44 ppm; ^{19}F NMR (372 MHz, CDCl$_3$, BF$_3$·Et$_2$O in CDCl$_3$ as an external standard); –154.07 ppm; MS (EI, 70 eV) m/z 641 (M$^+$, 100), 313 (16); HRMS (EI, 70 eV), Calculated (C$_{49}$H$_{53}^+$): 641.4142 (M$^+$), Found: 641.4139.

### 8,10-Dimesityl-4-(2,4,6-triisopropylphenyl)cyclohepta[*def*]fluorene 1d
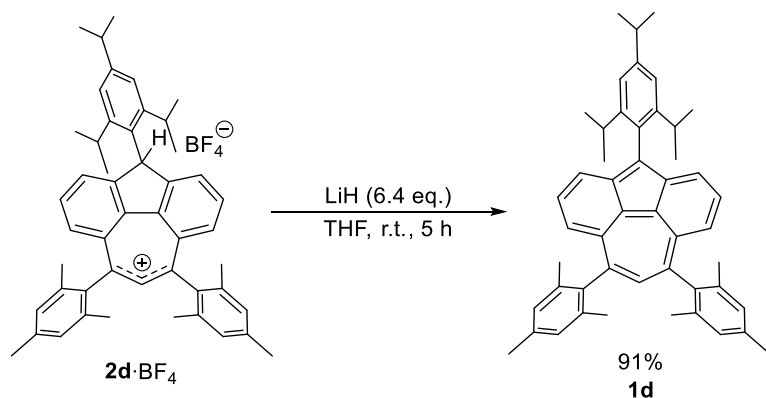
In a nitrogen-filled glove box, LiH (7.0 mg, 0.88 mmol) was added to a solution of **2d**·BF$_4$ in freshly dried THF (12 mL). The mixture was stirred at room temperature for 5 h. After insoluble materials were removed by filtration, the solvent was removed under vacuum. The residues were dissolved in hexane and insoluble materials were removed by filtration. The filtrate was

evaporated to give **1d** as dark blown solid (80.2 mg, 91%). The recrystallization of **1d** from a dichloromethane–hexane solution in a glove box afforded a single crystal suitable for the X-ray crystallographic analysis.

mp 180.2–182.0 °C; IR (KBr) $\nu = 3058$ (w), 2963 (s), 2921 (s), 2869 (m), 1607 (s), 1461 (m), 1426 (m), 1379 (m), 1361 (w), 850 (w), 795 (w), 719 (w) cm^{-1}; MS (EI$^+$, 70 eV) m/z 640 (M$^+$, 100); HRMS (EI$^+$, 70 eV), Calculated (C$_{49}$H$_{52}$): 640.4069 (M$^+$), Found: 640.4061 (M$^+$).

Over-reduction of 1d to radical anion 1d$^{\bullet-}$

2d·BF$_4$ Na·**1d**$^{\bullet-}$
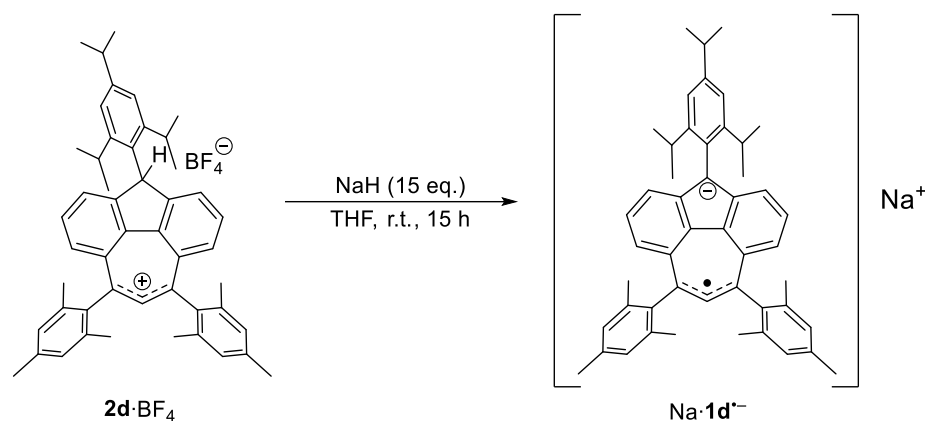
In a nitrogen-filled glove box, NaH (20 mg, 1.04 mmol) was added to a solution of **2d**·BF$_4$ (50.12 mg, 0.069 mmol) in freshly dried THF (5 mL). The mixture was stirred at room temperature for 15 h. After insoluble materials were removed by filtration, the solvent was removed under vacuum. The residues were dissolved in acetonitrile and insoluble materials were removed by filtration. The solvent was removed under vacuum and the residues were dissolved in THF (0.8 mL). After filtration, the filtrate was layered with hexane (3.2 mL) and placed at –45 °C. The recrystallization of the mixture from a tetrahydrofuran–hexane solution in a glove box afforded a blue single crystal of Na·**1d**$^{\bullet-}$ suitable for the X-ray crystallographic analysis.

4,5-dibromo-9-(2,6-dichlorophenyl)-9*H*-fluorene 3e
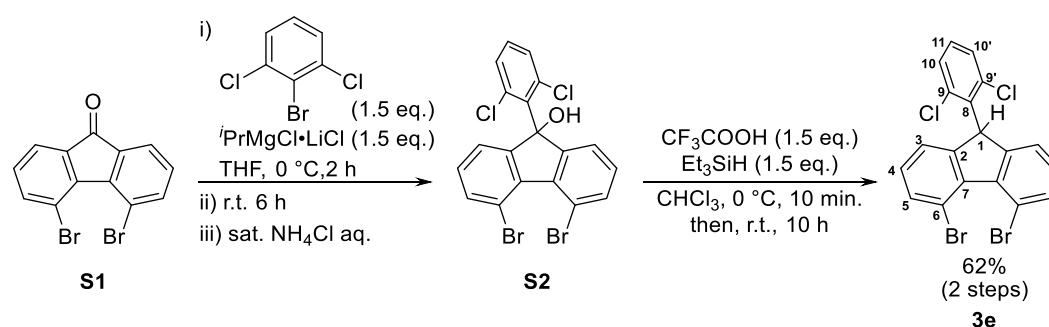
The Grignard reagent was prepared by the reaction of 1.3 M isopropyl magnesium chloride lithium chloride complex solution in THF (10.2 mL, 13.3 mmol) with 1-bromo-2,6-dichlorobenzene (2.99 g, 13.3 mmol) in THF (5 mL) at 0 °C. The mixture was stirred at 0 °C for 2 h to give a solution of the desired Grignard reagent in THF. A solid of **S1** (2.99 g, 8.84 mmol) was added to a solution of the Grignard reagent in THF at 0 °C and the mixture was stirred for 6 h at room temperature. The reaction was quenched by saturated aqueous NH$_4$Cl at 0 °C and the product were extracted with chloroform. The organic layer was washed with water and dried over MgSO$_4$. After filtration of the drying agent and the solvent was removed under vacuum, the mixture was subsequently reduced without further purification. To the mixture of **S2** and trifluoroacetic acid (1.02 mL, 13.3

mmol) in chloroform (10 mL) was added triethylsilane (1.44 mL, 13.3 mmol) at 0 °C. The mixture was stirred for 10 h at room temperature. The reaction was quenched by water and the products were extracted with chloroform. The organic layer was washed with water and dried over MgSO$_4$. After filtlation of the drying agent, the solvent was removed under vacuum. The residues were purified by column chromatography on silica gel with hexane to give **3e** (2.58 g, 62% in two steps).

R_f = 0.56 (hexane : EtOAc = 9:1); mp 128.2–128.5 °C; IR (KBr) ν = 3052 (w), 2895 (w), 1560 (w), 1434 (s), 1400 (m), 1157 (m), 1107 (m), 837 (s), 759 (s), 722 (s) cm^{-1}; ^{1}H NMR: (400 MHz, CDCl$_3$) 7.69–7.67 (m, 2H, 5-H), 7.50 (dd, J = 8.0 Hz, 1.2 Hz, 1H), 7.26–7.11 (m, 6H), 6.02 (s, 1H, 1-H); ^{13}C NMR (100 MHz, CDCl$_3$) 148.7 (s), 140.2 (s, C-7), 137.2 (s), 135.8 (s), 135.6 (s), 134.4 (d, C-5), 130.0 (d), 129.2 (d), 128.8 (d, C-4), 128.1 (d), 122.2 (d, C-3), 116.2 (s, C-6), 51.0 (d, C-1); MS (EI, 70 eV) m/z 474 ([M+8]$^+$, 1), 472 ([M+6]$^+$, 8), 470 ([M+4]$^+$, 22), 468 ([M+2]$^+$, 24), 466 (M$^+$, 9), 391 (45), 389 (100), 387 (61); HRMS (EI, 70 eV) Calculated (C$_{19}$H$_{10}$Br$_2$Cl$_2$): 465.8526 (M$^+$), Found: 465.8527.

5-Bromo-9-(2,6-dichlorophenyl)-9*H*-fluorene-4-carbaldehyde 4e
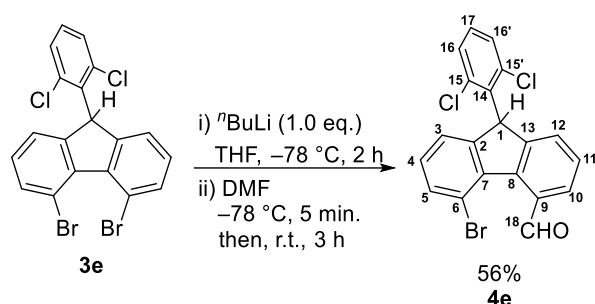
Under nitrogen atmosphere, ^{n}BuLi (1.6 M in hexane, 3.4 mL, 5.42 mmol) was added to a solution of **3e** (2.40 g, 5.42 mmol) in freshly dried THF (25 mL) at –78 °C. After stirred for 2 h at the temperature, anhydrous DMF (10 mL) was added to the reaction mixture. The reaction mixture was stirred for 5 min at –78 °C and was allowed to gradually warm to room temperature for 3 h. The reaction was quenched by saturated aqueous NH$_4$Cl at 0 °C. After the mixture was stirred for 30 min at 0 °C, the products were extracted with chloroform. The organic layer was washed with water and dried over MgSO$_4$. After filtration of the drying agent, the solvent was removed under vacuum. The residues were purified by column chromatography on silica gel with hexane and ethyl acetate (95:5) to give **4e** as a colorless solid (1.20 g, 56%).

R_f = 0.33 (hexane EtOAc = 9:1); mp 189.0–190.0 °C; IR (KBr) ν = 3068 (w), 2869 (w), 1686 (s), 1576 (m), 1557 (m), 1434 (s), 1384 (m), 1234 (m), 1180 (m), 1088 (m), 845 (m), 775 (s), 764 (s), 719 (m) cm^{-1}; ^{1}H NMR (400 MHz, CDCl$_3$) 10.99 (s, 1H, 18-H), 7.87 (d, J = 7.6 Hz, 1H, 10-H), 7.66–7.61 (m, 1H), 7.53 (dd, J = 8.4 Hz, 1.2 Hz, 1H), 7.44 (t, J = 7.6 Hz, 1H, 11-H), 7.39–7.36 (m, 1H, 12-H), 7.24–7.20 (m, 3H), 7.13 (dd, J = 8.0 Hz, 1.2 Hz, 1H), 6.06 (s, 1H, 1-H); ^{13}C NMR (100 MHz, CDCl$_3$) 191.6 (d, C-18), 149.0 (s), 146.7 (s, C-13), 140.8 (s, C-8), 140.0 (s), 137.3 (s), 135.6 (s), 135.0 (s), 133.3 (d), 132.4 (s, C-9), 130.0 (d), 129.5 (d), 129.4 (d), 128.25 (d), 128.16 (d, C-11), 127.5 (d, C-10, C-12, two signals were overlapped.), 123.1 (d), 117.6 (s), 51.0 (d, C-1); MS (EI, 70 eV) m/z 420 ([M+4]$^+$, 1), 418 ([M+2]$^+$, 3), 416 (M$^+$, 2), 339 (68), 337 (100); HRMS: (EI, 70 eV) Calculated (C$_{20}$H$_{11}$BrCl$_2$O) 415.9370 (M$^+$): Found: 415.9372.

9-(2,6-Dichlorophenyl)-5-((trimethylsilyl)ethynyl)-9*H*-fluorene-4-carbaldehyde 5e
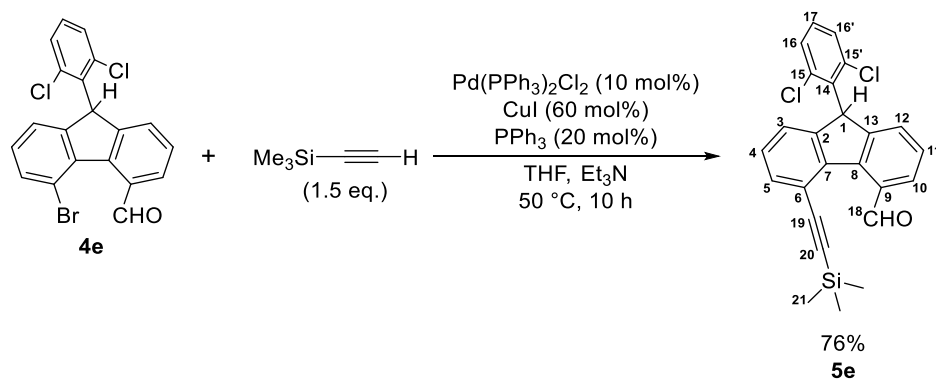
Under nitrogen atmosphere, PdCl₂(PPh₃)₂ (0.195 g, 0.278 mmol) was added to a mixture of **4e** (1.16 g, 2.78 mmol), CuI (0.320 g, 1.67 mmol) and PPh₃ (0.150 g, 0.56 mmol) in freshly dried THF (40 mL) and anhydrous Et₃N (20 mL) at room temperature. The mixture was heated to 50 °C and stirred for 10 h at the temperature. The reaction was quenched by saturated aqueous NH₄Cl at 0 °C and the products were extracted with chloroform. The organic layer was washed with water and dried over MgSO₄. After filtration of the drying agent, the solvent was removed under vacuum. The residues were purified by column chromatography on silica gel with hexane and ethyl acetate (95:5) to give **5e** as a colorless solid (0.914 g, 76%).

R_f = 0.47 (hexane : EtOAc = 9:1); mp 149.0–150.0 °C; IR (KBr) ν = 3058 (w), 2952 (w), 2885 (w), 2145 (m), 1685 (s), 1434 (m), 1388 (m), 1247 (m), 1232 (m), 991 (m), 862 (s), 843 (s), 763 (s), 724 (m), 655 (m) cm⁻¹; ¹H NMR (400 MHz, CDCl₃) 11.32 (s, 1H, 18-H), 7.94 (dd, *J* = 7.4 Hz, 1.4 Hz, 1H, 10-H), 7.64–7.61 (m, 1H, 5-H), 7.52 (dd, *J* = 8.0 Hz, 1.2 Hz, 1H, 16′-H), 7.44–7.40 (m, 1H, 11-H), 7.39–7.37 (m, 1H, 12-H), 7.30 (t, *J* = 7.4 Hz, 1H, 4-H), 7.24–7.19 (m, 2H, 3-H, 17-H), 7.12 (dd, *J* = 8.0 Hz, 1.6 Hz, 1H, 16-H), 5.99 (s, 1H, 1-H), 0,32 (s, 9H, 21-H); ¹³C NMR (100 MHz, CDCl₃) 192.0 (d, C-18), 147.0 (s, C-2), 146.8 (s, C-13), 141.7 (s, C-8), 140.4 (s, C-7), 137.4 (s, C-15′), 135.6 (s, C-15), 135.2 (s, C-14), 134.4 (d, C-5), 132.6 (s, C-9), 130.0 (d, C-16), 129.2 (d, C-17), 128.2 (d, C-16′), 127.9 (d, C-4), 127.8 (d, C-11), 127.7 (d, C-12), 127.0 (d, C-10), 124.3 (d, C-3), 119.1 (s, C-6), 104.9 (s, C-19), 99.4 (s. C-20), 50.4 (d, C-1), –0.52 (q, C-21); MS (EI, 70 eV) *m/z* 436 ([M+2]⁺, 3), 434 (M⁺, 5), 421 (83), 419 (100); HRMS (EI, 70 eV) Calculated (C₂₅H₂₀Cl₂OSi): 434.0660 (M⁺), Found: 434.0656.

## 4-(2,6-Dichlorophenyl)cyclohepta[*def*]fluoren-8(4*H*)-one 6e
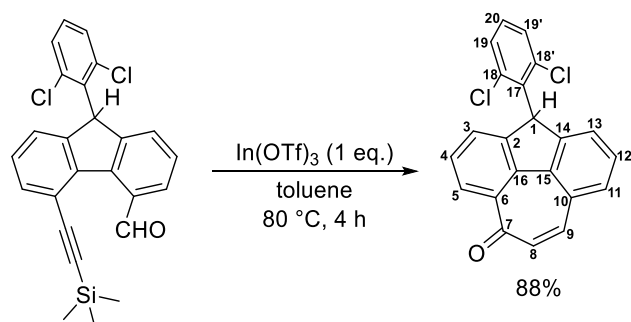
Under nitrogen atmosphere, In(OTf)₃ (1.14 g, 2.03 mmol) was added to a solution of **5e** (0.88 g, 2.03 mmol) in toluene (35 mL) at room temperature. The mixture was heated to 80 °C and stirred for 4 h at the temperature. The reaction was quenched by aqueous HCl (1 M) at 0 °C and the products were extracted with chloroform. The organic layer was washed with water and dried over MgSO₄. After filtration of the drying agent, the solvent was removed under vacuum. The residues were purified by column chromatography on silica gel with hexane and ethyl acetate (95:5) to give **6e** as a colorless solid (0.65 g, 88%).

R_f = 0.22 (hexane : EtOAc = 9:1); mp 205.0–206.0 °C; IR (KBr) ν = 3062 (w), 3021 (w), 2895 (w), 1624 (s), 1586 (s), 1435

(m), 1335 (m), 849 (m), 764 (m), 737 (s) cm^{-1}; ^{1}H NMR (400 MHz, CDCl$_3$) 8.48 (d, J = 7.2 Hz, 1H, 5-H), 7.65–7.50 (m, 6H), 7.44 (d, J = 7.2 Hz, 1H, 13-H), 7.23 (t, J = 8.0 Hz, 1H, 20-H), 7.12 (d, J = 8.0 Hz, 1H, 19-H), 6.96 (d, J = 12.8 Hz, 1H, 8-H), 6.17 (s, 1H, 1-H); ^{13}C NMR (100 MHz, CDCl$_3$) 187.3 (s, C-7), 146.5 (s), 145.9 (s), 140.75 (s), 140.66 (s), 140.3 (d), 137.4 (s, C-18′), 135.6 (s, C-18), 135.2 (s, C-17), 133.4 (s), 133.3 (d, C-8), 131.3 (s), 130.2 (d), 129.9 (d, C-19), 129.2 (d, C-20), 128.6 (d), 128.4 (d), 128.3 (d, two signals were overlapped.), 127.5 (d), 125.0 (d, C-13), 50.2 (d, C-1); MS (EI, 70 eV) m/z 366 ([M+4]$^+$, 12), 364 ([M+2]$^+$, 67), 362 (M$^+$, 100); HRMS (EI, 70 eV) Calculated (C$_{22}$H$_{12}$Cl$_2$O): 362.0265 (M$^+$), Found: 362.0263.

10-Mesityl-4-(2,6-dichlorophenyl)cyclohepta[*def*]fluoren-8(4*H*)-one 8e

6e

7e
^{1}H NMR observation

67%
(2 steps)
8e
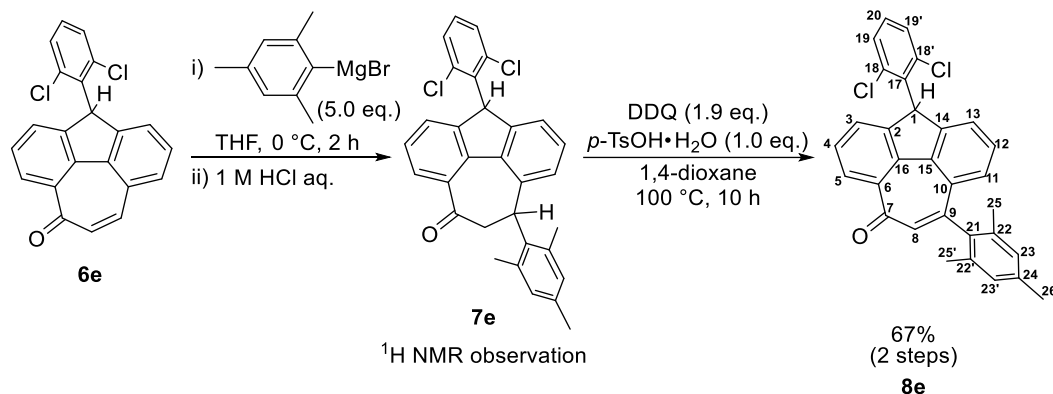
The Grignard reagent was prepared by the reaction of magnesium turnings (0.243 g, 10 mmol) and 2-bromomesitylene (1.27 mL, 8.46 mmol) in THF (10 mL) containing a small amount of 1,2-dibromoethane (0.1 mL) as the initiator. The mixture was refluxed for 1 h to give a solution of mesityl magnesium bromide in THF. Under nitrogen atmosphere, a solution of mesityl magnesium bromide in THF was added to a solution of **6e** (0.615 g, 1.69 mmol) in THF (10 mL) at 0 °C and stirred for 2 h at the temperature. The reaction was quenched by aqueous HCl (1 M) at 0 °C and the products were extracted with chloroform. The organic layer was washed with water and dried over MgSO$_4$. After filtration of the drying agent, the solvent was removed under vacuum. The residues were purified by column chromatography on silica gel with hexane and ethyl acetate (95:5) to give **7e** as colorless solids of diastereo mixture (*isomer A/B* = 1:1). After the confirmation of the products by ^{1}H NMR measurement, the diastereo mixture was subsequently oxidized without further purification. To a mixture of **7e** and 2,3-dichloro-5,6-dicyano-*p*-benzoquinone (DDQ) (0.768 g, 3.38 mmol) in 1,4-dioxane (10 mL) was added *p*-toluenesulfonic acid monohydrate (0.320 g, 1.69 mmol) at room temperature. The mixture was heated to 100 °C and stirred for 10 h at the temperature. After cooling to room temperature, the reaction was quenched by water and the products were extracted with chloroform. The organic layer was washed with water and dried over MgSO$_4$. After filtration of the drying agent, the solvent was removed under vacuum. The residues were purified by column chromatography on silica gel with hexane and ethyl acetate (90:10) to give **8e** (0.548 g, 67% in two steps).

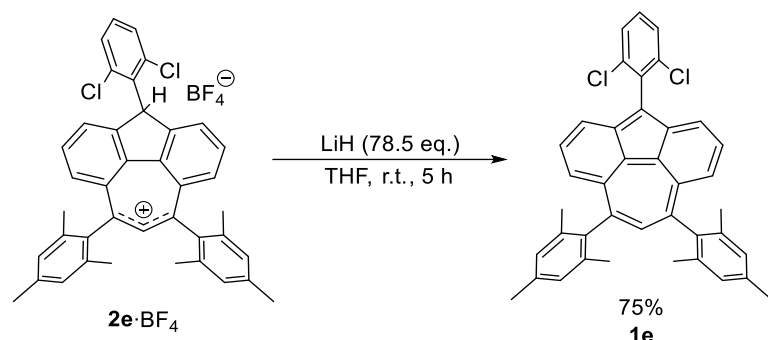### 10-Mesityl-4-(2,6-dichlororphenyl)-9,10-dihydrocyclohepta[*def*]fluoren-8(4*H*)-one 7e

^{1}H NMR (400 MHz, CDCl$_3$) 8.00 (t, J = 8.0 Hz, 2H), 7.55–7.52 (m , 2H), 7.48–7.46 (m, 1H), 7.43–7.35 (m, 3H), 7.23–7.10 (m, 7H), 6.95 (s, 2H), 6.92 (s, 2H), 6.81–6.71 (m, 3H), 6.14 (s, 1H), 6.02 (s, 1H), 5.02 (d, J = 12.0 Hz, 1H), 5.01 (d, J = 12.4 Hz, 1H), 3.96 (t, J = 12.6 Hz, 1H), 3.83 (t, J = 12.4 Hz, 1H), 3.07 (d, J = 12.4 Hz, 1H), 3.02 (d, J = 12.4 Hz, 1H), 2.34–2.33 (m, 12H), 2.21 (s, 6H).

10-Mesityl-4-(2,6-dichlororphenyl)cyclohepta[*def*]fluoren-8(4*H*)-one 8e

R_f = 0.36 (hexane : EtOAc = 9:1); mp 177.0–178.0 °C; IR (KBr) ν = 3068 (w), 2974 (w), 2916 (w), 2858 (w), 1615 (s), 1589 (s), 1559 (m), 1433 (s), 1331 (s), 851 (m), 788 (m), 768 (m), 739 (s) cm^{-1}; ^{1}H NMR (400 MHz, CDCl$_3$) 8.52–8.50 (m, 1H, 5-H), 7.65 (t, J = 7.2 Hz, 1H, 4-H), 7.63–7.61 (m, 1H, 3-H), 7.56 (dd, J = 8.2 Hz, 1.4 Hz, 1H, 19′-H), 7.42–7.40 (m, 1H, 13-H), 7.33 (t, J = 7.6 Hz, 1H, 12-H), 7.23 (t, J = 8.0 Hz, 1H, 20-H), 7.15–7.10 (m, 2H, 11-H, 19-H), 7.00 (s, 2H, 23-H, 23′-H), 6.94 (s, 1H, 8-H), 6.23 (s, 1H, 1-H), 2.38 (s, 3H, 26-H), 2.08 (s, 3H, 25′-H), 2.06 (s, 3H, 25-H); ^{13}C NMR (100 MHz, CDCl$_3$) 187.2 (s, C-7), 150.5 (s, C-9), 146.5 (s, C-2), 146.4 (s, C-14), 141.1 (s, C-16), 140.7 (s, C-15), 138.5 (s, C-21), 137.4 (s, C-18′), 137.2 (s, C-24), 135.7 (s, C-18), 135.4 (s, C-17), 135.25 (s), 135.15 (s), 135.11 (d, C-8), 133.3 (s, C-6), 131.7 (s, C-10), 130.0 (d, C-19), 129.2 (d, C-20), 128.6 (d, C-3, C-11, two signals were overlapped.), 128.44 (d, C-12), 128.36 (d, C-23, C-23′, two signals were overlapped.), 128.3 (d, C-19′), 128.0 (d, C-5), 127.6 (d, C-4), 125.0 (d, C-13), 50.1 (d, C-1), 21.1 (q, C-26), 19.94 (q), 19.93 (q); MS (EI, 70 eV) m/z 484 ([M+4]$^+$, 15), 482 ([M+2]$^+$, 72), 480 (M$^+$, 100), 465 (14); HRMS (EI, 70 eV) Calculated (C$_{31}$H$_{22}$Cl$_2$O) 480.1048 (M$^+$), Found: 480.1045.

8,10-Dimesityl-4-(2,6-dichlorophenyl)-4,8-dihydrocyclohepta[*def*]fluoren-8-ylium tetrafluoroborate 2e·BF$_4$
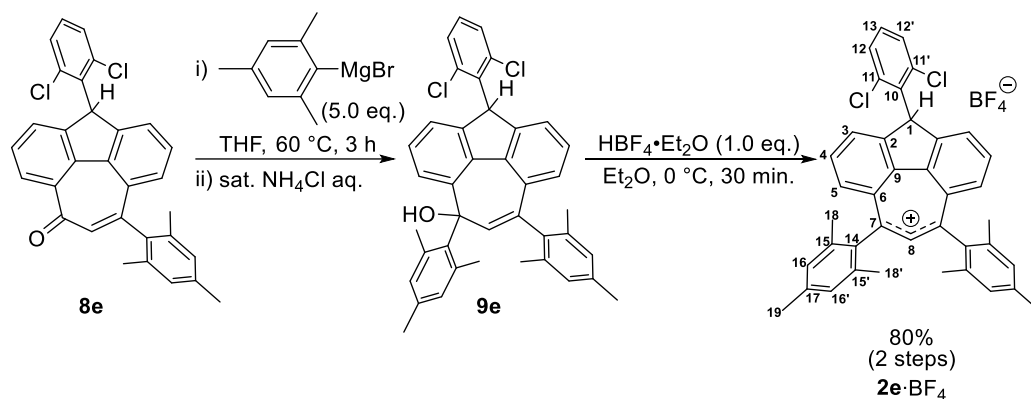
The Grignard reagent was prepared by the reaction of magnesium turnings (0.150 g, 6.17 mmol) and 2-bromomesitylene (0.77 mL, 5.16 mol) in THF (5 mL) containing a small amount of 1,2-dibromoethane (0.1 mL) as the initiator. The mixture was refluxed for 1 h to give a solution of mesityl magnesium bromide in THF. Under nitrogen atmosphere, a solution of mesityl magnesium bromide in THF was added to a solution of **8e** (0.497 g, 1.03 mmol) in THF (10 mL) at 0 °C and stirred for 3 h at 60 °C. The reaction was quenched by saturated aqueous NH$_4$Cl at 0 °C and the products were extracted with ethyl acetate. The organic layer was washed with water and dried over Na$_2$SO$_4$. After filtration of the drying agent, the solvent was removed under vacuum, the mixture including **9e** was subsequently treated by acid without further purification. A procedure from the literature[51] was modified as follows: To a mixture of **9e** in diethyl ether (20 mL) was added HBF$_4$·Et$_2$O (0.15 mL, 1.10 mmol). The reaction mixture was stirred at 0 °C for 2 h and allowed to warm to room temperature. After the reaction, the solvent was removed under vacuum and the residues were washed by dried hexane several times, to give **2e**·BF$_4$ (0.554 g, 80% in two steps).

mp >300 °C; IR (KBr) ν = 3068 (w), 2922 (w), 1608 (m), 1554 (m), 1491 (s), 1460 (s), 1435 (m), 1406 (s), 1084 (s), 1062 (s), 848 (m) cm^{-1}; ^{1}H NMR (400 MHz, CDCl$_3$) 8.50 (s, 1H, 8-H), 8.47 (d, J = 7.2 Hz, 2H, 3-H), 8.38 (t, J = 7.8 Hz, 2H, 4-H), 8.23 (d, J = 8.4 Hz, 2H, 5-H), 7.71 (d, J = 8.0 Hz, 1H, 12′-H), 7.40 (t, J = 8.2 Hz, 1H, 13-H), 7.20 (d, J = 8.0 Hz, 1H, 12-H), 7.13 (s, 4H, 16-H, 16′-H), 6.86 (s, 1H, 1-H), 2.44 (s, 6H, 19-H), 1.95 (s, 6H, 18′-H), 1.94 (s, 6H, 18-H); ^{13}C NMR (100 MHz, CDCl$_3$) 178.5 (s, C-7), 149.8 (s, C-2), 147.9 (s, C-9), 140.5 (s, C-17), 140.3 (d, C-8), 137.9 (s, C-11′), 137.6 (s, C-14), 136.4 (s, C-6), 134.9 (s, C-11), 134.6 (d, C-4), 134.2 (s, C-15′), 134.0 (d, C-3), 133.7 (s ,C-15), 132.4 (s, C-10), 132.3 (d, C-5), 130.8 (d ,C-

13), 130.2 (d, C-12), 129.3 (d), 129.1 (d, two signals were overlapped.), 50.0 (d, C-1), 21.1 (q, C-19), 20.3 (q), 20.2 (q); ^{11}B{^{1}H} NMR (127 MHz, CDCl$_3$, BF$_3$·Et$_2$O in CDCl$_3$ as an external standard) –1.25 ppm; ^{19}F NMR (372 MHz, CDCl$_3$, BF$_3$·Et$_2$O in CDCl$_3$ as an external standard) –154.38 ppm; MS (EI, 70 eV) m/z 587 ([M+4]$^+$, 16), 585 ([M+2]$^+$, 71), 583 (M$^+$, 100) ; HRMS (EI, 70 eV) Calculated (C$_{40}$H$_{33}$Cl$_2$$^+$): 583.1954 (M$^+$). Found: 583.1957.

8,10-Dimesityl-4-(2,6-dichlorophenyl)cyclohepta[*def*]fluorene 1e

In a nitrogen-filled glove box, LiH (94.3 mg, 11.9 mmol) was added to a solution of **2e·BF$_4$** (0.101 g, 0.14 mmol) in freshly dried THF (12 mL). The mixture was stirred at room temperature for 5 h. After insoluble materials were removed by filtration, the solvent was removed under vacuum. The residues were dissolved in hexane and insoluble materials were removed by filtration. The filtrate was evaporated to give **1e** (65.9 mg, 75%). The recrystallization of **1e** from a tetrahydrofuran–hexane solution in a glove box afforded a single crystal suitable for the X-ray crystallographic analysis.

mp 269.0–270.0 °C; IR (KBr) ν = 3062 (w), 2916 (w), 1634 (w), 1609 (m), 1539 (m), 1434 (m), 1298 (w), 1066 (s), 918 (m), 839 (w), 800 (m), 762 (s), 726 (w), 604 (w), 541 (m), 462 (m) cm^{-1}; MS (EI$^+$, 70 eV) m/z 586 ([M+4]$^+$, 31), 584 ([M+2]$^+$, 95), 582 (M$^+$, 100); HRMS (EI$^+$, 70 eV) Calculated (C$_{40}$H$_{32}$Cl$_2$): 582.1881 (M$^+$), Found: 582.1894 (M$^+$).

Supporting Information

Examinations of intramolecular cyclization catalyzed by Lewis acids

Under nitrogen atmosphere, Lewis acid was added to a solution of **S2**[67] (0.14 g, 0.5 mmol) in toluene (1 mL) at room temperature. The mixture was heated to 80 °C and stirred for 24 h at the temperature. The reaction was quenched by aqueous HCl (1 M) at 0 °C and the products were extracted with chloroform. The organic layer was washed with water and dried over MgSO$_4$. After filtration of the drying agent, the solvent was removed under vacuum. The residues were purified by column chromatography on silica gel with hexane and ethyl acetate (95:5) to give **S3**[67] as a colorless solid.
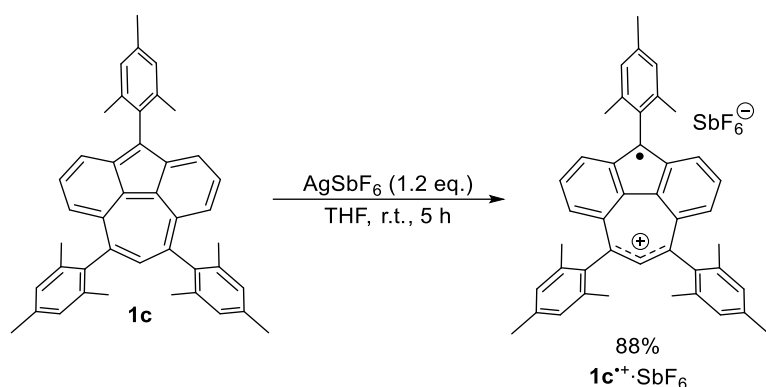
Table S1. Summary for intramolecular cyclization of **S2** catalyzed by Lewis acids.

entry	Lewis acid	X / mol%	yield of **S3** / %
1	$AlCl_3$	10	0
2	$InCl_3$	10	29
3	$InBr_3$	10	33
4	InI_3	10	2
5	$In(OTf)_3$	10	49
6	$In(OTf)_3$	30	85

Figure S1. Cyclic voltammograms of **1c–e** (V vs. Fc/Fc$^+$, in 0.1M nBu$_4$NClO$_4$/THF, scan rate = 100 mV/s, room temperature).

Table S2. Summary for the redox potentials for **1c–e.**

compound	$E_2^{ox, pa}$ / V	E_1^{ox} / V	E_1^{red} / V	$E_2^{red, pc}$ / V	$\Delta_{redox}E_1$ / V
1c	+0.76	–0.17	–1.31	–2.04	1.14
1d	+0.72	–0.15	–1.29	–2.02	1.14
1e	+0.91	–0.03	–1.18	–2.01	1.15

One-electron oxidation of 1c with AgSbF$_6$

In a nitrogen-filled glove box, AgSbF$_6$ (19.4 mg, 0.056 mmol) was added to a solution of **1c** (26.2 mg, 0.047 mmol) in freshly dried THF (4 mL). The mixture was stirred at room temperature for 5 h. After insoluble materials were removed by filtration, the solvent was removed under vacuum. The residues were dissolved in dichloromethane and insoluble materials were removed by filtration. The filtrate was evaporated to give radical cation **1c$^{•+}$·SbF$_6$** as black solid (32.8 mg, 88%). The recrystallization of radical cation of **1c$^{•+}$·SbF$_6$** from a dichloromethane–hexane solution in a glove box afforded a single crystal suitable for the X-ray crystallographic analysis.

mp 205.0–206.0 °C; IR: (KBr) ν = 3021 (w), 2922 (w), 2858 (w), 1655 (w), 1609 (w), 1542 (m), 1473 (w), 1451 (m), 1423 (w), 1400 (m), 1031 (w), 853 (w), 659 (s) cm^{-1}; MS (EI$^+$, 70 eV) m/z 556 (M$^+$, 93), 541 (8)**;** HRMS: (EI$^+$, 70 eV) Calculated (C$_{43}$H$_{40}$$^{•+}$) 556.3125 (M$^+$), Found: 556.3140 (M$^+$).
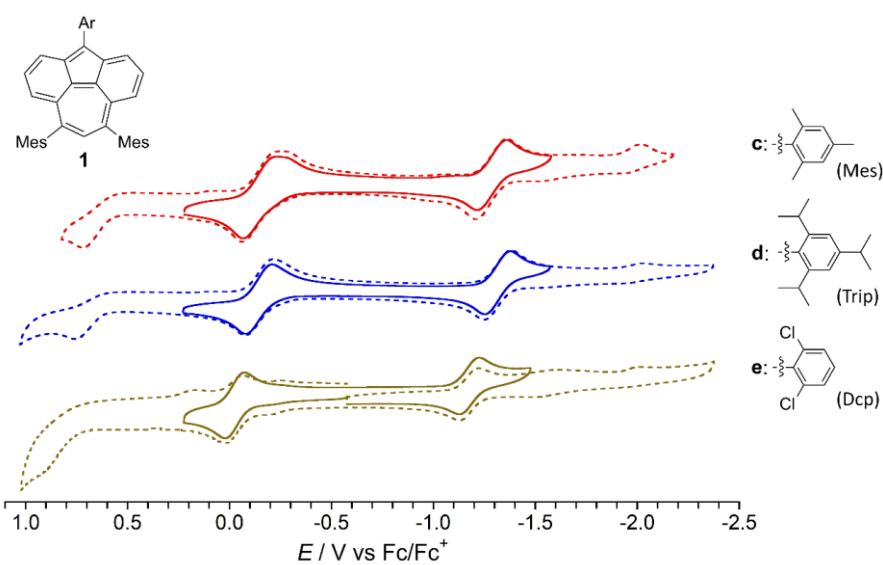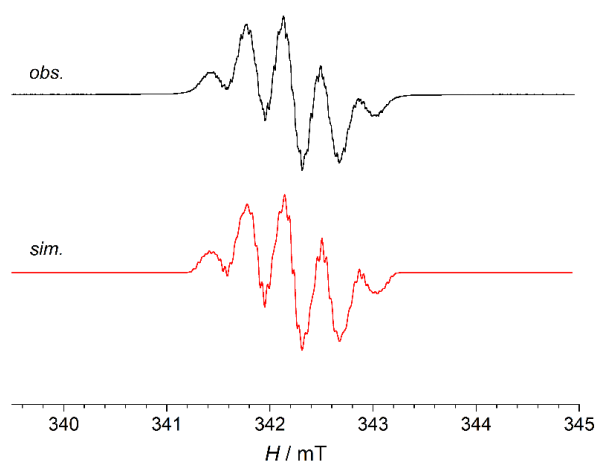
Figure S2. ESR spectrum of a CH$_2$Cl$_2$ solution of **1c$^{•+}$·SbF$_6$** at 295 K. 9.59252 GHz, g-value = 2.00260, Gain = 22500, sweep time = 3.4 min, modulation amplitude = 0.01 mT.
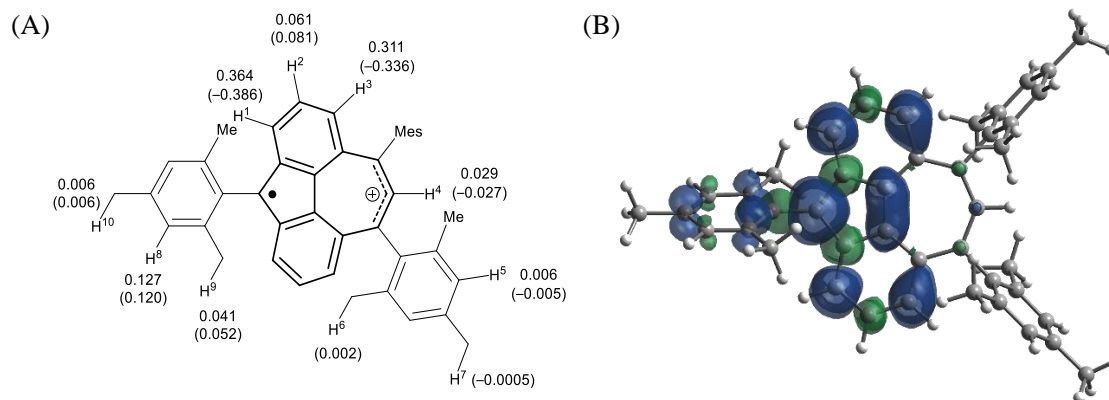
Figure S3. (A) Summary for hyper-fine coupling constants ($|A_H|$ /mT) for **1c**[•+]·SbF₆. The values in the parentheses were calculated by the UB3LYP/ESR-II//UB3LYP-D3(BJ)/6-311G* method. (B) Spin density map (the contour level of 0.001 / Å³) calculated by the UB3LYP-D3(BJ)/6-311G* method. Positive (blue) and negative (green) spin densities are shown.
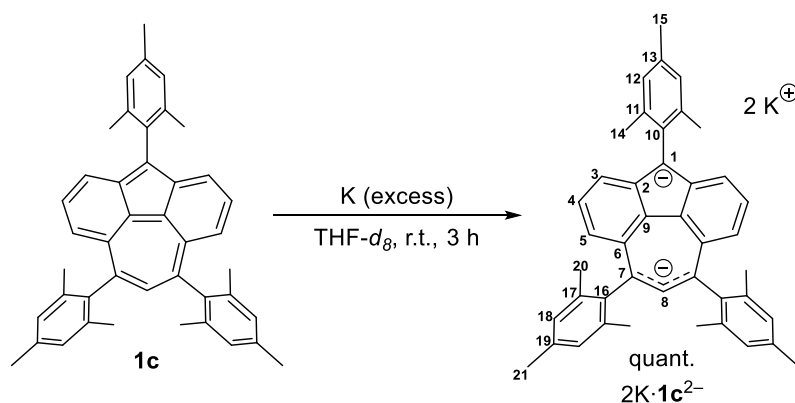
In a nitrogen-filled glove box, to a solution of **1c** (17 mg, 0.0310 mmol) in freshly dried THF-d_8 (0.4 mL) was added potassium metal (8.0 mg, 0.21 mmol) which was washed by hexane to remove mineral oil. After the reaction mixture was stirred for 3 h at room temperature, insoluble materials were removed by filtration to afford as a red solution of 2K·**1c**[2−]. According to the NMR monitoring, 2K·**1c**[2−] was generated quantitatively.

^{1}H NMR (600 MHz, THF-d_8) 6.61 (s, 2H, 12-H), 6.54 (s, 4H, 18-H), 5.06 (t, J = 7.5 Hz, 2H, 4-H), 4.79 (d, J = 7.8 Hz, 2H, 3-H), 3.26 (d, J = 7.2 Hz, 2H, 5-H), 2.94 (s, 1H, 8-H), 2.57 (s, 12H, 20-H) , 2.11 (s, 3H, 15-H) , 2.01 (s, 6H, 21-H) , 1.97 (s, 6H, 14-H); ^{13}C NMR (150 MHz, THF-d_8) 147.7 (s, C-6), 145.9 (s, C-16), 145.1 (d, C-8), 138.9 (s, C-17), 138.3 (s, C-10), 137.7 (s, C-11), 131.7 (s, C-13), 131.6 (s, C-19), 131.4 (s, C-2), 128.3 (d, C-18), 127.7 (d, C-12), 125.6 (s, C-9), 124.2 (d, C-4), 111.1 (d, C-3), 102.6 (d, C-5), 97.3 (s, C-7), 96.6 (s, C-1), 21.6 (q, C-14), 21.3 (q, C-20), 21.0 (q, C-15), 20.8 (q, C-21).

4,8,10-Trimesitylcyclohepta[*def*]fluorene 1c

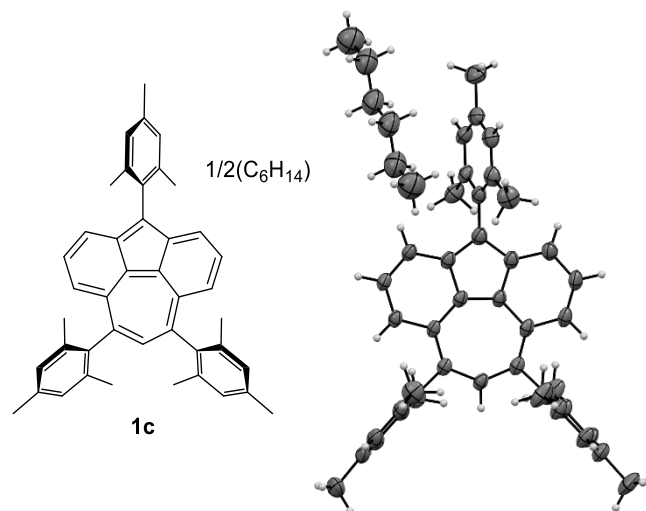**Figure S5.** ORTEP drawings of **1c** at the 50% probability level.

Empirical Formula	C$_{46}$H$_{47}$ (C$_{43}$H$_{40}$+1/2(C$_6$ H$_{14}$))	Space Group	*C2/c* (#15)
Formula Weight	599.83	*Z* value	8
Crystal Color, Habit	black, block	*D*$_{calc}$	1.142 g/cm^3
Crystal Dimensions	0.158 × 0.098 × 0.065 mm	*F*$_{000}$	2584.0
Crystal System	monoclinic	μ(CuK$_\alpha$)	0.478 mm^{-1}
Lattice Type	Centered on *C* faces	Temperature	123 K
Lattice Parameters	*a* = 31.0962(11) Å	Data/restraints/parameters	6941/0/425
	b = 7.51750(10) Å	Residuals: *R*1 (*I* > 2.00σ(*I*))	0.0867
	c = 32.6029(10) Å	Residuals: *wR*2 (*all data*)	0.2543
	β = 113.773(4) °	Goodness of Fit Indicator	1.073
	V =6974.8(4) Å^3		

8,10-Dimesityl-4-(2,4,6-triisopropylphenyl)cyclohepta[*def*]fluorene 1d
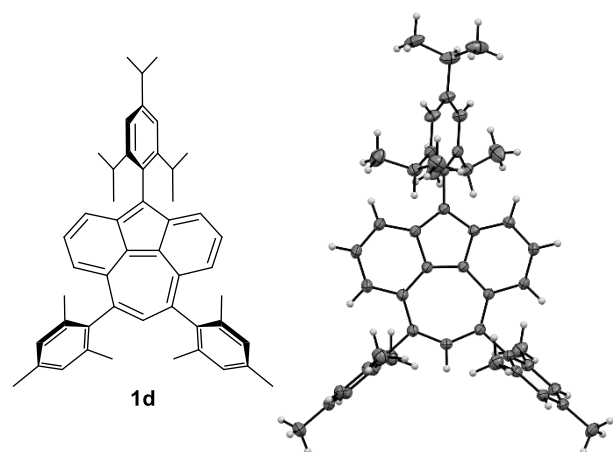
Figure S6. ORTEP drawings of **1d** at the 50% probability level.

Empirical Formula	C$_{49}$H$_{52}$	Space Group	P2$_1$/n (#14)
Formula Weight	640.90	Z value	4
Crystal Color, Habit	black, block	D$_{calc}$	1.116 g/cm^3
Crystal Dimensions	0.186 × 0.104 × 0.094 mm	F$_{000}$	1384.0
Crystal System	monoclinic	μ(CuK$_\alpha$)	0.465 mm^{-1}
Lattice Type	Primitive	Temperature	123 K
Lattice Parameters	a = 8.08290(10) Å	Data/restraints/parameters	7731/0/475
	b = 26.4830(3) Å	Residuals: R1 (I > 2.00σ(I))	0.0475
	c = 18.0574(2) Å	Residuals: wR2 (all data)	0.1225
	β = 99.2300(10) °	Goodness of Fit Indicator	1.026
	V =3815.31(8) Å^3		

8,10-Dimesityl-4-(2,6-dichlorophenyl)cyclohepta[*def*]fluorene 1e
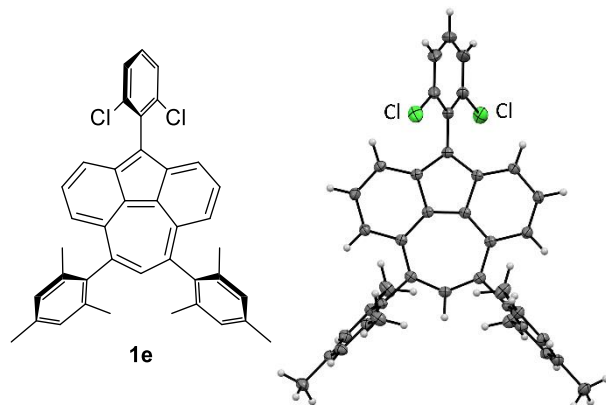
Figure S7. ORTEP drawings of **1e** at the 50% probability level.

Empirical Formula	C$_{40}$H$_{32}$Cl$_2$	Space Group	I2/a (#15)
Formula Weight	583.55	Z value	4
Crystal Color, Habit	black, block	D$_{calc}$	1.306 g/cm^3
Crystal Dimensions	0.169 × 0.144 × 0.116 mm	F$_{000}$	1224.0
Crystal System	monoclinic	μ(CuK$_\alpha$)	2.169 mm^{-1}
Lattice Type	Body centered	Temperature	123 K
Lattice Parameters	a = 12.8249(2) Å	Data/restraints/parameters	3019/0/195
	b = 17.2461(3) Å	Residuals: R1 (I > 2.00σ(I))	0.0363
	c = 13.4855(2) Å	Residuals: wR2 (all data)	0.0992
	β = 95.6800(10) °	Goodness of Fit Indicator	1.117
	V = 2968.07(8) Å^3		

4,8,10-Trimesityl-4,8-dihydrocyclohepta[*def*]fluoren-8-ylium tetrafluoroborate 2c·BF$_4$
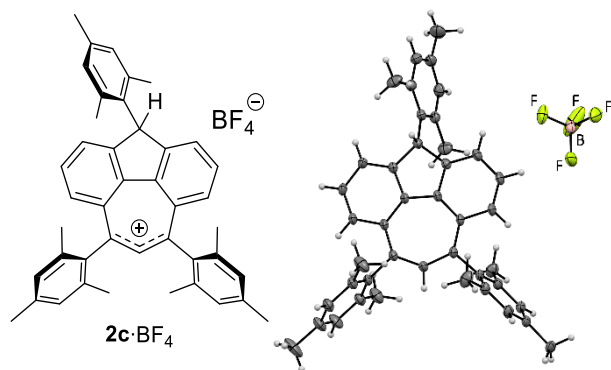
Figure S8. ORTEP drawings of **2c**·BF$_4$ at the 50% probability level.

Empirical Formula	C$_{43}$H$_{41}$BF$_4$	Space Group	P2$_1$/c (#14)
Formula Weight	644.57	Z value	4
Crystal Color, Habit	red, block	D$_{calc}$	1.226 g/cm^3
Crystal Dimensions	0.154 × 0.135 × 0.093 mm	F$_{000}$	1360.0
Crystal System	monomeric	μ(CuK$_\alpha$)	0.679 mm^{-1}
Lattice Type	Primitive	Temperature	123 K

Lattice Parameters	$a = 13.12580(10)$ Å	Data/restraints/parameters	7098/0/442
	$b = 17.3619(2)$ Å	Residuals: $R1$ ($I > 2.00\sigma(I)$)	0.0665
	$c = 15.5055(2)$ Å	Residuals: $wR2$ (all data)	0.1674
	$\beta = 98.9060(10)$ °	Goodness of Fit Indicator	1.056
	$V = 3490.93(7)$ Å^3		
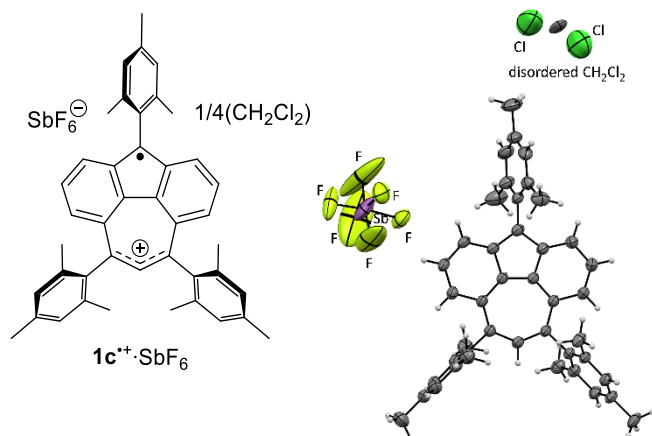
Figure S9. ORTEP drawings of **1c**•+·SbF$_6$ at the 50% probability level.

Empirical Formula	C$_{43.25}$H$_{40}$Cl$_{0.5}$F$_6$Sb	Space Group	$C2/c$ (#15)
	(C$_{43}$H$_{40}$+SbF$_6$+1/4(CCl$_2$))	Z value	8
	Due to the disorder of a CH$_2$Cl$_2$ molecule, the riding of hydrogen atoms failed.	D_{calc}	1.336 g/cm^3
		F_{000}	3304.0
		μ(CuK$_\alpha$)	6.184 mm^{-1}
Formula Weight	813.23	Temperature	123 K
Crystal Color, Habit	red, block	Data/restraints/parameters	8017/1/551
Crystal Dimensions	$0.163 \times 0.087 \times 0.063$ mm	Residuals: $R1$ ($I > 2.00\sigma(I)$)	0.0505
Crystal System	monoclinic	Residuals: $wR2$ (all data)	0.1486
Lattice Type	Centered on C faces	Goodness of Fit Indicator	1.059
Lattice Parameters	$a = 25.8138(8)$ Å		
	$b = 18.5685(6)$ Å		
	$c = 16.9257(4)$ Å		
	$\beta = 94.486(3)$ °		
	$V = 8088.0(4)$ Å^3		

Figure S10. ORTEP drawings of Na·**1d**•− at the 50% probability level.

Empirical	$C_{145}H_{192}N_2Na_2O_{11}$		Space Group	$P\,\text{-}1$ (#2)
Formula	$(2(C_{49}H_{52}+C_{20}H_{40}+C_4H_3N+Na)+$		Z value	1
	$(C_3H_2O))$		D_{calc}	1.116 g/cm^3
	Due to the disorder of a THF molecule, the perfect		F_{000}	1186.0
	atoms assignments for the molecule failed.		$\mu(\mathrm{CuK}_\alpha)$	0.589 mm^{-1}
Formula Weight	2184.97		Temperature	123 K
Crystal Color,	blue-green, block		Data/restraints/parameters	13172/0/818
Habit	$0.32 \times 0.276 \times 0.091$ mm		Residuals: $R1$ ($I > 2.00\sigma(I)$)	0.0879
	triclinic		Residuals: $wR2$ (all data)	0.2614
Crystal	Primitive		Goodness of Fit Indicator	1.035
Dimensions	$a = 12.8908(4)$ Å			
Crystal System	$b = 13.8879(4)$ Å			
Lattice Type	$c = 20.7783(4)$ Å			
Lattice	$\alpha = 73.757(2)$ °			
Parameters	$\beta = 84.208(2)$ °			
	$\gamma = 65.535(3)$ °			
	$V = 3250.25(17)$ Å^3			
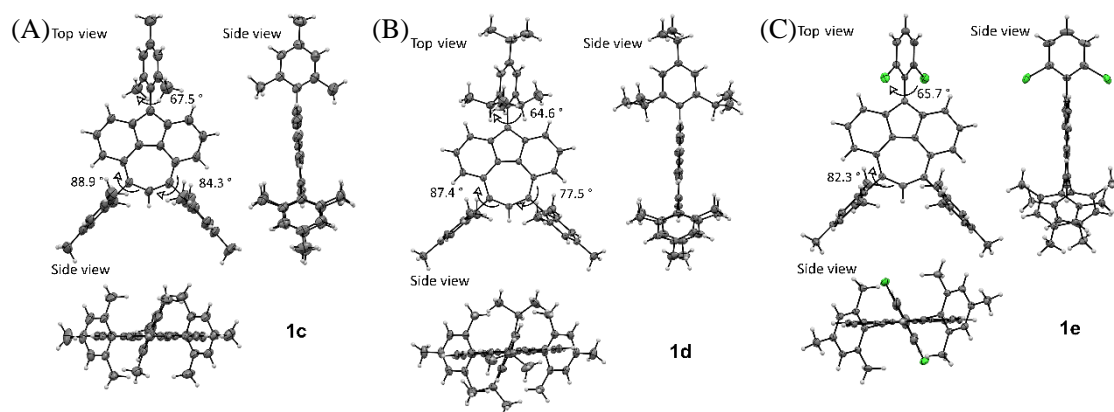
Figure S11. Comparisons of top and side views of **1c–e**. The thermal ellipsoids are set at the 50% probability level.
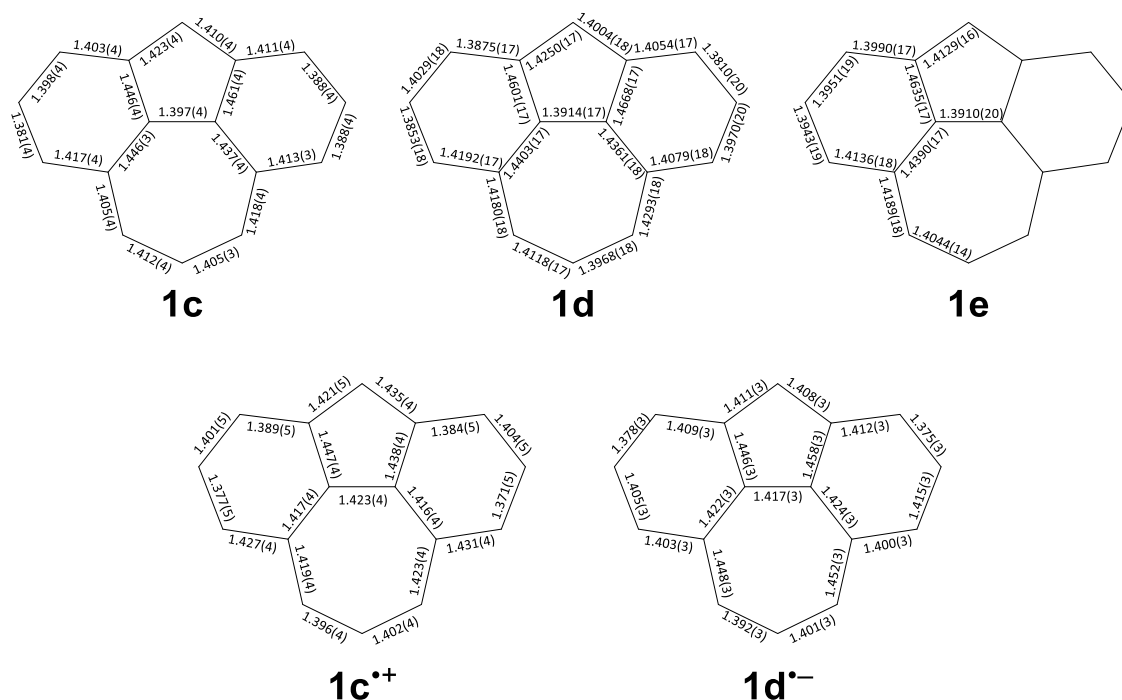
Figure S12. Summary for the observed bond lengths (/Å) for **1c–e**, **1c**$^{•+}$, and **1d**$^{•−}$.
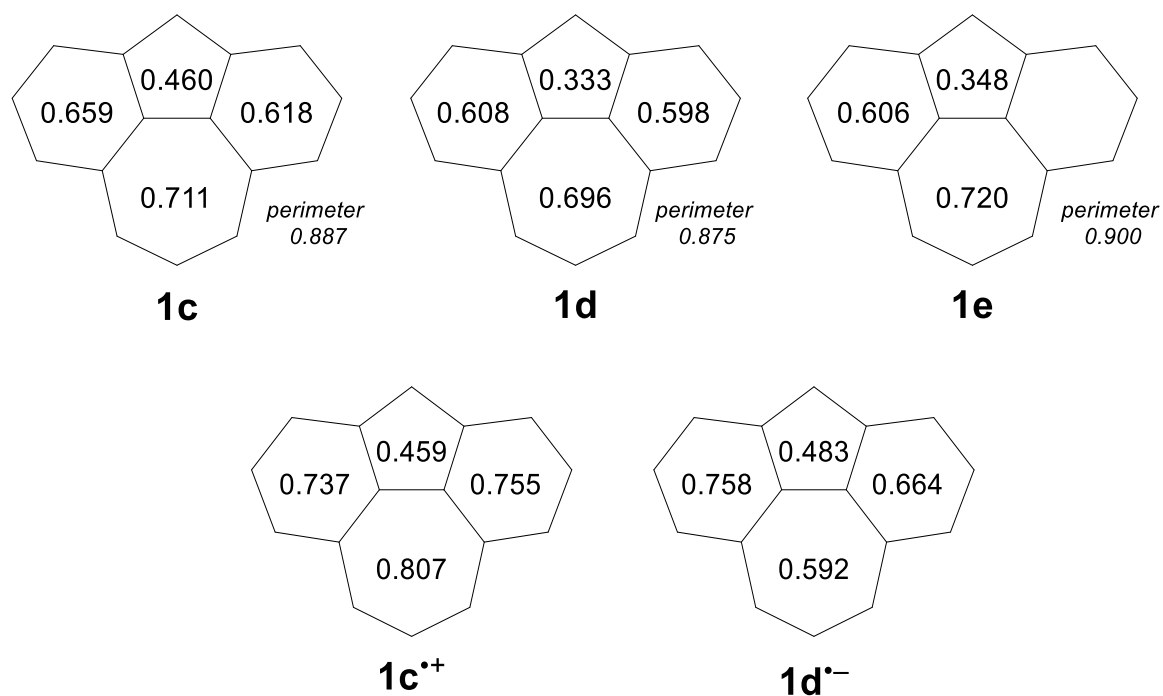
Figure S13. HOMA values calculated from the observed bond lengths for **1c–e**, **1c•+**, and **1d•−**.
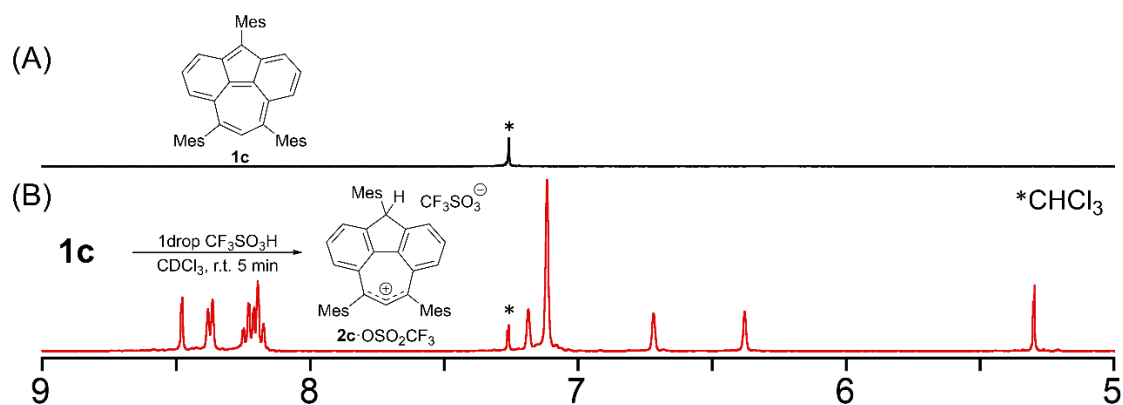
Figure S14. Partial ^{1}H NMR spectra of (A) **1c** and (B)**1c** with CF$_3$SO$_3$H in CDCl$_3$ (rt, 400 MHz). Due to the open-shell nature, no signal for **1c** except for solvent was observed at room temperature.
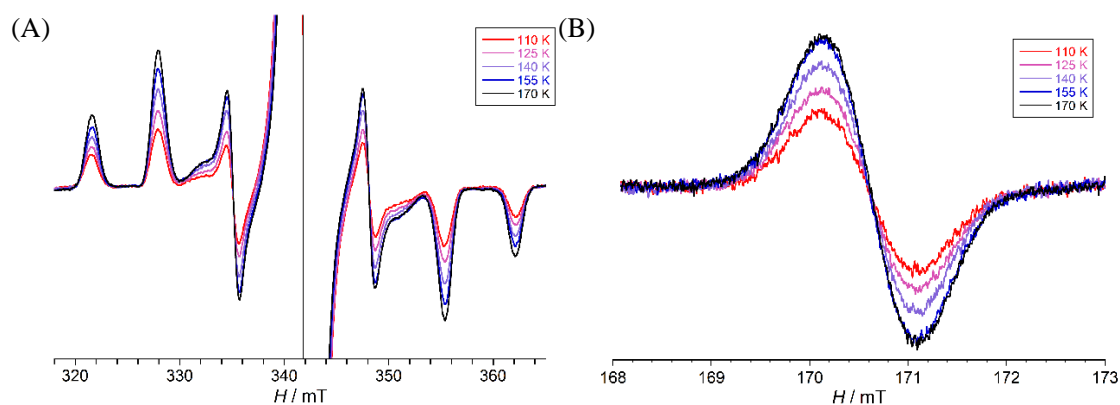
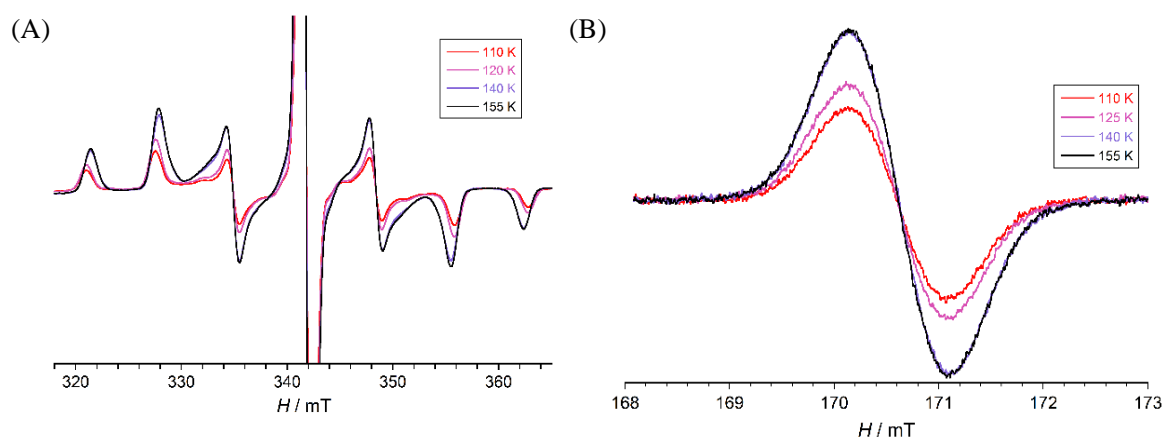**Figure S15.** ESR spectra of a glassy toluene sample of **1c** at 170–110 K. (A) Temperature-dependent ESR spectra for (A) $\Delta M_s = \pm 1$ and (B) $\Delta M_s = \pm 2$ half-field signals.
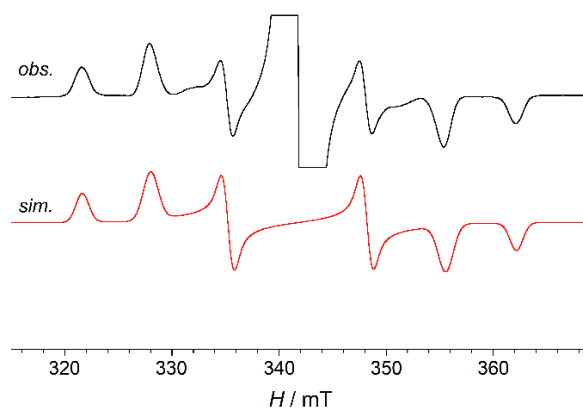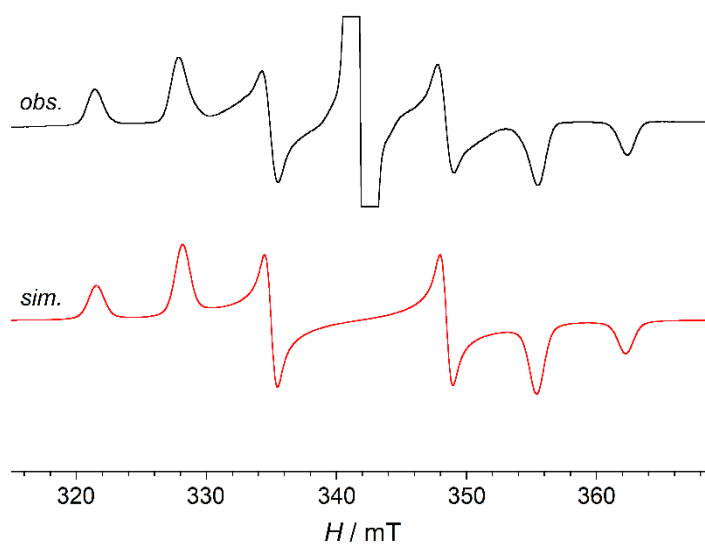

Figure S16. ESR spectrum of a glassy toluene sample of **1c** at 170 K (g-value = 2.0027). The microwave frequency used was 9.57856 GHz. The zero field splitting parameters were determined as $|D|$ = 20.3 mT = 0.0190 cm^{-1}, $|E|$ = 2.43 mT = 0.00227 cm^{-1} (line width parameters; x = 1.00 mT, y = 1.40 mT, z = 1.20 mT) by the spectral simulation.
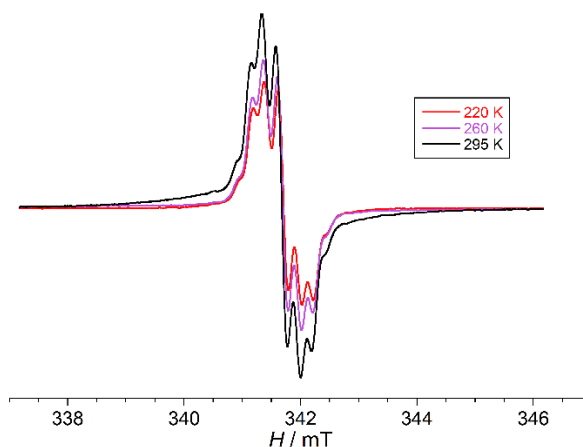
Figure S17. ESR spectra of a toluene solution of **1c** at 295–220 K. The microwave frequency used was 9.57728 GHz (at 295 K), g-value = 2.0027, Gain = 4480, sweep time = 2 min, modulation amplitude = 0.01 mT.

Figure S18. ESR spectra of a glassy toluene sample of **1d** at 155–110 K. (A) Temperature-dependent ESR spectra for (A) $\Delta M_s = \pm 1$ and (B) $\Delta M_s = \pm 2$ half-field signals.

Figure S19. ESR spectrum of a glassy toluene sample of **1d** at 155 K (*g*-value = 2.0025). The microwave frequency used was 9.57854 GHz. The zero field splitting parameters were determined as $|D|$ = 20.4 mT = 0.0190 cm^{-1}, $|E|$ = 2.30 mT = 0.00215 cm^{-1} (line width parameters; x = 0.70 mT, y = 1.10 mT, z = 1.10 mT) by the spectral simulation.
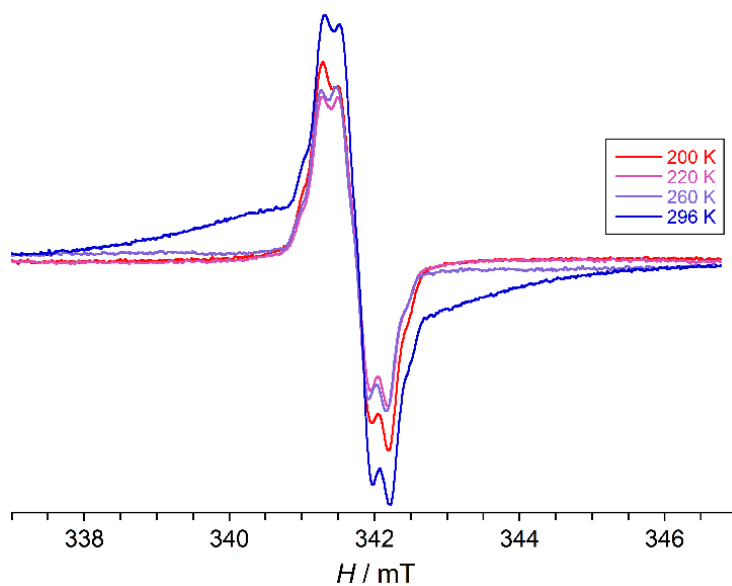
Figure S20. ESR spectra of a toluene solution of **1d** at 296–200 K. The microwave frequency used was 9.57880 GHz (at 296 K), *g*-value = 2.0025, Gain = 4480, sweep time = 2 min, modulation amplitude = 0.01 mT.
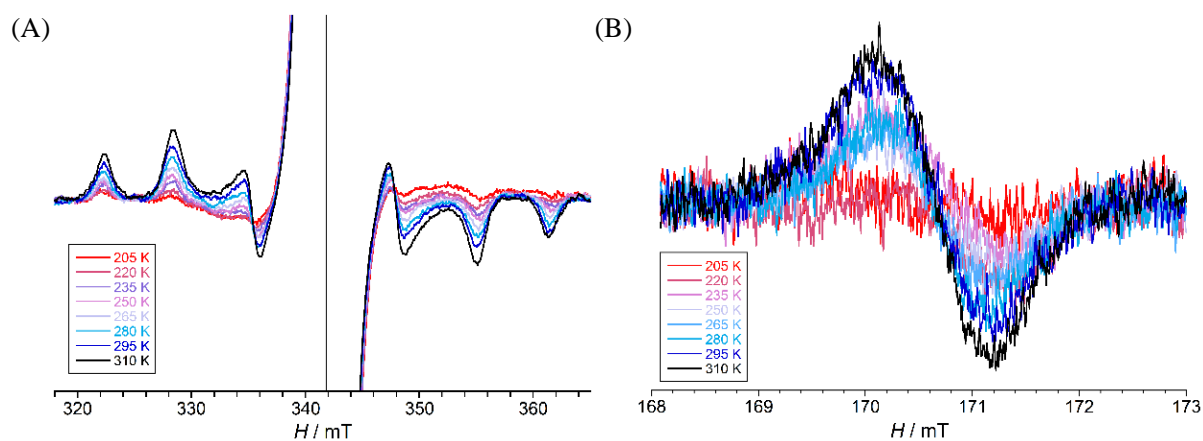

Figure S21. ESR spectra of a glassy *o*-terphenyl sample of **1e** at 310–205 K. (A) Temperature-dependent ESR spectra for (A) $\Delta M_s = \pm 1$ and (B) $\Delta M_s = \pm 2$ half-field signals.
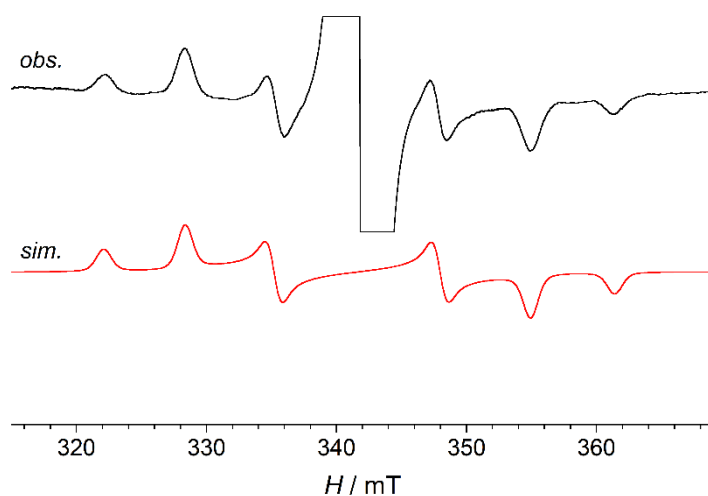
Figure S22. ESR spectrum of a glassy *o*-terphenyl sample of **1e** at 296 K (*g*-value = 2.0027). The microwave frequency used was 9.57854 GHz. The zero field splitting parameters were determined as |*D*| = 19.7 mT = 0.0184 cm^{-1}, |*E*| = 2.30 mT = 0.00215 cm^{-1} (line width parameters; *x* = 1.00 mT, *y* = 1.10 mT, *z* = 1.10 mT) by the spectral simulation.
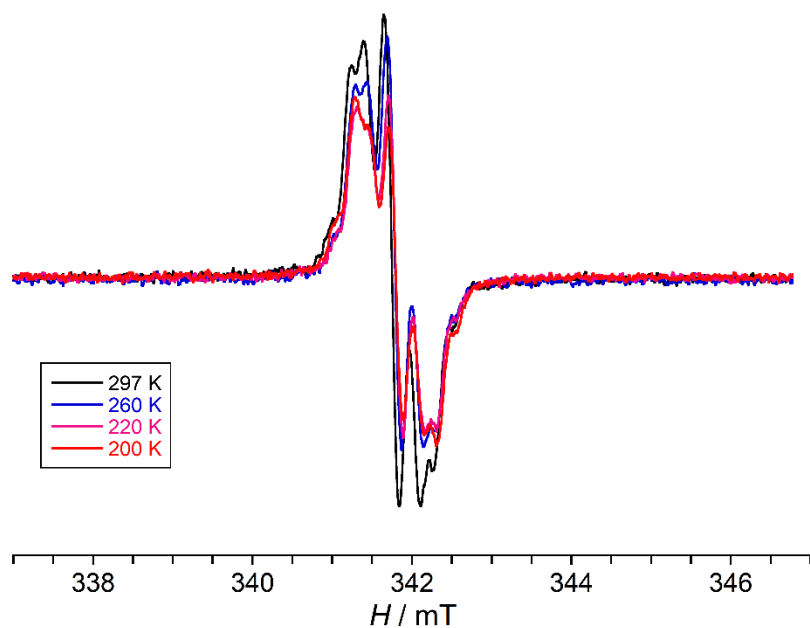

Figure S23. ESR spectra of a toluene solution of **1e** at 297–200 K. The microwave frequency used was 9.57912 GHz (at 297 K), *g*-value = 2.0027, Gain = 44800, sweep time = 2 min, modulation amplitude = 0.01 mT.
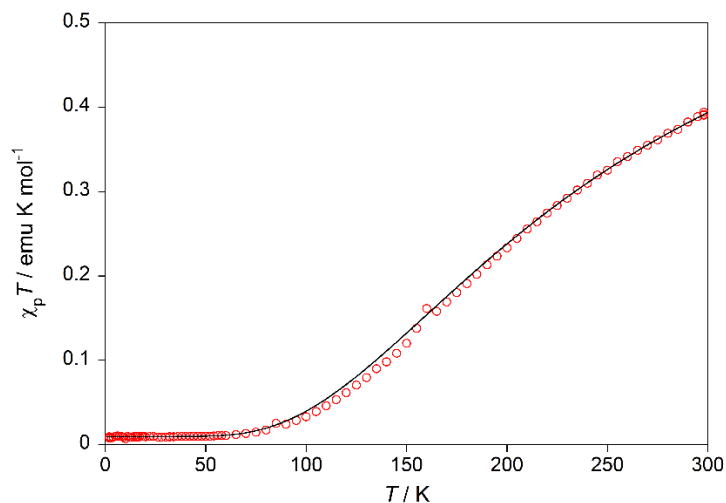
Figure S24. $\chi_p T$–T plot of the powdered **1d**. The measured data are plotted as open circles. The theoretical curve is drawn using the Bleaney–Bowers equation for the singlet–triplet model,[68] with the parameter of $2J/k_B$ (= ΔE_{S-T}) = –454 K (–0.90 kcal/mol), impurity spin contamination = 2.6%, g = 2.00, diamagnetic susceptibility = –470×10^{-6} emu/mol.
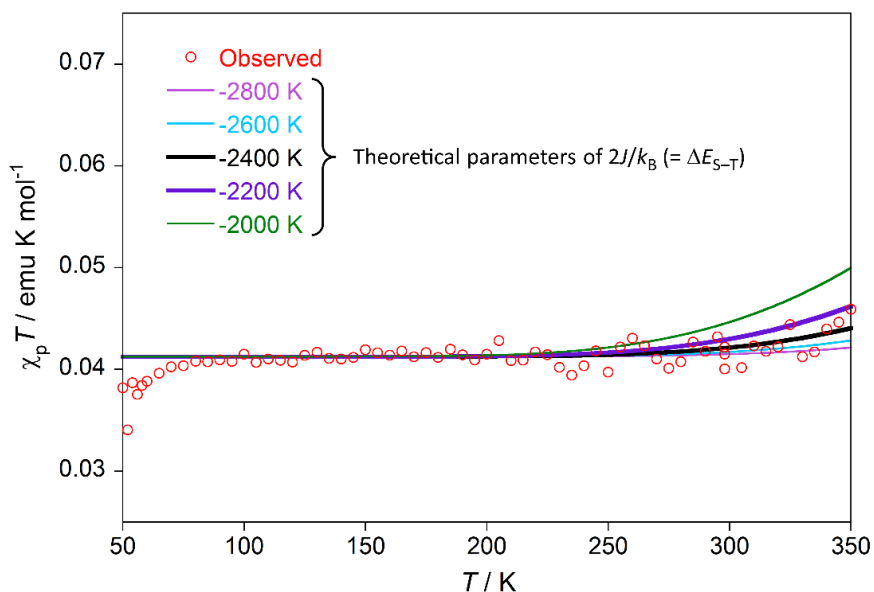

Figure S25. $\chi_p T$–T plot of the powdered **1e**. The measured data are plotted as open circles. The theoretical curve is drawn using the Bleaney–Bowers equation for the singlet–triplet model.[68] Due to the limitation of the measurement temperature, the increase of the magnetic susceptibility above 300 K was not clear. The parameter of $2J/k_B$ (= ΔE_{S-T}) was estimated to be in the range from –2400 K to –2200 K, impurity spin contamination = 11.0%, g = 2.00, diamagnetic susceptibility = –363×10^{-6} emu/mol. In order to determine the ΔE_{S-T} of **1e**, the temperature-dependent ESR measurements of the same sample was conducted (Figure S26).
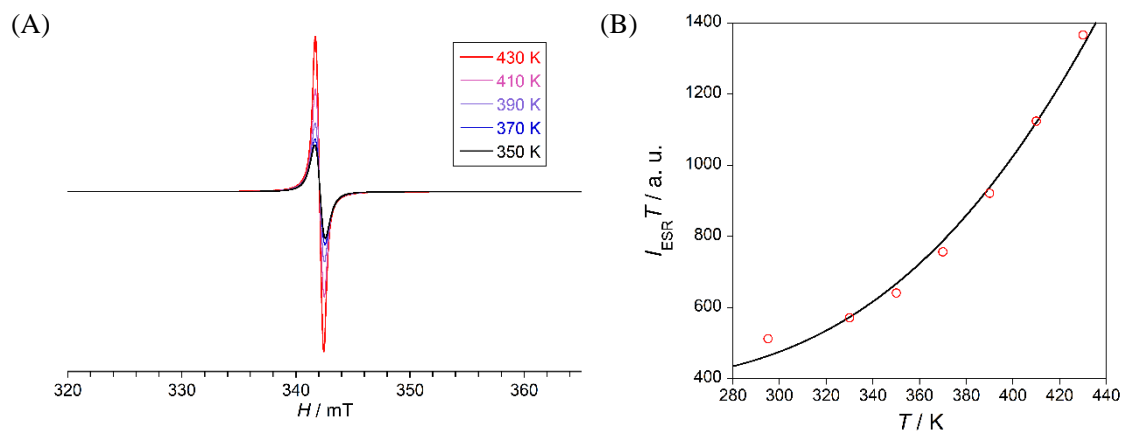
Figure S26. (A) Temperature-dependent ESR spectra of the solid sample of **1e** that was used for the SQUID measurements (Figure S25). (B) The change in ESR signal intensity with temperature (○) and the Bleaney–Bowers fit (——). The parameter of ΔE_{S-T} was estimated to be –2270 K (–4.5 kcal/mol).
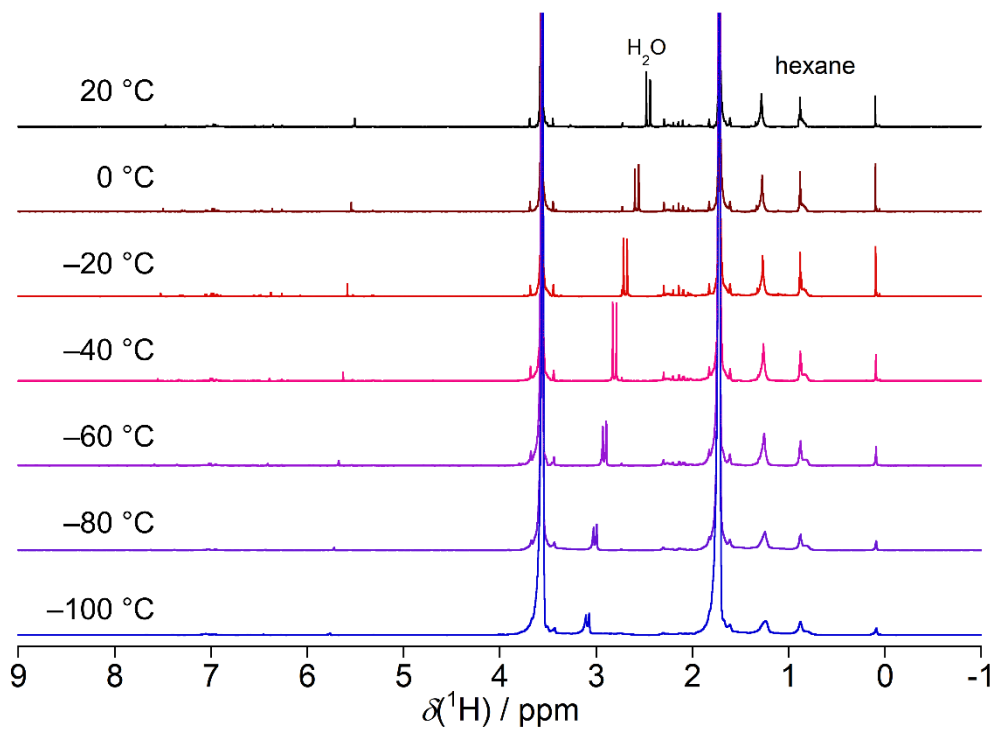

Figure S27. Temperature-dependent ^{1}H NMR spectra (600 MHz) of **1c** in THF-d_8.
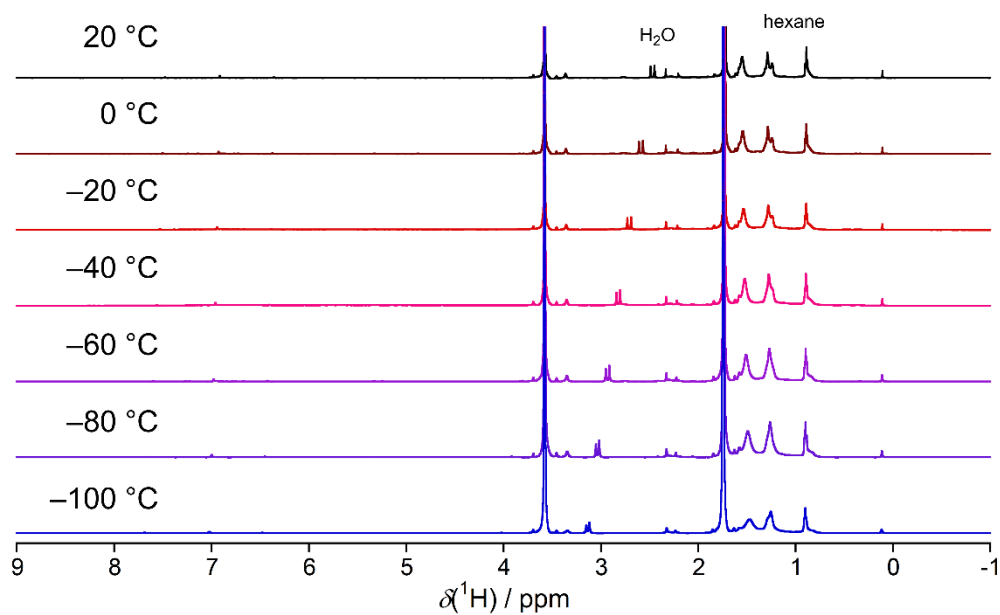
Figure S28. Temperature-dependent ^{1}H NMR spectra (600 MHz) of **1d** in THF-d_8.

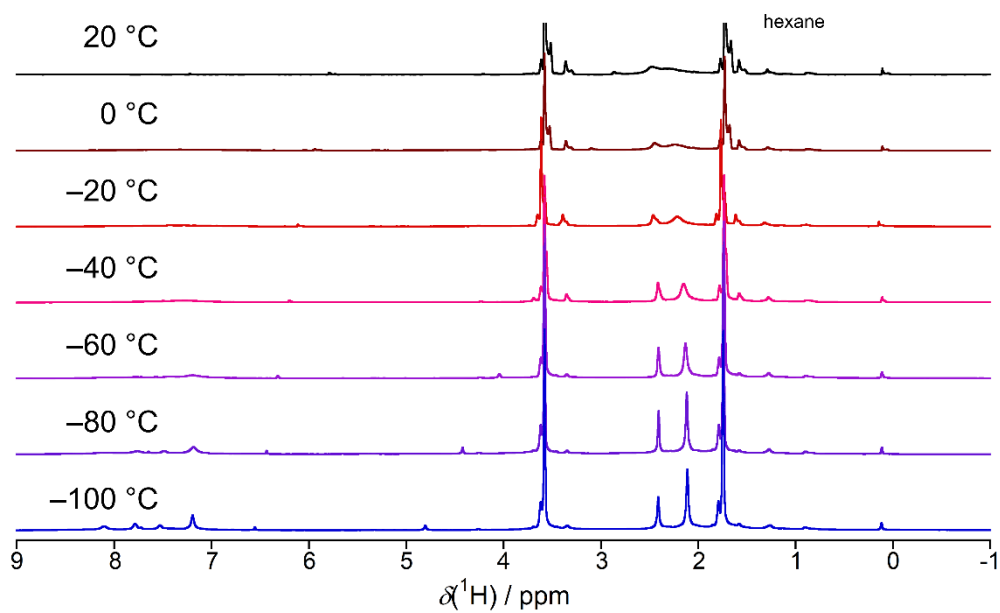**Figure S29.** Temperature-dependent ^{1}H NMR spectra (600 MHz) of **1e** in THF-d_8.
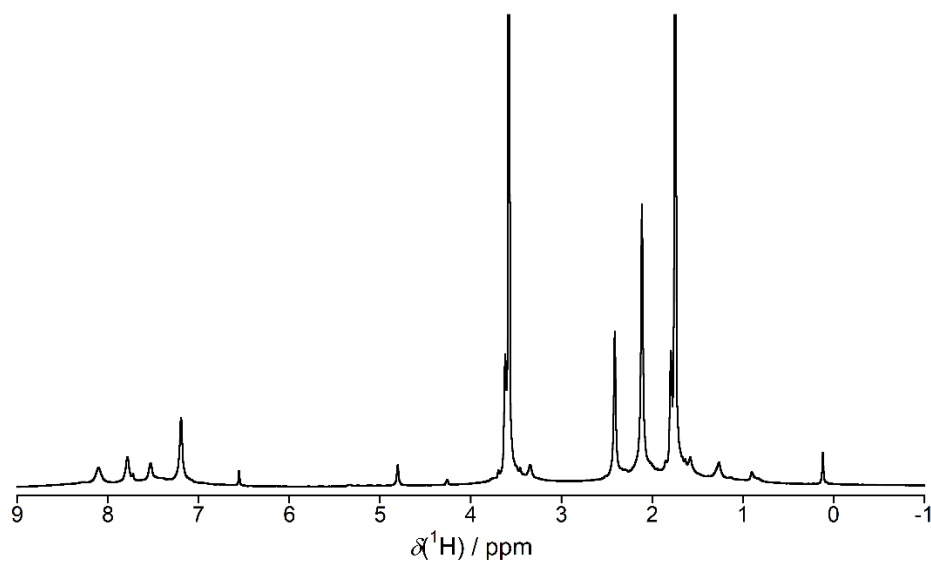
Figure S30. ^{1}H NMR spectrum (600 MHz, -100 ^{o}C) of **1e** in THF-d_8.

Because of the expanded ΔE_{S-T} of **1e**, some proton signals that are assigned to the aryl groups were observed.

Figure S31. Electronic absorption spectrum of **1c** in THF. Inset shows a magnified view.

134

Figure S32. Electronic absorption spectra of **1c** in THF (red), benzene (blue) and CH_2Cl_2 (green) in the region of visible to near-IR.

Figure S33. (A) Periodical measurements of electronic absorption of **1c** in THF at n the region of visible to near-IR upon exposure to air under room light at room temperature. (B) Plots of the absorbance at 1650 nm with time and the half-life time was estimated to be 146 min (2.4 h).
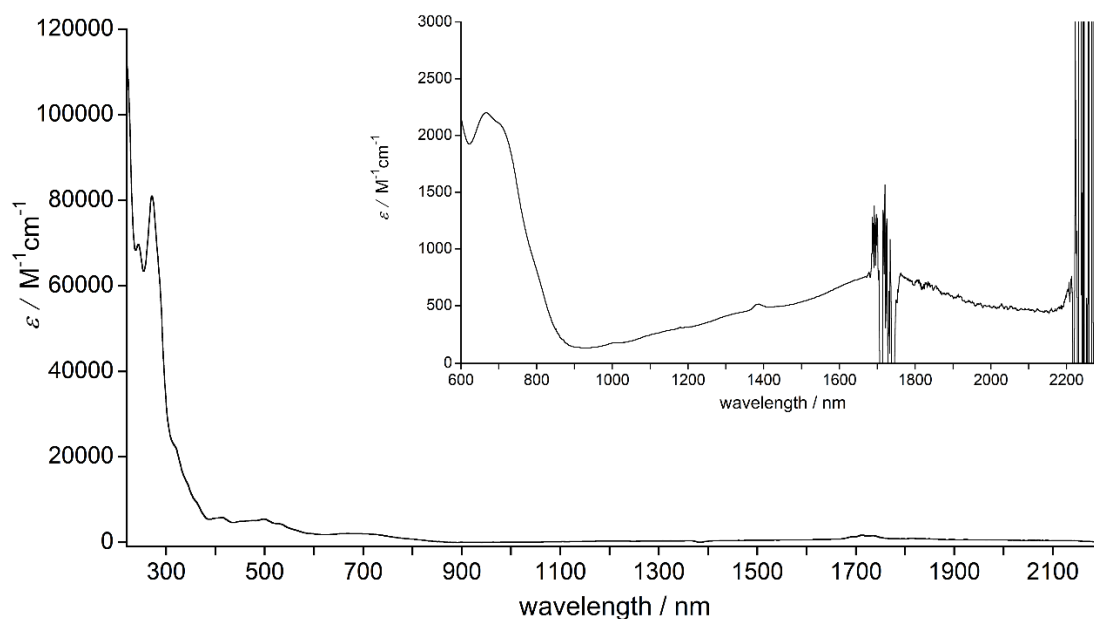
Figure S34. Electronic absorption spectrum of **1d** in THF. Inset shows a magnified view.
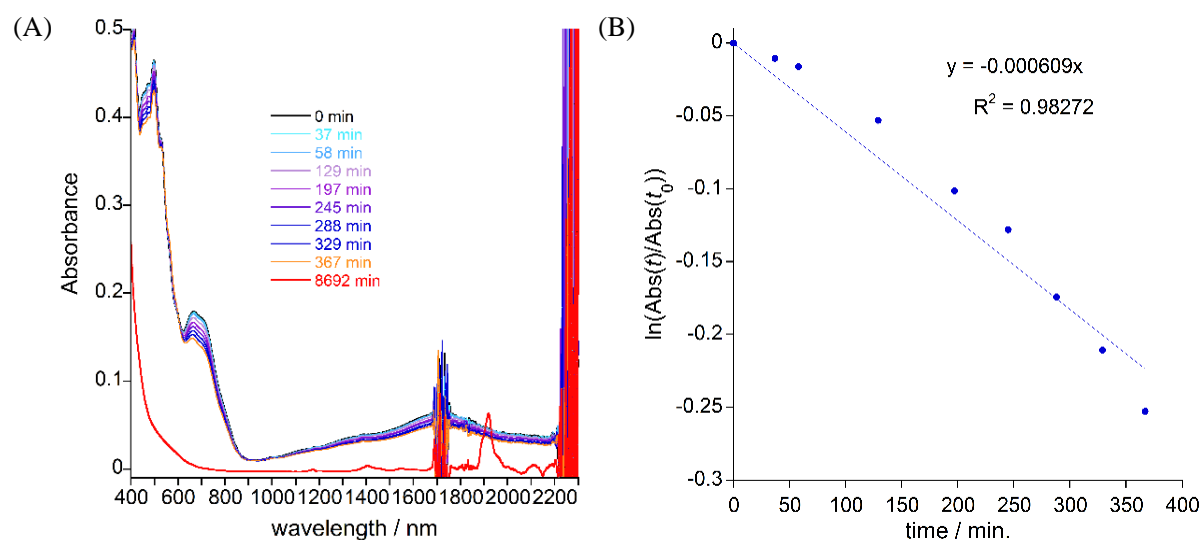
Figure S35. (A) Periodical measurements of electronic absorption of **1d** in THF at n the region of visible to near-IR upon exposure to air under room light at room temperature. (B) Plots of the absorbance at 1660 nm with time and the half-life time was estimated to be 1137 min (19 h).
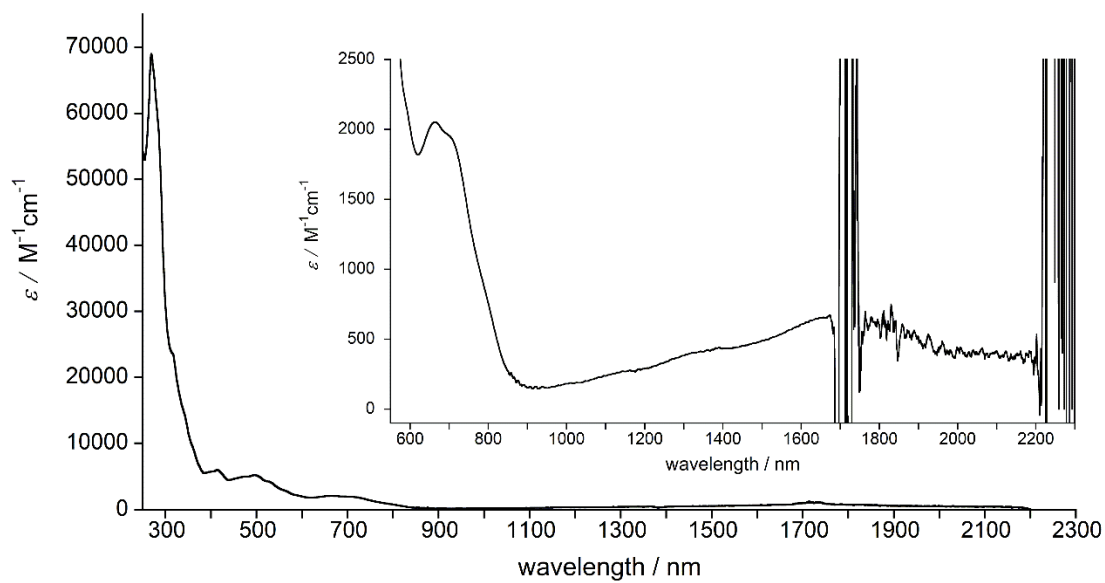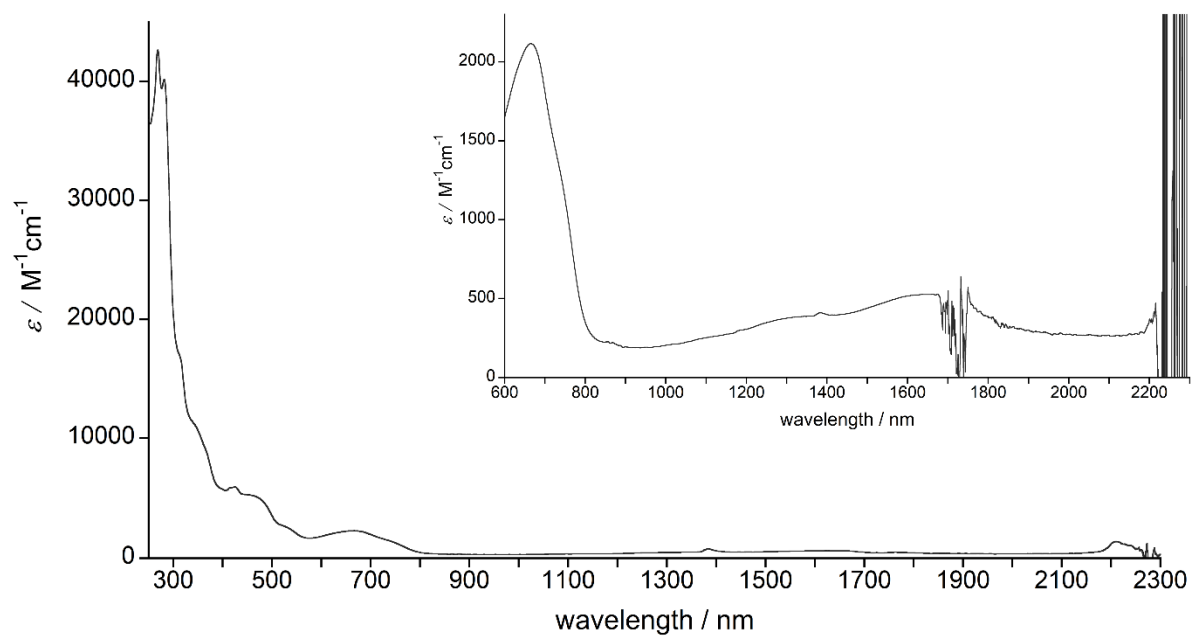
Figure S36. Electronic absorption spectrum of **1e** in THF. Inset shows a magnified view.
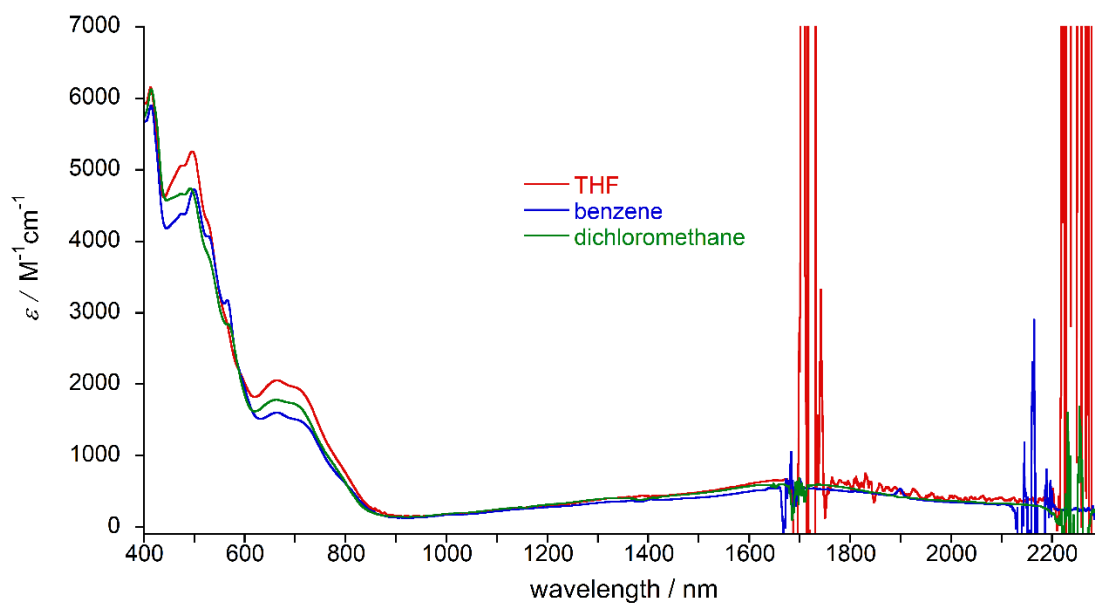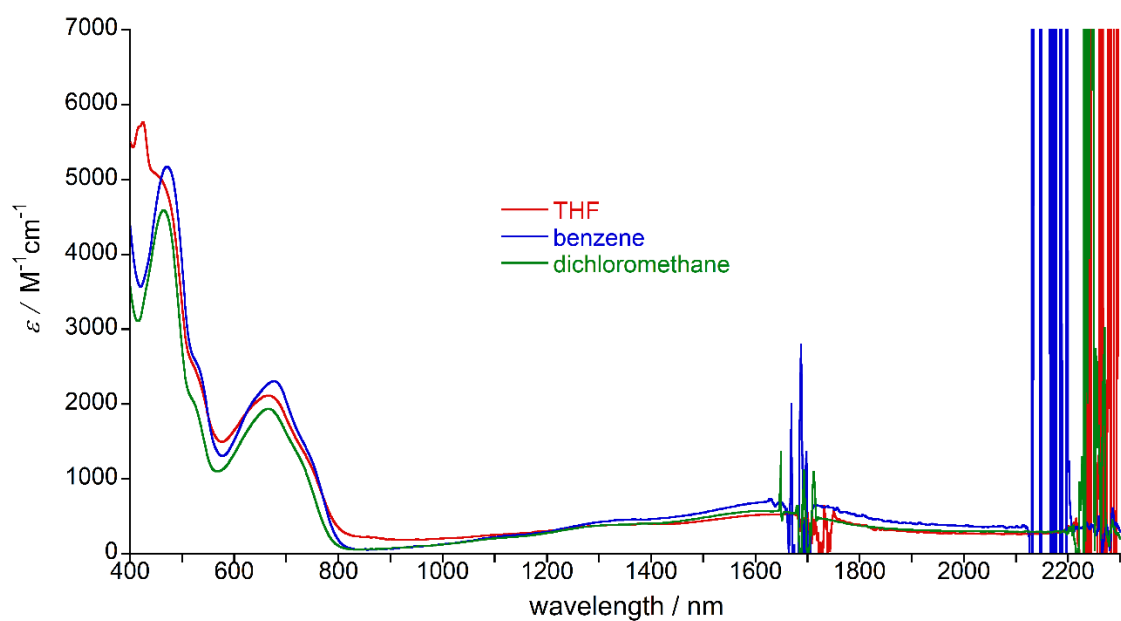

Figure S37. Electronic absorption spectra of **1e** in THF (red), benzene (blue) and CH_2Cl_2 (green) in the region of visible to near-IR.
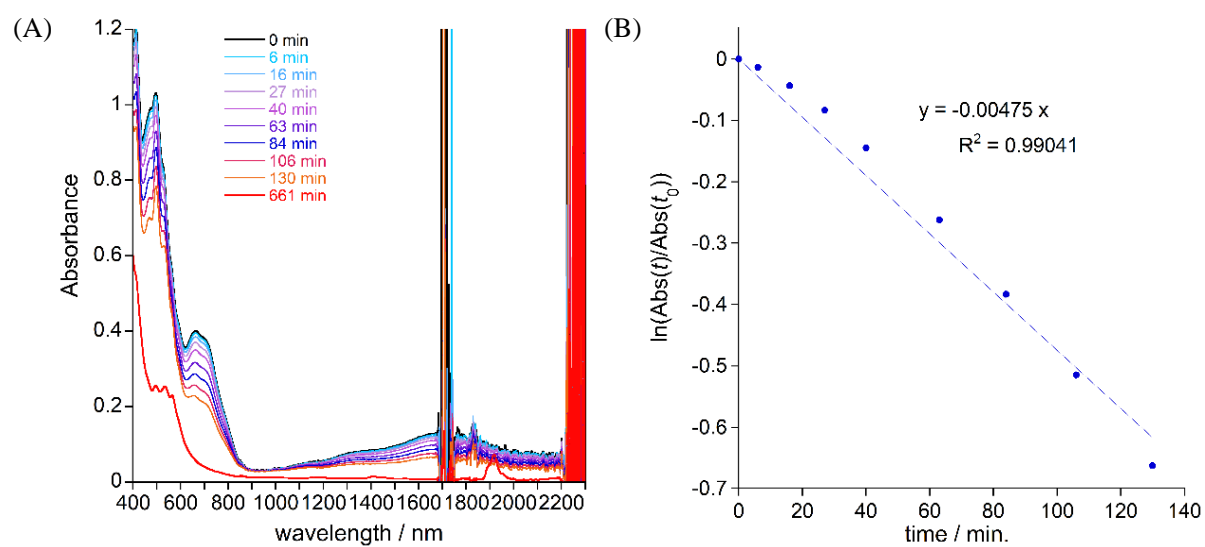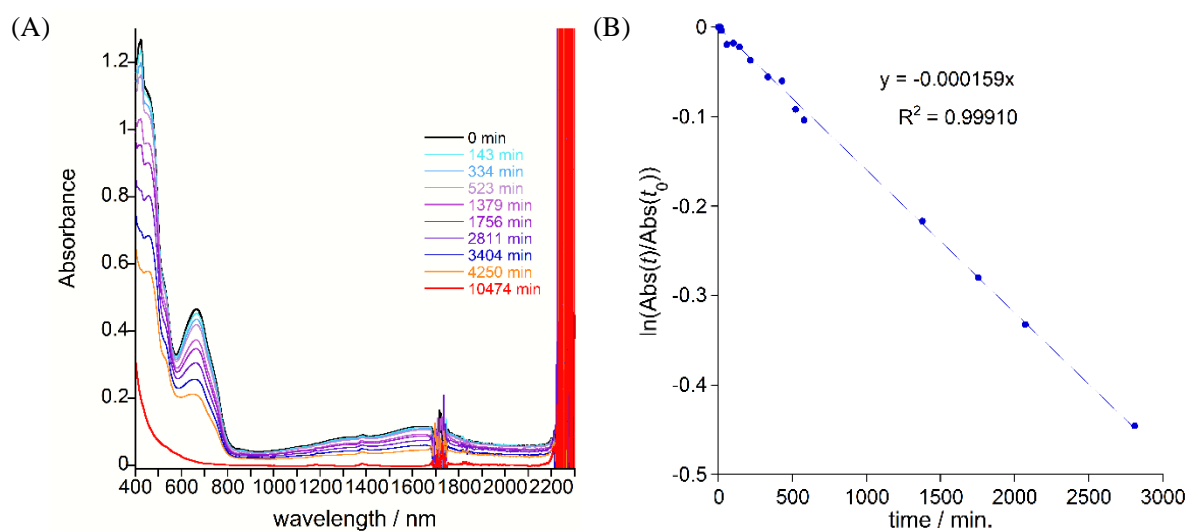
Figure S38. (A) Periodical measurements of electronic absorption of **1e** in THF at n the region of visible to near-IR upon exposure to air under room light at room temperature. (B) Plots of the absorbance at 1600 nm with time and the half-life time was estimated to be 4349 min (72.5 h = 3.0 days).
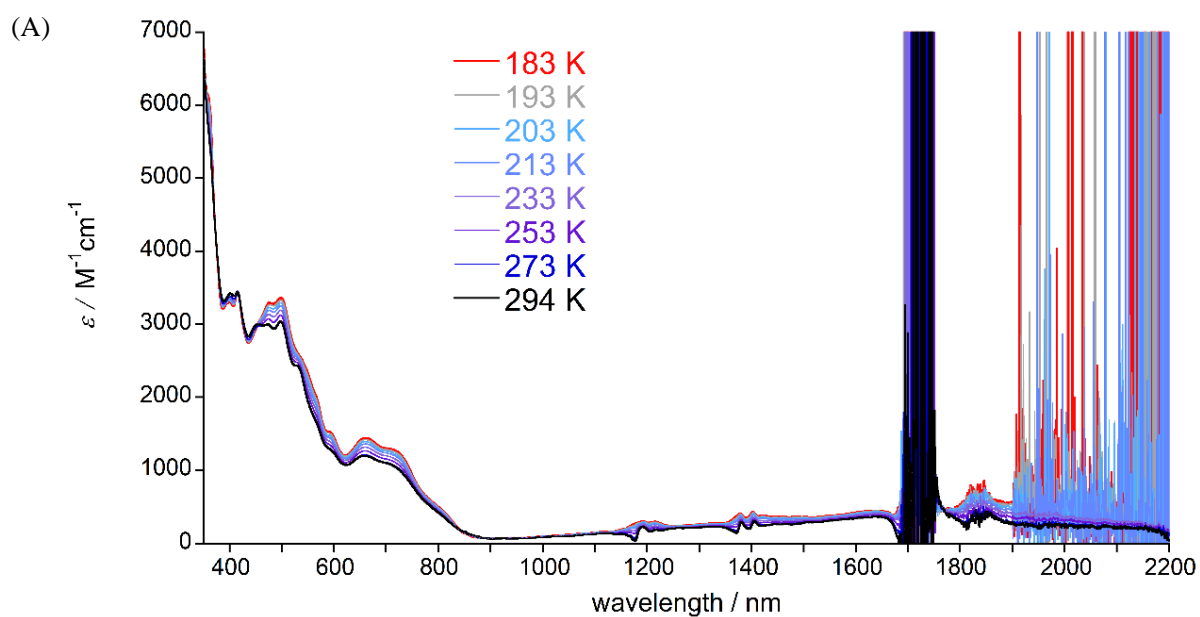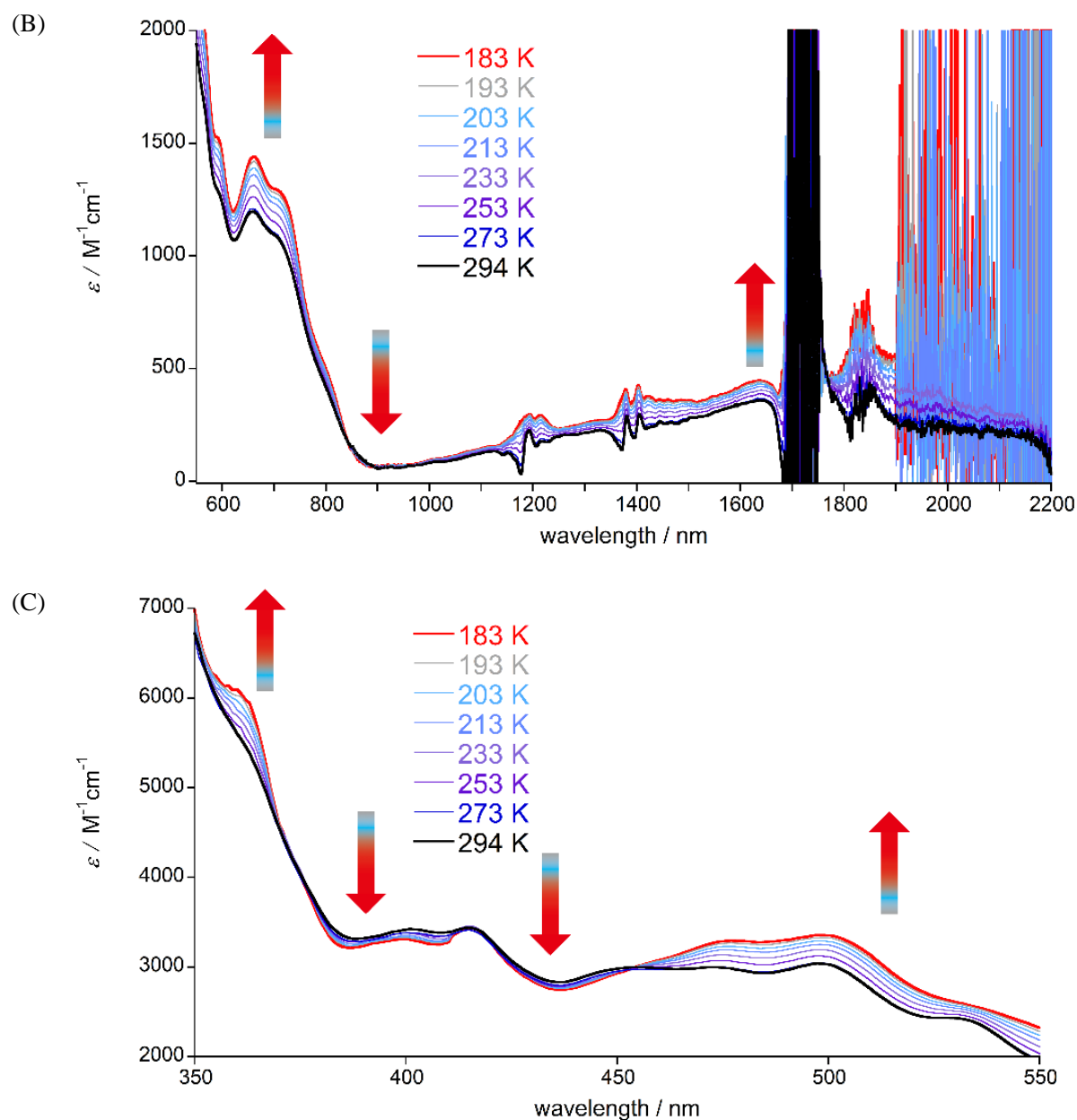
Figure S39. (A) Variable-temperature electronic absorption spectra for **1d** in THF and magnified views of (B) 2200–550 nm and (C) 550–350 nm regions.

Computational method

General

Electronic structures of open-shell molecular systems exhibiting spin- and charge-polarized resonance structures are in general difficult to be described by quantum chemical calculations. Results of geometries, energies, and properties from the quantum chemical calculations are very sensitive to the quality of approximation method, namely, balanced description of each canonical form in the resonance structure is needed. In principle, multi-configurational methodologies, such as multi-reference perturbation theory (MRPT) with sufficiently large active space, are necessary to gain the electron correlation effect, even though applications of such methods may usually be limited to the single-point calculations because of their high computational costs. Based on these features, we have carefully performed theoretical analysis on the geometries, electronic structures, and

139

properties of the present systems. All the calculations were performed using Gaussian 09 program package, except for the excitation properties.

Optimization

At first, we have performed geometry optimizations followed by frequency analysis for **1c–1e** in the singlet and triplet states at the spin-restricted (R) and -unrestricted (U)CAM-B3LYP-D3/def2-SVP levels, respectively. Figure S40 shows the results of optimized geometries in the singlet and triplet states. Structures of the bis-periazulene core part in the singlet state of **1c** and **1d** were predicted to have C_{2v}-like symmetry by theoretical calculations whereas those of the X-ray structures were more C_S-like. However, the theoretical and experimental bond lengths are found to be very close to each other.

	Singlet	**Triplet**
1c		
1d		
1e		

Figure S40. Comparison of theoretical geometries in the singlet (left) and triplet (right) states for **1c** (top), **1d** (middle) and **1e** (bottom). Bond lengths are given in Å.

NICS and AICD calculations

Aromatic characters of the bis-periazulene derivative were investigated by evaluating the nucleus-independent chemical shift (NICS) and the aromaticity of the induced current density (ACID). We evaluated the NICS(1) and ACID for the bis-periazulene core part (**1a'**) wh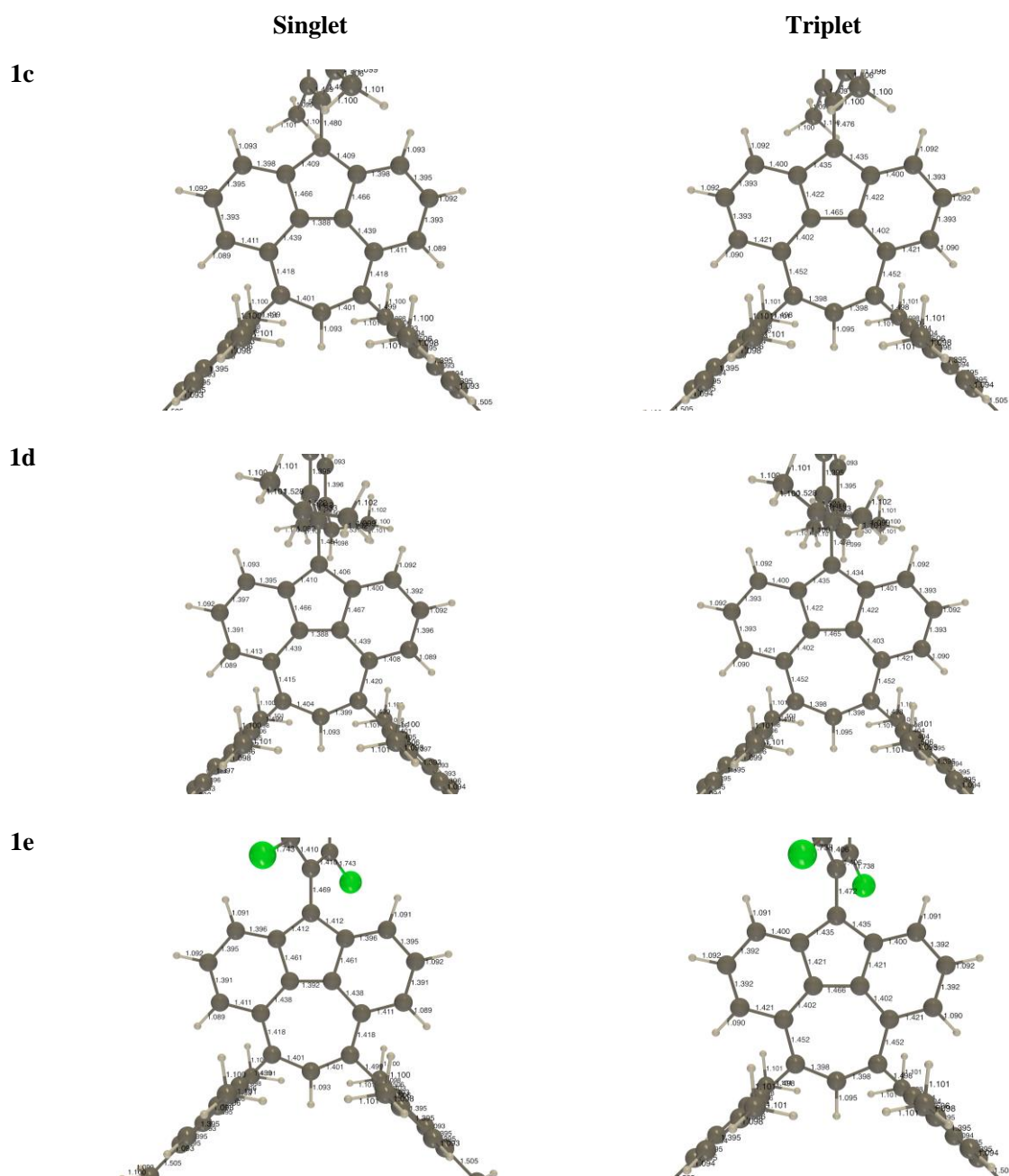ere the geometry was taken from that of X-ray geometry of **1d**. Here, all the Trip- and Mes- groups in **1d** were replaced by hydrogen (H) atoms, and then only the positions of H atoms were optimized at the RCAM-B3LYP/def2-SVP level. Magnetic response properties were evaluated at the GIAO- or CSGT-UCAM-B3LYP/def2-SVP level. Electrostatic potential (ESP) maps ware also evaluated at the same level. Since the X-ray geometry was very slightly deviated from the planar structure, the NICS(1) value for each ring was evaluated from the average of the NICS values 1 Å above and below the molecular plane.

(A)

(B)
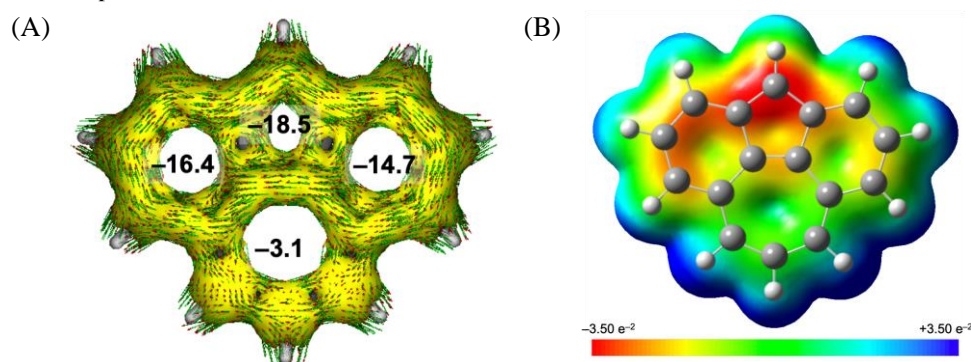
Figure S41. (A) AICD plots with NICS(1) values (/ppm, bold) of **1a'** at the GIAO- or CSGT-UCAM-B3LYP/def2-SVP level. (B) Electrostatic potential (ESP) map of **1a'** at the UCAM-B3LYP/def2-SVP level.

Molecular diagrams for the singlet and triplet states

We here compared the results of frontier π-MOs of **1c** in the singlet and triplet states calculated at the UCAM-B3LYP/def2-SVP level. Diradical characters y_i for the singlet state were evaluated at the PUHF/def2-SVP level. As shown in Table S3, these bis-periazulene derivatives are predicted to exhibit weak open-shell characters. Judging from the topologies and symmetries of MOs, the frontier π-MOs illustrated in Figures S43 and S44 are expected to be important to describe the electronic structures of bis-periazulene derivatives. Actually, the values of y_0 and y_1 are found to be comparable to each other, meaning that these systems are expected to show weak multiradical characters. Even though substituent effects on y_0/y_1 (wavefunction characters) in the singlet state are found to be very slight, singlet–triplet gaps (energetics) can be more sensitive to the substituent species.

Table S3. Results of y_i calculated at the PUHF/def2-SVP level.

	y_0	y_1
1c	0.229	0.168
1d	0.232	0.168
1e	0.218	0.164
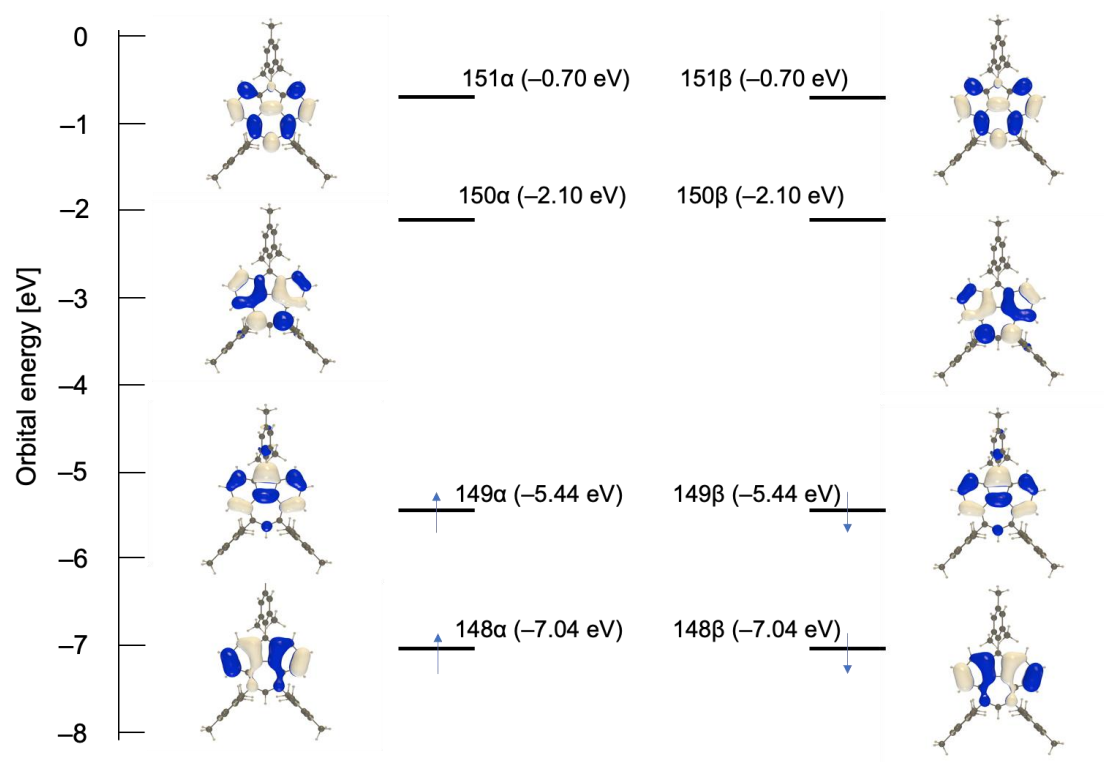
Figure S43. Frontier molecular orbitals of **1c** in the singlet state at the UCAM-B3LYP/def2-SVP//RCAM-B3LYP-D3/def2-SVP level.
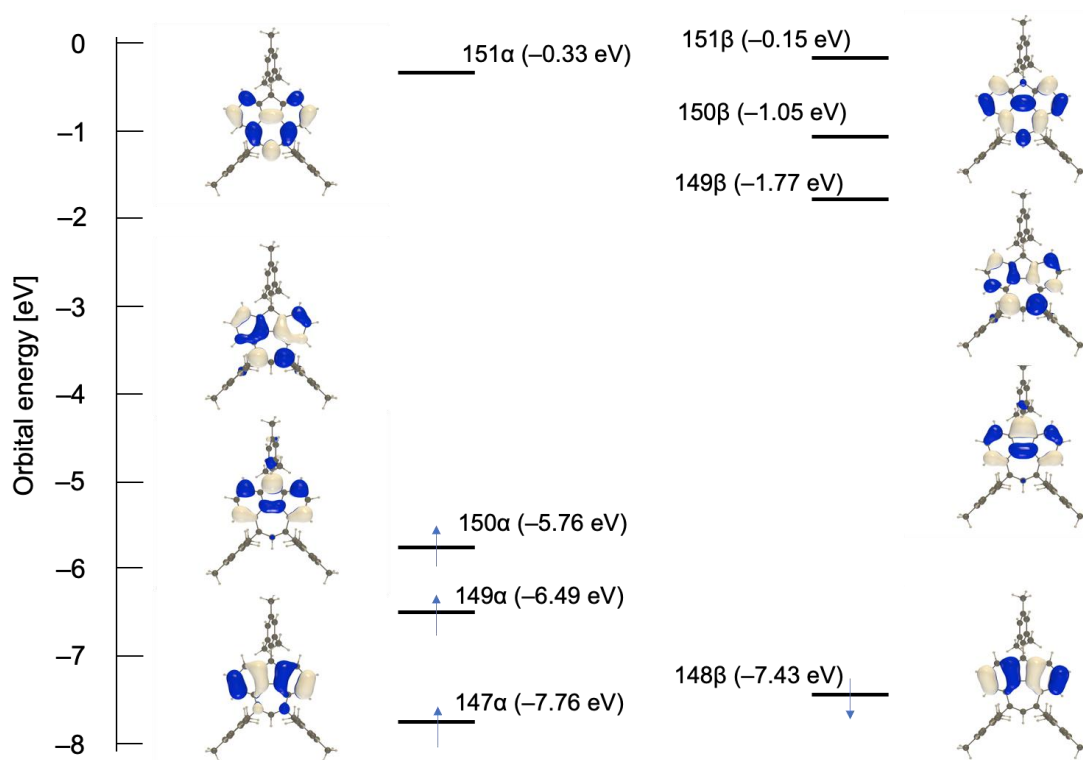
Figure S44. Frontier molecular orbitals of **1c** in the triplet state at the UCAM-B3LYP/def2-SVP//UCAM-B3LYP-D3/def2-SVP level.

Figure S45. Spin density maps of **1c** in the singlet and triplet states calculated at the UHF/def2-SVP level with the contour values of 0.06. Positive (blue) and negative (green) spin densities are shown.

Excited state calculations including singlet-triplet energy gaps

As explained in the previous section, electronic structures of the present systems are difficult to be treated theoretically. In general, well-balanced descriptions of both the charge- and spin-polarized electronic structures are needed for the open-shell singlet state. Judging from the frontier MO level structures and the results of y_0 and y_1, at least four frontier MOs, *i.e.*, HOMO–1, HOMO, LUMO and LUMO+1 should be considered as the active orbital space. We therefore performed th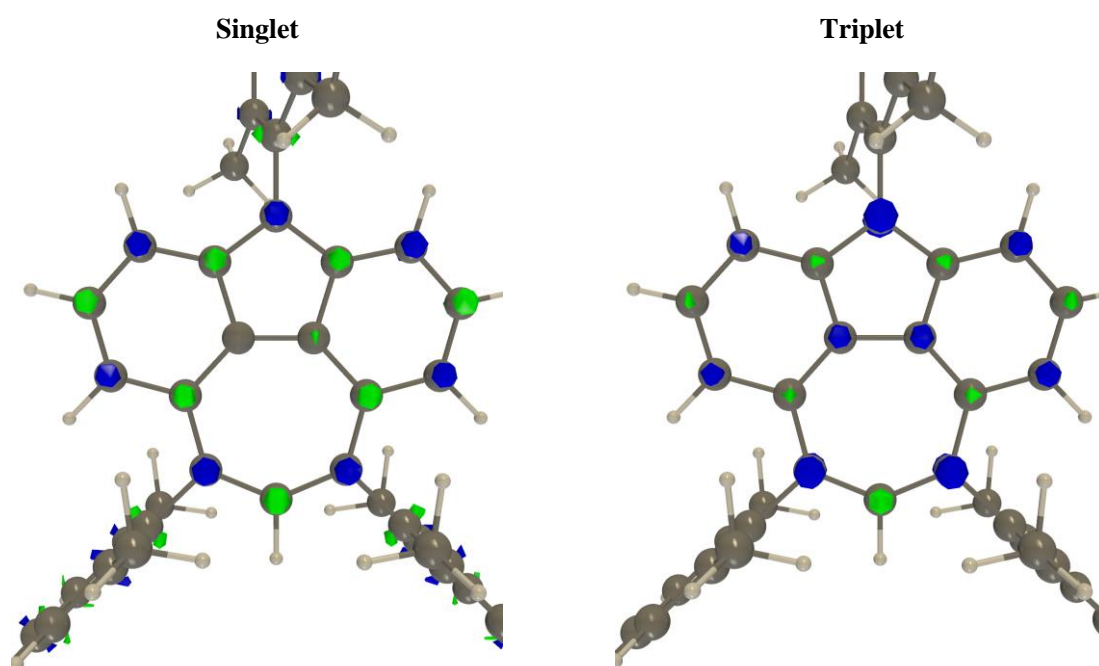e ground and excited state calculations at the state-averaged (SA-)CASSCF(4e,4o)/def2-SVP level. Here, density matrices of the lowest five roots in the CASSCF solution are averaged. Then, we performed the quasi-degenerate second-order n-electron valence state perturbation theory (QD-NEVPT2) calculations using the SA-CASSCF solution as the zeroth-order wavefunction. We employed strongly-contracted (SC-)NEVPT2 for the PT2 method, and explicitly Hermitian effective Hamiltonian during the QD calculations, *i.e.*, QD-SC-NEVPT2. During these calculations, we employed the def2-SVP/C auxiliary basis functions for the resolution of the identity (RI) approximation.[69] These calculations were performed using ORCA 4.2 program package.

For the singlet–triplet energy gaps, we performed the QD-SC-NEVPT2 calculations for both the singlet and triplet optimized geometries, and then the adiabatic singlet-triplet energy gaps were evaluated (Table S4). For the zero-point vibrational energy (ZPVE) corrections, we approximately employed the ZPVE values obtained from the frequency calculations at the R/U-CAM-B3LYP-D3/def2-SVP levels. Vertical singlet excitation energies related to the assignment of UV-vis absorption bands were also investigated at the time-dependent (TD-)UCAM-B3LYP/def2-SVP (Tables S5–S10) and QD-SC-NEVPT2 levels (Tables S11–S12). Theoretical calculations at the present level also predicted that the singlet-triplet gaps of **1c**/**1d** are larger than that of **1e**, although the results of y_0/y_1 are close to each other. Relative peak positions and intensities of UV-vis absorption bands (and its temperature dependence due to the thermal equilibrium of singlet and triplet states) were also reproduced well by both the present TD-UCAM-B3LYP and QD-SC-NEVPT2 calculations, even though the TD-UCAM-B3LYP results tend to overestimate the experimental excitation energies to some extent. Weak absorption band in the long-wavelength region is characterized by the HOMO-LUMO single-electron transition.

Table S4. Results of singlet–triplet gaps.

	Adiabatic / kcal mol^{-1}	Adiabatic + ZPVE / kcal mol^{-1}
1c	-3.37	-2.67
1d	-2.97	-2.77
1e	-5.29	-4.65

Table S5. TD-DFT results of vertical singlet-singlet transitions ($f > 0.01$) for **1c** at the S_0 optimized geometry calculated at the TD-UCAM-B3LYP/def2-SVP//RCAM-B3LYP-D3/def2-SVP. [a)]

Root number	Excitation energy / eV (wavelength / nm)	Excitation amplitudes (abs. > 0.3)		Oscillator strength f
2 ($<S^2> = 0.012$)	0.7554 (1641.3)	0.70105 −0.70061	(149β – 150β) (149α – 150α)	0.0107
5 ($<S^2> = 0.017$)	2.2902 (541.4)	0.70079 0.70069	(149β – 151β) (149α – 151α)	0.0754
6 ($<S^2> = 0.064$)	2.4935 (497.2)	0.69510 0.69493	(148β – 150β) (148α – 150α)	0.0814
17 ($<S^2> = 0.073$)	3.6467 (340.0)	0.44006 −0.43873 −0.39008 0.39011	(147β – 150β) (147α – 150α) (148β – 151β) (148α – 151α)	0.0115
21 ($<S^2> = 0.847$)	3.8627 (321.0)	−0.30432 0.30935	(141β – 150β) (141α – 150α)	0.0460

a) $<S^2>$ of the initial (S_0) state at the UCAM-B3LYP/def2-SVP level is calculated to be 0.0198. Here, the 149th and 150th MOs are HOMO and LUMO, respectively.

Table S6. TD-DFT results of vertical triplet-triplet transitions ($f > 0.01$) for **1c** at the T_1 optimized geometry calculated at the TD-UCAM-B3LYP/def2-SVP//UCAM-B3LYP-D3/def2-SVP. [a)]

Root number	Excitation energy / eV (wavelength / nm)	Excitation amplitudes (abs. > 0.3)		Oscillator strength
2 ($<S^2> = 2.144$)	2.3363 (530.7)	0.78847 −0.58066	(148β – 149β) (150α – 151α)	0.0111
3 ($<S^2> = 2.494$)	3.1585 (392.5)	0.67792 −0.46846	(145β – 149β) (149α – 151α)	0.0520
8 ($<S^2> = 2.733$)	3.5083 (353.4)	0.63343	(148β – 150β)	0.0319
10 ($<S^2> = 2.125$)	3.6802 (336.9)	0.80738 −0.36213	(141β – 150β) (145β – 150β)	0.0468

a) $<S^2>$ of the initial (T_1) at the UCAM-B3LYP/def2-SVP level is calculated to be 2.1354. Here, the 148th MO is the highest doubly occupied MO, the 149th and 150th MOs are singly occupied MOs, and the 151th MO is the lowest vacant MO, respectively, in the triplet configuration.

Table S7. TD-DFT results of vertical singlet-singlet transitions ($f > 0.01$) for **1d** at the S_0 optimized geometry calculated at the TD-UCAM-B3LYP/def2-SVP//RCAM-B3LYP-D3/def2-SVP. [a)]

Root number	Excitation energy / eV (wavelength / nm)	Excitation amplitudes (abs. > 0.3)		Oscillator strength f
2 ($<S^2> = 0.017$)	0.7443(1665.7)	0.67302 0.72754	(173β – 174β) (173α – 174α)	0.0100
5 ($<S^2> = 0.035$)	2.2838 (542.9)	0.70624 0.69376	(173β – 175β) (173α – 175α)	0.0758
6	2.4928 (497.4)	0.70008	(172β – 174β)	0.0852

		−0.68141	(172α – 174α)	
21	3.8403 (322.9)	0.35569	(165β – 174β)	0.0696
($<S^2>$ = 0.329)		0.34350	(165α – 174α)	
		−0.34240	(173β – 182β)	
		0.30178	(173α – 182α)	
		0.32714	(172β – 175β)	
		−0.35111	(172α – 175α)	

a) $<S^2>$ of the initial (S_0) state at the UCAM-B3LYP/def2-SVP level is calculated to be 0.0411. Here, the 173th and 174th MOs are HOMO and LUMO, respectively.

Table S8. TD-DFT results of vertical triplet-triplet transitions ($f > 0.01$) for **1d** at the T_1 optimized geometry calculated at the TD-UCAM-B3LYP/def2-SVP//UCAM-B3LYP-D3/def2-SVP. *a*)

Root number	Excitation energy / eV (wavelength / nm)	Excitation amplitudes (abs. > 0.3)		Oscillator strength
2	2.3499 (527.6)	0.80486	(172β – 173β)	0.0104
($<S^2>$ = 2.150)		−0.55698	(174α – 175α)	
3	3.1808 (389.8)	0.85659	(173α – 175α)	0.0498
($<S^2>$ = 2.315)				
8	3.4966 (354.6)	0.57388	(172β – 174β)	0.0306
($<S^2>$ = 2.870)		−0.33815	(169β – 173β)	
10	3.6768 (337.2)	0.83511	(165β – 174β)	0.0434
($<S^2>$ = 2.124)		−0.30780	(169β – 174β)	

a) $<S^2>$ of the initial (T_1) at the UCAM-B3LYP/def2-SVP level is calculated to be 2.1345. Here, the 172th MO is the highest doubly occupied MO, the 173th and 174th MOs are singly occupied MOs, and the 175th MO is the lowest vacant MO, respectively, in the triplet configuration.

Table S9. TD-DFT results of vertical singlet-singlet transitions ($f > 0.01$) for **1e** at the S_0 optimized geometry calculated at the TD-UCAM-B3LYP/def2-SVP//RCAM-B3LYP-D3/def2-SVP. *a*)

Root number	Excitation energy / eV (wavelength / nm)	Excitation amplitudes (abs. > 0.3)		Oscillator strength f
2	0.8583 (1444.5)	0.70285	(153β – 154β)	0.0126
($<S^2>$ = 0.000)		0.70285	(153α – 154α)	
5	2.3972 (517.2)	0.70103	(153β – 155β)	0.0776
($<S^2>$ = 0.000)		0.70103	(153α – 155α)	
6	2.4975 (496.4)	0.70108	(152β – 154β)	0.0795
($<S^2>$ = 0.000)		0.70108	(152α – 154α)	
20	3.8546 (321.7)	0.50080	(152β – 155β)	0.1200
($<S^2>$ = 0.000)		0.50080	(152α – 155α)	
		−0.35332	(153β – 162β)	
		−0.35332	(153α – 162α)	

a) $<S^2>$ of the initial (S_0) state at the UCAM-B3LYP/def2-SVP level is calculated to be 0.0000, meaning that the open-shell solution reduces to the closed-shell one. Here, the 153th and 154th MOs are HOMO and LUMO, respectively.

Table S10. TD-DFT results of vertical triplet-triplet transitions ($f > 0.01$) for **1e** at the T_1 optimized geometry calculated at the TD-UCAM-B3LYP/def2-SVP//UCAM-B3LYP-D3/def2-SVP. *a*)

Root number	Excitation energy / eV (wavelength / nm)	Excitation amplitudes (abs. > 0.3)		Oscillator strength
2	2.2809 (543.6)	0.70449	(152β – 153β)	0.0123
($<S^2>$ = 2.129)		0.68180	(154α – 155α)	
3	3.1572 (392.7)	0.80034	(147β – 153β)	0.0284
($<S^2>$ = 2.527)				
5	3.3146 (374.1)	0.72026	(153α – 155α)	0.0221

($\langle S^2 \rangle$ = 2.604)		-0.43599	(152β – 154β)	
8	3.5238 (351.9)	0.71256	(152β – 154β)	0.0238
($\langle S^2 \rangle$ = 2.358)		0.38795	(153α – 155α)	
		0.31219	(143β – 153β)	
9	3.6557 (339.2)	0.74077	(145β – 153β)	0.0281
($\langle S^2 \rangle$ = 2.529)		-0.37015	(151α – 155α)	
		0.30997	(146β – 153β)	
10	3.6937 (335.7)	0.82940	(147β – 154β)	0.0288
($\langle S^2 \rangle$ = 2.243)				

a) $\langle S^2 \rangle$ of the initial (T_1) at the UCAM-B3LYP/def2-SVP level is calculated to be 2.1371. Here, the 152th MO is the highest doubly occupied MO, the 153rd and 154th MOs are singly occupied MOs, and the 155th MO is the lowest vacant MO, respectively, in the triplet configuration.

Table S11. QD-SC-NEVPT2 results of vertical singlet-singlet transitions at the S_0 optimized geometry.

	1c	1d	1e
S_0–S_1	1887.5 nm (f = 0.017)	1896.5 nm (f = 0.017)	1698.0 nm (f = 0.020)
S_0–S_2	780.3 nm (f = 0.050)	782.8 nm (f = 0.045)	739.5 nm (f = 0.067)
S_0–S_3	582.2 nm (f = 0.019)	579.8 nm (f = 0.020)	576.2 nm (f = 0.013)
S_0–S_4	542.7 nm (f = 0.127)	548.3 nm (f = 0.129)	508.6 nm (f = 0.120)

Table S12. QD-SC-NEVPT2 results of vertical triplet-triplet transitions at the T_1 optimized geometry.

	1c	1d	1e
T_1–T_2	751.5 nm (f = 0.002)	752.2 nm (f = 0.002)	757.7 nm (f = 0.000)
T_1–T_3	645.3 nm (f = 0.036)	643.9 nm (f = 0.033)	662.8 nm (f = 0.044)
T_1–T_4	472.4 nm (f = 0.038)	477.0 nm (f = 0.038)	457.5 nm (f = 0.020)
T_1–T_5	451.8 nm (f = 0.038)	452.9 nm (f = 0.037)	447.3 nm (f = 0.053)

We also compared the diradical properties of **1c** using the theoretical and experimental geometries, since the (pseudo-)symmetry of the bis-periazulene core part are C_{2v}-like and C_s-like, respectively. For the X-ray geometry, only the positions of H atoms were optimized at the RCAM-B3LYP/def2-SVP level. Then, calculation results of diradical characters and vertical singlet–triplet gaps were compared (Table S13). Difference of the results using theoretical and experimental geometries is found to be small (e.g., ~1 kcal/mol in the vertical singlet–triplet gap).

Table S13. Results of vertical singlet–triplet gaps of **1c** (-Mes) using the theoretical (C_{2v}-like) and experimental (C_s-like) geometries.

	Theoretical geometry / kcal mol^{-1}	Experimental geometry / kcal mol^{-1}
y_0/y_1	0.229/0.168	0.237/0.166
Vertical singlet–triplet gap	-10.51	-9.32

4-5. Reference

(1)   Tobe, Y. Non-Alternant Non-Benzenoid Aromatic Compounds: Past, Present, and Future. *Chem. Rec.* **2015**, *15*, 86–96.

(2)   Tobe, Y. Quinodimethanes Incorporated in Non-Benzenoid Aromatic or Antiaromatic Frameworks. *Top. Curr. Chem.* **2018**, *376*, 12.

(3)   Frederickson, C. K.; Rose, B. D.; Haley, M. M. Explorations of the Indenofluorenes and Expanded Quinoidal Analogues. *Acc. Chem. Res.* **2017**, *50*, 977–987.

(4)   Dressler, J. J.; Haley, M. M. Learning How to Fine-tune Diradical Properties by Structure Refinement. *J. Phys. Org. Chem.* **2020**, *33*, 4114.

(5)   Konishi, A.; Yasuda, M. Breathing New Life into Nonalternant Hydrocarbon Chemistry: Syntheses and Properties of Polycyclic Hydrocarbons Containing Azulene, Pentalene, and Heptalene Frameworks. *Chem. Lett.* **2021**, *50*, 195–212.

(6)   Chaolumen; Stepek, I. A.; Yamada, K. E.; Ito, H.; Itami, K. Construction of Heptagon-Containing Molecular Nanocarbons. *Angew. Chem. Int. Ed.* **2021**, *60*, 23508–23532.

(7)   Márquez, I. R.; Castro-Fernández, S.; Millán, A.; Campaña, A. G. Synthesis of Distorted Nanographenes Containing Seven- and Eight-Membered Carbocycles. *Chem. Commun.* **2018**, *54*, 6705–6718.

(8)   Fei, Y.; Fu, Y.; Bai, X.; Du, L.; Li, Z.; Komber, H.; Low, K.; Zhou, S.; Phillips, D. L.; Feng, X.; Liu, J. Defective Nanographenes Containing Seven-Five-Seven (7–5–7)-Membered Rings. *J. Am. Chem. Soc.* **2021**, *143*, 2353–2360.

(9)   Liu, P.; Chen, X.; Cao, J.; Ruppenthal, L.; Gottfried, J. M.; Müllen, K.; Wang, X. Revisiting Acepleiadylene: Two-Step Synthesis and π-Extension toward Nonbenzenoid Nanographene. *J. Am. Chem. Soc.* **2021**, *143*, 5314–5318.

(10)   Mallada, B.; de la Torre, B.; Mendieta-Moreno, J. I.; Nachtigallová, D.; Matěj, A.; Matoušek, M.; Mutombo, P.; Brabec, J.; Veis, L.; Cadart, T.; Kotora, M.; Jelínek, P. On-Surface Strain-Driven Synthesis of Nonalternant Non-Benzenoid Aromatic Compounds Containing Four- to Eight-Membered Rings. *J. Am. Chem. Soc.* **2021**, *143*, 14694–14702.

(11)   Kantarod, K.; Worakul, T.; Soorukram, D.; Kuhakarn, C.; Reutrakul, V.; Surawatanawong, P.; Wattanathana, W.; Leowanawat, P. Dibenzopleiadiene-Embeded Polyaromatics via [4 + 3] Annulative Decarbonylation/Decarboxylation. *Org. Chem. Front.* **2021**, *8*, 522–530.

(12)   Gleiter, R.; Haberhauer, G.; Hoffmann, R. *Aromaticity and Other Conjugation Effects*; Wiley-VCH, 2012.

(13)   Michl, J.; Thulstrup, E. W. Why Is Azulene Blue and Anthracene White? A Simple Mo Picture. *Tetrahedron* **1976**, *32*, 205–209.

(14)   Xin, H.; Gao, X. Application of Azulene in Constructing Organic Optoelectronic Materials: New Tricks for an Old Dog. *Chempluschem* **2017**, *82*, 945–956.

(15)   Huang, J.; Huang, S.; Zhao, Y.; Feng, B.; Jiang, K.; Sun, S.; Ke, C.; Kymakis, E.; Zhuang, X. Azulene-Based Molecules, Polymers, and Frameworks for Optoelectronic and Energy Applications. *Small Methods* **2020**, *4*, 2000628.

(16)   Xin, H.; Hou, B.; Gao, X. Azulene-Based π-Functional Materials: Design, Synthesis, and Applications. *Acc. Chem. Res.* **2021**, *54*, 1737–1753.

(17)   Jiang, Q.; Tao, T.; Phan, H.; Han, Y.; Gopalakrishna, T. Y.; Herng, T. S.; Li, G.; Yuan, L.; Ding, J.; Chi, C. Diazuleno-*s*-Indacene Diradicaloids: Syntheses, Properties, and Local (Anti)Aromaticity Shift from Neutral to Dicationic State. *Angew. Chem. Int. Ed.* **2018**, *57*, 16737–16741.

(18)   Pigulski, B.; Shoyama, K.; Würthner, F. NIR-Absorbing Π-Extended Azulene: Non-Alternant Isomer of Terrylene Bisimide. *Angew. Chem. Int. Ed.* **2020**, *59*, 15908–15912.

(19)   Xin, H.; Li, J.; Lu, R.; Gao, X.; Swager, T. M. Azulene–Pyridine-Fused Heteroaromatics. *J. Am. Chem. Soc.* **2020**, *142*, 13598–13605.

(20)   Fan, Q.; Martin-Jimenez, D.; Ebeling, D.; Krug, C. K.; Brechmann, L.; Kohlmeyer, C.; Hilt, G.; Hieringer, W.; Schirmeisen, A.; Gottfried, J. M. Nanoribbons with Nonalternant Topology from Fusion of Polyazulene: Carbon Allotropes beyond Graphene. *J. Am. Chem. Soc.* **2019**, *141*, 17713–17720.

(21)   Nishimura, H.; Ishida, N.; Shimazaki, A.; Wakamiya, A.; Saeki, A.; Scott, L. T.; Murata, Y. Hole-Transporting Materials with a Two-Dimensionally Expanded π-System around an Azulene Core for Efficient Perovskite Solar Cells. *J. Am. Chem. Soc.* **2015**, *137*, 15656–15659.

(22)   Yamaguchi, Y.; Takubo, M.; Ogawa, K.; Nakayama, K.; Koganezawa, T.; Katagiri, H. Terazulene Isomers: Polarity Change of OFETs through Molecular Orbital Distribution Contrast. *J. Am. Chem. Soc.* **2016**, *138*, 11335–11343.

(23)   Yang, C.; Schellhammer, K. S.; Ortmann, F.; Sun, S.; Dong, R.; Karakus, M.; Mics, Z.; Löffler, M.; Zhang, F.; Zhuang, X.; Cánovas, E.; Cuniberti, G.; Bonn, M.; Feng, X. Coordination Polymer Framework Based On-Chip Micro-Supercapacitors with AC Line-Filtering Performance. *Angew. Chem. Int. Ed.* **2017**, *56*, 3920–3924.

(24)   Xin, H.; Ge, C.; Jiao, X.; Yang, X.; Rundel, K.; McNeill, C. R.; Gao, X. Incorporation of 2,6-Connected Azulene Units into the Backbone of Conjugated Polymers: Towards High-Performance Organic Optoelectronic Materials. *Angew. Chem. Int. Ed.* **2018**, *57*, 1322–1326.

(25)   Boekelheide, V.; Langeland, W. E.; Liu, C.-T. A Study of the Synthesis and Some Properties of Acepleiadiene. *J. Am. Chem. Soc.* **1951**, *73*, 2432–2435.

(26)   Boekelheide, V.; Vick, G. K. A Synthesis of Pleiadiene and Acepleiadylene 1. *J. Am. Chem. Soc.* **1956**, *78*, 653–658.

(27)   Reid, D. H.; Stafford, W. H.; Ward, J. P. The Fine Structure of Azulene. Part I. CycloHepta[*bc*]Acenaphthylene and Cyclohepta[*def*]Fluorene. *J. Chem. Soc.* **1955**, *84*, 1193–1201.

(28)   Gardner, P. D.; Wulfman, C. E.; Osborn, C. L. Cyclohepta[*klm*]Benz[*e*]Indene. Further Considerations on the Stability of Complex Polynuclear Systems. *J. Am. Chem. Soc.* **1958**, *80*, 143–148.

(29)   Hafner, K.; Fleischer, R.; Fritz, K. Pentaleno[2,1,6-*def*]Heptalene– a Non-Benzenoid Isomer of Pyrene. *Angew. Chem. Int. Ed. Engl.* **1965**, *4*, 69–70.

(30)   Anderson, A. G.; MacDonald, A. A.; Montana, A. F. Dicyclopenta[*ef,kl*]Heptalene (Azupyrene). *J. Am. Chem. Soc.* **1968**, *90*, 2993–2994.

(31)   Reel, H.; Vogel, E. Dicyclohepta[*cd,gh*]Pentalene?A New Pyrene Isomer. *Angew. Chem. Int. Ed. Engl.* **1972**, *11*, 1013–1014.

(32)   Munday, R.; Sutherland, I. O. Synthetic Approaches to the Cyclohepta[*def*]Fluorene System. *Chem. Commun.* **1967**, 569–570.

(33)   Munday, R.; Sutherland, I. O. Synthesis of Compounds Related to Cyclohepta[*def*]Fluorene. *J. Chem. Soc. C* **1969**, 1427–1434.

(34)   Grieser, U.; Hafner, K. Synthesis and Properties of Kinetically Stabilized Cyclohepta[*def*]Fluorene Derivatives. *Chem. Ber.* **1994**, *127*, 2307–2314.

(35)   Das, S.; Wu, J. Toward Singlet–Triplet Bistable Nonalternant Kekulé Hydrocarbons: Azulene-to-Naphthalene Rearrangement. *Org. Lett.* **2015**, *17*, 5854–5857.

(36)   Baumgartner, P.; Weltin, E.; Wagnière, G.; Heilbronner, E. Ist Die Molekel Ein Biradikal? *Helv. Chim. Acta* **1965**, *48*, 751–764.

(37)   Nendel, M.; Goldfuss, B.; Houk, K. N.; Grieser, U.; Hafner, K. Bis-Periazulene: A Simple Kekulé Biradical with a Triplet Ground State. *Theor. Chem. Acc.* **1999**, *102*, 397–400.

(38)   Guihery, N.; Maynau, D.; Jean-Paul Malrieu, A. Search for Singlet-Triplet Bistabilities in Conjugated Hydrocarbons. *New J. Chem.* **1998**, *22*, 281–286.

(39)   Konishi, A.; Okada, Y.; Kishi, R.; Nakano, M.; Yasuda, M. Enhancement of Antiaromatic Character via Additional Benzoannulation into Dibenzo[*a,f*]Pentalene: Syntheses and Properties of Benzo[*a*]Naphtho[2,1-*f*]Pentalene and Dinaphtho[2,1-*a,f*]Pentalene. *J. Am. Chem. Soc.* **2019**, *141*, 560–571.

(40)   Konishi, A.; Horii, K.; Shiomi, D.; Sato, K.; Takui, T.; Yasuda, M. Open-Shell and Antiaromatic Character Induced by the Highly Symmetric Geometry of the Planar Heptalene Structure: Synthesis and Characterization of a Nonalternant Isomer of Bisanthene. *J. Am. Chem. Soc.* **2019**, *141*, 10165–10170.

(41)   Yang, X.; Shi, X.; Aratani, N.; Gonçalves, T. P.; Huang, K.-W.; Yamada, H.; Chi, C.; Miao, Q. Benzo[4,5]Cyclohepta[1,2-*b*]Fluorene: An Isomeric Motif for Pentacene Containing Linearly Fused Five-, Six- and Seven-Membered Rings. *Chem. Sci.* **2016**, *7*, 6176–6181.

(42)   Fu, X.; Han, H.; Zhang, D.; Yu, H.; He, Q.; Zhao, D. A Polycyclic Aromatic Hydrocarbon Diradical with PH-Responsive Magnetic Properties. *Chem. Sci.* **2020**, *11*, 5565–5571.

(43)   Zhen, C.; Lu, S.; Lin, M.; Wu, J.; Chao, I.; Lin, C. Singlet Biradical Versus Triplet Biradical/Zwitterion Characteristics in Isomers of $C_6-C_5-C_6-C_7-C_6$-Fused Pentacyclic Aromatic Hydrocarbons Revealed through Reactivity Patterns. *Chem. Eur. J.* **2021**, 1–9.

(44)   Borden, W. T. *Diradicals*; Borden, W. T., Ed.; Wiley-Interscience: New York, 1982.

(45)   Rajca, A. Organic Diradicals and Polyradicals: From Spin Coupling to Magnetism? *Chem. Rev.* **1994**, *94*, 871–893.

(46)   Abe, M. Diradicals. *Chem. Rev.* **2013**, *113*, 7011–7088.

(47)   Oyama, H.; Akiyama, M.; Nakano, K.; Naito, M.; Nobusawa, K.; Nozaki, K. Synthesis and Properties of [7]Helicene-like Compounds Fused with a Fluorene Unit. *Org. Lett.* **2016**, *18*, 3654–3657.

(48)   Savela, R.; Majewski, M.; Leino, R. Iron-Catalyzed Arylation of Aromatic Ketones and Aldehydes Mediated by Organosilanes. *Eur. J. Org. Chem.* **2014**, 4137–4147.

(49)   Pérez Sestelo, J.; Sarandeses, L. A.; Martínez, M. M.; Alonso-Marañón, L. Indium(III) as π-Acid Catalyst for the Electrophilic Activation of Carbon–Carbon Unsaturated Systems. *Org. Biomol. Chem.* **2018**, *16*, 5733–5747.

(50)   Nishimoto, Y.; Yasuda, M. Carbometalation and Heterometalation of Carbon-Carbon Multiple-Bonds Using Group-13 Heavy Metals: Carbogallation, Carboindation, Heterogallation, and Heteroindation. *Chem. Asian J.* **2020**, *15*, 636–650.

(51)   Hagel, M.; Liu, J.; Muth, O.; Estevez Rivera, H. J.; Schwake, E.; Sripanom, L.; Henkel, G.; Dyker, G. *P*-Quinoid Compounds by Nucleophilic Aromatic Substitution with Hydride as Leaving Group. *Eur. J. Org. Chem.* **2007**, 3573–3582.

(52)   Arikawa, S.; Shimizu, A.; Shintani, R. Azoniadibenzo[*a,j*]Phenalenide: A Polycyclic Zwitterion with Singlet Biradical Character. *Angew. Chem. Int. Ed.* **2019**, *58*, 6415–6419.

(53)   Katayama, K.; Konishi, A.; Horii, K.; Yasuda, M.; Kitamura, C.; Nishida, J.; Kawase, T. Isolation and Characterisation of a Stable 2-Azaphenalenyl Azomethine Ylide. *Commun. Chem.* **2019**, *2*, 136.

(54)   Liu, J.; Mishra, S.; Pignedoli, C. A.; Passerone, D.; Urgel, J. I.; Fabrizio, A.; Lohr, T. G.; Ma, J.; Komber, H.; Baumgarten, M.; Corminboeuf, C.; Berger, R.; Ruffieux, P.; Müllen, K.; Fasel, R.; Feng, X. Open-Shell Nonbenzenoid Nanographenes Containing Two Pairs of Pentagonal and Heptagonal Rings. *J. Am. Chem. Soc.* **2019**, *141*, 12011–12020.

(55)   Dittrich, B.; Fabbiani, F. P. A.; Henn, J.; Schmidt, M. U.; Macchi, P.; Meindl, K.; Spackman, M. A. Azulene Revisited: Solid-State Structure, Invariom Modeling and Lattice-Energy Minimization of a Classical Example of Disorder. *Acta Crystallogr. Sect. B* **2018**, *74*, 416–426.

(56)   Kruszewski, J.; Krygowski, T. M. Definition of Aromaticity Basing on the Harmonic Oscillator Model. *Tetrahedron Lett.* **1972**, *13*, 3839–3842.

(57)   Krygowski, T. M. Crystallographic Studies of Inter- and Intramolecular Interactions Reflected in Aromatic Character of π-Electron Systems. *J. Chem. Inf. Comput. Sci.* **1993**, *33*, 70–78.

(58)   Herges, R.; Geuenich, D. Delocalization of Electrons in Molecules. *J. Phys. Chem. A* **2001**, *105*, 3214–3220.

(59)   Geuenich, D.; Hess, K.; Köhler, F.; Herges, R. Anisotropy of the Induced Current Density (ACID), a General Method To Quantify and Visualize Electronic Delocalization. *Chem. Rev.* **2005**, *105*, 3758–3772.

(60)   Hafner, K.; Hafner-Schneider, G.; Bauer, F. Azuleno[8,8a,1,2-Def]Heptalene. *Angew. Chem. Int. Ed. Engl.* **1968**, *7*, 808–809.

(61)   Nakasuji, K.; Todo, E.; Murata, I. Azuleno[4,5,6-*cd*] Phenalene; A Novel Nonalternant Isomer of Benzo[*a*] Pyrene. *Angew. Chem. Int. Ed. Engl.* **1977**, *16*, 784–785.

(62)   Todo, E.; Yamamoto, K.; Murata, I. BENZO[4,5]CYCLOHEPT[1,2,3-*bc*]ACENAPHTHYLENE AND BENZO[*a*]NAPHTH[3,4,4a,5-*cde*]AZULENE. NONALTERNANT ISOMERS OF BENZO[*a*]PYRENE. *Chem. Lett.* **1979**, *8*, 537–540.

(63)   Yoshida, Z.; Shibata, M.; Ogino, E.; Sugimoto, T. A New Cata-Condensed Nonalternant Tetracyclic Hydrocarbon Azuleno[2,1-*e*]Azulene. *Tetrahedron Lett.* **1984**, *25*, 3343–3346.

(64)   Yamane, K.; Yamamoto, H.; Nitta, M. Synthesis, Stability, and Spectroscopic and Electronic Properties of Three Benzocyclohepta[*a*]Azulenylium Ions 1. *J. Org. Chem.* **2002**, *67*, 8114–8122.

(65)   Konishi, A.; Morinaga, A.; Yasuda, M. Construction of Polycyclic π-Conjugated Systems Incorporating an Azulene Unit Following the Oxidation of 1,8-Diphenyl-9,10-Bis(Phenylethynyl)Phenanthrene. *Chem. Eur. J.* **2018**, *24*, 8548–8552.

Conclusion

This thesis descibes the synthesis and characterization of benzo-annulated non-alternant hydrocarbons with (anti)aromaticity and/or open-shell character. The author focused on bicyclic non-alternant hydrocarbons, pentalene, heptalene, and azulene. The embedded quinoidal subunits in π-extended non-alternant hydrocarbons played a pivotal role in determining their electronic properties.

In Chapter 1, the author examined the interrelation between open-shell and anti-aromatic characters by comparing four types of diareno[*a*,*f*]pentalenes. Two simple principles as the main factors to determine the balance between open-shell and antiaromatic characteristics were demonstrated: the mode of the *o*-quinoidal moiety and the formal molecular symmetry. This conclusion can easily be broadened to other open-shell 4nπ-conjugated systems.

In Chapter 2, the author described the potential application of diareno[*a*,*f*]pentalene to organic devices. A dinaphtho[2,1-*a*:2,3-*f*]pentalene was adequately stable under ambient conditions and showed the intermolecular contacts derived from CH–π interactions in the crystal packing. These features suggests its potential as an organic hole transport material. The amorphous layer of this molecule showed moderate mobility despite having bulky substituents, and further molecular modification is expected to improve the mobility.

In Chapter 3, the author focused on the comparison of optoelectronic properties between alternant and non-alternant hydrocarbons under the same molecular symmetry. The author designed the derivative of difluorenoheptalene. Notably, it is the first report dealing with a planar heptalene derivative. The synthesized difluorenoheptalene showed the harmonization of the open-shell character with antiaromatic properties. The interconversion of two *o*-quinoidal units in difluorenoheptalene effectively induced the antiaromatic nature on the heptalene unit. Because of the antiaromatic and open-shell character of difluorenoheptalene, the electronic HOMO–LUMO gap was smaller than that of bistanethene.

In Chapter 4, the author synthesized and characterized bis-periazulene derivatives, which had not been synthesized for several decades. Although some previous theoretical reports showed a pristine bis-periazulene has a triplet ground state, the derivative with three aryl groups was experimentally disclosed its ground state was singlet. The energy gap between singlet ground state and thermally excited triplet state was considerably small and critically affected by the substituent on its pentagon.

The findings of this study show that the characteristic properties of non-alternant hydrocarbons can be realized with minimal π-extension. It is expected to be an important guideline for future molecular design using conjugated hydrocarbons.